Studying the Effects of Different Cosolutes on Protein Conformational Stability, Hydration Dynamics and Activity

A thesis submitted for the award of the degree of

Doctor of Philosophy (Science)
in
Chemistry (Experimental)

by

Nirnay Samanta

Department of Chemistry

University of Calcutta

2017

Dedicated to

My beloved Parents &

the Supervisor.

Abstract

This dissertation documents detail investigations of the protein structure, conformation, hydration and enzyme activity in presence of different kinds of cosolutes (e.g. macromolecules, osmolytes, chemical denaturants) at the physiological condition. Our goal is to understand how proteins fold/unfold, hydrates and function in *crowded* cellular environment through *in vitro* studies. With this end in view, we have chosen some synthetic polymers and some biologically relevant small cosolutes to study protein stabilization and functionality by both spectroscopy and thermodynamic studies. We investigate the effect of short chain polyethylene glycol (PEG) on the physical properties of a model protein human serum albumin and found unusual behaviour in thermal stability as well as in the hydration of the protein which cannot be explained only by so called *excluded volume theory* rather one needs to consider weak attractive interactions between protein and PEG. We have addressed a debatable issue whether some molecules (urea, guanidinium chloride, amino acids) denature or stabilize proteins due to modification of water networks. Our studies using terahertz (THz) spectroscopy tool reveal the interesting correlation of protein stabilization or denaturation with the modification in sub-ps to ps collective hydrogen bond dynamics of water. Finally we have investigated enzyme activity in presence of cosolutes and found an unusual enhancement of the activity in very dilute concentration region of cosolutes; activity decreases in the higher concentration regime.

List of Publications

This thesis is based upon the following publications and manuscripts:

1. Samanta, N., Mahanta, D. D., Hazra, S., Kumar, G. S., and Mitra, R. K. (2014) Short Chain Polyethylene Glycols Unusually Assist Thermal Unfolding of Human Serum Albumin, *Biochimie 104*, 81-89.
2. Samanta, N., Mahanta, D. D., and Mitra, R. K. (2014) Does Urea Alter the Collective Hydrogen Bond Dynamics in Water: A Dielectric Relaxation Study in the THz Frequency Region, *Chemistry - An Asian Journal 9*, 3457-3463.
3. Samanta, N., Mahanta, D. D., and Mitra, R. K. (2014) Collective Hydration Dynamics of Guanidinium Chloride Solutions and its Possible Role in Protein Denaturation: A Terahertz Spectroscopic Study, *Physical Chemistry Chemical Physics 16*, 23308-23315.
4. Samanta, N., Mahanta, D. D., and Mitra, R. K. (2015) Urea and guanidinium chloride act as 'water structure breakers': The debate revisited by dielectric relaxation study in THz range, *Infrared, Millimeter, and Terahertz waves (IRMMW-THz), 2015 40th International Conference*, IEEE.(*Conference Proceeding*).
5. Samanta, N., Luong, T. Q., Mahanta, D. D., Mitra, R. K., and Havenith, M. (2016) Effect of Short Chain Polyethyleneglycols on the Hydration Structure and Dynamics around Human Serum Albumin, *Langmuir*.32(3), 831-837.
6. Samanta, N., Mahanta, D. D., Choudhury, S., Barman, A., and Mitra, R. K. (2017) Collective Hydration dynamics in some amino acid solutions: A combined GHz-THz Spectroscopy study, *Journal of Chemical Physics* 146 (12), 125101-125108.
7. Samanta, N., Mahanta, D. D., and Mitra, R. K. THz spectroscopic study unravels why chloride salt of guanidinium is a protein denaturing agent while sulphate salt is not *(Manuscript to be submitted).*
8. Samanta, N., Mahanta, D. D., Patra, A., and Mitra, R. K. Lysozyme activity on Micrococcus Lysodeikticus cell wall in crowded environments *(Manuscript to be submitted).*

I have also contributed to the following publications:

9. Mahanta, D. D., Samanta, N., and Mitra, R. K. (2016) The effect of monovalent cations on the collective dynamics of water and on a model protein, *Journal of Molecular Liquids 215*, 197-203.
10. Patra, A., Hazra, S., Samanta, N., Kumar, G. S., and Mitra, R. K. (2016) Micelle induced dissociation of DNA–ligand complexes: The effect of ligand binding specificity, *International journal of biological macromolecules 82*, 418-424.
11. Mahanta, D. D., Patra, A., Samanta, N., Luong, T. Q., Mukherjee, B., and Mitra, R. K. (2016) Non-monotonic dynamics of water in its binary mixture with 1,2-dimethoxyethane: A combined THz spectroscopic and MD simulation study, *The Journal of Chemical Physics* 145, 164501-164512.

12. Patra, A., Samanta, N., Das, D. K., and Mitra, R. K. Enhanced catalytic activity of α-chymotrypsin in cationic surfactant solutions: The component specificity revisited *Journal of Physical Chemistry B 121, 1457-1465.*

13. Mahanta, D. D., Samanta, N., and Mitra, R. K. The Decisive Role of Hydrophobicity on the Effect of Alkylammonium Chlorides on Protein Stability: A Terahertz Spectroscopic Finding *(Under review).*

14. Pal, S., Samanta, N., Mahanta, D. D., Mitra, R. K., and Chattopadhyay A. Effect of phospholipid head group on the structure and dynamics of water around membrane bilayers: A THz study *(Manuscript to be submitted).*

Acknowledgements

Without acknowledging some persons it will remain incomplete to write my thesis. It is my great pleasure to acknowledge them, who helped and encouraged me directly or indirectly during my Ph.D. days.

First of all, I express my deepest respect to my Mother who is my first teacher, and then to my Father. Their love, affection, ideology always reflects in my mind. Today I am here due to their incessant support and inspiration. I have no word to acknowledge them.

I wish to convey my sincere gratitude to my Ph.D. supervisor Dr. Rajib Kumer Mitra. His continual guidance, support, motivation and knowledge helped me in all the time of my Ph.D. and writing of this thesis. I have learned from him even very basic things like preparing presentable graphs, poster presentation and writing scientific reports in a proper way. I express my gratitude to him for all the suggestions and advices which helped to improve my Ph.D. work and knowledge. His incessant curiosity on my work gave the will to carry on going forward. I always believe that I was lucky enough to have an opportunity of working under the guidance of such a man with goodness, welcoming behaviour and sense of humour.

Besides my supervisor, I would like to express gratitude to Dr. Gopinatha Suresh Kumar (IICB, Kolkata) and Prof. Anjan Barman (SNBNCBS, Kolkata) for giving me an opportunity to access their laboratories and research facilities. I would also like to acknowledge my other collaborators Dr. Trung Quan Luong, Prof. Martina Havenith (Ruhr University, Germany) and Prof. Amitabha Chattopadhyay (CCMB, Hyderabad) for their valuable suggestions and supports.

I would like to thank my past and present lab mates: Dr. Animesh Patra, Dr. Debanjan Polley, Debasish Das Mahanta, Dr. Dipak kr. Das, Dr. Semanti Pal, Dr. Arindam Das, Debkumar Rana, Partha Pyne,

Kumar Neeraj, Amit Barh, Saikat Pal, Sk Imadul Islam and Anulekha De for working together in an amusing atmosphere, the stimulating discussions, for all the fun we have had during the last five years. A very special thank goes to Animesh Da, from whom I have learned a lot, like experimental techniques, lab attitudes, data analysis etc. Without his help my research work would be very difficult. I wish to thank Debasish for all the helps and supports throughout my PhD work. I am thankful to Debanjan Da for helping me to learn the THz spectroscopy and the measurements. Thanks to Dipak Da for giving tips and suggestions to understand some basic instrumentations and the techniques to align the optics. I would like to thank Christopher McRaven (Opto-Mechanical engineer) for helping to learn the alignment of THz time domain spectroscopy in our lab. I express my acknowledgment and special thanks to Semanti Di, from whom I learnt so many things like the use of "endnote", different techniques in MS Word, drawing presentable schematic, some of the basic instrumentations, which help me a lot in writing the thesis and also thanks her for all the helps and suggestions. I would like to thank Dipak da, Debasish, Partha, Debanjan da, Amit and Sonali di for helping a lot in proof corrections of the thesis. Each and every one's help and cooperation affluences my research work and I must say that this is the best lab in the world.

We, the lab members, spent some delightful evenings in the sweet home of our Sir and Madam (Dr. Sukanya Chakrabarty). Thanks Madam and thanks again to Sir for those cheerful moments and for those special dinners.

Apart from my lab mates I would like to acknowledge some persons who helped me in my Ph.D. work. I would like to thank Dr. Soumitra Hazra for doing DSC study at IICB. Thanks Samiran for helping me during Dielectric relaxation study in GHz frequency. I am thankful to Dr. Ranajay Saha (helped to learn protein structure

analysis in CDNN software), Dr. Surajit Rakhsit, Dr. Nirmal Goswami, Sushovan, Anuradha di, Kallol da for helping me to understand some experimental techniques. Thanks to Sreetama (CCMB, Hyderabad) for sharing the knowledge of lipid membrane and some fruitful scientific discussions during the collaborative work. I am thankful to my friend Nayim Sepay (organic Chemist) for the scientific discussions, suggestions. His enthusiasm in research always motivates me.

Nonetheless it is beyond acknowledgement, I express my special thanks to Nivedita Samanta (my Didi), Dipak Roy (brother in law), nieces (my little angels: Rai & Rinki) and my loving nephew (Rohan) for giving me all the love, happiness and pleasures.

During my Ph.D. life through the last five years, I have had some nice persons who gave me some lasting memories full of happiness and lots of fun. Among them my heartiest thanks go to Semanti Di, Animesh Da for all their affection, guidance, unconditional love, keeping me smile always. They are always with me in my all good and bad days. I'll never forget the kindness and care of Semanti Di. After them my special thanks goes to Partha, one of my labmates for giving continuous company, support and caring. I am very thankful to Krishnendu, Sonali di, Debkumar, Sayani di, Arghya da, CS, Ishita di, Subhasish da for making me so happy and for all the supports. Thanks to Abhijit, Sandip, Suman Aich, Rajkumar, Suman Som, GBD, Tuhin, Indranil, Atanu, Mithun, Chiranjit da, Tilak da. I remember the sense of humour of Animesh da, Semanti Di, Amit, Imadul, Krishnendu, Suman Aich, Debkumar, without their presence my life would be boring and hectic. I am so grateful to have the awesome group ("Vat" group) of Semanti Di, Animesh Da, Sonali Di and Nitish Da for all the amusing moments we spent.

I would like to express special thanks to my close friends and classmates: Rabin, Swarnadip, Nayim, Ankur da, Sujit, Arpan, Samrat, Sumanta da for all the chats and cheering me up all-the time.

I am indebted to my beloved teachers whose inspiration all the time helps me to go forward. I am grateful to my school teachers Gautam Mishra, Malay Kumar Basu, Dipak Bhattacharya, Dinesh Das, Krishna Mahanti, Raju da. I am also grateful to the Prof. Sanjeeb Bagchi, Prof. DCM, Dr. SB, Dr. CKB, Prof. GNM, Dr. Souvik Chatterjee, Dr. Suman Das, Prof. HKC, Dr. SBM for enlightening me during my Master and Graduate days.

I express my gratitude to Prof. Samir Kumar Pal, Prof. Sandip K. Chakrabarty, Dr. Kinsuk Acharyya, and Dr. PKM for teaching during Ph. D. course work programme. I am also thankful to the reviewers for their judicial comments of different journals and thank to the thesis committee.

Thanks to all the academic and non-academic personnel of SNB for their cooperation. Finally, I would like to acknowledge S.N. Bose National Centre for Basic Sciences and DST for the financial support and giving me the opportunity to research.

Sign:_____ Date:

NIRNAY SAMANTA (*e-mail:* mail2nirnay@gmail.com)

S. N. Bose National Centre for Basic Sciences
Block JD, Sector III, Salt Lake, Kolkata 700106 (W.B.), INDIA.

Acronyms

AA	Amino Acid
BSA	Bovine Serum Albumin
CD	Circular Dichroism
DLS	Dynamic Light Scattering
DSC	Differential Scanning Calorimeter
EG	Ethylene Glycol
FTIR	Fourier Transform Infrared Spectroscopy
FIR	Far Infrared Spectroscopy
GdmCl	Guanidinium Chloride
HEWL	Hen Egg White Lysozyme
HSA	Human Serum Albumin
PEG	Poly(Ethylene) Glycol
SASA	Solvent Accessible Surface Area
TCSPC	Time Correlated Single Photon Counting
THz	Terahertz
TMGdm	Tetramethylguanidinium
TRFS	Time Resolved Fluorescence Spectroscopy
Trp	Tryptophan
TTDS	Terahertz Time Domain Spectroscopy
UV	Ultra Violet

Table of Contents

Chapter 1

1. Introduction

Proteins from "birth to death" is extremely fascinating from their biosynthesis to their folding, signalling and degradation. Prof. George Rose said in a lecture, *"The fold of the protein links the one-dimensional, linear world of DNA to the three-dimensional world of biological function; accordingly, protein folding is a cornerstone of life on earth"*. Proteins have evolved to function in cellular *crowded environments*, and it, therefore, is important to understand how it folds, interacts, hydrates *in vivo*. From amino acids to polypeptides to "protein" – this journey takes place at ribosome (*protein factory*) which is embedded in crowded cytoplasm. After transcription *messenger RNA* (*mRNA*) moves out from the nucleus to the ribosome where *transfer RNA* (*tRNA*) attached with a specific amino acid (AA) translates the amino acid one after another following the codons of *mRNA* and thus forms primary structure with a specific sequence. [1, 2] Finally it undergoes certain steps to build a fully functioning protein by minimizing the free energy by forming hydrogen bonds, disulphide bridges, ionic, van der Waals interaction between amino acids and lowering configurational entropy. Protein folding process takes place within real time in a highly heterogeneous media and sometimes it fails to follow the right pathway and it misfolds.[1] In living cell upto 40% (w/v) volume is crowded by various macromolecules and other cosolutes. Such environment is termed as "*crowded"* rather than concentrated because no individual molecule may exist at high concentration.[3] Both intra as well as extra cellular (e.g., blood plasma) environments are heterogeneous due to the presence of several organic and inorganic compounds including *macromolecules* like lipids, nucleic acids, proteins, *osmolytes (small organic molecules, termed as osmolytes, which are ubiquitously found in living organisms, primarily involved in maintaining osmotic pressure in the cell)* like sugars, trimethylamine N-oxide (TMAO), metabolites, along with macromolecular arrays (e.g. cytoskeleton fibre etc.).[4, 5] For instance, erythrocytes content ~35% (w/v) protein, in cytoplasm (Escherichia coli)[6] and in human lens[7] there are ~34% (w/v) protein.

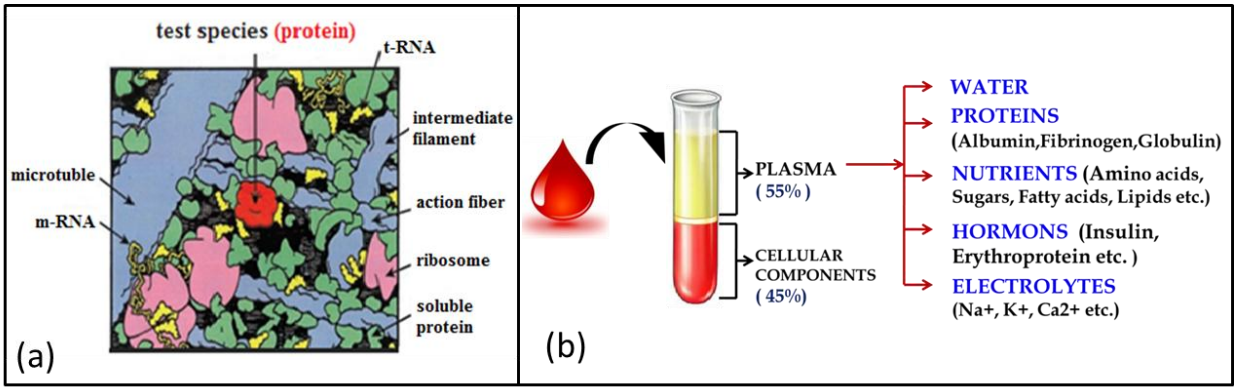

Scheme 1.1: (a) Cartoon of eukaryotic cytoplasm at a magnification of 1,000,000 ×. The test protein molecule (*red*) is in a fluid medium that is crowded by soluble proteins (*green*), RNA species (*yellow*), and ribosomes (*pink*) and confined by cytoskeletal fibers (*blue*).[8] (b) Composition of blood plasma to represent the extracellular crowding.

In such crowded media protein stability is very crucial to explore as proteins are biologically active mostly in its native form and misfolding could often lead to malfunction and diseases.[9, 10] Under certain pathological conditions (e.g, Alzheimer's disease, Parkinson's disease, Type II diabetes, mad cow disease, prion disease, Huntington's disease etc.)[11] there appears fibrillation/aggregation which might enhance further crowding.[12-14] In such cases, osmolytes are proving to be successful therapeutic agents. For example, in case of Alzheimer's disease the formation of β-amyloid plaque, which leads to neuronal cell death, was found to be inhibited in presence of osmolytes like TMAO and glycerol.[15] Hence it is of utmost importance to understand the conformational stability, the associated hydration dynamics in its solvation sheathe as well as the activity of proteins in presence of different types of *cosolutes*. Due to experimental challenges to observe a particular protein in living species scientists have successfully mimicked[4] the *crowding effects* by adding apparently inert cosolutes which serve to mimic such cellular crowding effect. To comprehend the factors for protein stability, some synthetic polymers (e.g. dextran, ficoll, polyethylene glycol), and small molecules (sucrose, glycerol, TMAO) as well as protein itself are often employed to investigate how the structure, thermal stability, hydration and function or activity of a protein are modified.[16-19] Theoretical studies using simple analytical calculations based on the *scaled particle theory* (*SPT*) have shown that artificial macromolecules can be modelled as simple hard spheres or rods in shape.[20] Protein folding in a crowded medium was first investigated applying *coarse-grained molecular simulation* by Cheung et al.[21] It was found that the folding stabilities in such mimicking crowding environment obtained from simulations agrees well with the experimentally measured values.[16, 22]

To properly assess the physiological role of a particular process/reaction *in vivo*, it is important to consider all the possible influence of the cosolutes on the process/reaction in its physiological milieu. So it is crucial to study proteins in presence of different types of cosolutes. These are broadly categorized as – *'macromolecular crowders'*[23] (e.g. proteins, DNA, dextran, polyethylene glycol, Ficol), '*bioprotective osmolytes'* (e.g. polyols, sugars, methylamines, amino acids), and '*chemical denaturants'* (e.g. guanidinium chloride, urea)[24]. It has been recognized that proteins behave differently in crowded environment as compared to normal *in vitro* aqueous environments, and such altered behaviours could often be identified with those observed in cellular environments.[25-29]Such modification in physical properties has so far been correlated to the idea of *'volume exclusion'*[21, 30-34] which is based on the principle that the volume occupied by macromolecules is not accessible to other solutes.

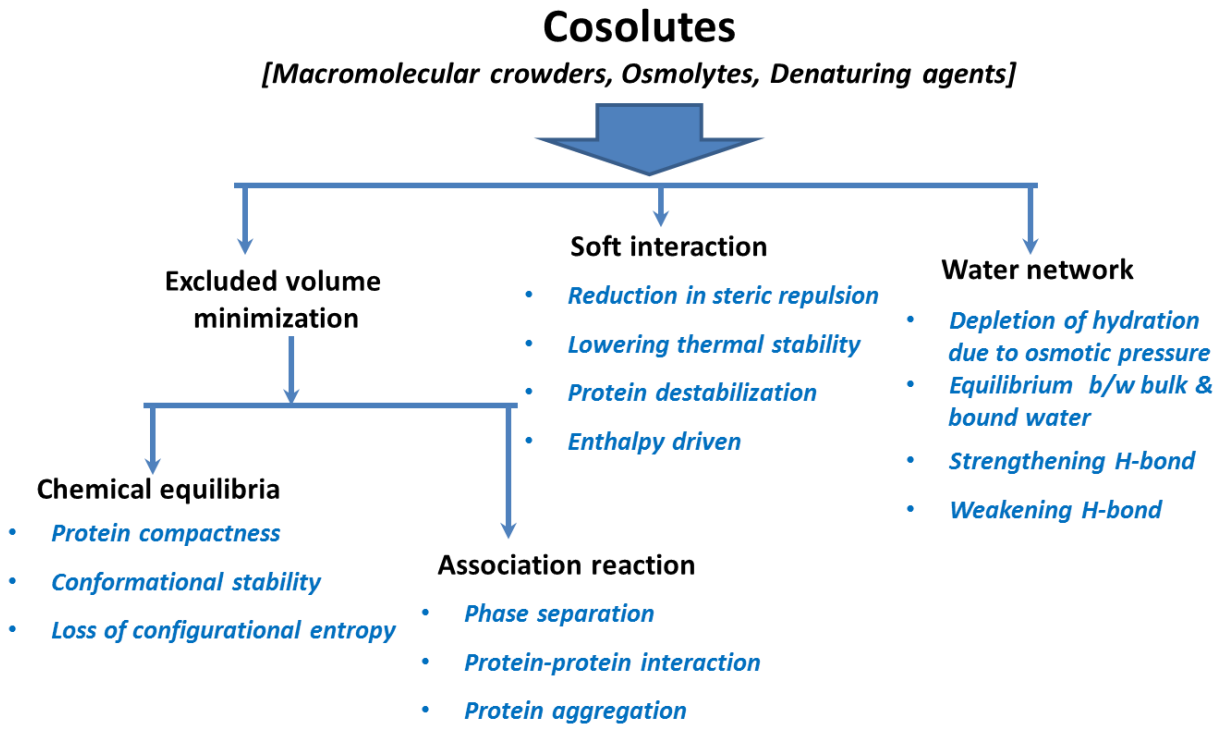

Scheme 1.2: Possible effects of cosolutes to modulate the physical properties of protein.

The *excluded volume theory* is based on the assumption of mutual impenetrability of seemingly hard sphere solute molecules that generate steric repulsion. In the simplest case of spherical particles the closest two such molecules can approach is a distance equal to the sum of their radii (see details in chapter 2). This makes a spherical excluded volume around each molecule which is inaccessible to the centers of all the other molecules. It is obvious that in

the available space. As a consequence there is a decrease in the randomness of distribution of the particles i.e. lowering of configurational entropy. In earlier studies the observed increase in the native→unfolded transition temperature has been explained on the basis of the relative stabilization of the folded state of the protein in comparison to the destabilization of the unfolded state in the potential energy landscape by making the unfolded state more compact to minimize steric repulsion and thereby energetically less favourable.[4, 31, 35] However, recent studies have shown that the excluded volume effect is not the sole factor, there are several other factors to be considered in crowded environments like viscosity, perturbed diffusion, direct physical interactions between the crowding agents and proteins, "soft" interactions (e.g. electrostatic, hydrophobic, and van der Waals interactions) between the crowding agent and the protein, and, most importantly, the effects of crowders on solvent properties.[36] Macromolecules inside real cellular environment do not show compactness as expected by excluded volume effect as the attractive, nonspecific interactions counteract the excluded-volume effect.[37] In a recent study Ebbinghaus *et al.* have introduced a thermodynamic overview to understand the effects of different cosolutes on proteins in the following way—*i) Ideal excluded volume effect* (for ficoll, sugar) does increase the thermal stability (increase in the melting temperature, T_m) and decrease in the change in entropy with marginal change in enthalpy during unfolding of protein, *ii) preferential hydration* (for glucose, KCl, dextran) of protein causes an enthalpic stabilisation and protect the protein to interact directly, *iii) preferential binding* of the cosolutes (for urea) causes a decrease in enthalpy and thermal stability (decrease in melting temperature), *iv)* when both the *preferential hydration* of protein and *preferential binding* of cosolutes to the protein simultaneously work (e.g. for PEG), there occurs an increase in enthalpy and decrease in thermal stability (lowering of melting temperature) of proteins.[24] Therefore PEG can be considered as an intermediate between stabilizing osmolytes and chemical denaturant and the overall effect depends on the chain length and the protein used. It is not a trivial task to predict the effect of different PEGs on the physical properties of a specific protein. This makes it interesting to study PEG as a crowding agent. The effect of several small and large molecular weight osmolytes on the biomolecular stability has theoretically been investigated by the group of Record *et al.*[38-40] However, the exact mechanism of the stabilization (whether direct or indirect interaction) has not yet been properly understood for small polymers which also behave as osmolytes. Recent studies by Chowdhury *et al.* have concluded direct evidence of substantial *soft interaction* rather than *excluded volume repulsion* to prevail between proteins and crowding agents.[41, 42]

The authors proposed that in dilute concentration region such polymers (not in enough entangled form) are more prone to interact directly with the proteins. Despite all these studies it is evident that the interaction cannot be predicted as it is highly dependent on the protein as well as the crowding agents. A detailed understanding regarding the hydration state of protein surface under such strained environment has not yet been well rationalized, and is a demanded study as conformation and functionality of proteins are slaved by these factors. The present research work is an attempt to explore the effect of *crowded environment* on different physical processes of protein molecules as manifested in the solvation dynamics and associated energy cost during the processes.

There exists some otherwise indifferent biologically relevant small solutes e.g. urea, guanidinium chloride (GdmCl), amino acids, which are well known to denature or stabilise proteins. Amino acids often act as intermediates in metabolism as well as osmolytes that can stabilize proteins.[43-45] Moreover hydrophobicity of amino acids is believed to be a key parameter that regulates phenomena like protein folding-unfolding, aggregation, activity, protein-ligand binding and protein hydration in aqueous environments.[46-50] The exact molecular mechanism of the processes involved still remains a strongly debatable issue. Interaction of these molecules with proteins has been envisaged either as a result of a direct interaction with the protein backbone or as an indirect effect in which these molecules perturb the water network structure.[51-53] Some earlier studies have reckoned urea[54] and GdmCl[55-58] to be *'water structure breaker'*. This hypothesis has, however, not received considerable support from experimental or simulation studies with only a few reports documented in the literatures[59-65].

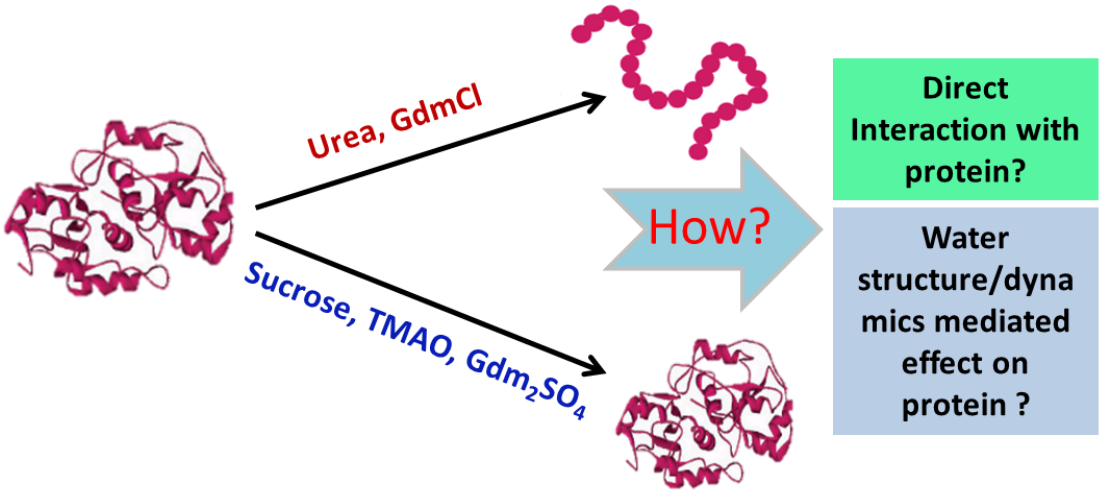

Scheme 1.3: The mechanism of protein denaturation or stabilisation by cosolutes is still a debatable issue

The concept of these molecules being enacted as a 'water structure breaker' has been challenged by a series of simulation and experimental studies.[66-68] In this notion the denaturing ability of GdmCl is believed to be due to direct interaction of Gdm^+ with the protein.[69, 70] But question arises when Gdm_2SO_4 has been found to stabilize the proteins.[71] In an early study von Hippel and Wong reported that thermal melting temperature of ribonuclease increases with the Gdm_2SO_4 concentration in contrast to GdmCl.[72] In this regard another interesting fact is that arginine (Arg) having considerable structural similarity to that of guanidinium (Gdm^+) cation, however, shows remarkably contrasting behaviour with proteins: while Gdm^+ denatures them, Arg modestly stabilizes them[73]. This makes it worth comparing their hydration behaviour. So investigation of the mechanism of denaturation/stabilization of proteins by small solutes is still on demand.

How proteins function in presence of different cosolutes is vital to understand as they act as biological catalyst to almost all life processes. Study of protein function in crowded milieu is a widespread topic of research.[74, 75] It is not a trivial task to predict the effect of different crowding agents or cosolutes on protein activity because each protein behaves in different ways in presence of materials due to their variable hydrophilic and hydrophobic residues on the surface and on the binding sites. Lee *et al.* reported the enzyme activity of α-chymotrypsin in presence of different osmolytes and denaturants.[76] They found reduced activity of the enzyme when introduced the stabilizing osmolytes (sucrose, TMAO, betaine, sacrosine and proline) and in presence of urea, GdmCl the enzyme activity almost finishes. Most of the previous studies revealed lowering of protein activity owing to the volume exclusion and an increase in the viscosity has been believed to affect the diffusion or encounter rates of enzyme and substrate.[77, 78] On the other hand ~6% enhancement of enzyme activity was reported by Pancera *et al.*[79] for yeast hexokinase in presence of very dilute PEG 400 solution, however, the activity was lower in PEG 1500 and 4000 solutions. The activity of glucose-6-phosphate dehydrogenase was reported to increase in presence of 20% (w/v) PEG 400 and 4000 solutions.[80] But a molecular level plausible mechanism is still lacking due to several juxtaposed factors which control the protein function.

The principal objective of this thesis is to understand protein folding/unfolding process and the associated changes in the structure and dynamics of the protein hydration sheathe in presence of model crowding agents, osmolytes of variable hydrophobicity and chemical denaturants. Conformational stability of protein molecules (e.g. human serum albumin, lysozyme, bovine serum albumin etc.) in presence of macromolecular crowding

agents (e.g. PEG), osmolytes (amino acids) and chemical denaturants (e.g. urea, GdmCl) has been determined using *circular dichroism* (CD) spectroscopy. The overall hydrodynamic diameter of the proteins has been obtained using *dynamic light scattering* (DLS) technique. Intrinsic fluorescence from the constituent tryptophan residues of proteins is a potential marker of the local environment of that protein. Additional information on the hydration structure of proteins is extracted from absorption spectroscopy, *acoustic* (high precision density and sound velocity analyser), *FTIR* (by measuring the spectra in the O-H stretching (3000-3800 cm^{-1}) or O-D (in D_2O solution) stretching (2200-2700 cm^{-1}), and intermolecular O-H stretching in the FIR region (30-600 cm^{-1})). Enzymatic activity of proteins in such environments has been determined by UV spectrophotometer. The free energy, enthalpy and entropy changes associated with the above mentioned processes (like protein conformational changes, enzymatic activity etc.) in both the environments is underlined using *differential scanning calorimetry* (DSC) technique and temperature dependent optical property study.

Hydration dynamics around cosolutes and proteins has been measured using two complementary techniques: *time resolved fluorescence spectroscopy* (TRFS) and *THz time domain spectroscopy* (TTDS). In the former one, relaxation of polar environment (water) around an excited fluorophore is measured using ps-resolved *time-correlated single photon counting* (TCSPC) technique.[81-83] The collective H-bond network and ultrafast dynamics of hydration water is studied using *THz spectroscopy* (1 THz = 10^{12} Hz = 1 ps^{-1}), which has recently been emerged as a potential tool to *label free* determination of the *collective dynamics* of water around biomolecules.[84-89] The main advantage of THz radiation is its low energy (1THz corresponds to ~ 4 meV) which leaves biomolecules unharmed and the perfect timescale that probes the ultrafast collective dynamics of the hydrogen bond network in the solvation water in its *extended hydration sheathe* which extends up to several hydration layer about the solute surface and is otherwise wiped off in conventional spectroscopic techniques.[90, 91] TTDS offers with an additional advantage of measuring both the phase and the amplitude of the transmitted radiation in a single experiment enabling the calculation of various optical parameters (e.g. absorption coefficient, complex refractive index, complex dielectric constant etc.) of the solutions by numerically solving Fresnel's transmittance equations[92], such parameters are used to extract the collective hydration dynamics of solvents around biomolecules using multiple *Debye relaxation model*[90, 93] (details provided in chapter 2). It is a reliable tool to extract ultrafast water dynamics in ps-sub ps time scale. It is very sensitive to detect the times scales of ~ 8 ps, ~ 200 fs and ~ 80 fs for water and any alteration

induced by the cosolutes or biomolecules.[90] The ~ 8 ps and ~ 200 fs timescales are due to the well-known cooperative rearrangement of the hydrogen bonded network and the rotational modes of individual polar water molecules, respectively.[94] The ~ 80 fs timescale has its origin rooted to the 60 cm^{-1} vibrational band due to the hydrogen-bond bending and the related transverse acoustic phonons which propagate in a direction normal to the hydrogen bonds in between two neighbouring water molecules.[95, 96]

The present thesis is based on the investigation of structure, conformation, thermal stability, hydration and finally the activity/function of some model proteins/enzymes in presence of a special kind of crowding agent PEG of different chain lengths,[97, 98] and some bio-relevant small cosolutes (urea, GdmCl, amino acids).[99-101]

This thesis consists of the following seven chapters as described in brief.

Chapter 1 discusses the introduction and motivation behind this thesis work.

Chapter 2 is based on some relevant basic theories, information and experimental methods that we have used. This chapter also provides the chemical structure of the samples used.

Chapter 3 represents all the instruments used and briefly describes their basic working principles.

Chapter 4 describes the effect of short chain PEGs on the physical properties of human serum albumin and unusual behaviour of thermal stability as well as hydration of the protein. We have found the primary nature of interaction of the PEG with the protein changes from a non-interacting or weakly repulsive (as an osmolyte) to interacting (as a non-specific ligand) mode with the increase in concentration of PEG. Here we have shown the effect of the crowding agents on the collective hydrogen bonded water network structure by using THz spectroscopy.

Chapter 5 discusses the investigations to understand the process of how protein folds or unfolds by cosolutes in water medium. Our study reveals the collective hydrogen bond dynamics in presence of some protein-denaturing (urea, GdmCl) and stabilizing cosolutes (TMAO, sucrose, amino acids).

Chapter 6 reveals the study of the enzyme activity of hen egg white lysozyme (HEWL) on the cell wall of a *micrococcus* bacterium in presence of cosolutes and found an unusual enhancement of activity in very dilute concentration region of cosolutes whereas activity decreases in the higher concentration regime.

Chapter 7 provides the summary of the present thesis work and also a brief discussion about some future plans.

References

1. Lodish, H., Baltimore, D., Berk, A., Zipursky, S. L., Matsudaira, P., and Darnell, J. (1995) *Molecular cell biology*, Vol. 3, Scientific American Books New York.
2. Bryngelson, J. D., Onuchic, J. N., Socci, N. D., and Wolynes, P. G. (1995) Funnels, pathways, and the energy landscape of protein folding: a synthesis, *Proteins: Structure, Function, and Bioinformatics 21*, 167-195.
3. Minton, A. P. (1997) Influence of excluded volume upon macromolecular structure and associations in 'crowded" media, *Current opinion in biotechnology 8*, 65-69.
4. Zimmerman, S. B., and Minton, A. P. (1993) Macromolecular Crowding: biochemical, biophysical and physiological consequences, *Annu. Rev. Biophys. Biomol. Struct. 22*, 27-75.
5. Fulton, A. B. (1982) How crowded is the cytoplasm?, *Cell 30*, 345-347.
6. Zimmerman, S. B., and Trach, S. O. (1991) Estimation of macromolecule concentrations and excluded volume effects for the cytoplasm of Escherichia coli, *Journal of Molecular Biology 222*, 599-620.
7. Harding, J. (1991) *Cataract: biochemistry, epidemiology, and pharmacology*, Chapman and Hall.
8. Minton, A. P. (2001) The Influence of Macromolecular Crowding and Macromolecular Confinement on Biochemical Reactions in Physiological Media, *THE JOURNAL OF BIOLOGICAL CHEMISTRY 276*, 10577-10580.
9. Chiti F, D. C. (2006) Protein misfolding, functional amyloid, and human disease, *Annu Rev Biochem 75*, 333–336.
10. Thirumalai D, K. D., Dima RI (2003) Emerging ideas on the molecular basis of protein and peptide aggregation, *Curr Opin Struct Biol 13*, 146-159.
11. Bhat, M. Y., Singh, L. R., and Dar, T. A. (2017) Modulation of Protein Aggregation/Fibrillation by Osmolytes, In *Cellular Osmolytes: From Chaperoning Protein Folding to Clinical Perspectives*, pp 121-142, Springer Singapore, Singapore.
12. Dobson, C. M. (2004) In the footsteps of alchemists, *Science 304*, 1259-1262.
13. Uversky, V. N., Oldfield, C. J., Midic, U., Xie, H., Xue, B., Vucetic, S., Iakoucheva, L. M., Obradovic, Z., and Dunker, A. K. (2009) Unfoldomics of human diseases: linking protein intrinsic disorder with diseases, *BMC genomics 10*, S7.
14. Habchi, J., Tompa, P., Longhi, S., and Uversky, V. N. (2014) Introducing protein intrinsic disorder, *Chemical reviews 114*, 6561-6588.
15. Chaudhuri, T. K., and Paul, S. (2006) Protein-misfolding diseases and chaperone-based therapeutic approaches, *FEBS Journal 273*, 1331-1349.
16. Stagg, L., Zhang, S.-Q., Cheung, M. S., and Wittung-Stafshede, P. (2007) Molecular crowding enhances native structure and stability of α/β protein flavodoxin, *Proceedings of the National Academy of Sciences 104*, 18976-18981.
17. Perham, M., Stagg, L., and Wittung-Stafshede, P. (2007) Macromolecular crowding increases structural content of folded proteins, *FEBS letters 581*, 5065-5069.
18. Ellis, R. J. (2001) Macromolecular crowding: obvious but underappreciated, *Trends in Biochemical Sciences 26*, 597-604.
19. Verma, P. K., Kundu, A., Ha, J.-H., and Cho, M. (2016) Water Dynamics in Cytoplasm-Like Crowded Environment Correlates with the Conformational Transition of the Macromolecular Crowder, *Journal of the American Chemical Society 138*, 16081-16088.

20. Zhou, H.-X., Rivas, G., and Minton, A. P. (2008) Macromolecular Crowding and Confinement: Biochemical, Biophysical, and Potential Physiological Consequences, *Annu. Rev. Biophys. 37*, 375-397.
21. Cheung, M. S., Klimov, D., and Thirumalai, D. (2005) Molecular crowding enhances native state stability and refolding rates of globular proteins, *Proc. Natl. Acad. Sci. USA 102*, 4753-4758.
22. Christiansen A, W. Q., Samiotakis A, Cheung MS, Wittung-Stafshede P. . (2010) Factors defining effects of macromolecular crowding on protein stability: An in vitro/in silico case study using cytochrome c, *Biochemistry 49*, 6519–6530.
23. Minton, A. P., and Wilf, J. (1981) Effect of macromolecular crowding upon the structure and function of an enzyme: glyceraldehyde-3-phosphate dehydrogenase, *Biochemistry 20*, 4821-4826.
24. Senske, M., Törk, L., Born, B., Havenith, M., Herrmann, C., and Ebbinghaus, S. (2014) Protein stabilization by macromolecular crowding through enthalpy rather than entropy, *Journal of the American Chemical Society 136*, 9036-9041.
25. Yamin, G., Munishkina, L. A., Karymov, M. A., Lyubchenko, Y. L., Uversky, V. N., and Fink, A. L. (2005) Forcing Nonamyloidogenic β-Synuclein To Fibrillate†, *Biochemistry 44*, 9096-9107.
26. Aisenbrey, C., Bechinger, B., and Gröbner, G. (2008) Macromolecular Crowding at Membrane Interfaces: Adsorption and Alignment of Membrane Peptides, *Journal of Molecular Biology 375*, 376-385.
27. McPhie, P., Ni, Y.-s., and Minton, A. P. (2006) Macromolecular Crowding Stabilizes the Molten Globule Form of Apomyoglobin with Respect to Both Cold and Heat Unfolding, *Journal of Molecular Biology 361*, 7-10.
28. Morán-Zorzano, M. T., Viale, A. M., Muñoz, F. J., Alonso-Casajús, N., Eydallín, G. G., Zugasti, B., Baroja-Fernández, E., and Pozueta-Romero, J. (2007) Escherichia coli AspP activity is enhanced by macromolecular crowding and by both glucose-1,6-bisphosphate and nucleotide-sugars, *FEBS Letters 581*, 1035-1040.
29. Sasaki, Y., Miyoshi, D., and Sugimoto, N. (2007) Regulation of DNA nucleases by molecular crowding, *Nucleic acids research 35*, 4086-4093.
30. Knoll, D., and Hermans, J. (1983) Polymer-protein interactions. Comparison of experiment and excluded volume theory, *J. Biol. Chem. 258*, 5710-5715.
31. Stagg, L., Zhang, S.-Q., Cheung, M. S., and Wittung-Stafshede, P. (2007) Molecular crowding enhances native structure and stability of α/β protein flavodoxin, *Proc. Natl. Acad. Sci. USA 104*, 18976-18981.
32. Waegele, M. M., and Gai, F. (2011) Power-law dependence of the melting temperature of ubiquitin on the volume fraction of macromolecular crowders *J. Chem. Phys. 134*, 095104.
33. Sotomayor-Pérez, A.-C., Subrini, O., Hessel, A., Ladant, D., and Chenal, A. (2013) Molecular Crowding Stabilizes Both the Intrinsically Disordered Calcium-Free State and the Folded Calcium-Bound State of a Repeat in Toxin (RTX) Protein, *J. Am. Chem. Soc. 135*, 11929-11934.
34. Perham, M., Stagg, L., and Wittung-Stafshede, P. (2007) Macromolecular crowding increases structural content of folded proteins, *FEBS Lett. 581*, 5065-5069.
35. Minton, A. P. (2005) Models for Excluded Volume Interaction between an Unfolded Protein and Rigid Macromolecular Cosolutes: Macromolecular Crowding and Protein Stability Revisited, *Biophys. J. 88*, 971-985.
36. Kuznetsova, I. M., Zaslavsky, B. Y., Breydo, L., Turoverov, K. K., and Uversky, V. N. (2015) Beyond the excluded volume effects: mechanistic complexity of the crowded milieu, *Molecules 20*, 1377-1409.

37. Gnutt, D., Gao, M., Brylski, O., Heyden, M., and Ebbinghaus, S. (2015) Excluded-Volume Effects in Living Cells, *Angewandte Chemie International Edition 54*, 2548-2551.
38. Courtenay, E. S., Capp, M. W., Anderson, C. F., and Record, M. T. (2000) Vapor pressure osmometry studies of osmolyte-protein interactions: Implications for the action of osmoprotectants in vivo and for the interpretation of "osmotic stress" experiments in vitro, *Biochemistry 39*, 4455-4471.
39. Diehl, R. C., Guinn, E. J., Capp, M. W., Tsodikov, O. V., and Record, M. T. (2013) Quantifying Additive Interactions of the Osmolyte Proline with Individual Functional Groups of Proteins: Comparisons with Urea and Glycine Betaine, Interpretation of m-Values, *Biochemistry 52*, 5997-6010.
40. Knowles, D. B., LaCroix, A. S., Deines, N. F., Shkel, I., and Record, J., M.T. (2011) Separation of preferential interaction and excluded volume effects on DNA duplex and hairpin stability *Proc. Natl. Acad. Sci. USA 108*, 12699-12704.
41. Kundu, J., Kar, U., Gautam, S., Karmakar, S., and Chowdhury, P. K. (2015) Unusual effects of crowders on heme retention in myoglobin, *FEBS Letters 589*, 3807-3815.
42. Mukherjee, S. K., Gautam, S., Biswas, S., Kundu, J., and Chowdhury, P. K. (2015) Do macromolecular crowding agents exert only an excluded volume effect? A protein solvation study, *The Journal of Physical Chemistry B 119*, 14145-14156.
43. Jamal, S., Poddar, N. K., Singh, L. R., Dar, T. A., Rishi, V., and Ahmad, F. (2009) Relationship between functional activity and protein stability in the presence of all classes of stabilizing osmolytes, *The FEBS journal 276*, 6024-6032.
44. Stambolic, V., and Woodgett, J. R. (1994) Mitogen inactivation of glycogen synthase kinase-3β in intact cells via serine 9 phosphorylation, *Biochemical Journal 303*, 701-704.
45. Shiraki, K., Kudou, M., Fujiwara, S., Imanaka, T., and Takagi, M. (2002) Biophysical effect of amino acids on the prevention of protein aggregation, *Journal of biochemistry 132*, 591-595.
46. Zhou, R., Huang, X., Margulis, C. J., and Berne, B. J. (2004) Hydrophobic Collapse in Multidomain Protein Folding, *Science 305*, 1605.
47. Cheung, M. S., García, A. E., and Onuchic, J. N. (2002) Protein folding mediated by solvation: water expulsion and formation of the hydrophobic core occur after the structural collapse, *Proceedings of the National Academy of Sciences 99*, 685-690.
48. Chandler, D. (2005) Interfaces and the driving force of hydrophobic assembly, *Nature 437*, 640-647.
49. Estell, D. A., Graycar, T. P., Miller, J. V., Powers, D. B., Wells, J. A., Burnier, J. P., and Ng, P. G. (1986) Probing Steric and Hydrophobic Effects on Enzyme-Substrate Interactions by Protein Engineering, *Science 233*, 659.
50. Breydo, L., Sales, A. E., Frege, T., Howell, M. C., Zaslavsky, B. Y., and Uversky, V. N. (2015) Effects of Polymer Hydrophobicity on Protein Structure and Aggregation Kinetics in Crowded Milieu, *Biochemistry 54*, 2957-2966.
51. Rossky, P. J. (2008) Protein denaturation by urea: Slash and bond, *Proc. Nat. Acad. Sci. 105*, 16825-16826.
52. Tanford, C. (1970) Protein Denaturation: Part C. Theoretical Models for The Mechanism of Denaturation, *Adv. Protein Chem. 24*, 1-95.
53. Schellman, J. A. (2002) Fifty years of solvent denaturation, *Biophys. Chem. 96*, 91.
54. Frank, H. S., and F., F. (1968) Structural Approach to the Solvent Power of Water for Hydrocarbons; Urea as a Structure Breaker, *J. Chem. Phys. 48*, 4746-4757.
55. Mountain, R. D., and Thirumalai, D. (2004) Alterations in Water Structure Induced by Guanidinium and Sodium Ions, *J. Phys. Chem. B 108*, 19711–19716.

56. Mason, P. E., Neilson, G. W., Enderby, J. E., Saboungi, M.-L., Dempsey, C. E., MacKerell, J., A.D. , and Brady, J. W. (2004) The Structure of Aqueous Guanidinium Chloride Solutions, *J. Am. Chem. Soc. 126*, 11462-11470.
57. Scott , J. N., Nucci, N. V., and Vanderkooi, J. M. (2008) Changes in Water Structure Induced by the Guanidinium Cation and Implications for Protein Denaturation, *J. Phys. Chem. A 112*, 10939-10948.
58. Wernersson, E., Heyda, J., Vazdar, M., Lund, M., Mason, P. E., and Jungwirth, P. (2011) Orientational Dependence of the Affinity of Guanidinium Ions to the Water Surface, *J. Phys. Chem. B 115*, 12521-12526.
59. Walrafen, G. E. (1966) Raman Spectral Studies of the Effects of Urea and Sucrose on Water Structure, *J. Chem. Phys. 44*, 3726-3727.
60. Finer, E. G., Franks, F., and Tait, M. J. (1972) Nuclear magnetic resonance studies of aqueous urea solutions, *J. Am. Chem. Soc. 94*, 4424-4429.
61. Idrissi, A., Cinar, E., Longelin, S., and Damay, P. (2004) The effect of temperature on urea-urea interactions in water: a molecular dynamics simulation, *J. Mol. Liq. 110*, 201-208.
62. Idrissi, A., Gerard, M., Damay, P., Kiselev, M., and Puhovsky, Y. (2010) The Effect of Urea on the Structure of Water: A Molecular Dynamics Simulation, *J. Phys. Chem. B 114*, 4731-4738.
63. Herskovits, T. T., and Kelly, T. M. (1973) Viscosity studies of aqueous solutions of alcohols, ureas, and amides, *J. Phys. Chem. 77*, 381-388.
64. Sacco, A., and Holz, M. (1997) NMR studies on hydrophobic interactions in solution Part 2.-Temperature and urea effect on the self-association of ethanol in water *J. Chem. Soc., Faraday Trans. 93*, 1101-1104.
65. Das, A., and Mukhopadhyay, C. (2009) Urea-Mediated Protein Denaturation: A Consensus View, *J. Phys. Chem. B 113*, 12816-12824.
66. Rezus, Y. L. A., and Bakker, H. J. (2006) Effect of urea on the structural dynamics of water, *Proc. Natl. Acad. Sci. USA 103*, 18417-18420.
67. Shimizu, A., Fumino, K., Yukiyasu, K., and Taniguchi, Y. (2000) NMR studies on dynamic behavior of water molecule in aqueous denaturant solutions at 25 °C: Effects of guanidine hydrochloride, urea and alkylated ureas, *J. Mol. Liq. 85*, 269-278.
68. Hua, L., Zhou, R., Thirumalai, D., and Berne, B. J. (2008) Urea denaturation by stronger dispersion interactions with proteins than water implies a 2-stage unfolding, *Proc. Nat. Acad. Sci. 105*, 16928-16933.
69. O'Brien, E. P., Dima, R. I., Brooks, B., and Thirumalai, D. (2007) Interactions between Hydrophobic and Ionic Solutes in Aqueous Guanidinium Chloride and Urea Solutions: Lessons for Protein Denaturation Mechanism, *Journal of the American Chemical Society 129*, 7346-7353.
70. Godawat, R., Jamadagni, S. N., and Garde, S. (2010) Unfolding of Hydrophobic Polymers in Guanidinium Chloride Solutions, *The Journal of Physical Chemistry B 114*, 2246-2254.
71. Graziano, G. (2011) Contrasting the denaturing effect of guanidinium chloride with the stabilizing effect of guanidinium sulfate, *Physical Chemistry Chemical Physics 13*, 12008-12014.
72. TRAKSITION, T. R., and VON HIPPEL, P. H. (1965) On the conformational stability of globular proteins, *The Journal of Biological Chemistry 240*, 3909-3923.
73. Shah, D., and Shaikh, A. R. (2016) Interaction of arginine, lysine, and guanidine with surface residues of lysozyme: implication to protein stability, *Journal of Biomolecular Structure and Dynamics 34*, 104-114.

74. Laurent, T. C. (1971) Enzyme reactions in polymer media, *European Journal of Biochemistry 21*, 498-506.
75. Totani, K., Ihara, Y., Matsuo, I., and Ito, Y. (2008) Effects of Macromolecular Crowding on Glycoprotein Processing Enzymes, *Journal of the American Chemical Society 130*, 2101-2107.
76. Attri, P., Venkatesu, P., and Lee, M.-J. (2010) Influence of Osmolytes and Denaturants on the Structure and Enzyme Activity of α-Chymotrypsin, *The Journal of Physical Chemistry B 114*, 1471-1478.
77. Shahid, S., Ahmad, F., Hassan, M. I., and Islam, A. (2015) Relationship between protein stability and functional activity in the presence of macromolecular crowding agents alone and in mixture: An insight into stability-activity trade-off, *Archives of biochemistry and biophysics 584*, 42-50.
78. Stojanovski, B. M., Breydo, L., Uversky, V. N., and Ferreira, G. C. (2016) Macromolecular crowders and osmolytes modulate the structural and catalytic properties of alkaline molten globular 5-aminolevulinate synthase, *RSC Advances 6*, 114541-114552.
79. Pancera, S., Petri, D., and Itri, R. (2004) The effect of poly (ethylene glycol) on the activity, structural conformation and stability of yeast hexokinase, *Surface and Colloid Science*, 301-334.
80. Pancera, S. M., da Silva, L. H., Loh, W., Itri, R., Pessoa, A., and Petri, D. F. (2002) The effect of poly (ethylene glycol) on the activity and structure of glucose-6-phosphate dehydrogenase in solution, *Colloids and Surfaces B: Biointerfaces 26*, 291-300.
81. Lakowicz, J. R. (2006) *Principles of fluorescence spectroscopy*, 3rd ed., Kluwer Academic/Plenum, New York.
82. O'Connor, D. (2012) *Time-correlated single photon counting*, Academic Press.
83. Amiri, M., Jankeje, K., and Albani, J. R. (2010) Origin of fluorescence lifetimes in human serum albumin. Studies on native and denatured protein, *Journal of fluorescence 20*, 651-656.
84. Ebbinghaus, S., Kim, S. J., Heyden, M., Yu, X., Heugen, U., Gruebele, M., Leitner, D. M., and Havenith, M. (2007) An extended dynamical hydration shell around proteins, *Proceedings of the National Academy of Sciences 104*, 20749-20752.
85. Heyden, M., Ebbinghaus, S., and Havenith, M. (2006) Terahertz Spectroscopy as a Tool to Study Hydration Dynamics, In *Encyclopedia of Analytical Chemistry*, John Wiley & Sons, Ltd.
86. Leitner, D. M., Gruebele, M., and Havenith, M. (2008) Solvation dynamics of biomolecules: modeling and terahertz experiments, *HFSP journal 2*, 314-323.
87. Penkov, N., Shvirst, N., Yashin, V., Fesenko Jr, E., and Fesenko, E. (2015) Terahertz spectroscopy applied for investigation of water structure, *The Journal of Physical Chemistry B 119*, 12664-12670.
88. Hunger, J., Bernecker, A., Bakker, H. J., Bonn, M., and Richter, R. P. (2012) Hydration dynamics of hyaluronan and dextran, *Biophysical journal 103*, L10-L12.
89. Bye, J. W., Meliga, S., Ferachou, D., Cinque, G., Zeitler, J. A., and Falconer, R. J. (2013) Analysis of the hydration water around bovine serum albumin using terahertz coherent synchrotron radiation, *The Journal of Physical Chemistry A 118*, 83-88.
90. Polley, D., Patra, A., and Mitra, R. K. (2013) Dielectric relaxation of the extended hydration sheathe of DNA in the THz frequency region, *Chem. Phys. Lett. 586*, 143-147.

91. Ebbinghaus, S., Kim, S. J., Heyden, M., Yu, X., Heugen, U., Gruebele, M., Leitner, D. M., and Havenith, M. (2007) An extended dynamical hydration shell around proteins., *Proc. Natl. Acad.Sci.USA 104*, 20749-20752.
92. Beard, M. C., Turner, G. M., and Schmuttenmaer, C. A. (2002) Terahertz Spectroscopy, *J. Phys. Chem. B 106*, 7146-7159.
93. Elton, D. C. (2017) The origin of the Debye relaxation in liquid water and fitting the high frequency excess response, *Physical Chemistry Chemical Physics*.
94. Kindt, J. T., and Schmuttenmaer, C. A. (1996) Far-infrared dielectric properties of polar liquids probed by femtosecond terahertz pulse spectroscopy, *J. Phys. Chem. 100*, 10373-10379.
95. Walrafen, G. E., Chu, Y. C., and Piermarini, G. J. (1996) Low-Frequency Raman Scattering from Water at High Pressures and High Temperatures, *J. Phys. Chem. 100* 10363-10372.
96. Vij, J. K., Simpson, D. R. J., and Panarina, O. E. (2004) Far infrared spectroscopy of water at different temperatures: GHz to THz dielectric spectroscopy of water *J. Mol. Liq. 112*, 125-135.
97. Samanta, N., Mahanta, D. D., Hazra, S., Kumar, G. S., and Mitra, R. K. (2014) Short chain polyethylene glycols unusually assist thermal unfolding of human serum albumin, *Biochimie 104*, 81-89.
98. Samanta, N., Luong, T. Q., Mahanta, D. D., Mitra, R. K., and Havenith, M. (2016) The Effect of Short Chain Polyethyleneglycols on the Hydration Structure and Dynamics around Human Serum Albumin, *Langmuir 32*, 831-837.
99. Samanta, N., Mahanta, D. D., and Mitra, R. K. (2014) Does Urea Alter the Collective Hydrogen Bond Dynamics in Water: A Dielectric Relaxation Study in the THz Frequency Region, *Chemistry - An Asian Journal 9*, 3457-3463.
100. Samanta, N., Mahanta, D. D., and Mitra, R. K. (2014) Collective Hydration Dynamics of Guanidinium Chloride Solutions and its Possible Role in Protein Denaturation: A Terahertz Spectroscopic Study, *Physical Chemistry Chemical Physics 16*, 23308-23315.
101. Samanta, N., Mahanta, D. D., Choudhury, S., Barman, A., and Mitra, R. K. (2017) Collective hydration dynamics in some amino acid solutions: A combined GHz-THz spectroscopic study, *The Journal of Chemical Physics 146*, 125101-125108.

Chapter 2

2. Basic Theories & Experimental Methods

This section provides some relevant theories, information and experimental methods applied for the chapters 4, 5 and 6. This section also introduces the chemicals used in this thesis work.

2.1. Basic Theories

2.1.1. Noncovalent Interactions and the Energies

Noncovalent interactions are weaker than covalent bonds but have a great role to control the structure of all biomolecules. The energy required to break noncovalent interactions is only 4–20 kJ/mol, much lesser than those of covalent bonds (~110-700 kJ/mol). Hence noncovalent bonds form and break at room temperature as the thermal energy is 2.5 kJ/mol at 298 K.[1] Although these interactions are individually weak and have a transient existence at physiological temperature (25–37 ºC) multiple noncovalent interactions can act collectively to produce highly stable and specific associations between different parts of a large molecule or between different macromolecules.

Table 2.1: Noncovalent and covalent bond distances and bond energies[1, 2]

Interaction	Distance (Å)	Energy (kJ/mol)
Thermal energy at 298 K		~ 2.5
Van der Waals	~ 3.5	~ 2.0-4.0
Electrostatic	variable	~ 6.0
Hydrogen bond	2.8-3.0	~ 4.0-13.0
Covalent bond	0.9-1.5	~ 110-700

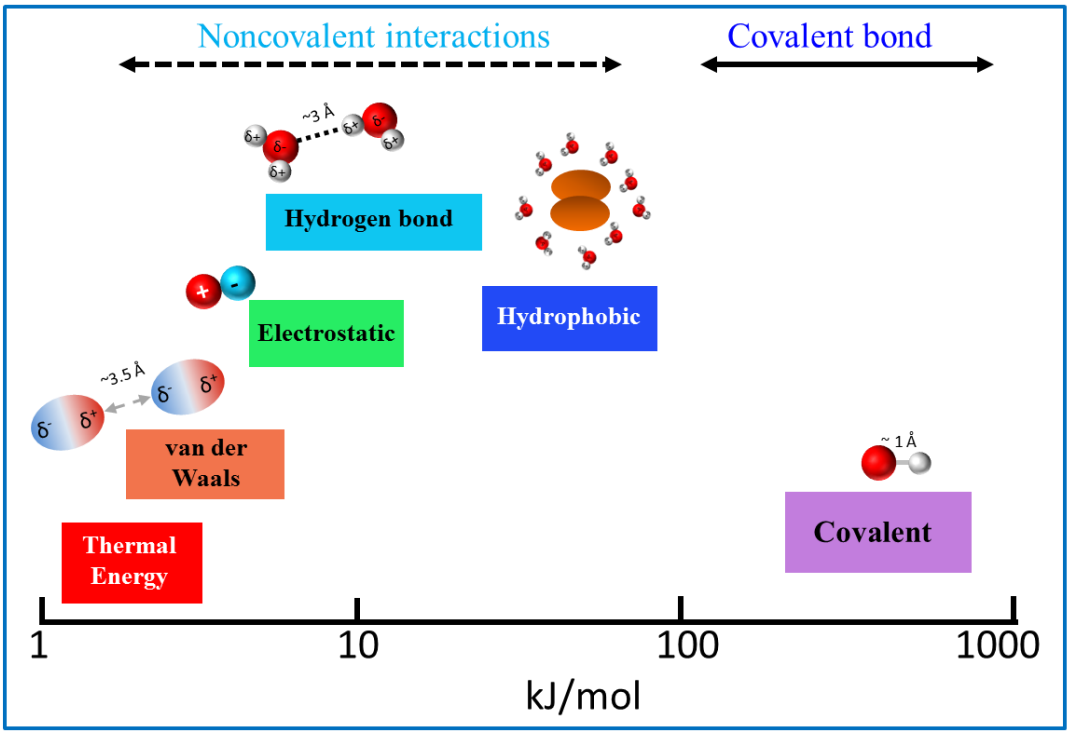

Scheme 2.1: Relative energies of noncovalent interactions and covalent bond. (Drawn using the data given in the table 2.1).

2.1.2. Cooperativity in Hydrogen Bond Networks

The term *cooperativity* is often used for hydrogen bonded networks which means that each H-bond assists its neighbouring H-bond to get stronger.[3] All the H-bonds are affected by the presence of each other: if one is removed the entire network could get weaker; add one and the whole system could get stronger.

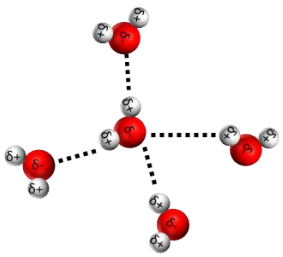

Scheme 2.2: Hydrogen bonding in water

2.1.3. Protein Structure

Proteins are built of *amino acids* (H_2N-HCR-COOH). Nature has selected only L-amino acids to constitute all proteins. There are four levels of protein structure **— i) Primary structure**: Series of amino acids linked one after another by peptide bonds to polypeptide chain**. ii)**

Secondary structure: Polypeptide chains fold into α-helix, β-sheet, turns and coil by hydrogen bonding. **iii) Tertiary structure**: Water soluble proteins further fold into compact structure by hydrogen bonding, van der Waals interaction, electrostatic interaction and

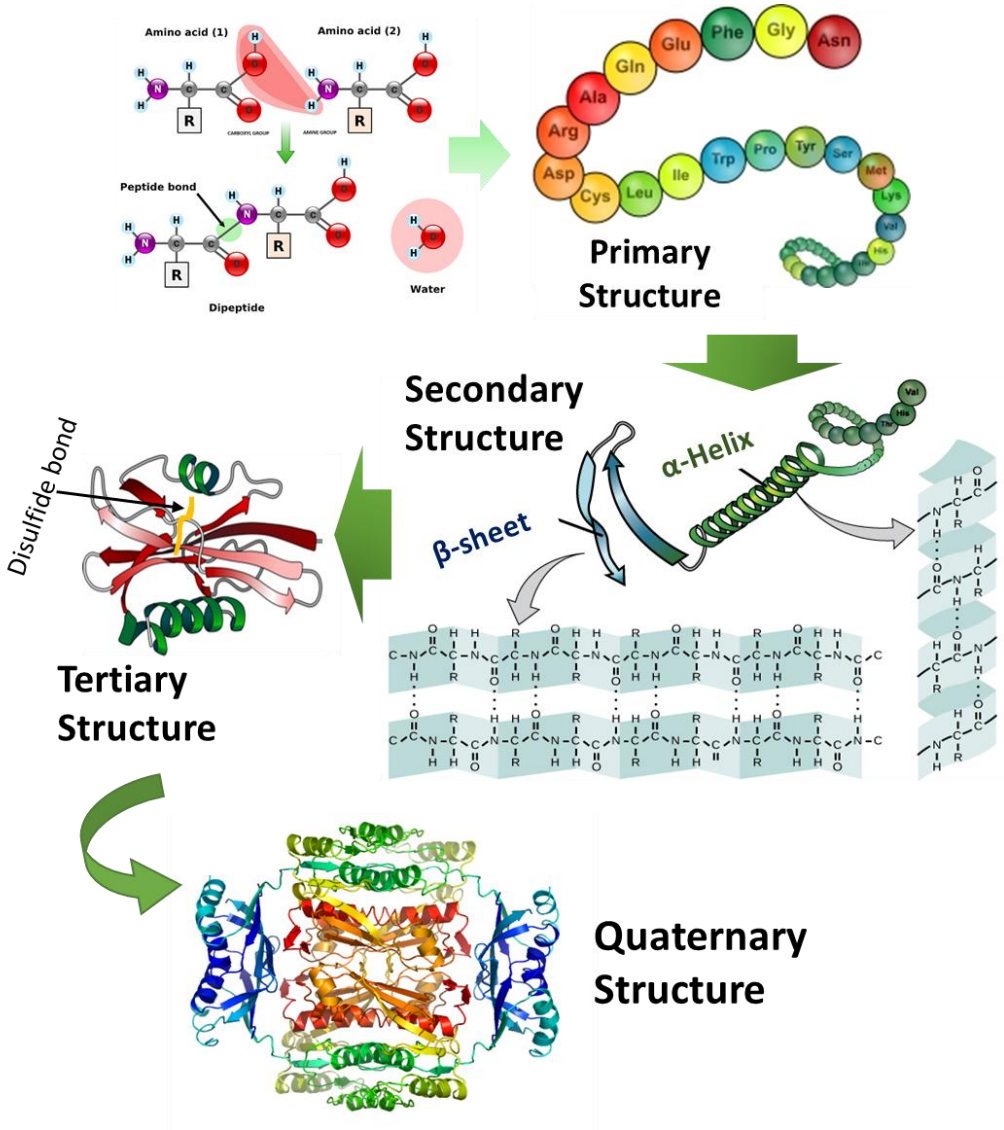

Scheme 2.3: Four levels of protein structure — primary, secondary, tertiary and quaternary structure. (Modified from the source file: *https://en.wikipedia.org/wiki/File:Main_protein_structure_levels_en.svg*).

di-sulphide bridges (covalent bonds formed between cysteine residues in different parts of the protein). **iv) Quaternary structure:** Sometimes folded polypeptide chains assemble into multisubunit structures.

2.1.4. Excluded Volume Effect

The concept of '*excluded volume'* was introduced by Werner Kuhn in 1934 and was applied to polymer molecules shortly thereafter by Paul Flory. In liquid state theory, the '*excluded volume*' of a molecule is the volume that is inaccessible to other molecules in the system as a result of the presence of the first molecule. This model is based on hard-core repulsion assuming that no solute penetrates each other. Following is a schematic to elucidate the excluded volume principle.

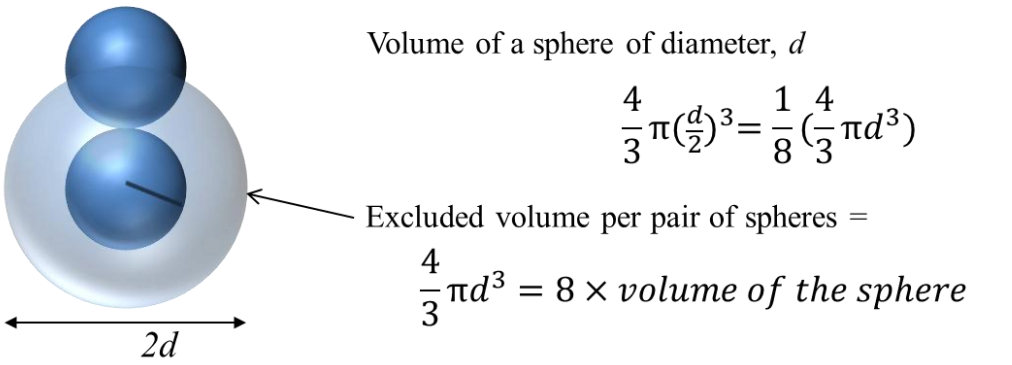

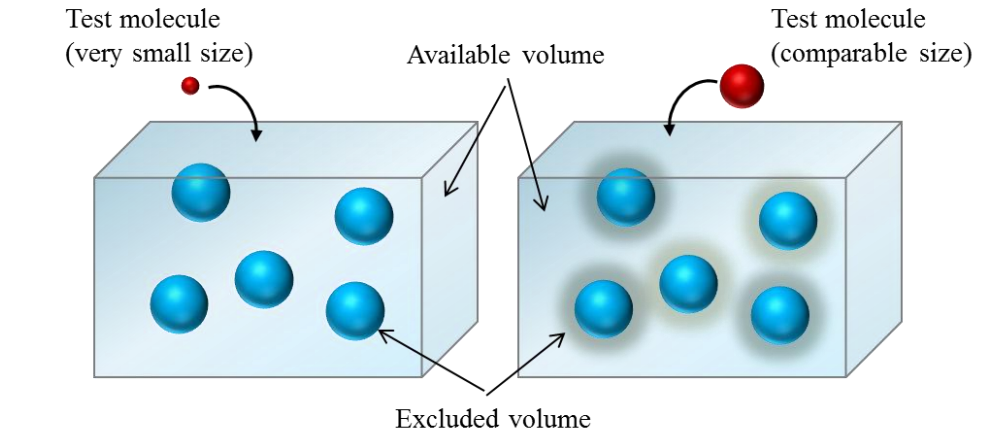

Scheme: 2.4: Representation of excluded volume assuming hard sphere.

This excluded volume theory is applied for a globular protein in presence of macromolecular crowding agents.

2.1.5. Electromagnetic Spectrum

The full electromagnetic spectrum is as follows:

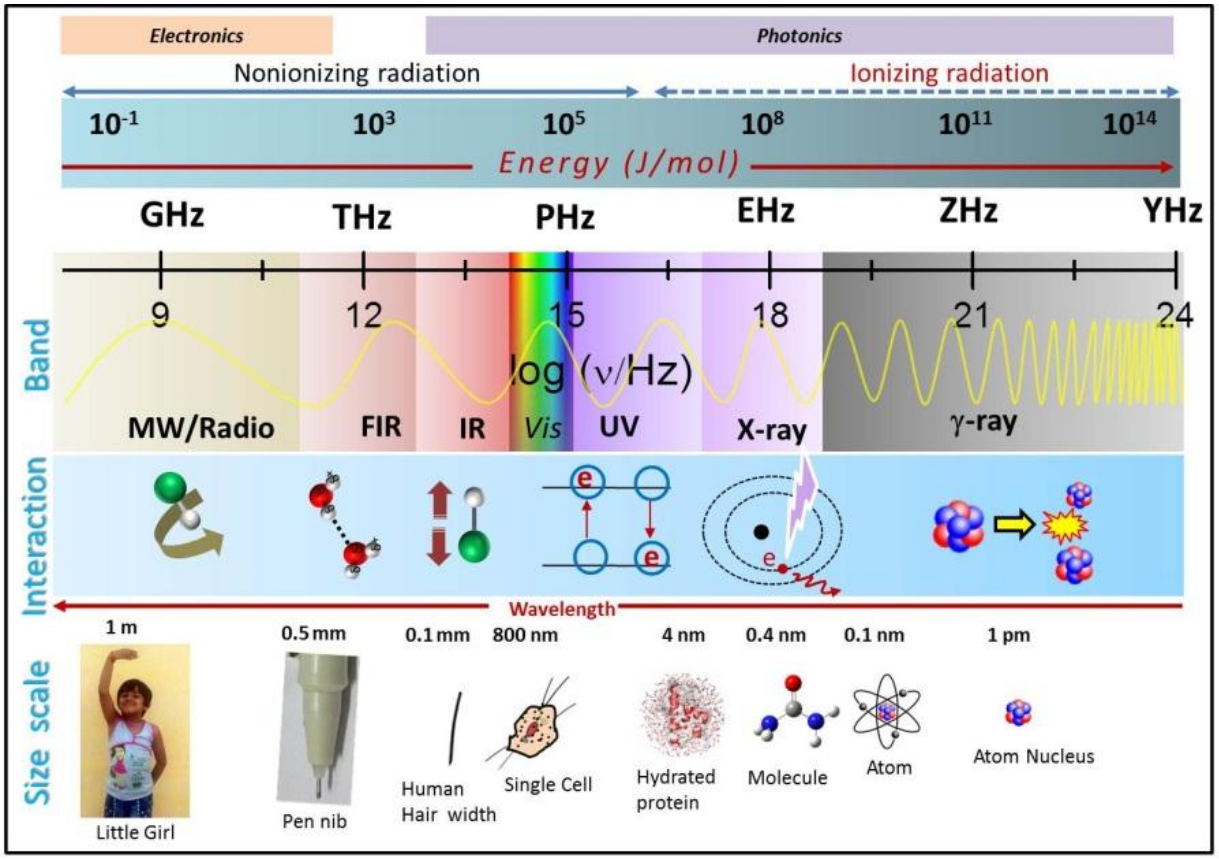

Scheme 2.5: Electromagnetic spectrum from low (left) to high (right) frequency (Gigahertz, Terahertz, Petahertz, Exahertz, Zettahertz and Yottahertz) and corresponding energy, wavelength, matter-wave interaction, comparable size scale.

In this thesis work we are concerned in GHz (dielectric relaxation study), THz (study of the collective hydrogen bond dynamics of water), IR (covalent bond vibration) and PHz (study of the absorption, fluorescence emission corresponding to electronic transitions) regimes.

2.1.6 Dielectric Relaxation: Origin of Debye Model

Dielectric relaxation measurement is a sound method to investigate intermolecular interactions and capable to monitor cooperative processes at the molecular level.[4-6] This method is more appropriate than any other to monitor such different scales of molecular motions. It is a widely used method to study the structure, dynamics, and macroscopic behaviour of complex systems.[7]

A brief discussion (detail is found elsewhere[7]) about basic principle of dielectric polarization is presented in the following section.

Dielectric Polarization in Static Electric Field:

If dielectric materials are placed in an external static electric field $\vec{E}$, there occurs a charge displacement which in turn creates a *macroscopic dipole moment* ($\vec{M}$) and this process is known as polarization ($\vec{P}$) or dipole density (scheme 2.6).

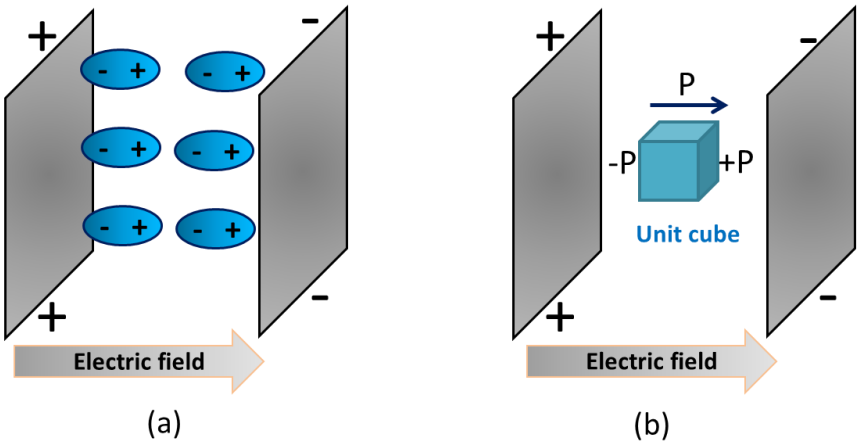

Scheme 2.6: (a) Polarization of dielectric. (b) Polarization vector.

The polarization is related to the $<\vec{M}>$ (ensemble average) and volume (V) of the sample by the following equation,

$$\vec{P} = \frac{<\vec{M}>}{V} \tag{2.1}$$

If a static electric field of strength $\vec{E}$ is applied to an isotropic and uniform dielectric material of dielectric susceptibility χ then the macroscopic polarization can be expressed as

$$\vec{P} = \varepsilon_0 \chi \vec{E} \tag{2.2}$$

where ε_0 is the dielectric permittivity of the vacuum. Applying the macroscopic Maxwell theory the electric displacement (electric induction) vector, $\vec{D}$ can be written as

$$\vec{D} = \varepsilon_0 \vec{E} + \vec{P} = \varepsilon_0 (1 + \chi) \vec{E} \tag{2.3}$$

As we know that the relative dielectric permittivity (or *dielectric constant*) as in the linear regime it is independent of the field strength, $\varepsilon = 1 + \chi$. Therefore,

$$\vec{D} = \varepsilon_0 \varepsilon \vec{E}$$

There are different types of polarization mechanisms by an applied electric field in different frequency regions (scheme 2.7): i) *Ionic polarisation*, ii) *Orientation or dipolar rotation polarisation*, iii) *Deformation (Atomic and Electronic) polarisation*.

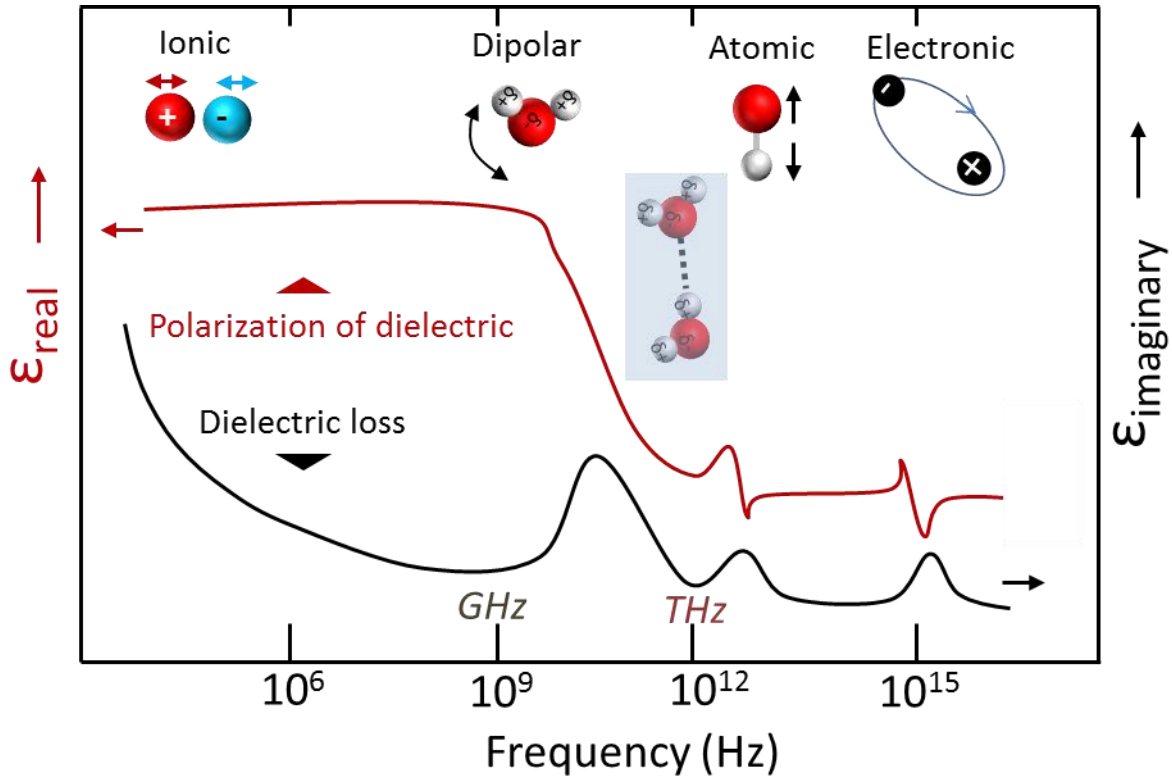

Scheme 2.7: Frequency dependent real and imaginary permittivity and corresponding processes: ionic, dipolar relaxations and atomic, electronic resonances. *[Reference: Wikipedia]*

The total polarization ($\vec{P}$) is the sum of *induced polarization* ($\vec{P}_\alpha$) and *dipole polarization* ($\vec{P}_\mu$).

Therefore, $$\vec{P}_\alpha + \vec{P}_\mu = \varepsilon_0(\varepsilon - 1)\vec{E} \qquad (2.4)$$

For *polar dielectric* the individual molecule possess a permanent dipole moment even in the absence of external electric field but for the *nonpolar* one there is no dipole moment unless an electric field is applied. Due to the long range of the dipolar forces, an accurate calculation of the interaction of a particular dipole with all other dipoles of a specimen would be very complicated. However, a good approximation can be made by considering that the dipoles beyond a certain distance can be replaced by a continuous medium having the macroscopic

dielectric properties. Assuming a continuum with dielectric constant ε_∞ in which point dipoles with a moment μ_d are embedded, we can write the induced polarization as follows,

$$\vec{P}_\alpha = \varepsilon_0(\varepsilon_\infty - 1)\vec{E} \tag{2.5}$$

The orientation polarization is given by the dipole density due to the dipoles $\vec{\mu}_d$. If we consider a sphere with volume V comprised of dipoles, we can write

$$\vec{P}_\mu = \frac{<\vec{M}_d>}{V} = \frac{\sum_i(\vec{\mu}_d)_i}{V} \tag{2.6}$$

Dielectric Polarization in Time Dependent Electric Field:

When a time dependent electric field is applied the decay function of dielectric polarization is given by,

$$\phi(t) = \frac{\vec{P}(t)}{\vec{P}(0)} \tag{2.7}$$

where $\vec{P}(t)$ is the time dependent polarization vector. Time dependent displacement vector $\vec{D}(t)$ can be written as follows,

$$\vec{D}(t) = \varepsilon_0\vec{E}(t) + \vec{P}(t) \tag{2.8}$$

$$\vec{D}(t) = \varepsilon_0\left[\varepsilon_\infty\vec{E}(t) + \int_{-\infty}^{t}\Phi(t')\vec{E}(t-t')dt'\right] \tag{2.9}$$

where $\Phi(t)$ is the dielectric response function, $\Phi(t) = (\varepsilon_s - \varepsilon_\infty)/[1-\varphi(t)]$. ε_s and ε_∞ are the dielectric permittivity at low and high frequency, respectively. The frequency dependent complex permittivity $\varepsilon^*(\omega)$ is connected to the above relaxation function through Laplace transformation,[8-10]

$$\frac{\varepsilon^*(\omega)-\varepsilon_\infty}{\varepsilon_s-\varepsilon_\infty} = \hat{L}[-\frac{d}{dt}\varphi(t)] \tag{2.10}$$

where $\hat{L}$ is the operator of the Laplace transformation, which is defined for the arbitrary time dependent function *f(t)* as

$$\hat{L}[f(t)] \equiv F(\omega) = \int_0^\infty e^{-pt}f(t)dt \tag{2.11}$$

where $p = x + i\omega$ and $x \to 0$.

Equation 2.10 gives equivalent information on dielectric relaxation properties of the sample both in frequency domain and time domain measurements. Therefore the dielectric response might be measured experimentally as a function of either frequency or time, providing data in the form of a dielectric spectrum $\varepsilon^*(\omega)$ or the macroscopic relaxation function $\varphi(t)$. For instance, when a macroscopic relaxation function obeys the simple exponential law

$$\varphi(t) = \exp(-\frac{t}{\tau_m}) \tag{2.12}$$

where τ_m indicates the relaxation time. Equation 2.11 and 2.12 give rise to the following relation

$$\frac{\varepsilon^*(\omega)-\varepsilon_\infty}{\varepsilon_s-\varepsilon_\infty} = \frac{1}{1+i\omega\tau_m} \tag{2.13}$$

$$\text{i.e, } \varepsilon^*(\omega) = \varepsilon_\infty + \frac{\varepsilon_s-\varepsilon_\infty}{1+i\omega\tau_m} \tag{2.14}$$

This is known as the Debye model for frequency dependent dielectric permittivity.

2.2. Experimental Methods

2.2.1 Analysis of Protein Structure

Protein secondary and tertiary structure can be obtained from CD spectra analysis. It is a very reliable tool to underline the protein conformational changes. When multiple chromophores in a chiral environment are in close vicinity, the excited states of the chromophores can mix resulting in an *exciton coupled circular dichroism*. This phenomenon is highly dependent on the relative orientation and proximity of the chromophores (amide bonds). The region 190-260 nm (far UV CD) and 250-310 nm (near UV CD) can sense the secondary and tertiary structure, respectively. α-helix, β-sheet, and a random coil have amide bonds in different orientations at different distances and thus give CD signals with different amplitudes of different signs as a function of wavelength. For each pure secondary conformation the distinctive CD spectrum is shown in scheme 2.8.

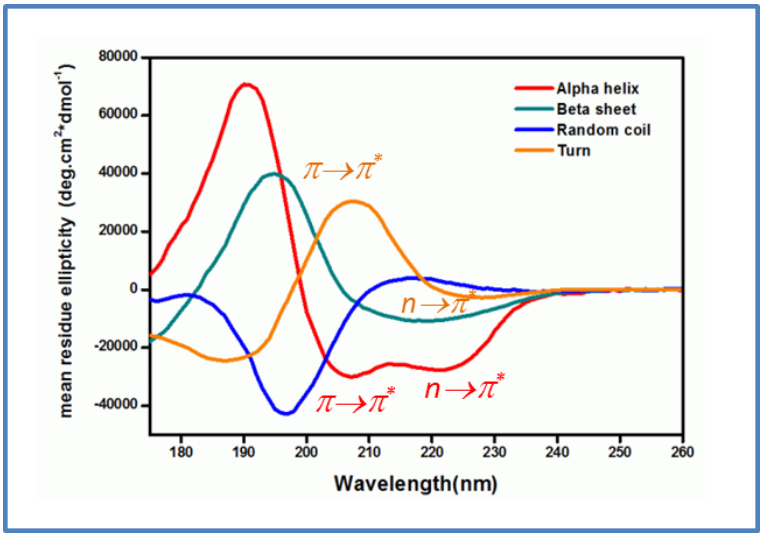

Scheme 2.8.: Typical CD spectra for each secondary structure content.[11]

The CD spectra of α-helices are characterized by a negative peak with separate maxima of comparable magnitude at 208 nm and 222 nm. The negative 222 nm band is due to the peptide n→π* transition, while the 208 nm band results from the exciton splitting of the lowest peptide π→π* transition[12, 13]. The spectrum features arising in near UV region are due to the absorption of the aromatic residues (phenylalanine, tyrosine, and tryptophan) and di sulphide bonds.

The secondary structural analysis is done by deconvoluting the CD spectra using CDNN software (http//bioinformatik.biochemtech.uni-halle.de/cdnn).

2.2.2 Thermal Stability of Protein

Thermal denaturation process of a protein can be considered as a two state transition between the native and the unfolded states,[14]

$$N(native) \rightleftarrows D(denatured)$$

The corresponding equilibrium constant for the unfolding process (K_u) can analytically be expressed as,

$$K_u = \frac{Fraction\ of\ the\ unfolded\ protein\ (f_D)}{Fraction\ of\ the\ native\ protein\ (f_N)} \qquad (2.15)$$

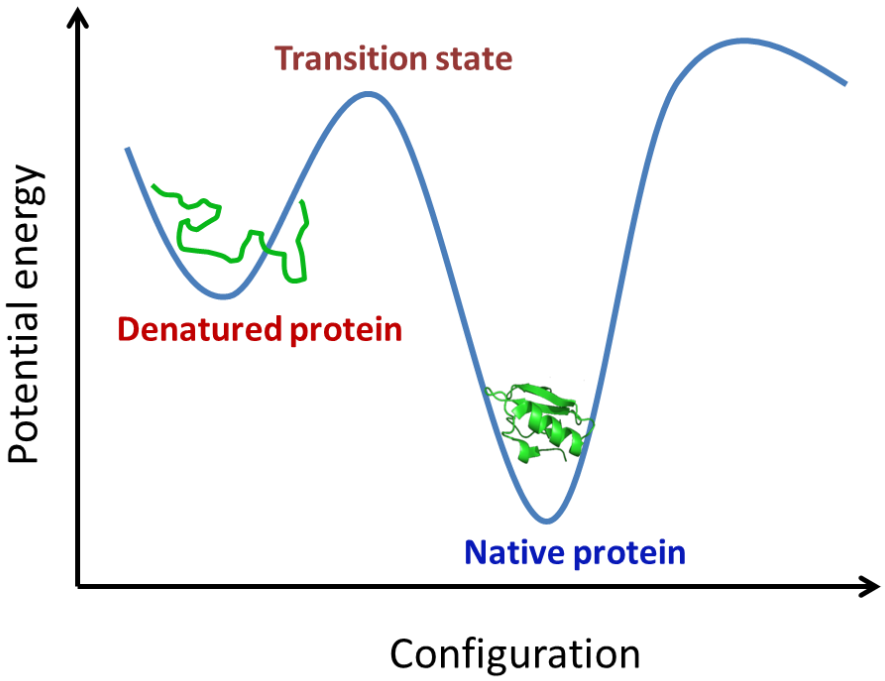

Scheme 2.9.: Representation of native and denatured state of protein in energy landscape.

The native fraction of protein can be determined by temperature dependent spectroscopic study e.g., CD, fluorescence or UV. The optical property at a particular wavelength is related to the native fraction by the following equation,

$$f_N = \frac{Y_T - Y_D}{Y_N - Y_D} \tag{2.16}$$

where Y_T, Y_N and Y_D represents the optical property at any temperature T, in the native state and in the complete denatured state, respectively. The Gibbs free energy change for the unfolding process is given by, $\Delta G_u = -RTlnK_u$, where R is the gas constant.

The van't Hoff enthalpy change (ΔH) for the process is obtained from the following equation,

$$\frac{\partial(\Delta G_u/T)}{\partial(1/T)} = \Delta H \tag{2.17}$$

The corresponding entropy change (ΔS) is obtained as,

$$\Delta G_u = \Delta H - T\Delta S \tag{2.18}$$

Van't Hoff enthalpy is often obtained from calorimetric measurement (DSC) which reckons the global unfolding of the protein.[15, 16] The area under the experimental heat

capacity (C_p) curve is used to determine the calorimetric transition enthalpy (ΔH_{cal}) given by the relation: $\Delta H_{cal} = \int C_p \, dT$. This calorimetrically determined enthalpy is model-independent and is thus unrelated to the nature of the transition. The temperature at which the excess heat capacity is maximum, defines the transition temperature (T_m). The model-dependent van't Hoff enthalpy (ΔH_{vh}) was obtained as,

$$\Delta H_{vh}(T_m) = 4RT_m^2 \frac{\Delta C_p(T_m)}{\Delta H_{cal}} \tag{2.19}$$

where $\Delta C_p(T_m)$ is the height of the heat absorption peak at the midpoint (T_m) of the transition.[17, 18] The entropy change (ΔS) for the unfolding process is obtained using the relation,

$$\Delta S = \int \frac{\Delta C_p}{T} dT. \tag{2.20}$$

Flory Exponent:

Cheung and co-workers proposed a direct relation between the size of the confinement space and the thermal stability of proteins in a crowded environment according to the relation, $\Delta T_m \approx \chi \varphi_c^{\alpha/3}$, where $\Delta T_m = T_m^{crowder} - T_m^{buffer}$, ϕ_c is the volume fraction of macromolecule or crowder, χ is a constant including dimension of the crowder and the accessible volume and α is a parameter related to the Flory exponent (ν) and is determined from the plot $\ln(\Delta T_m)$ vs. $\ln(\phi_c)$,

$$\ln \Delta T_m = \frac{\alpha}{3} \ln \varphi + \ln \chi \tag{2.21}$$

For a spherical shape ν can be calculated from α values according to the relation,[19-21]

$$\nu = \frac{1}{\alpha} + \frac{1}{3} \text{ and for slit shape } \nu = \frac{1}{\alpha}.$$

The Flory exponent is related to the behaviour of the macromolecules in a space of defined dimensions (d) according to P.J. Flory by the equation, $\upsilon = \frac{3}{d+2}$

For d=2, ν=0.75 indicates elongated coil while for d=3, ν=0.6 indicates random coil.

2.2.3. Partial Volume and Adiabatic Compressibility of a Solute

According to scaled particle theory by Prof. Reiss (*1965*), the partial molar volume V^0 of a solute can be considered as the sum of four terms,

$$V^0 = V_M + V_T + V_I + \beta_{T^0} RT \qquad (2.22)$$

where V_M is the intrinsic molar volume of the solute, V_T is the thermal volume (this corresponds to an empty domain around the solute molecule which results from the mutual thermal motions of the solute and solvent molecules), V_I is interaction volume which represents the change in the solvent volume due to hydration, $\beta_{T^0} RT$ is an ideal term where β_{T^0} is the coefficient of solvent isothermal compressibility.

Partial specific volume v^0 of a protein of molecular mass M can be considered equal to the sum of only three terms

$$v^0 = v_m + v_T + v_I = \frac{V_M}{M} + \frac{V_T}{M} + \frac{V_I}{M} \qquad (2.23)$$

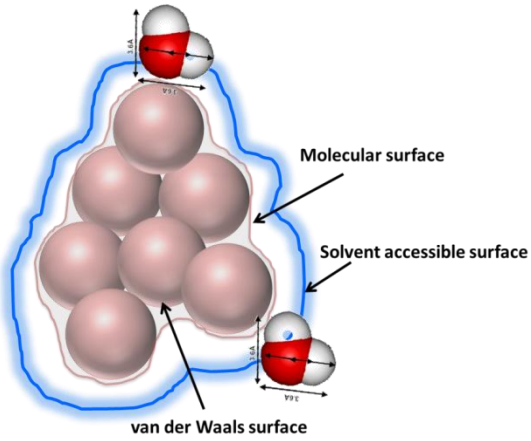

Scheme 2.10.: Molecular surface, van der Waals surface and solvent accessible surface (SASA)

$$v_I = n_h \frac{V_h^0 - V_o^0}{M} \qquad (2.24)$$

where V_h^0 is the partial molar volume of water in the hydration shell. V_o^0 is the partial molar volume of water in the bulk state. V_M is the sum of van der Waals volume of the constituent atoms and total volume of the voids inside protein molecule which result from its imperfect packing.

2.2.3.I. Apparent Specific Volume & Apparent Adiabatic Compressibility:

Adiabatic compressibility (β_p) of the protein solution can be determined by measuring the protein solution density (ρ_p) and sound velocity (u_p) and applying Laplace's equation,

$$\beta_p = \frac{1}{\rho_p u_p^2} \tag{2.25}$$

The apparent specific volume of the protein, ϕ_v is obtained by,

$$\phi_v = \frac{1}{\rho_0} + \frac{\rho_0 - \rho_p}{[P]\rho_0} \tag{2.26}$$

where $[P]$ is the concentration of the protein solution and ρ_0 and ρ_p are the densities of the solvent and protein solutions, respectively. The corresponding partial apparent adiabatic compressibility (ϕ_k) is obtained from the following relation,

$$\phi_k = \beta_0 \left(2\varphi_v - 2[u] - \frac{1}{\rho_0}\right) \tag{2.27}$$

where $[u]$ is the relative specific sound velocity increment given by, $[u] = \frac{u_p - u_0}{[P]u_0}$, with u_0 and u_p being the sound velocities in solvent and protein solutions, respectively.

2.2.4. Steady State and Time Resolved Fluorescence to Study Protein

Fluorescence spectroscopy is a very widespread method to acquire domain specific information of protein.[22] Tryptophan (Trp), tyrosine (Tyr) and phenylalanine (Phe) are the three intrinsic fluorophores present in protein.

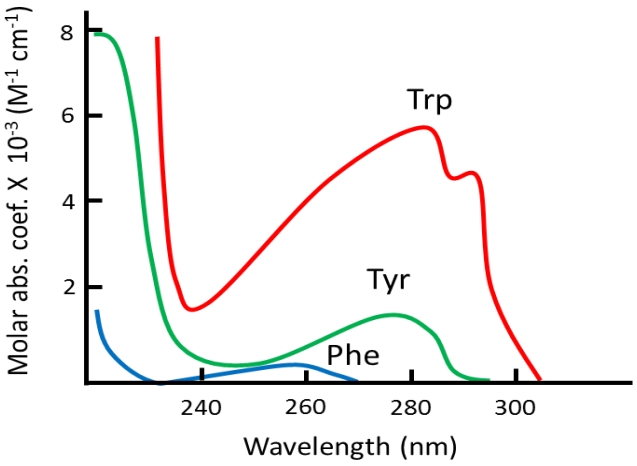

Figure 2.1: Absorption spectra of tryptophan, tyrosine and phenylalanine in water of pH 7. *[Modified from literature[22] plot.]*

Tryptophan absorbs at the longest wavelength among the three and displays the largest extinction coefficient (ε_{280}=5579 M^{-1} cm^{-1}). So the emission of proteins is mostly dominated by the Trp. At wavelengths longer than 295 nm, the absorption is mostly due to the Trp which can be selectively excited at 295–305 nm. Therefore we excited the protein at 299 nm to avoid excitation of Tyr and Phe. In our study we have chosen the Trp emission as it is highly sensitive to the local environment, while that of tyrosine is rather insensitive. Besides, the number of Trp residues in a protein are limited (e.g., HSA contains single Trp) which helps to interpret more precisely the local environment around fluorophore of a protein.

2.2.4.I. ***Steady State Fluorescence Anisotropy Measurements:***

Anisotropy is defined as the extent of polarization of the emission from a fluorophore. It is based on the principle of photo selective excitation of those fluorophore molecules whose absorption transition dipoles are parallel to the electric vector of the polarized excitation light. In an isotropic solution, fluorophores are oriented randomly. When exposed to polarized light, those fluorophores that have their absorption transition moments oriented along the electric vector of the incident light are preferentially excited. Hence the excited-state population is partially oriented. A significant fraction of the excited molecules have their transition moments oriented along the electric vector of the polarized exciting light. For the steady state anisotropy measurement emission polarization is adjusted to be parallel or perpendicular to that of the excitation and anisotropy is obtained by the following equation,

$$r = \frac{I_{\parallel} - I_{\perp}}{I_{\parallel} + 2I_{\perp}} \qquad (2.28)$$

where $I_{\parallel}$ and $I_{\perp}$ are the intensities measured with a linear polarizer for emission (the analyzer) parallel and perpendicular, respectively, to the electric vector of linearly polarized incident light.

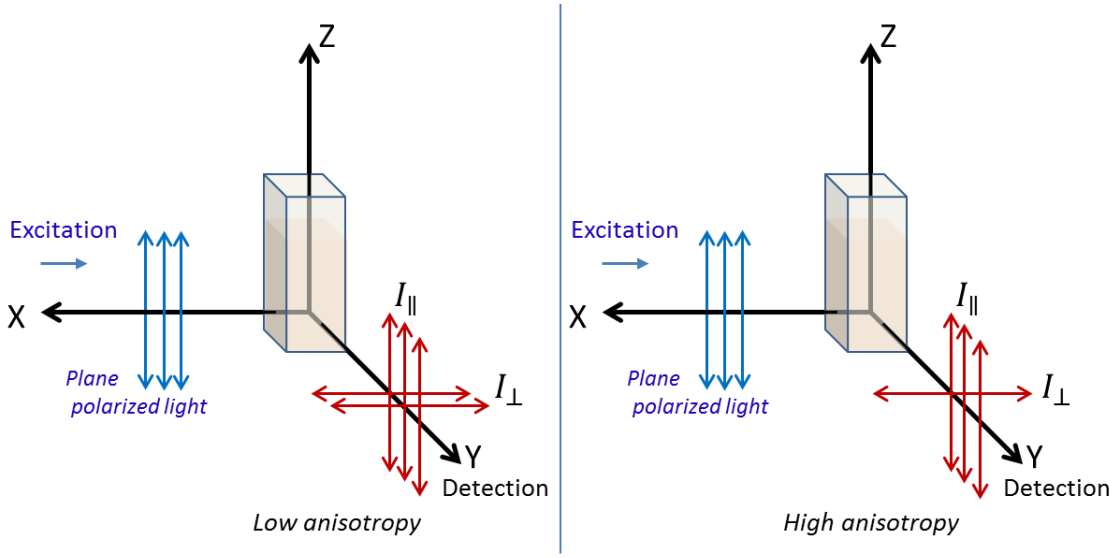

Scheme 2.11.: Representation for steady state anisotropy.

2.2.4.II. *Time Resolved Fluorescence Measurements:*

Time resolved fluorescence study measures the time the fluorophore spends in the excited state before coming back to its ground state. Lifetime measurements are advantageous in many cases over steady state measurements. For example, a protein contains two Trp residues, each with distinct lifetimes. Because of spectral overlap of their absorption and emission, it is not usually possible to resolve the emission from the two residues from the steady-state data. However, the time resolved data can reveal two decay times, which can be used to resolve the emission spectra and relative intensities of the two tryptophan residues. The time resolved measurements can reveal how each of the tryptophan residues in the protein is affected by their respective local environments.

A fluorophore is excited with a narrow pulse of light. If n_0 is the initial population of fluorophore molecules in the excited state it decays in different ways (radiative, non-radiative, intersystem crossing, photochemistry) with a rate of $k_r+k_{nr}+k_{isc}+k_{pr}$. The number of excited molecules at time t is given by,

$$-\frac{dn(t)}{dt} = (k_r + k_{nr} + k_{isc} + k_{pr})n(t) \qquad (2.29)$$

On integration,

$$n(t) = n(0)\exp(-kt) = n(0)\exp(-t/\tau) \qquad (2.30)$$

where $k = k_r + k_{nr} + k_{isc} + k_{pr}$ and the lifetime is the inverse of total decay rate, $\tau = k^{-1}$. In terms of intensity,

$$I(t) = I_0 \exp(-t/\tau) \quad (2.31)$$

This is a single exponential decay. However, most of the systems show multi-exponential decay,

$$I(t) = \sum_i a_i \exp(-t/\tau_i) \quad (2.32)$$

where $\sum_i a_i = 1$ and the average lifetime is given by the following equation,

$$\langle \tau \rangle = \sum_i a_i \tau_i \quad (2.33)$$

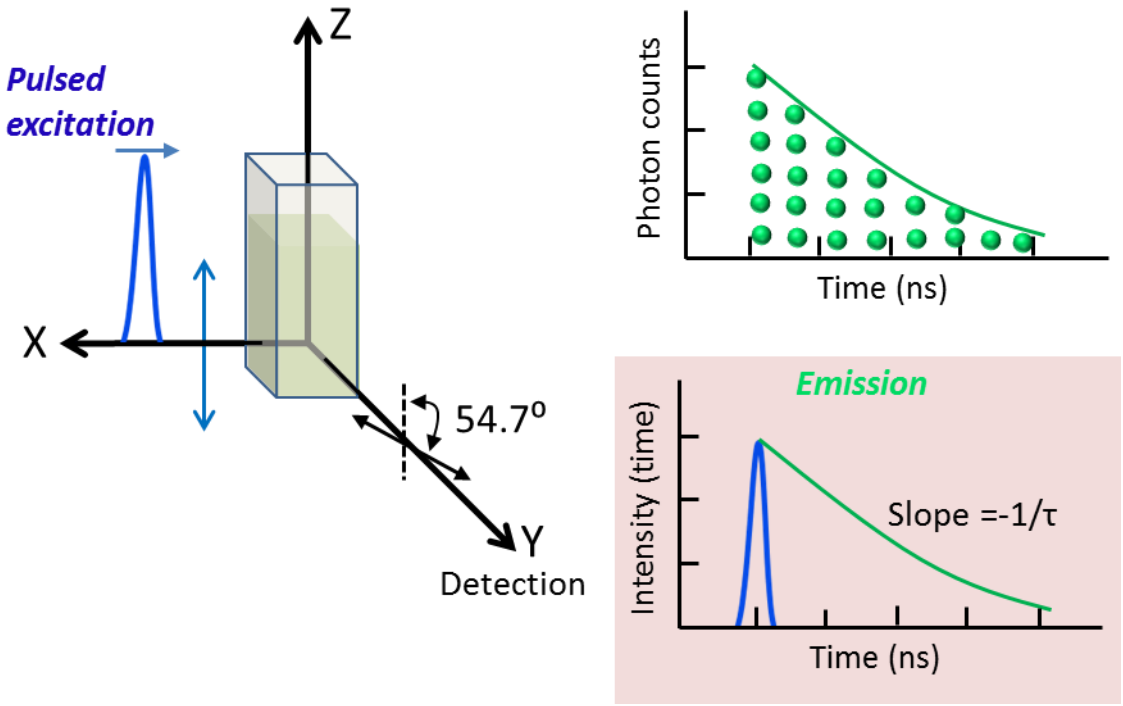

Scheme 2.12.: Time resolved fluorescence lifetime measurement by exciting with a pulsed light.

In our study we observed the lifetime of free Trp and the Trp of HSA by using 299 nm LED. The instrument response function (IRF) is measured from the Raleigh scattering (using dust in water) at the excitation wavelength (299 nm) and then the emission decay (at λ_{max}) of the sample was measured. Both the decays are fitted by reconvolution method and then the

lifetimes are obtained by fitting in multi exponential equation using F900 software (Edinburgh).[22]

2.2.6. THz Measurement

THz (1 THz = 10^{12} Hz = 1 ps^{-1}) frequency region has recently been evolved as a potential and sensitive tool to label free probe the sub-ps intermolecular collective dynamics of water network which is otherwise wiped off in conventional spectroscopic techniques.[23-25] The GHz as well as MIR frequency range are limited to the intra-molecular stretching band of water and does not protrude into the global collective motion of water which extends to more than one hydration layer[23]. Such global collective information can only be realized in the THz frequency domain.[26]

Data analysis: By varying the time delay between the probe and the pump beam (details in chapter 3) the amplitude and phase of the THz electric field are measured as a function of time. Frequency dependent power and phase of the transmitted pulse are obtained using Fourier analysis of the measured electric field amplitude $E_{THz}(t)$. In this thesis work we have used Tera K8, MenloSystems time domain THz spectroscopy where the extracted frequency domain THz spectra in air is fairly smooth with a high signal to noise ratio and minimal water absorption lines up to ~2.5 THz which enables us to extract the optical parameters with high precision up to ~2 THz. Different optical parameters are extracted from this frequency domain data.

The absorption coefficient, $$\alpha(\nu) = \frac{\ln I_0(\nu) - \ln I_S(\nu)}{d} \qquad (2.34)$$

where $I_0(\nu)$ and $I_s(\nu)$ represent the intensities in air (reference) and in presence of sample, d indicates the sample thickness.

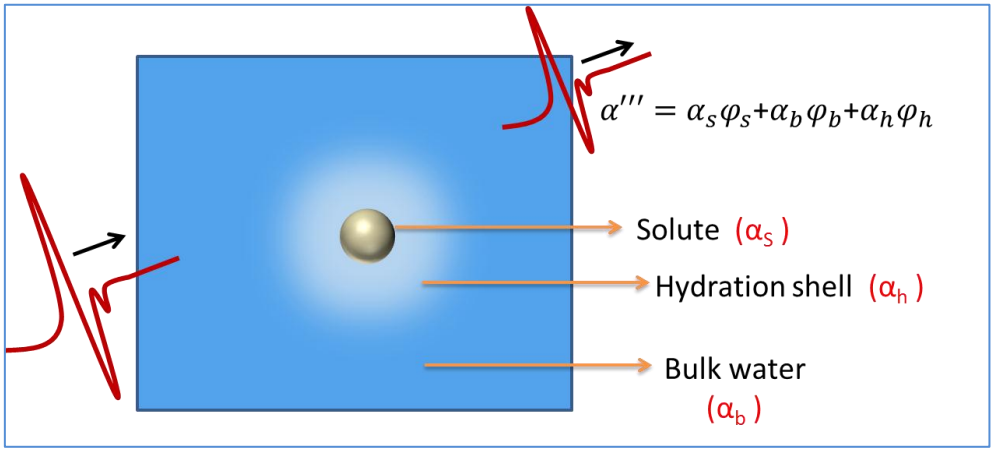

Scheme 2.13: Interpretation of THz absorption of an aqueous solution of a solute with known volume fraction (φ_s).

The refractive index can be calculated by measuring the phase in air and in sample,

$$n(\nu) = \frac{\phi_s(\nu) - \phi_0(\nu)}{2\pi\nu d} \quad (2.35)$$

The imaginary refractive index, $k(\nu) = \frac{c.\alpha(\nu)}{4\pi\nu}$ (2.36)

The frequency dependent real (ε') and imaginary (ε'') dielectric constants of the samples are extracted as, $\varepsilon'(\nu) = n^2(\nu) - k^2(\nu)$ and $\varepsilon''(\nu) = 2n(\nu)k(\nu)$, where the complex refractive index is given as, $\tilde{n}(\nu) = n(\nu) - ik(\nu)$.

We have extracted all the parameters by commercially available TeraLyzer Terahertz software (http://www.menlosystems.com/products/thz-time-domain-solutions/teralyzer-single/).

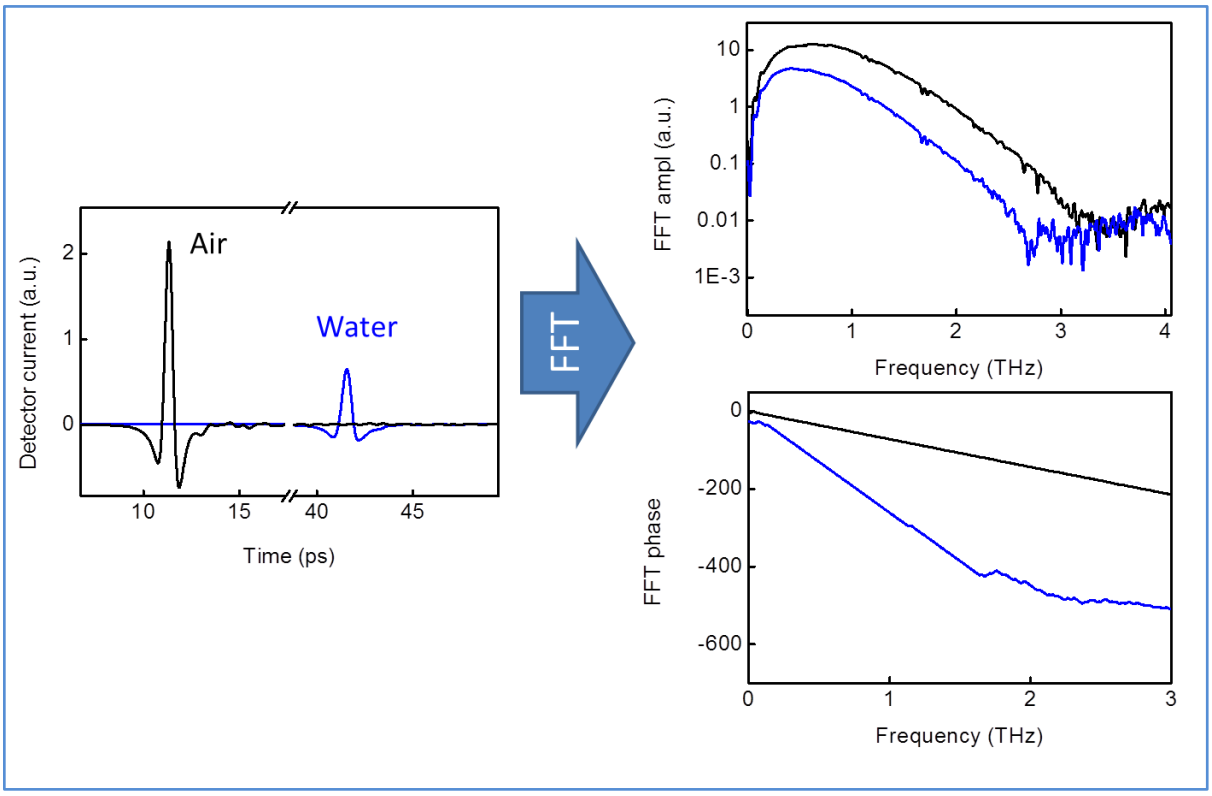

Figure 2.2: TTDS data extraction: Time domain to frequency domain conversion by Fast Fourier Transform (FFT) method using origin 8.5 software.

2.2.7. Dielectric Relaxation Fitting (GHz-THz Regime)

We have employed a multiple Debye model[25, 27, 28] to describe the dynamics of water molecules in cosolute solutions. According to the Debye model, the complex frequency dependent dielectric response [$\tilde{\varepsilon}(\nu) = \varepsilon_{real}(\nu) - i\varepsilon_{imaginary}(\nu)$] can be described as:

$$\tilde{\varepsilon}(\nu) = \varepsilon_\infty + \sum_{j=1}^{m} \frac{\varepsilon_j - \varepsilon_{j+1}}{1+i2\pi\nu\tau_j} \quad (2.37)$$

where, τ_j is the relaxation time for the *j*-th relaxation mode, ε_1 is the static dielectric constant, ε_j are the dielectric constants for different relaxation processes, ε_∞ is the extrapolated dielectric constant at a very high frequency and *m* describes the number of relaxation modes. The magnitude of induced polarization is given by the dispersion amplitude, $S_j = \varepsilon_j - \varepsilon_{j+1}$. We fit the relaxation data of water in this frequency range using three relaxation modes. Keeping in mind that a considerable fraction of water molecules in these concentrated solutions move rather slowly, we model the DR by introducing an additional Debye mode; the following equation describes the frequency-dependent complex permittivity, $\tilde{\varepsilon}(\omega)$:

$$\tilde{\varepsilon}(\omega) = \varepsilon_\infty + \frac{S_{slow}}{1+i\omega\tau_1} + \frac{S_2}{1+i\omega\tau_2} + \frac{S_3}{1+i\omega\tau_3} + \frac{S_4}{1+i\omega\tau_4} \quad (2.38)$$

where S_i is the relaxation strength of the i-th mode and ω is the angular frequency.

The following equation is to describe frequency-dependent complex permitivities $\tilde{\varepsilon}(\omega)$ in a solution containing considerable number of ions[29]

$$\tilde{\varepsilon}(\omega) = \varepsilon_\infty + \sum_{j=1}^{m} \frac{S_j}{1+i\omega\tau_j} + \frac{\sigma}{i\omega\varepsilon_0} \quad (2.39)$$

where S_j is the relaxation strength of the j-th relaxation mode, σ is the dc conductivity of the solution and ε_0 is the permittivity in free space.

2.2.8. Measurement of Enzyme Kinetics

Following is the simplest mechanism to show enzyme (*E*) kinetic reaction on a substrate (*S*) to form a product (*P*):

$$E + S \leftrightarrows ES \rightarrow ES^{\#} \longrightarrow E + P \quad (2.40)$$

where *ES* is the enzyme-substrate complex and $ES^{\#}$ is an intermediate transition state before product formation. At a fixed enzyme concentration we measured the initial rate (V_0) in presence of varying concentration of the substrate (S). Most of the enzymes follow the Michaelis-Menten equation[2],

$$V_0 = \frac{V_{max}\times[S]}{K_M+[S]} \quad (2.41)$$

where V_{max} is the maximum rate attainable at saturating substrate concentration, K_M represents Michaelis-Menten constant defined by the substrate concentration at which the rate is given by, $V_0=V_{max}/2$. The enzyme kinetic parameters are obtained by using Lineweaver-Burk (LB) plot i.e. $1/V_0$ vs. $1/[S]$ plot in the lower concentration regime of the substrate concentration,

$$\frac{1}{V_0} = \frac{1}{V_{max}} + \frac{K_M}{V_{max}}\frac{1}{[S]} \quad (2.42)$$

$$k_{cat} = \frac{V_{max}}{[E]} \quad (2.43)$$

Catalytic constant, k_{cat} represents the turn over number which can be defined as the number of substrate molecules converted to the product per unit time when the enzyme is fully saturated with the substrate. The enzyme catalytic efficiency is given by the ratio k_{cat}/K_M.

2.3. Chemicals Used

2.3.I. Protein, Enzyme and Bacteria Cell:

Human serum albumin (HSA) is a principal extracellular globular protein abundantly present in blood plasma[30] consisting of three structurally similar domains (I, II, and III), each containing two sub-domains (A and B) and stabilized by 17 disulfide bridges[31]. It contains 585 amino acids. The molecular weight of HSA is 66.5 kDa and the molar extinction coefficient (ε) at 280 nm is 36500 $cm^{-1}M^{-1}$. The choice of this protein lies on the fact that the crystal structure of the protein is well established, and the various steps involved in its thermal denaturation have now been well understood.[32, 33] Furthermore, the protein has an intrinsic fluorophore in the form of a single tryptophan (Trp214) moiety in the IIA sub-domain which can selectively be used to extract domain specific information.

Bovine serum albumin (BSA) is an extracellular globular protein (~70 % similar to HSA) present in blood plasma of cow. It contains about 583 amino acids with 17 disulphide bridges with 1 sulfhydryl group. The molecular weight of BSA is 66.4 kDa and the molar extinction coefficient (ε) at 279 nm is 44318.9 $cm^{-1}M^{-1}$.[34, 35]

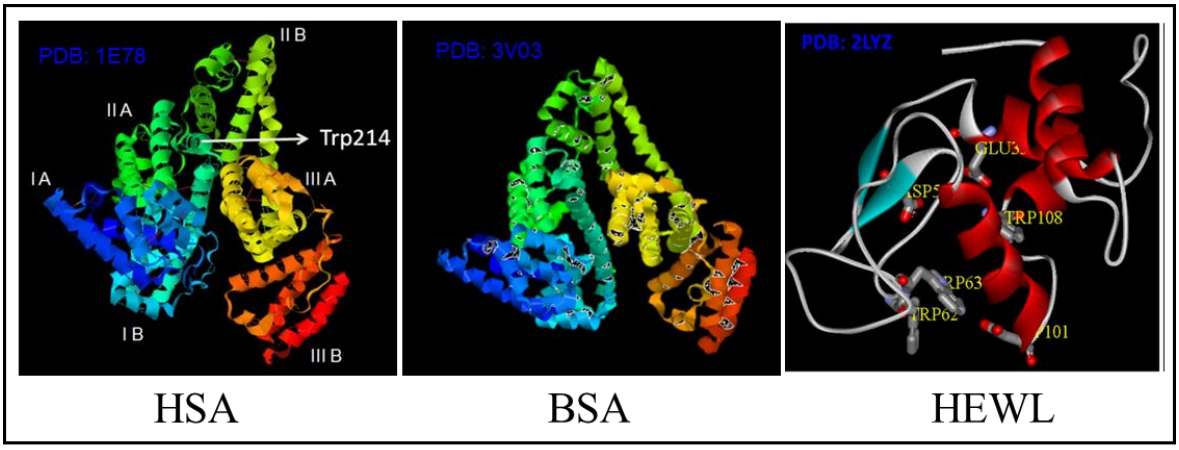

Scheme 2.14: 3D structure of the proteins (HSA, BSA and HEWL) as obtained from protein data bank. *[modified by Viewer Lite software]*.

Hen egg white lysozyme (HEWL) is a single chain polypeptide of 129 amino acids cross-linked with four disulphide bridges and the peptide chain is arranged in two equal size segments disjointed by a deep cleft.[36] The molecular weight of HEWL is 14.307 kDa[37], molar extinction coefficient[38], ε_{280nm}=36000 $M^{-1}cm^{-1}$. Substrates and inhibitors bind in this cleft and are hydrolyzed under the action of key residues Glu35 and Asp52 (Trp62, Trp63, Asp101, Trp108 are involved in substrate binding)[39] in the active site of the protein. Lysozyme catalyses the hydrolysis of β (1→4) glycosidic bond between N-acetyl glucosamine (NAG) and N-acetyl muramic acid (NAM) which form the backbone of many bacterial cell wall.[40] In the first step of mechanism lysozyme gets attached to the large surface cell wall through electrostatic interaction.[41] As the isoelectric point (pI) of lysozyme is 11.35,[42] it, as a whole, is positively charged at least upto pH 11 (as pH < pI) whereas the cell wall is negatively charged [*Ref: M. R, J. Salton, Proc. 3rd Intern. Symp. Fleming's Lysozyme, Miilan (I964), Società Prodotti Antibiotic, p. 5/RT*] even at neutral pH.

Lysozyme substrate: Micrococcus lysodeikticus cell is a gram positive, to gram variable bacterium which is found in soil, dust, water and air. It is also found is mammal skin, mouth, mucosae and upper respiratory tract. The cell wall is composed of N-acetyl glucosamine (NAG) and N-acetyl muramic acid (NAM).

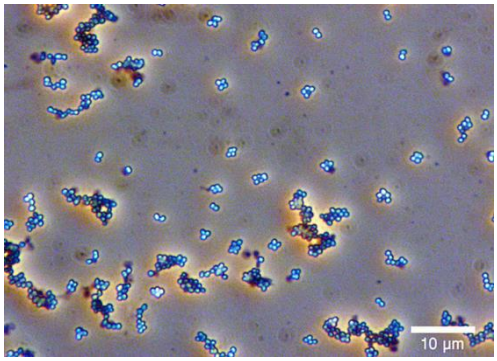

Scheme 2.15.: Micrococcus lysodeikticus bacteria gram stain. [*Source: Wikipedia*].

Following is the composition of Micrococcus lysodeikti cell wall:

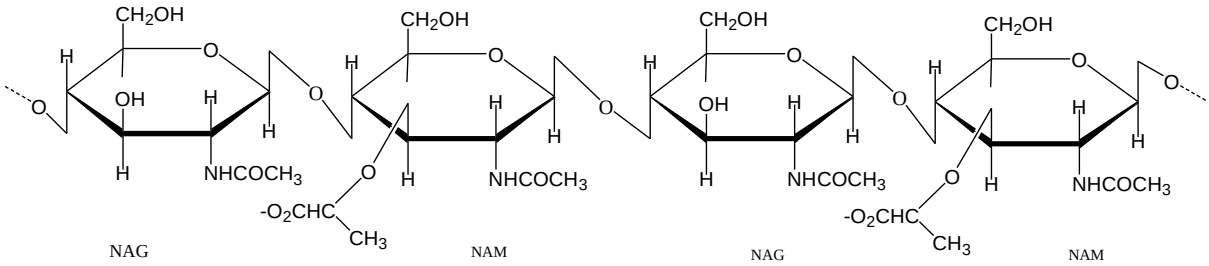

2.3.II. Macromolecular Crowding Agents:

We have used polyethylene glycols (PEGs) of different chain length. PEG is a water soluble synthetic polymer which is used as *macromolecular crowding agent*. The general chemical structure of polyethylene glycol (PEG) is as follows:

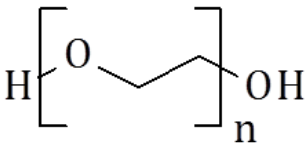

Molecular formula $C_{2n}H_{4n+2}O_{n+1}$

n-value	Name	Molecular weight (Da)
1	Ethylene glycol (EG)	62
4-5	PEG 200	194-238
8-9	PEG 400	370-414
90-91	PEG 4000	3978-4022
227-231	PEG 10000	10006-10182

2.3.III. Denaturing Agents:

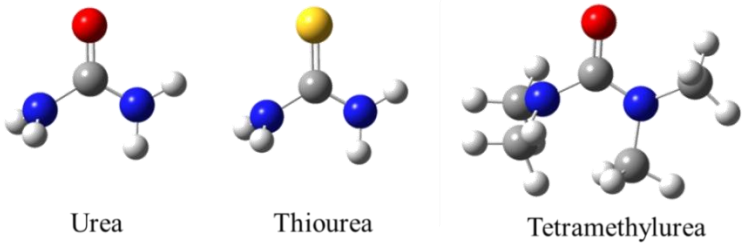

Urea Thiourea Tetramethylurea

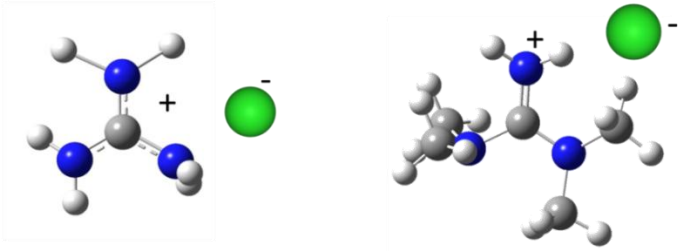

Guanidinium Chloride Tetramethylguanidinium Chloride

2.3.IV. Osmolytes:

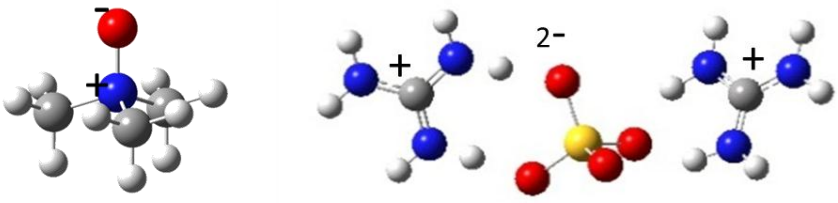

Trimethylamine N-oxide Guanidine sulfate

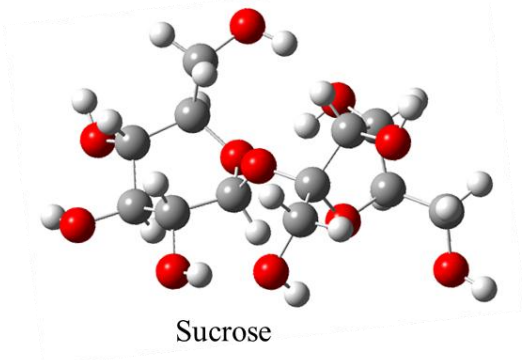

Sucrose

Amino Acids:

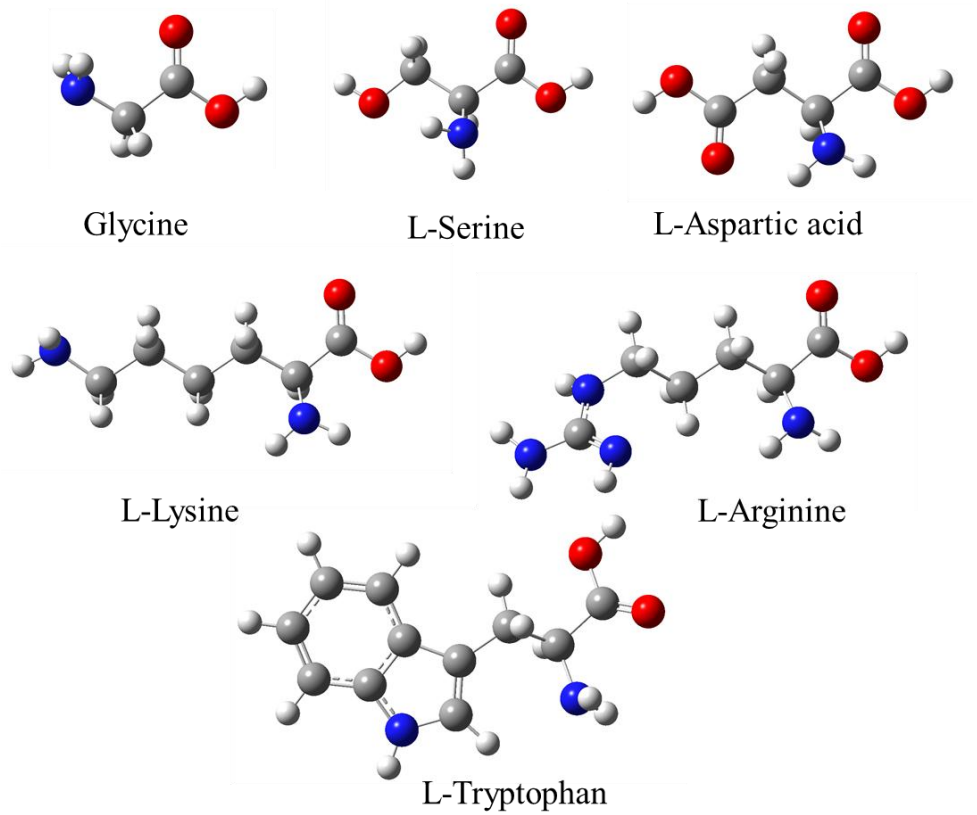

*** The previous pictures have been drawn by "Gauss View 05 software" and the symbols used are as follows:*

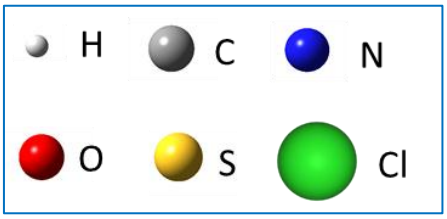

2.4. References

1. Lodish, H., Baltimore, D., Berk, A., Zipursky, S. L., Matsudaira, P., and Darnell, J. (1995) *Molecular cell biology*, Vol. 3, Scientific American Books New York.
2. Berg, J. M., Tymoczko, J. L., and Stryer, L. (2002) *Biochemistry*, W.H. Freeman & Company, New York.
3. Williamson, M. (2012) *How Proteins Work*, Garland Science, Taylor & Francis Group, LLC, USA.
4. Nee, T. W., and Zwanzig, R. (1970) Theory of dielectric relaxation in polar liquids, *The Journal of Chemical Physics 52*, 6353-6363.
5. Nandi, N., Bhattacharyya, K., and Bagchi, B. (2000) Dielectric relaxation and solvation dynamics of water in complex chemical and biological systems, *Chemical Reviews 100*, 2013-2046.
6. Agieienko, V., Horinek, D., and Buchner, R. (2017) Hydration and self-aggregation of a neutral cosolute from dielectric relaxation spectroscopy and MD simulations: the case of 1, 3-dimethylurea, *Physical Chemistry Chemical Physics 19*, 219-230.
7. Yuri Feldman, P. B. I., Alexander Puzenko, Valerică Raicu. (2015) Elementary Theory of the Interaction of Electromagnetic Fields with Dielectric Materials, Oxford University Press, Oxford.
8. Fröhlich, H. (1958) *Theory of dielectrics: dielectric constant and dielectric loss*, Clarendon Press.
9. Bötcher, C., and Bordewijk, P. (1978) Theory of Electric Polarization, vol. II, Dielectrics in Time-Dependent Fields, Elsevier Science.
10. Feldman, Y., Puzenko, A., and Ryabov, Y. (2006) Dielectic Relaxation Phenomena in Complex Materials, *Advances in chemical physics 133*, 1.
11. Rodger, A., and Ismail, M. A. (2000) In *Spectrophotometry and Spectrofluorimetry A Practical Approach* (Gore, M. G., Ed.), pp 99-139, Oxford University Press, Oxford, New York.
12. Woody, R. W., and Tinoco Jr., I. (1967) Optical Rotation of Oriented Helices. III. Calculation of the Rotatory Dispersion and Circular Dichroism of the Alpha- and 310-Helix, *J. Chem. Phys. 46*, 4927-4945.
13. Nordén, B. (1997) *Circular dichroism and linear dichroism*, Vol. 1, Oxford University Press, USA.
14. Tamura, Y., and Gekko, K. (1995) Compactness of thermally and chemically denatured ribonuclease A as revealed by volume and compressibility, *Biochemistry 34*, 1878-1884.
15. Zielenkiewicz, W., Swierzewski, R., Attanasio, F., and Rialdi, G. (2006) Thermochemical,volumetric and spectroscopic properties of lysozyme–poly(ethylene) glycolsystem, *Journal of Thermal Analysis and Calorimetry 83*, 587-595.
16. Samanta, N., Mahanta, D. D., Hazra, S., Kumar, G. S., and Mitra, R. K. (2014) Short chain polyethylene glycols unusually assist thermal unfolding of human serum albumin, *Biochimie 104*, 81-89.
17. Privalov, P. L., and Khechinashvili, N. N. (1974) A thermodynamic approach to the problem of stabilization of globular protein structure: A calorimetric study, *J. Mol. Biol. 86*, 665-684.
18. Creighton, T. E., (Ed.) (1992) *Protein Folding*, Freeman, New York.

19. Cheung, M. S., Klimov, D., and Thirumalai, D. (2005) Molecular crowding enhances native state stability and refolding rates of globular proteins, *Proc. Natl. Acad. Sci. USA 102*, 4753-4758.
20. Sotomayor-Pérez, A.-C., Subrini, O., Hessel, A., Ladant, D., and Chenal, A. (2013) Molecular Crowding Stabilizes Both the Intrinsically Disordered Calcium-Free State and the Folded Calcium-Bound State of a Repeat in Toxin (RTX) Protein, *J. Am. Chem. Soc. 135*, 11929-11934.
21. Waegele, M. M., and Gai, F. (2011) Power-law dependence of the melting temperature of ubiquitin on the volume fraction of macromolecular crowders *J. Chem. Phys. 134*, 095104.
22. Lakowicz, J. R. (2006) *Principles of Fluorescence Spectroscopy*, Springer Science & Business Media, New York, USA.
23. Heyden, M., Sun, J., Funkner, S., Mathias, G., Forbert, H., Havenith, M., and Marx, D. (2010) Dissecting the THz spectrum of liquid water from first principles via correlations in time and space *Proc. Natl. Acad.Sci.USA 107*, 12068-12073.
24. Heugen, U., Schwaab, G., Bründermann, E., Heyden, M., Yu, X., Leitner, D. M., and Havenith, M. (2006) Solute-induced retardation of water dynamics probed directly by terahertz spectroscopy, *Proc. Natl. Acad.Sci.USA 103*, 12301-12306.
25. Polley, D., Patra, A., and Mitra, R. K. (2013) Dielectric relaxation of the extended hydration sheathe of DNA in the THz frequency region, *Chem. Phys. Lett. 586*, 143-147.
26. Ebbinghaus, S., Kim, S. J., Heyden, M., Yu, X., Heugen, U., Gruebele, M., Leitner, D. M., and Havenith, M. (2007) An extended dynamical hydration shell around proteins., *Proc. Natl. Acad.Sci.USA 104*, 20749-20752.
27. Kindt, J. T., and Schmuttenmaer, C. A. (1996) Far-infrared dielectric properties of polar liquids probed by femtosecond terahertz pulse spectroscopy, *J. Phys. Chem. 100*, 10373-10379.
28. Rønne, C., Åstrand, P. O., and Keiding, S. R. (1999) THz Spectroscopy of Liquid H2O and D2O, *Phys. Rev. Lett. 82*, 2888-2891
29. van der Post, S. T., Tielrooij, K.-J., Hunger, J., Backus, E. H. G., and Bakker, H. J. (2013) Femtosecond study of the effects of ions and hydrophobes on the dynamics of water, *Faraday Discuss. 160*, 171-189.
30. Peters, T. (1996) *All About Albumin: Biochemistry, Genetics, and Medical Applications*, Academic Press, San Diego.
31. He, X. M., and Carter, D. C. (1992) Atomic structure and chemistry of human serum albumin, *Nature 358*, 209 - 215.
32. Flora, K., Brennan, J. D., Baker, G. A., Doody, M. A., and Bright, F. V. (1998) Unfolding of Acrylodan-Labeled Human Serum Albumin Probed by Steady-State and Time-Resolved Fluorescence Methods, *Biophys. J. 75*, 1084-1096.
33. Luong, T. Q., Verma, P. K., Mitra, R. K., and Havenith, H. (2011) Do Hydration Dynamics Follow the Structural Perturbation during Thermal Denaturation of a Protein: A Terahertz Absorption Study, *Biophys. J. 101*, 925-933.
34. Arnaud, P. (1986) The plasma proteins: Structure, function, and genetic control, Academic Press, Orlando, Fla.
35. Hirayama, K., Akashi, S., Furuya, M., and Fukuhara, K.-i. (1990) Rapid confirmation and revision of the primary structure of bovine serum albumin by ESIMS and Frit-FAB LC/MS, *Biochemical and biophysical research communications 173*, 639-646.
36. Jollès, P. (1969) Lysozymes: A Chapter of Molecular Biology, *Angewandte Chemie International Edition in English 8*, 227-239.

37. Canfield, R. E. (1963) The Amino Acid Sequence of Egg White Lysozyme, *Journal of Biological Chemistry 238*, 2698-2707.
38. Davies, R. C., Neuberger, A., and Wilson, B. M. (1969) The dependence of lysozyme activity on pH and ionic strength, *Biochimica et Biophysica Acta (BBA) - Enzymology 178*, 294-305.
39. Blake, C., Koenig, D., Mair, G., North, A., Phillips, D., and Sarma, V. (1965) Structure of hen egg-white lysozyme: a three-dimensional Fourier synthesis at 2 Å resolution, *Nature 206*, 757-761.
40. Gorin, G., Wang, S.-F., and Papapavlou, L. (1971) Assay of lysozyme by its lytic action on M. lysodeikticus cells, *Analytical biochemistry 39*, 113-127.
41. Davies, R., Neuberger, A., and Wilson, B. (1969) The dependence of lysozyme activity on pH and ionic strength, *Biochimica et Biophysica Acta-Enzymology 178*, 294-305.
42. Wetter, L., and Deutsch, H. (1951) Immunological studies on egg white proteins IV. Immunochemical and physical studies of lysozyme, *Journal of Biological Chemistry 192*, 237-242.

Chapter 3

3. Instrumentation and Basic Principles

3.1. Ultra Violet-Visible Spectrophotometer (UV-Vis)

UV-Vis absorption was measured with Shimadzu UV-2600 spectrophotometer. A tungsten lamp (W1) is used as visible light source and a deuterium lamp (D2) is used as ultraviolet light source with a lamp interchange wavelength of 282-293 nm. The only monochromator used in this instrument consists of high performance blazed holographic grating which spreads the beam of light into its component wavelengths. This is a typical double beam instrument; the light emanating from source is split into two beams the reference beam and sample beam. A photomultiplier tube (PMT) is used as a detector.

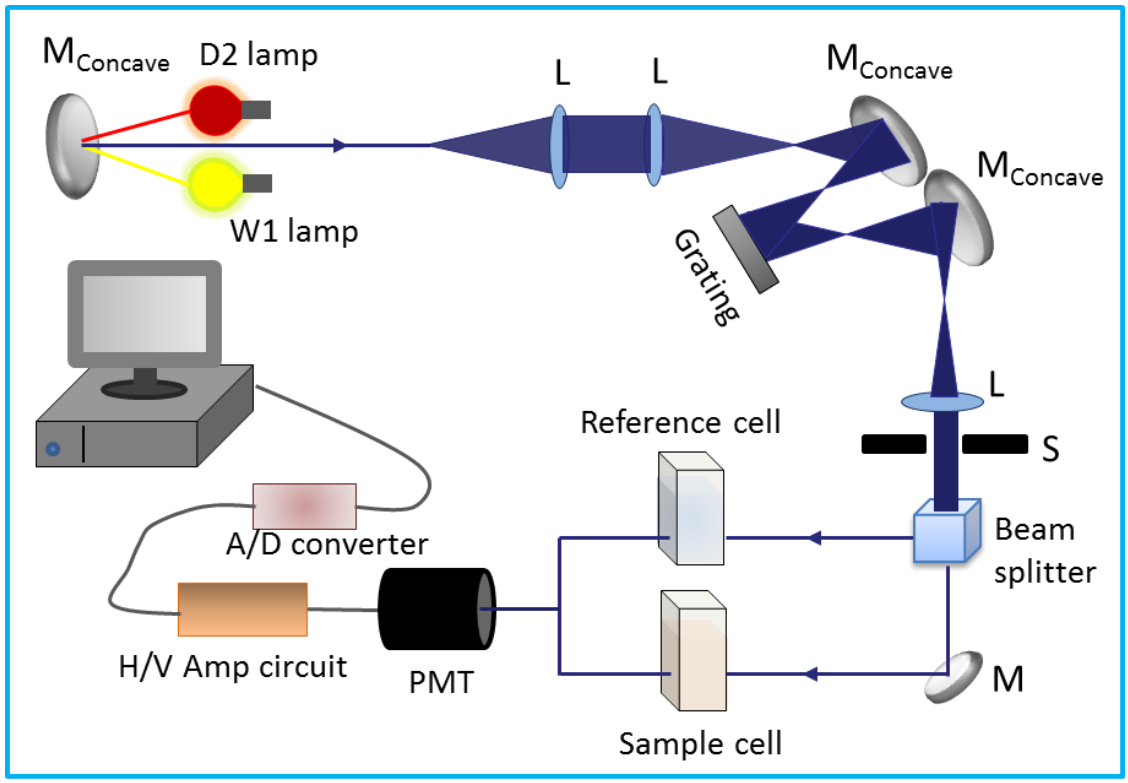

Scheme 3.1: Representation of an absorption spectrophotometer. Tungsten halogen (W1) and Deuterium lamps (D2) are used as light sources in the visible and UV regions, respectively. $M_{concave}$, M, L, S, PMT represent concave mirror, plane mirror, lens, shutter and photomultiplier tube, respectively. A/D converter and HV/Amp indicate analog to digital converter and High-voltage/Amplifier circuit, respectively.

When continuous radiation passes through a material, a portion of the radiation may be absorbed. If that occurs, the residual radiation, when it is passed through a prism, yields a spectrum with gaps in it, called an absorption spectrum. In the case of UV-visible spectroscopy, the absorption of electromagnetic radiation occurs due to the transitions from lower energy electronic state to higher energy state. An electronic transition of a molecule is always associated with both vibrational and rotational transitions. So each electronic

transition consists of a vast number of lines spaced so closely that spectrophotometer cannot resolve them. Rather, the instrument traces an 'envelope'. That's why the UV spectrum of a molecule usually consists of a broad band centered near the wavelength of the major transition.

Regarding the extent of absorption of a molecule there is an empirical equation known as Beer-Lambert law as given below,

$$A = \log(I_0/I) = \varepsilon c l \quad \text{(for a given wavelength)} \qquad (3.1)$$

where A=absorption, I_0 is the intensity of light incident upon sample cell, I is the intensity of light leaving sample cell, ε is molar absorptivity, c is the molar concentration of solute and l is the length of sample cell.

3.2. Circular Dichroism (CD) Spectrometer

CD was measured by JASCO J-815. Spectropolarimeter with a Peltier temperature controller attachment. A Xe-lamp is used as source of light. N_2 is purged to remove O_3 gas.

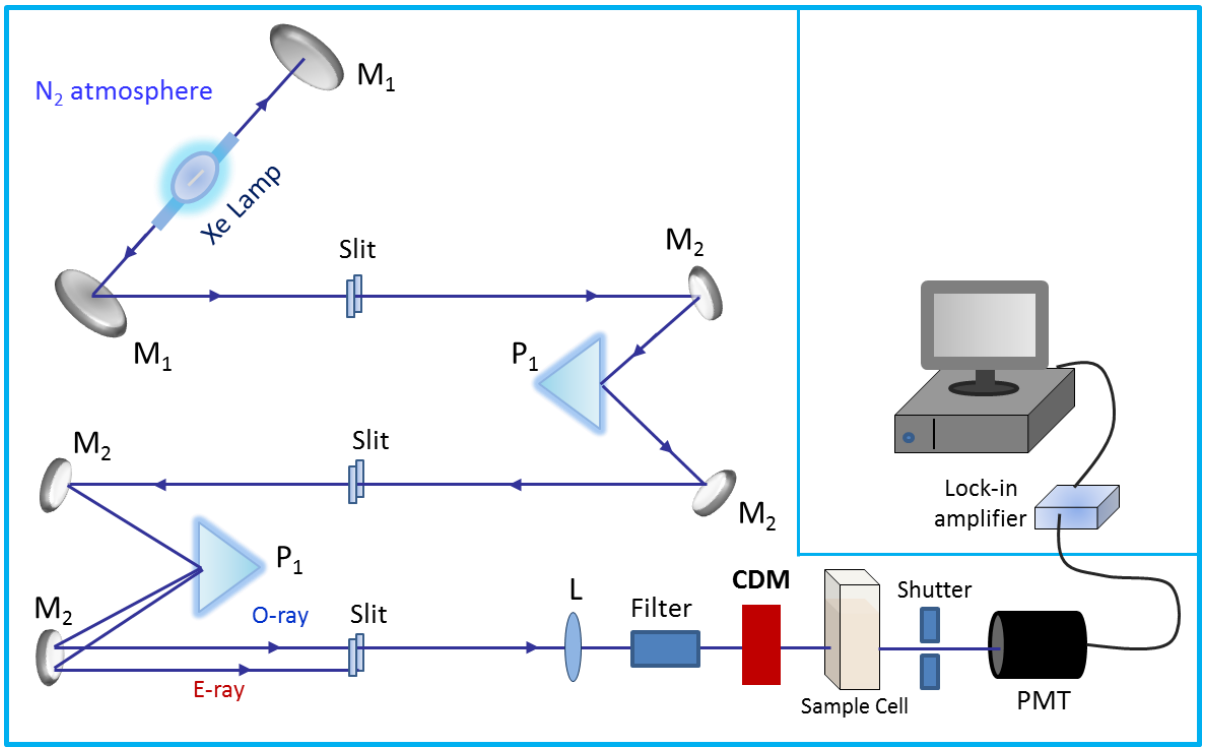

Scheme 3.2: Ray diagram of a Circular Dichroism (CD) spectropolarimeter. M_1, M_2, P_1, L, PMT, CDM, O-ray and E-ray represent concave mirror, plain mirror, reflecting prism, lens, photomultiplier tube, CD-modulator, ordinary ray and extraordinary ray, respectively.

CD is defined as the difference in absorbance of left-handed (L) and right-handed (R) circularly polarized light and occurs when a molecule contains one or more chiral chromophores (light absorbing groups).

$$CD = A_L(\lambda) - A_R(\lambda) \tag{3.2}$$

Molar ellipticity [θ] is defined as,

$$[\theta] = \frac{\theta\ (mdeg)}{C_M \times l \times 10}\ (\text{deg cm}^2\ \text{decmol}^{-1}) \tag{3.3}$$

where $\theta\ (mdeg)$ is the CD in mdeg unit, C_M is the molar concentration of the sample, l is the path length of the cell in cm unit.

3.3. Steady State Fluorescence Spectroscopy

We have used Fluorolog, Horiba-Jobin Yvon, Edison, NJ (Model LFI-3751). Ozone free Xe-Arc lamp has been used as a source of continuous wave light. There are two monochromators[1] which are excitation and emission monochromator. The essential part of these monochromators is reflection grating, containing 1200 grooves/mm and are blazed at 330 nm (excitation) and 500 nm (emission).

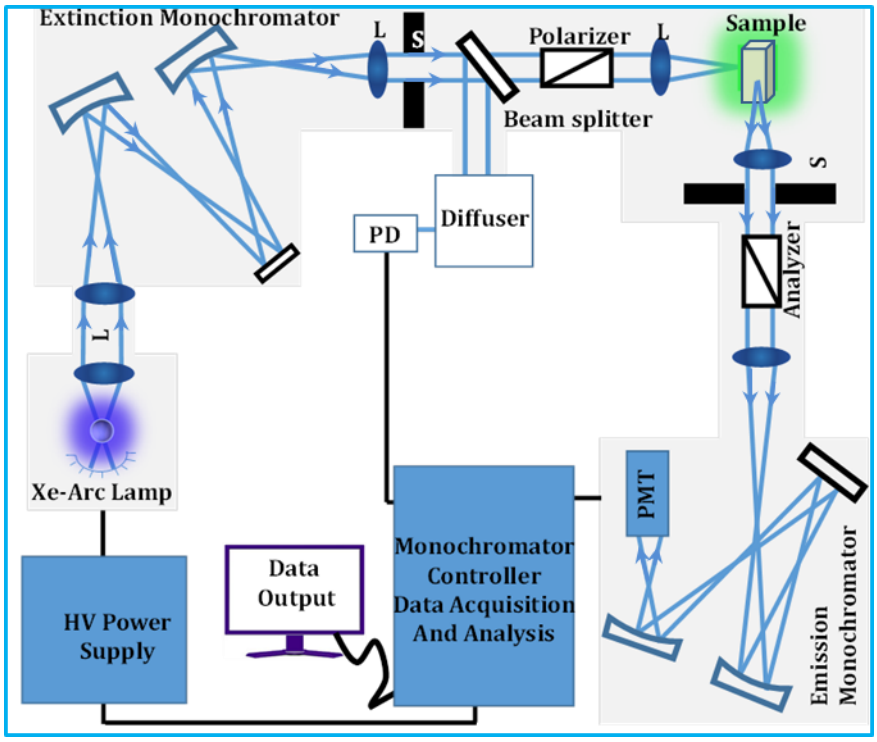

Scheme 3.3: Ray diagram of an emission spectrofluorimeter. M, G, L, S, PMT and PD represent mirror, grating, lens, shutter, photomultiplier tube and reference photodiode, respectively.

These gratings give an excitation wavelength coverage 220-600 nm and emission wavelength coverage 290-850 nm.

3.4. Time Resolved Fluorescence Spectroscopy (TRFS)

Picosecond-resolved fluorescence[2] transients were recorded using time correlated single photon counting (TCSPC) technique.[1] The schematic block diagram of a TCSPC system is shown in scheme 3.4. TCSPC setup (Edinburgh instruments, U.K.) was used during fluorescence decay acquisitions. The instrument response functions (IRFs) of the laser sources at different excitation wavelengths varied from 60 ps to 400 ps. Fluorescence signal from the samples was detected by a photomultiplier after dispersion through a grating monochromator. For all the transients, the polarizer in the emission side was adjusted to be at 54.7° (magic angle) with respect to the polarization axis of the excitation beam.

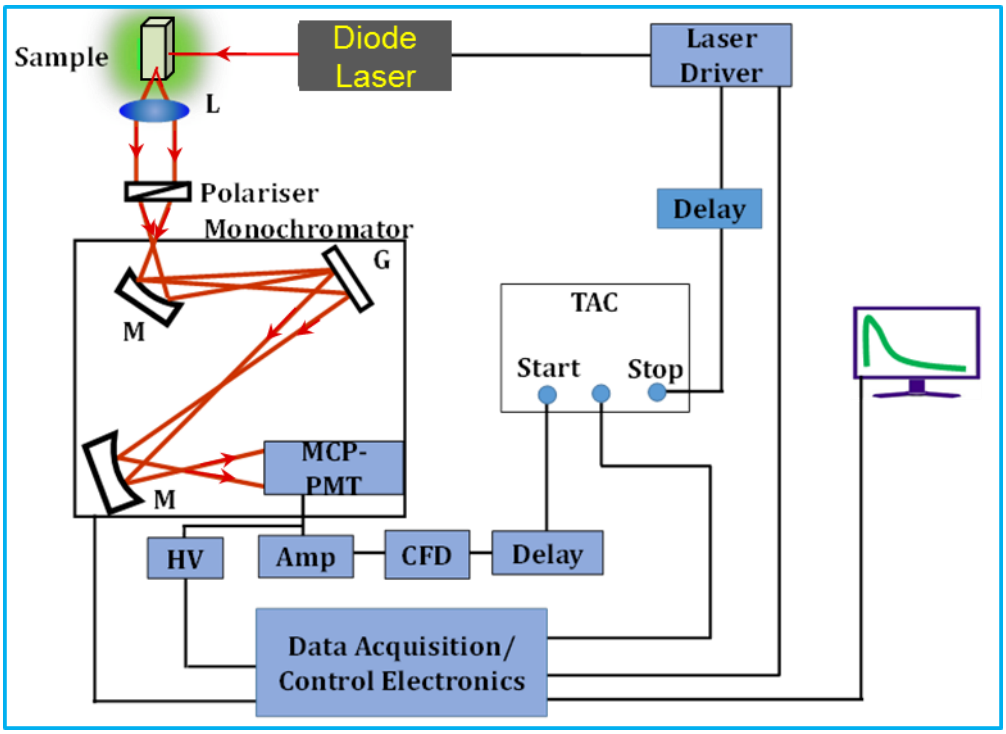

Scheme 3.4: Ray diagram of a TCSPC spectrophotometer. A signal from microchannel plate photomultiplier tube (MCP-PMT) is amplified (Amp) and connected to start channel of time to amplitude converter (TAC) via constant fraction discriminator (CFD) and delay. The stop channel of the TAC is connected to the laser driver via a delay line. L, M, G and HV represent lens, mirror, grating and high voltage source, respectively.

3.5. Oscillating U-tube Density Meter

Density and sound velocity were measured using a high precision density meter (model DSA5000) from Anton Parr (Austria) with an accuracy of 5×10^{-6} g cc^{-1} and 0.5 m s^{-1} in density and sound velocity measurements, respectively.

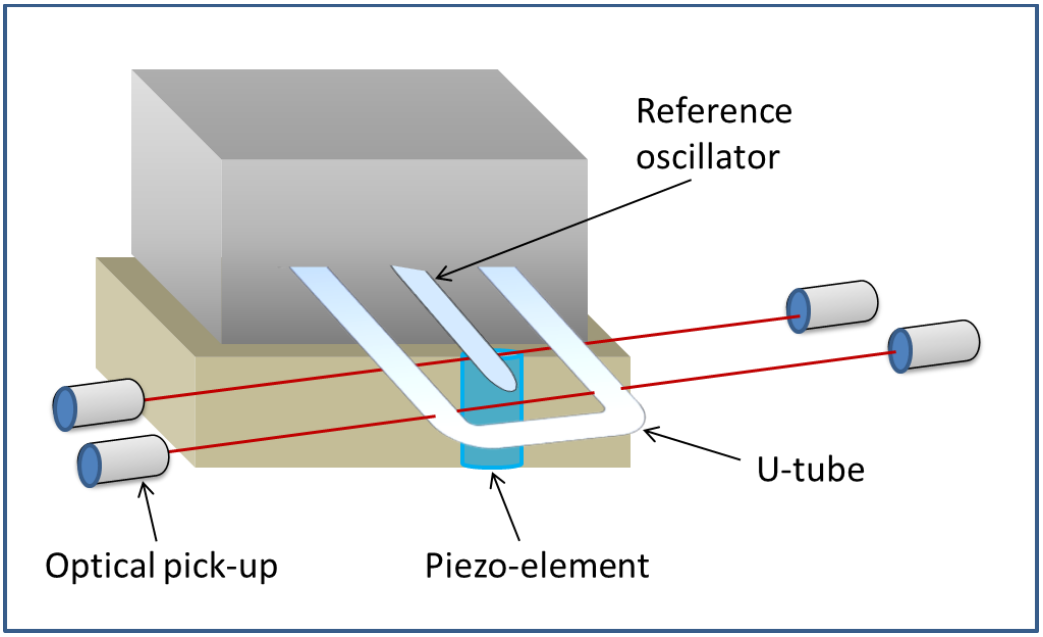

Scheme 3.5: Density meter based on oscillating U-tube principle

A hollow U-shaped glass tube of known volume and mass is filled with the liquid sample and excited electronically by a Piezo-element. The U-tube is periodically oscillating with a frequency (say) *f*. Optical pick-ups record the oscillating period *P* as *P=1/f*. The frequency is inversely proportional to the density (ρ) of the filled liquid. The density is obtained from the following equation,

$$\rho = A \times P^2 - B \qquad (3.4)$$

where *A* and *B* are parameters. Thus the density of the sample can be determined after adjusting the instrument with air and water (water must be free of air bubble).

3.6. Viscosity Meter

Viscosity of a liquid sample was measured by an automated Micro Viscometer [AMVn, Anton Parr (Austria)].

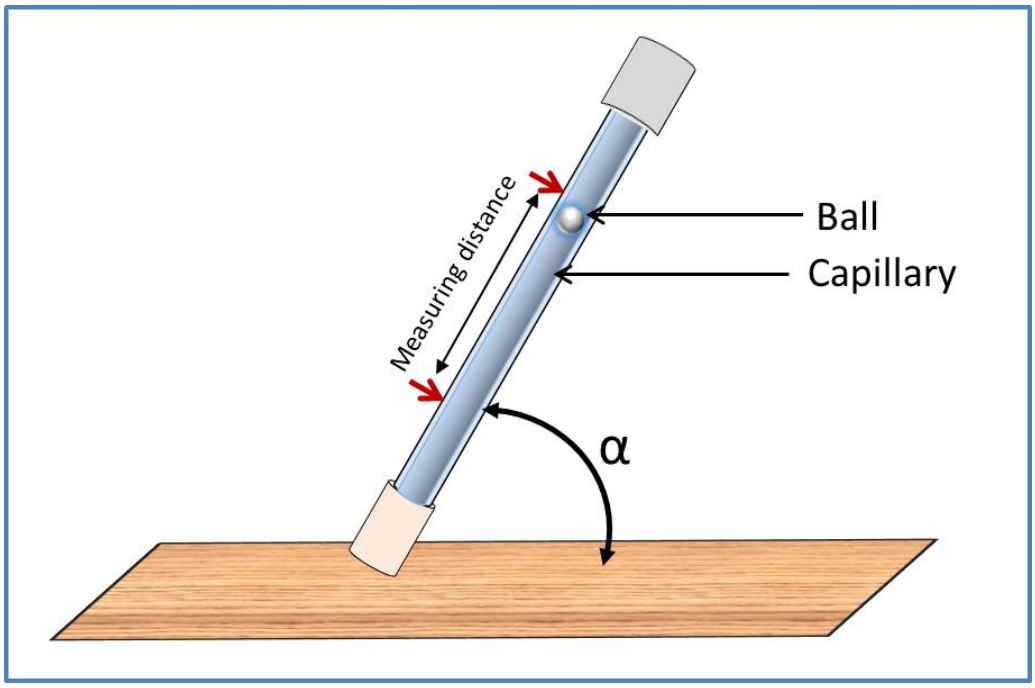

Scheme 3.6: Representation for micro viscometer based on falling ball principle

This instrument measures viscosity by the Höppler falling ball principle. In this method the elapsed time is required for the ball to fall under gravity through a liquid sample-filled capillary tube inclined at an angle. The tube is mounted on a pivot bearing which quickly allows rotation of it by 180 degrees, thus allowing a repeated measurement to run immediately. The average time is converted into a viscosity value in centipoise (cP). The dynamic viscosity is calculated by the following eq^{n}.

$$\eta = t(\rho_1 - \rho_2)K \times F \qquad (3.5)$$

where η is the dynamic viscosity (mPaS), t is the travelling time of the ball, $\rho_1$and ρ_2 is the density (g cm^{-3}) of the ball and the sample, respectively, K is the ball constant (mPa.cm^{-3}g^{-1}) and F is working angle constant.

3.7. Dynamics Light Scattering (DLS)

Dynamic light scattering (DLS), also known as photon correlation spectroscopy (PSC) or quasi elastic light scattering (QELS) is one of the reliable technique to determine the hydrodynamic diameter of the particle. In our lab measurements were carried out with *Nano S Malvern* instrument employing a 4mW He-Ne LASER (λ= 632.8 nm) equipped with a thermostated sample chamber. When light hits small particles compared to the wavelength, the light scatters in all directions (Rayleigh scattering).

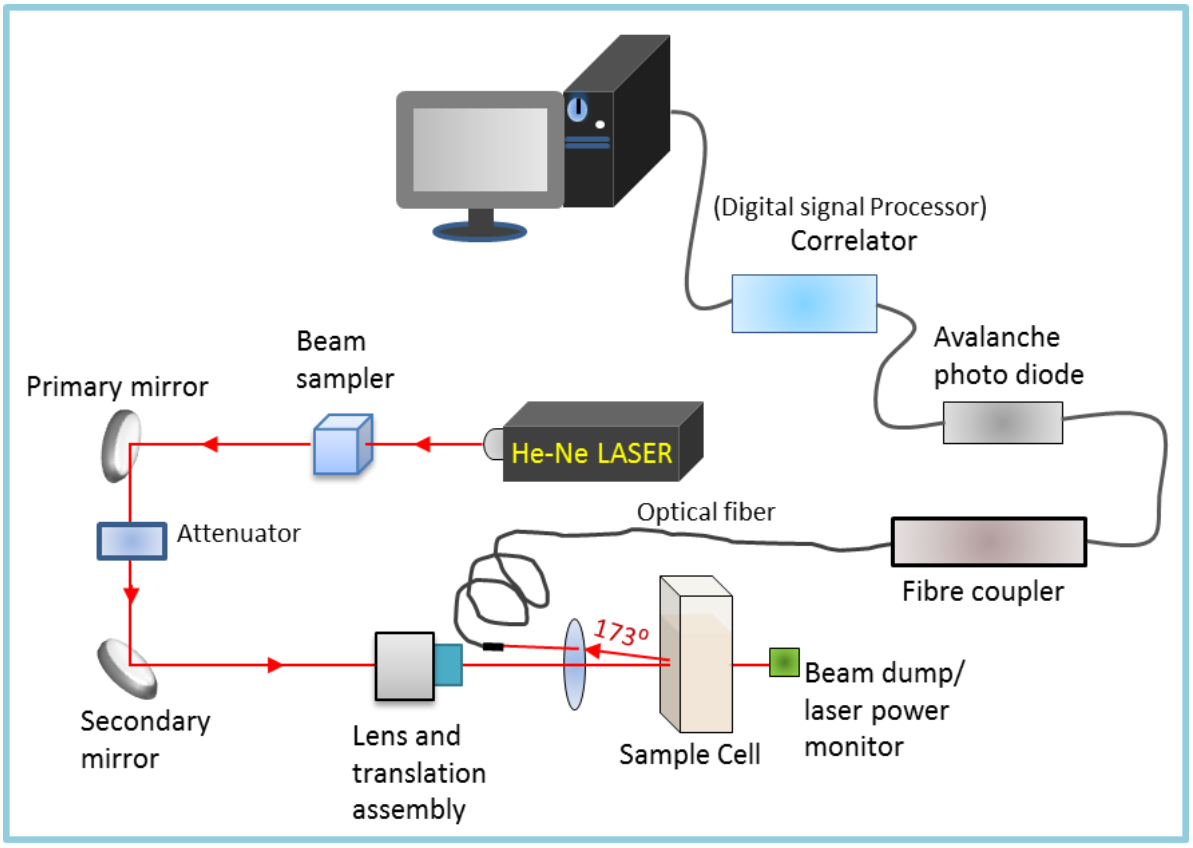

Scheme 3.7: Ray diagram of dynamic light scattering (DLS).

For the monochromatic and coherent light, the scattering intensity fluctuates over time due to small molecules in solutions undergoing Brownian motion, and so the distance between the scatterers in the solution is constantly changing with time. This scattered light then undergoes either constructive or destructive interference by the surrounding particles, and within this intensity fluctuation, information is contained about the time scale of movement of the scatterers. All the scattered photons are collected at 173° scattering angle. The details of DLS measurements has been reported elsewhere.[3] The measured data in DLS experiment is the correlation curve. Embodied within this correlation curve is all of the information regarding

the diffusion of particles within the sample that has been measured. By fitting the correlation curve to an exponential function, the diffusion coefficient (*D*) can be calculated (*D* is proportional to the lifetime of the exponential decay).

Hydrodynamic diameter (d_H) of the particle is estimated from the intensity autocorrelation function of the time-dependent fluctuation in intensity. According to Stokes-Einstein (SE) model the d_H is related to the viscosity and the diffusion coefficient of the solution as given below,

$$d_H = \frac{k_B T}{3\pi\eta D} \tag{3.6}$$

where k_B is the Boltzmann constant, η is the viscosity.

3.8. Fourier Transform Infrared (FTIR) Spectroscopy

FTIR measurements were performed on a JASCO FTIR-6300 spectrometer (transmission mode). Michelson interferometer[4] is the heart of FTIR spectrometer. It consists of a fixed mirror (M4), a moving mirror (M5) and a beam-splitter (BS), as illustrated in figure 3.8. The collimated IR beam from the source is partially transmitted to the moving mirror and partially reflected to the fixed mirror by the beam-splitter. The two IR beams are then reflected back to the beam-splitter by the mirrors. The detector then senses the transmitted beam from the fixed mirror and reflected beam from the moving mirror, simultaneously. The two combined beams interfere constructively or destructively depending on the wavelength of the light (or frequency in wavenumbers) and the optical path difference introduced by the moving mirror. The resulting signal is called an interferogram which has the unique property that every data point (a function of the moving mirror position) which makes up the signal has information about every infrared frequency which comes from the source. The measured interferogram signal is then processed through a Fourier transform to obtain the final spectrum. Each spectrum consists of 100 scans (1500−4000 cm^{-1}) acquired at 0.5 cm^{-1} resolution.

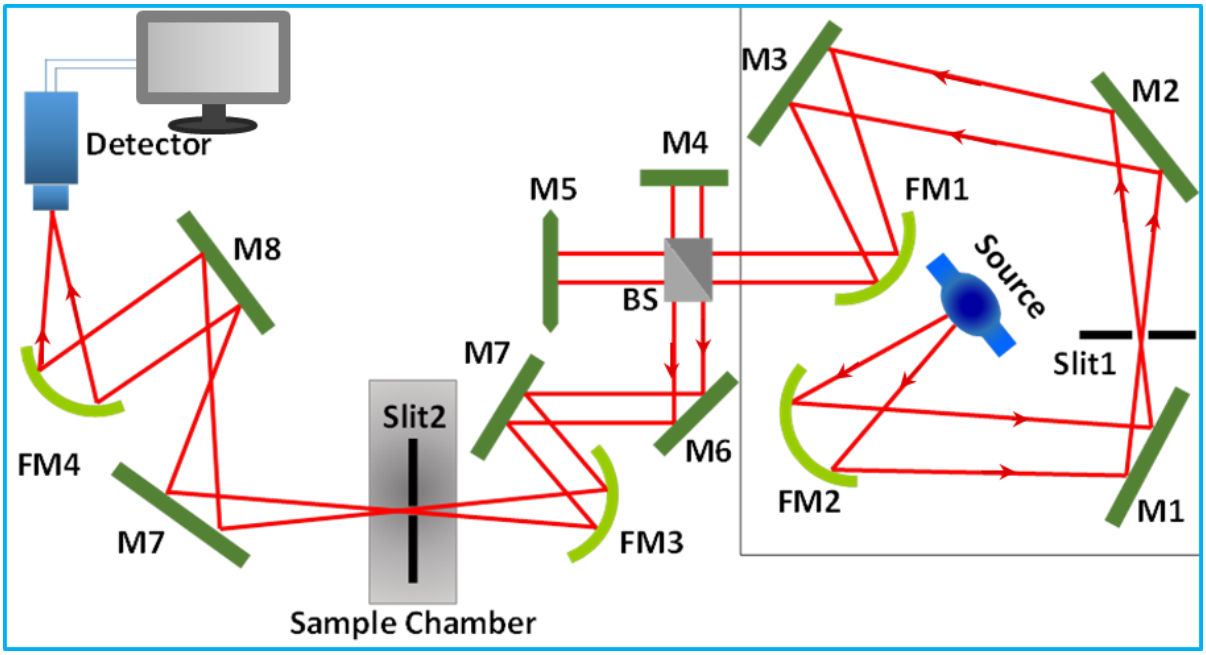

Scheme 3.8. Ray diagram of Fourier Transform Infrared (FTIR) spectrometer. It is mainly a Michelson interferometer in which one of the two fully-reflecting mirrors is movable, allowing a variable delay (in the travel-time of the light) to be included in one of the beams. M, FM and BS represent the mirror, focussing mirror and beam splitter, respectively. M5 is a moving mirror.

FIR (in collaboration with Ruhr University, Germany): FTIR spectra were recorded using a VERTEX 80v FTIR Spectrometer (Bruker Optics) under nitrogen gas flow in the sample compartment. The data were collected and processed using OPUS software. For spectra acquisition in the FIR region (30-450 cm^{-1}), a mercury-lamp served as an FIR source, a liquid-helium-cooled silicon bolometer was used as a detector. All the measurements were performed using a liquid cell (model A145, Bruker Optics, diamond windows) with a thickness of 28.5 ± 0.3 µm.

3.9. Terahertz Time Domain Spectroscopy (TTDS)

TTDS measurements were carried out in a commercial THz spectrophotometer (*TERA K8, Menlo System*). [5, 6] A 780 nm Er doped fiber laser having pulse width of <100 fs and a repetition rate of 100 MHz excites a THz emitter antenna producing a THz radiation having a bandwidth up to 3.0 THz (> 60 dB). This THz radiation is then focused on sample and the

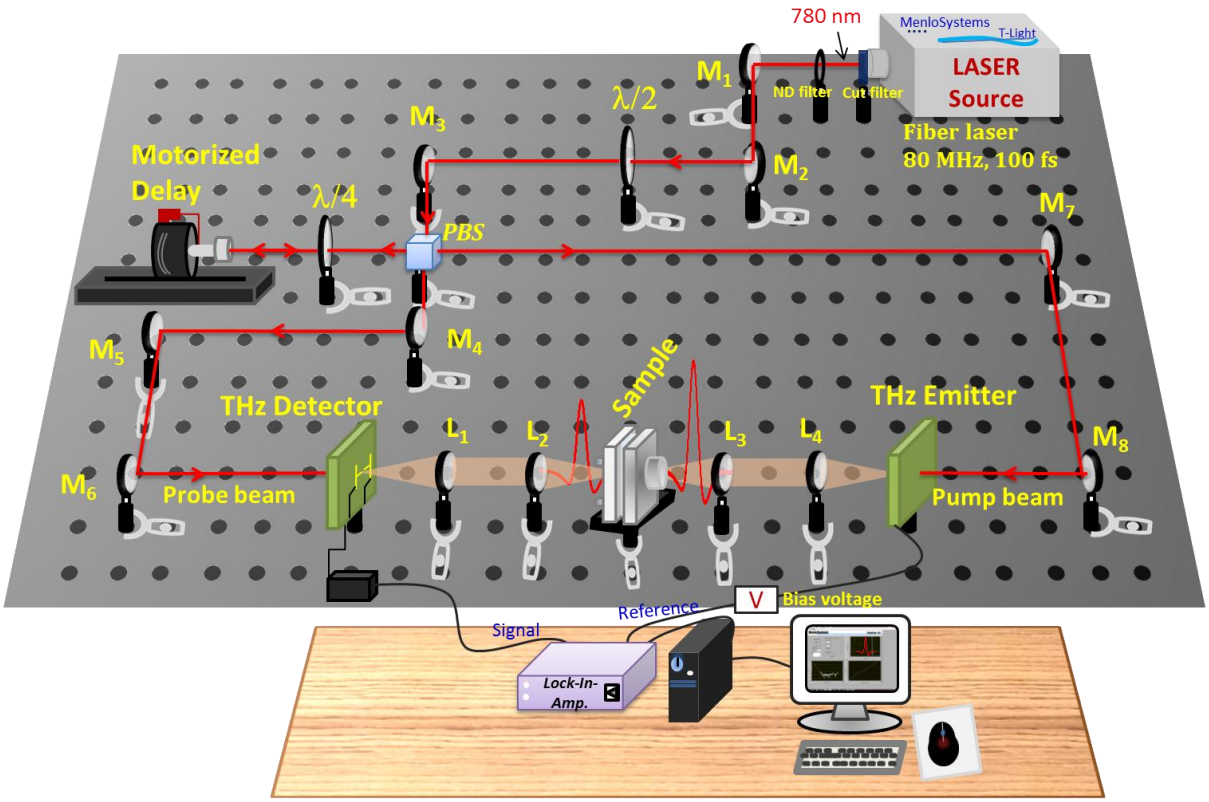

Scheme 3.9. Schematic diagram of Terahertz time domain spectroscopy. M, L, λ/2 and λ/4 representing mirror, TPX polymer convex lens, half wave plate and quarter wave plate respectively. Both the detector and emitter are photo conductive antennas made of gold dipole deposited on GaAs semiconductor (low temperature grown).

transmitted THz radiation is further focused on a THz detector antenna which is gated by the probe laser beam. Both the THz antennas are gold dipoles with a dipole gap of 5μm deposited on LT (low temperature grown) GaAs substrate (mobility μ ~400 cm/s, carrier lifetime τ~1 ps). With applied bias voltage (~20 V, 10 kHz) the electric energy is stored in the gap area. When laser light focuses on the gap, electron hole pairs are created. These charge carriers are accelerated by the bias field. In this case, the fs laser pulses act transient switches to open the stored electric energy and releases it in the form of the emission of a time dependent THz field $E_{THz}(t)$ which is proportional to the derivation of the current density $J(t)$.

$$E_{THz}(t) = \frac{1}{4\pi\varepsilon_0}\frac{A}{zc^2}\frac{\partial J(t)}{\partial t} \tag{3.7}$$

$$J(t) = N(t)e\mu E_b \tag{3.8}$$

By varying the time delay between the probe and the pump beam the amplitude and phase of the THz electric field are measured as a function of time. Frequency dependent power and

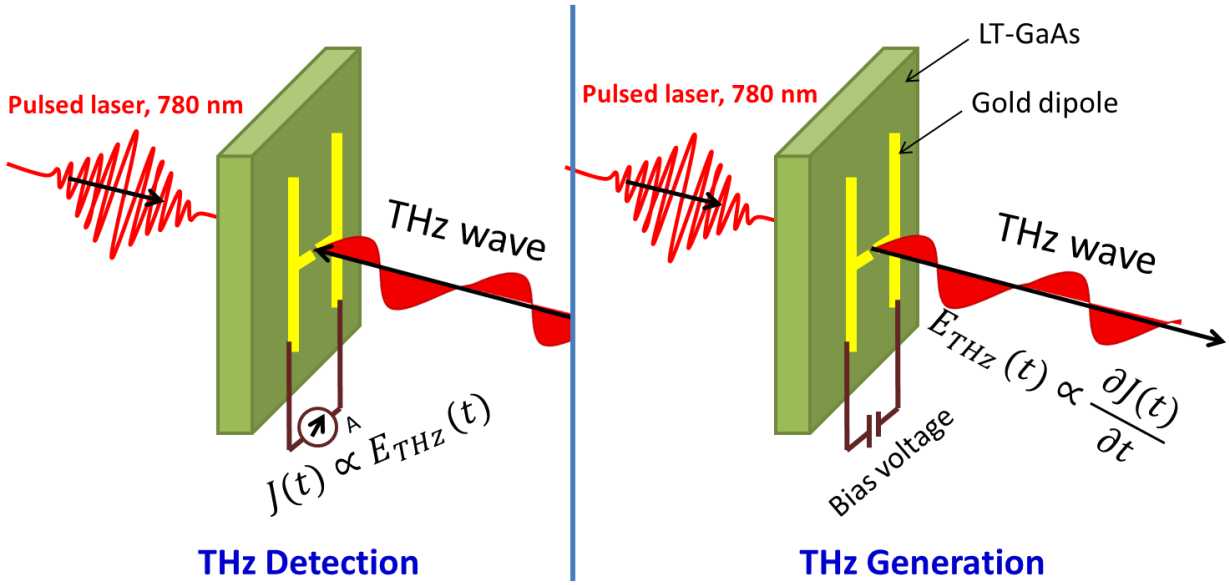

Scheme 3.10: THz generation and detection by using photo conducting antenna.

phase of the transmitted pulse are obtained using Fourier transform of the measured electric field amplitude $E_{THz}(t)$.

3.10. p-Germanium Terahertz

(In collaboration with Ruhr University, Germany): In the p-Ge (p-Germanium) difference spectrometer measurements the THz radiation source used is a high-power (1 W) p-Ge laser.[7] This set-up has been described in elsewhere.[8] The p-Ge crystal emits THz radiation in the range of 1 to 4 THz, accessing the intermolecular collective modes of the hydrogen-bonding network of water. The THz radiation emitted from the p-Ge laser is split by a chopper into a probe and a reference beam, propagating through the sample cell containing the solvated protein, and the reference cell containing the buffer solution, respectively. Both beams are focused to the detector (bolometer) by a polyethylene lens. We used the p-Ge difference spectrometer to record the integrated absorption of the protein solution relative to that of the buffer in the frequency range of 2.1 to 2.8 THz. For each measurement, 30,000 pulses each for the sample and for the reference were recorded and averaged. The change of THz absorption of the samples compared to that of the reference was deduced.

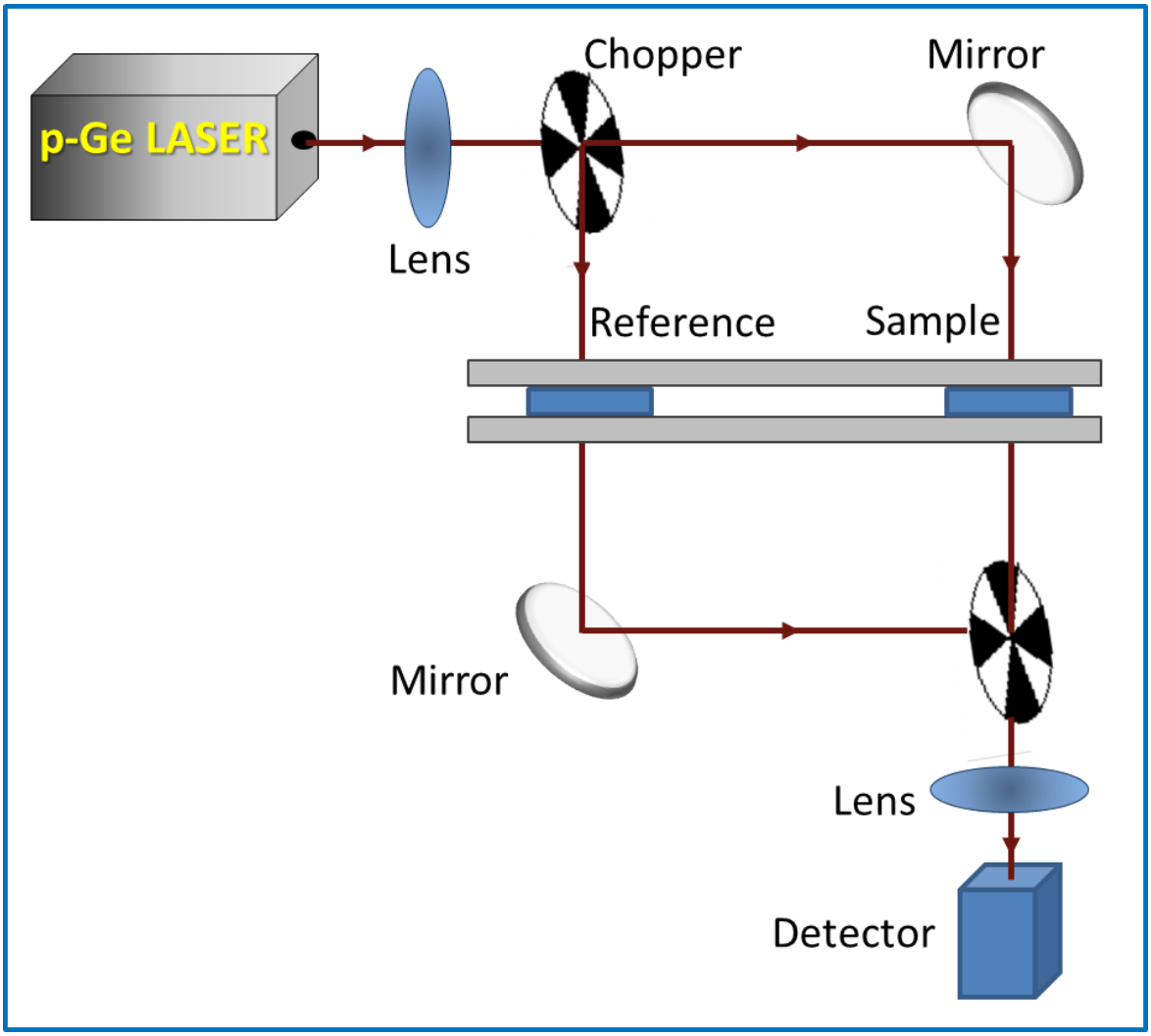

Scheme 3.11: p-Ge THz spectroscopy

3.11. Vector Network Analyser (Dielectric in GHz Frequency)

Dielectric relaxation (DR) in GHz regime is measured in PNA-L network analyser with an open ended coaxial probe which is in direct contact with solution. Both the magnitude and phase of the reflected power is measured by the network analyser that can give the information of real and imaginary dielectric constants at each frequency sweep.

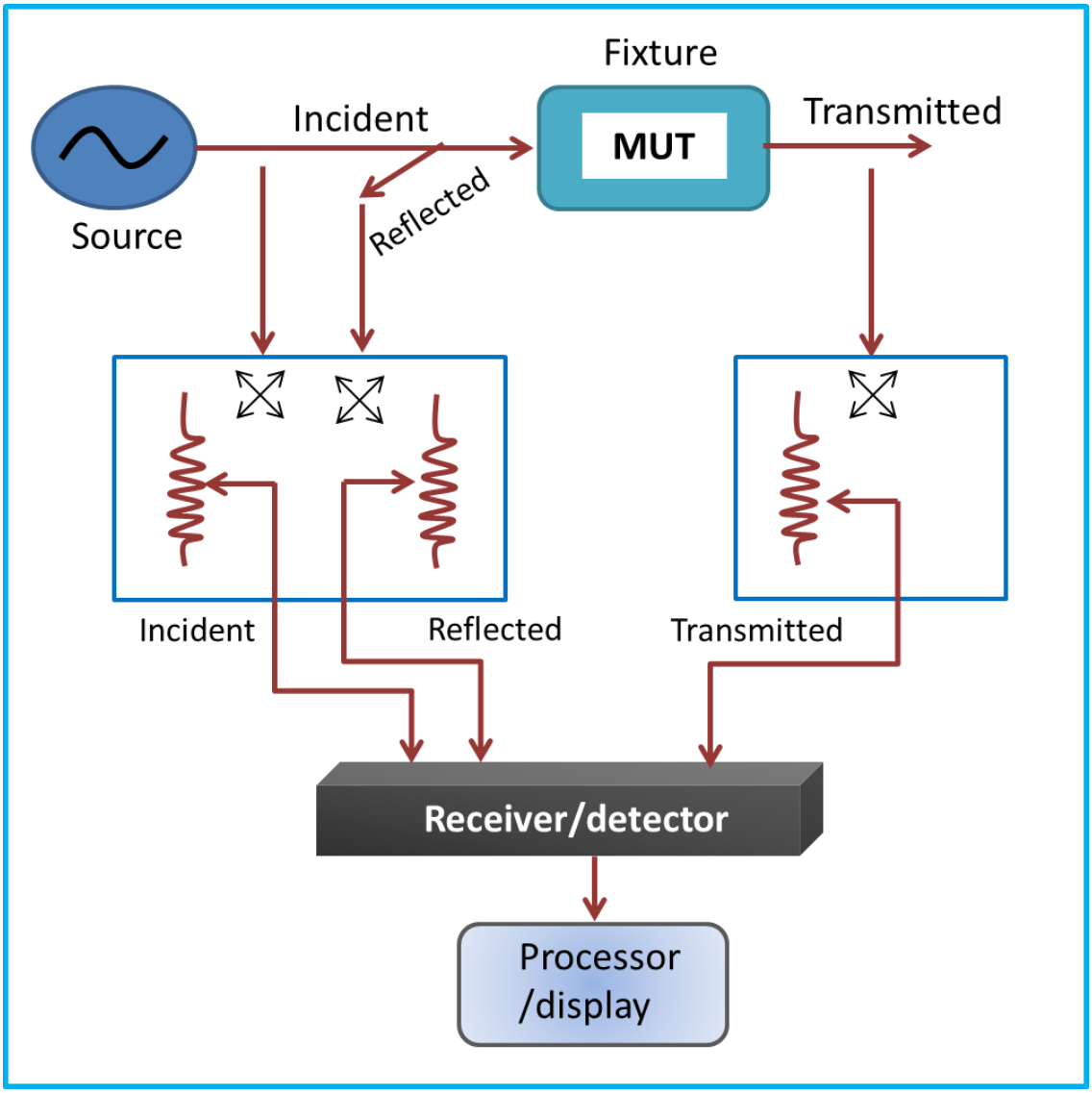

Scheme 3.12: Vector network analyser. MUT means material under test.

3.12. Differential Scanning Calorimeter (DSC)

*(In collaboration with IICB, Kolkata):*The temperature dependent transitions in the protein were measured on a Microcal VP-differential scanning calorimeter (DSC) (MicroCal, Inc., Northampton, MA) by monitoring excess heat capacities as a function of temperature as described elsewhere.[9]

References

1. Lakowicz, J. R. (2013) *Principles of fluorescence spectroscopy*, Springer Science & Business Media.
2. O'Conner, D. V., and Philips, D. (1984) *Time correlated single photon counting*, Academic Press, London.
3. Mitra, R. K., Sinha, S. S., and Pal, S. K. (2007) Hydration in protein folding: Thermal unfolding/refolding of human serum albumin *Langmuir 23*, 10224-10229.
4. Saptari, V. (2004) *Fourier transform spectroscopy instrumentation engineering*, SPIE Optical Engineering Press.
5. Polley, D., Ganguly, A., Barman, A., and Mitra, R. K. (2013) Polarizing effect of aligned nanoparticles in terahertz frequency region, *Opt. Lett. 38*, 2754-2756.
6. Polley, D., Patra, A., and Mitra, R. K. (2013) Dielectric relaxation of the extended hydration sheathe of DNA in the THz frequency region, *Chem. Phys. Lett. 586*, 143-147.
7. Bergner, A., Heugen, U., Bründermann, E., Schwaab, G., Havenith, M., Chamberlin, D. R., and Haller, E. E. (2005) New p-Ge THz laser spectrometer for the study of solutions: THz absorption spectroscopy of water, *Rev. Sci. Instr. 76*, 063110.
8. Luong, T. Q., Verma, P. K., Mitra, R. K., and Havenith, H. (2011) Do Hydration Dynamics Follow the Structural Perturbation during Thermal Denaturation of a Protein: A Terahertz Absorption Study, *Biophys. J. 101*, 925-933.
9. Giri, P., and Kumar, G. S. (2008) Binding of protoberberine alkaloidcoralyne with double stranded poly(A): a biophysical study, *Mol. BioSyst. 4*, 341-348.

Chapter 4

4. Effect of Crowding Agents on Protein Conformational Stability and Hydration Dynamics

To mimic the real cellular environment biomolecules are studied in presence of crowding agents (e.g., polyethylene glycol, ficoll etc.). We aim to study the structure, thermal stability and collective hydration dynamics of a globular protein human serum albumin (HSA) in presence of two short chain crowding agents, namely polyethyleneglycols (PEG 200 and 400). The secondary as well as tertiary structures of HSA have been studied by using circular dichroism (CD) spectroscopy. The alteration in the collective water network structure is investigated using FTIR spectroscopy in the far-infrared (FIR) frequency range (30-450 cm^{-1}) and site specific changes are obtained by time-resolved fluorescence spectroscopic technique using the intrinsic fluorophore tryptophan (Trp214) of HSA. The collective hydration dynamics of HSA in presence of PEG molecules are obtained using Terahertz (THz) spectroscopy. Our study affirms that PEG 200 and 400 interact with HSA differently in comparison to higher chain PEG 10000 and smaller solute sucrose. For PEG 200 and 400 we have found a critical concentration beyond which the hydration of HSA alters abruptly.

4.1. Introduction

Cellular environments are crowded (see scheme 1.1, chapter 1) with several macromolecules like lipids, sugars, nucleic acids and proteins, along with macromolecular arrays (e.g. cytoskeleton fibre) and the large volume occupied by such molecules can have profuse effect on a number of processes of biological importance[1]. Such non-specific influence of this high macromolecular concentration affects the structure and dynamics of proteins as they experience volume restriction owing to the surrounded macromolecules as well as restricting the allowed protein conformations[2]. The phenomenon of macromolecular crowding has generally been explained in terms of the 'exclusion volume' model which predicts a relative stabilization of the native state compared to the fully unfolded states[1, 3] as has also been experimentally realized in many earlier studies[4-9] including those in which weak attractive protein-crowder interaction has been envisaged.[2, 10-18] In all

these studies increase in native→unfolded transition temperature has been explained on the basis of the relative stabilization of the folded state of the protein in comparison to the destabilization of the unfolded state in the potential energy landscape by making the unfolded state more compact and thereby energetically less favourable.[1, 6, 19] This model is based on hard-core repulsion which arises because the crowders decrease the space available to the proteins. Such an effect is mostly entropy driven as it involves only the arrangement of molecules and not the interaction among themselves.[15, 20] However, a point of concern that emerges is whether there exist any 'true' crowding agent that does not cause any additional effect apart from the volume exclusion[2], also direct effect of the crowding agent on the folded as well as unfolded states of proteins could not be ruled out[3] as there have been reports available in which crowding agents are found to ease the unfolding process[21, 22]. This could make a-priori prediction on the effect of macromolecular crowding on protein stability counterintuitive and a proper experimental as well as theoretical drive on rationalizing the effect on the type and content of the crowding agent is still on demand. In this regard hydration of protein in such crowded milieu is a matter of study as we know water, an integral and active component of life, plays both dynamic as well as structural roles in most of the biophysical processes.[23] It is an essential component for protein structure, defining the collapse of the hydrophobic core in maintaining its structure.[24] It is interesting to note that only small amount of bulk water is available in the real cellular environment which is crowded with macromolecules at a concentration of about 300 $mg \cdot ml^{-1}$.[25] A considerable effort has been put forward on protein-crowder interactions with a major point devoted to the protein stability and refolding kinetics[1, 9, 12, 26] whereas the effect of crowding on the structure and dynamics of hydration around proteins has rarely been addressed.[27-29] Highly crowded environment is expected to alter the hydration structure of proteins following the 'excluded volume' model as well as significant interactions with nearby macromolecules which may result in a reduction of the diffusion rate[30] and can affect various biological processes.[31] In an earlier study crowding induced alteration in hydration dynamics has been reported to modify the enzymatic activity of α-chymotrypsin.[29] A recent MD simulation study by Harada et al.[27] have reported that macromolecular crowding at low crowder concentration moderately affects the hydration structure and dynamics at the protein surface, whereas a significant change has been recorded beyond a certain concentration (~30%) of the crowders. 2D IR study by the group of Kurbaryh et al.[28] has shown that both PEG and protein themselves induce a dynamical transition wherein the coupled protein-hydration dynamics exhibits a sharp

retardation beyond a certain concentration of PEG (~30-40 %v/v) indicative of an independent-to-collective hydration transition. A more recent study showed that in contrast to the prediction of the excluded volume theory, an enthalpic stabilization and an entropic destabilisation was observed upon addition of PEG.[32] In summary we can state that a proper understanding of the fate of hydration dynamics at protein surface is still strongly in demand. In the present contribution we have carried out an experimental investigation to study the effect of small chain polyethylene glycols (PEG 200 and 400) on the conformation stability as well as hydration structure and dynamics of a globular serum protein human serum albumin (HSA).

Polyethylene glycol (PEG) is a highly water-soluble synthetic polymer which has extensively been used as a macromolecular crowing agent.[33-35] PEG is best modelled as a spherical particle and belongs to one of the 'modificator' groups which are essentially treated as protein structure stabilizers.[36] PEG is regarded as a flexible spherical coil in the dilute regime and in the semi dilute as well as in concentrated regime the polymers begin to penetrate one another forming a mesh-like entangled network.[33, 35, 37] PEG molecules are associated with a hydration of 20-200 water molecules which are essentially stabilized by dipole-dipole forces in the form of hydrogen bonding.[38] Large molecular weight PEGs experience predominantly repulsive interaction with proteins and induce macromolecular association and compaction in accordance to the crowding theory[39]. However, a number of studies have shown that this interaction cannot exclusively be described in terms of excluded volume alone[40, 41], rather an attractive interaction between PEG and nonpolar or hydrophobic side chains on the protein surface needs to be taken into consideration[42, 43]. Such dual behaviour of PEG to act both as a crowding agent obeying the excluded volume theory as well as being covalently or non-covalently adsorbed at the protein surface seems intriguing. PEGs of higher molecular weights (e.g., M_w 8000, 10000) stabilize the native compact structure of HSA; the interaction between these polymers and HSA is thermodynamically unfavourable and becomes even more unfavourable for the denatured protein[22], PEG 3500 has been found to bind HSA non-specifically and induces its conformational change at high PEG concentration[44]. On the other hand, higher molecular weight PEGs (M_w 6000, 10000) have been found to stabilize the unfolded state of lysozyme and consequently reduce the unfolding temperature of the protein[21] whereas they offer only marginal effect on the thermal denaturation of ribonuclease.[45] Most of these previous studies involve high molecular weight (M_w>1000) PEGs and the role of PEG in modifying protein stabilization either in the form of

an osmolyte or as a ligand has not explicitly been addressed. A systematic and thorough understanding of the way small chain PEG molecules interact with proteins is still demanded. Recently Knowles et al.[46] have studied the concentration dependent effect of PEGs with varying chain length (starting from the monomer) on intramolecular hairpin and intermolecular duplex DNA formation. The stability of the formation is found to be dependent on two factors, namely, the excluded volume and the preferential interaction. The authors reported that for the large PEGs the later factor has a positive stabilizing effect whereas the former one offers a less destabilizing effect compared to the smaller PEGs. Interestingly the destabilization to stabilization transition shows a threshold for PEG 200 and 400. This prompted us to carry out the present investigation with these two small chain PEGs, namely PEG 200 and PEG 400 to understand their effect on the stability of HSA. The structure of the protein in the presence of PEG has been studied using far-UV circular dichroism (CD) spectroscopy. Static hydration at the surface of the protein has been analyzed using high precision densimetry and sound velocity measurements. Temperature induced unfolding of the protein in the presence of the polymer has been studied using CD, fluorescence spectroscopic technique and the corresponding energetics are measured using differential scanning calorimetry (DSC) technique. Here we have further addressed the question how the hydration dynamics, especially in the collective network structure at the protein surface is affected in presence of the small chain PEG molecules around the critical concentration. To address this issue we have investigated the hydration behaviour of HSA in presence of short chain PEGs using far-infrared (FIR) FTIR and fluorescence spectroscopy, while the hydration dynamics has been explored using THz time domain spectroscopy. The elusive spectral range of THz has proven to be an important tool to study hydration dynamics around biomolecules.[47-51] This technique is sensitive to the subtle changes of these vibrational modes of water which can extend up to several layers beyond the solute surface.[52] In order to compare the behaviour of PEG 200 and 400 we study the effect of two other otherwise indifferent or moderately protein stabilizing crowding agents sucrose and PEG 10000.

4.2. Materials and Methods

HSA (Human serum albumin), and poly ethylene glycols (PEG 200, PEG 400, PEG 10000), sucrose and L- tryptophan were purchased from Sigma-Aldrich with a purity of ~99%. All the chemicals were used without further purification. All aqueous solutions were prepared in sodium phosphate buffer (50 mM) at pH 7.0 and used after filtration with syring-driven filter (Millex) of diameter 0.22 μm. For far-UV CD measurements the protein concentration was

fixed at 2 μM. For near-UV CD and volumetric study 30 μM protein was used, while for DSC and DLS measurements 20 μM protein solution was used. For fluorescence measurements it was fixed at 1 μM.

We have used following instruments and methods (for details see chapters 2, 3). Protein structure was measured by the *CD spectroscopy*. Volume and compressibility of HSA solution in the absence and in the presence of PEG were calculated using the density and sound velocity data obtained with a high precision *density meter*. The hydrodynamic diameter of HSA was detected by *Dynamic Light Scattering (DLS)*. To probe the local environment *fluorescence* measurements were done by both *steady state* and *time resolved* experiments. During time resolved fluorescence study 299 nm LED was used for excitation and found 480 ps instrument response function (IRF). The decay profile is fitted with a multi-exponential equation using F900 software provided by Edinburgh Instruments. Thermal stability of the protein was studied by *Differential scanning calorimeter (DSC).*After buffer or buffer-PEG solution subtraction and base line adjustments, the DSC thermograms of HSA in buffer or buffer-PEG solutions depicting the excess heat capacity vs. temperature were analyzed using Origin 7.0 software. The data obtained from the DSC measurements is of analysis of a non-two state model. The area under the experimental heat capacity (C_p) curve was used to determine the calorimetric transition enthalpy (ΔH_{cal}) given by the relation: $\Delta H_{cal} = \int C_p \, dT$, where T is the temperature in Kelvin. This calorimetrically determined enthalpy is model-independent and is thus unrelated to the nature of the transition. The temperature at which excess heat capacity is maximum defines the transition temperature (T_m). The model-dependent van't Hoff enthalpy (ΔH_{vh}) was obtained as,

$$\Delta H_{vh}(T_m) = 4RT_m^2 \frac{\Delta C_p(T_m)}{\Delta H_{cal}} \qquad (4.1)$$

where $\Delta C_p(T_m)$ is the height of the heat absorption peak at the midpoint (T_m) of the transition[53, 54]. The entropy change (ΔS) for the unfolding process is obtained using the relation, $\Delta S = \int \frac{\Delta C_p}{T} dT$.

To study the collective hydration we used the *FTIR spectra* (FIR regime) and *THz (TTDS* and *p-Ge THz*) spectroscopy. We employed a Debye model[55-57] to describe the dynamics of water molecules in PEG solutions. The details of the Debye fitting model are described in Chapter 2. In the p-Ge (p-germanium) difference spectrometer measurements the

THz radiation source used is a high-power (1 W) p-Ge laser.[58] The change of THz absorption of the samples compared to that of the reference was deduced. In order to obtain the hydration dynamics of PEG we measure the difference absorbance of PEG 200 and 400 solutions at different concentrations ($\Delta\alpha = \alpha_{(buffer+PEG)} - \alpha_{buffer}$). The net change in the absorption coefficient of the protein solutions compared to the respective buffers is obtained as:

$$\Delta\Delta\alpha = \Delta\alpha_{(buffer+PEG+HSA)} - \Delta\alpha \qquad (4.2)$$

where $\Delta\alpha_{(buffer+PEG+HSA)} = \alpha_{(buffer+HSA+PEG)} - \alpha_{buffer}$.

4.3. Results and Discussion

4.3.I. Effect of Short Chain Polyethylene Glycols on the Structure & Thermal Unfolding of Human Serum Albumin

CD Measurements:

Far-UV CD measurements of HSA in the range of 200-260 nm are shown in figure 4.3.I.1.(a). At 20^0C the protein retains its native structure in the buffer with two characteristic negative peaks at 208 and 222 nm. The protein is mostly constituted of α-helix (67.1%) with smaller contributions of other secondary structures like random coils, β-turn etc.[44, 59, 60] As PEG 400 is added into the protein solution the negative signal increases gradually up to a concentration of 30% (v/v) and further addition of PEG (up to 50%) does not effectively change the spectrum. The corresponding α-helical content increases up to ~71% with fractional changes in the other secondary structural components. A similar trend is also observed for PEG 200. Earlier studies of HSA using high molecular weight PEGs exhibited a steady decrease in the α-helical content with increasing

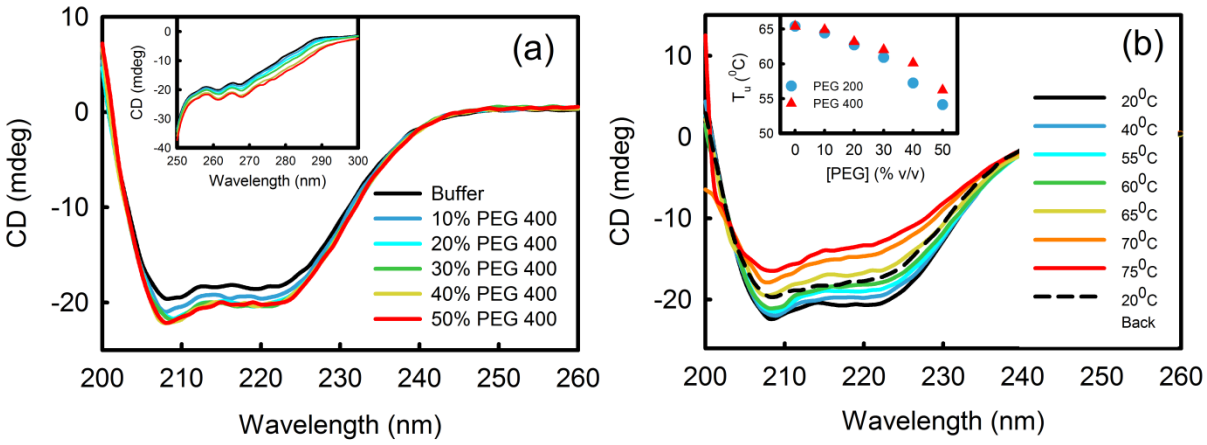

Figure 4.3.I.1. (a) Far UV CD spectra of HSA in 50 mM phosphate buffer at different concentrations of PEG 400. The inset shows the corresponding near-UV spectra. (b) Temperature dependent CD spectra of HSA in 30% (v/v) PEG 400 solution. The inset figure represents the unfolding temperature (T_u) as observed from the CD signal of HSA measured at 222 nm as a function of PEG concentrations.

PEG concentration[22, 44], whereas in a separate study with a globular protein concanavalin A with lower molecular weight PEG, a marginal effect was reported up to 30% PEG concentration, beyond which there occurred a significant loss in the secondary structure[61]. The observed increase in the α-helical content in the present investigation suggests the formation of a more compact structure which perhaps renders a greater stability to the native protein structure as a result of the addition of the crowding agent. CD spectrum in the near-UV region (between 250 and 300 nm wavelength) probes the asymmetry of a protein's aromatic amino acid environment[62, 63]. The Near-UV CD spectrum of HSA at 20^{0}C reveals two distinct peaks at 262 and 268 nm along with a shoulder ~290 nm (figure 1a, inset). With gradual addition of PEG 400 all these spectral features remain intact, with a steady increase of negative signals indicating the protein to become more folded with increase in PEG concentration. A similar trend has also been observed in case of PEG 200. The absence of any drastic change in both the CD signals strongly suggests that both the secondary as well as the tertiary structure of HSA suffers only subtle modifications towards higher folded states upon addition of PEG.

DLS Measurements:

Hydrodynamic diameter of the protein in buffer and at different PEG concentrations is measured using DLS technique (Figure 4.3.I.2a). HSA is a globular protein with a hydrodynamic diameter of ~10 nm in aqueous solution[60]. Considering a hydration shell of ~5 Å thickness this value is in good agreement with the crystal structure[59, 64]. As observed from

figure 4.3.I.2a, the size of the protein does not undergo substantial modification with a marginal decrease in size up to 20% PEG concentration, which is corroborated with the increased compaction of the protein as evidenced from the CD measurements (figure 4.3.I.1a).

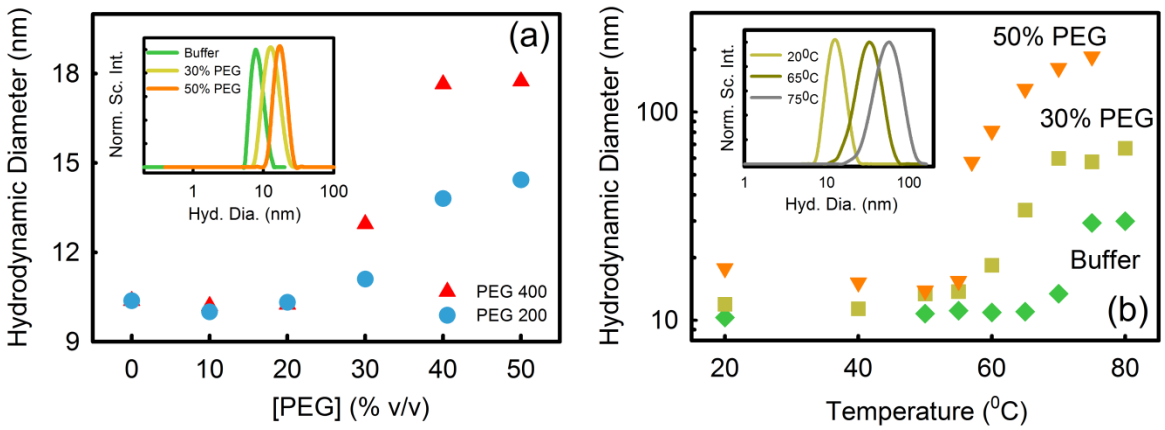

Figure 4.3.I.2. (a) Hydrodynamic diameter of HSA in presence of PEG of different concentrations. The inset shows a representative scattering intensity distribution of HSA in buffer and different PEG concentrations. (b) Hydrodynamic diameter of HSA in presence of PEG 400 of different concentrations as a function of temperature. The inset shows a representative scattering intensity distribution of HSA in 30% (v/v) PEG at 20^0C, 65^0C and 75^0C.

With further increase in the PEG concentration the size increases considerably, with an effect more prominent in case of PEG 400. CD studies have provided evidence that both the secondary and tertiary structures of the protein do not suffer adverse modification upon the addition of PEG. So no apparent swelling or denaturation of the protein can be envisaged at higher PEG concentrations. A probable reason for the observed increase in size might be the association of the PEG molecules at the protein surface, a phenomenon reported earlier in which ligands bind at the protein surface without effectively perturbing the CD signals.[65]

Densimetry Measurements:

An easy and convenient way to study the intermolecular interaction in a protein is to measure the apparent specific volume (ϕ_v) and apparent compressibility (ϕ_k) which are the two very important macroscopic observations particularly sensitive to the hydration properties of solvent exposed amino acids, as well as to the structure and conformational properties of the solvent inaccessible protein interior.[66-68] ϕ_v and ϕ_k of HSA are measured in the absence and in the presence of different concentrations of PEG and representative results with PEG 400 are depicted in figure 4.3.I.3. The partial specific volume (ϕ_v) of PEG solution is ~9×10^{-4} m^3 kg^{-1}

remains almost constant with the concentration of PEG in solution. The observed values of ϕ_v and ϕ_k for HSA in buffer are found to be in good agreement with those reported in earlier studies[67]. With increasing PEG concentration ϕ_v increases gradually up to 30% PEG, beyond which it starts decreasing. A similar trend is also observed in the ϕ_k profile. The present trend of increasing ϕ_v and ϕ_k up to certain PEG concentration is consistent with our previous study in which an increase in ϕ_v and ϕ_k were observed upon addition of PEG 400 into α-chymotrypsin[29]. It is worth mentioning here that both ϕ_v and ϕ_k values for PEG-water mixture do not change appreciably with increasing PEG concentration[69]. The partial molar volume (V^0) of a protein is a sum of two different contributions[67, 70],

$$V^0 = V_{int} + V_h \qquad (4.3)$$

where the V_h is the change in the volume of solvent due to hydration and V_{int} is the specific intrinsic volume which is the sum of two contributions, namely the intrinsic molar volume of the protein (V_m) which water cannot penetrate and the 'thermal volume' (V_T) which corresponds to the void volume due to imperfect packing of the protein. The V_{int} term usually contributes a positive share towards V^0 whereas the contribution of the V_h term towards the total molar volume is usually negative. The initial increase in ϕ_v is attributed to a decrease in the V_h contribution due to the dehydration of the protein surface. CD measurements have concluded a gradual increase in the α-helix content with PEG addition which corresponds to a more compact structure and correspondingly a partial dehydration at the protein surface, corroborating the observed change in ϕ_v. The sharp decrease in ϕ_v beyond 30% PEG is striking, as it suggests a drastic change in the hydration structure at the protein surface. The observed decrease in volume might have the following reasons[70]: higher hydration of the charged and polar groups, or, volume changes associated with the transfer of non-polar groups from hydrophobic environment to solvent water[71], or, the loss of void volume due to imperfect packing in the protein interior. As observed from the CD measurements, the tertiary and quaternary structures of the protein do not suffer any major change even at 50% PEG concentration. Consequently, a drastic change in the void volume can safely be ruled out. The direct interaction of the protein surface with PEG might modify the V_h which produces the overall decrease in ϕ_v.

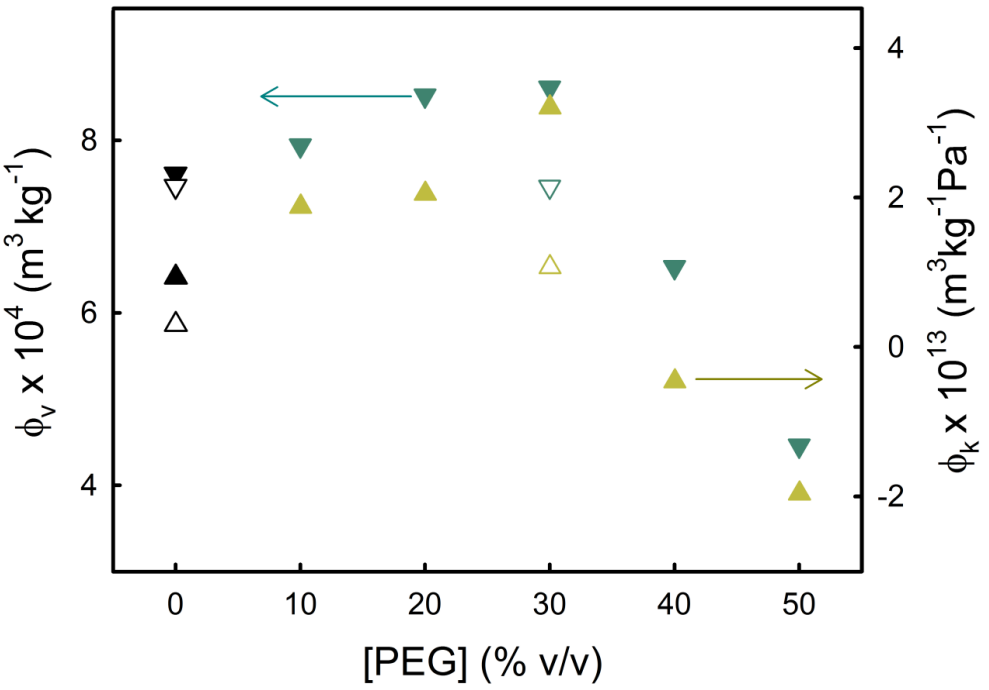

Figure : 4.3.I.3. The apparent specific volume (ϕ_v, down triangle) and partial apparent adiabatic compressibility (ϕ_k, up triangle) of HSA at different concentration of PEG 400 at 20^0C.

ϕ_k also gets a positive intrinsic contribution (k_{int}) and a negative hydration contribution (k_h)[66, 72] with k_{int} usually predominating over k_h.[73] The intrinsic contribution corresponds to the compressible atomic contacts due to imperfect packing in the solvent-inaccessible interior of proteins while the hydration contribution corresponds to the difference in the compressibility between water in the hydration shell and in bulk.[70] ϕ_k value of HSA increases with increasing PEG content revealing a positive contribution emanating as a result of the compaction of the protein structure coupled with a less negative k_h contribution due to the partial dehydration of the protein surface. Beyond 30% PEG, ϕ_k decreases sharply and acquires a negative value, indicating either to the loss of imperfect packing as well as exposure of a large number of amino acid residues to water[74] and/or compressible inter-atomic contacts in the protein to be replaced by atomic group-water contacts in the unfolded proteins.[75] As evidenced from the CD data k_{int} is not expected to change much. Thus the major negative contribution eventually comes from the k_h term as a result of direct interaction of PEG with the amino acid residues as has also been observed during the volumetric changes.

Fluorescence Measurements:

The intrinsic fluorescence profile is an excellent parameter to monitor the polarity of the Trp environment in the protein and is sensitive to the protein conformation[76]. We measure the emission from Trp in the absence and in the presence of PEG at different concentrations and the results are depicted in figure 4.3.I.4. It is worthy to note here that PEG itself does not contribute to the emission profile in the studied wavelength range. HSA in buffer produces an emission maximum at ~350 nm, a considerably blue shifted peak with respect to that of Trp dissolved in water[77] due to the much hydrophobic exposure of Trp in the protein compared to that in bulk water[78, 79].

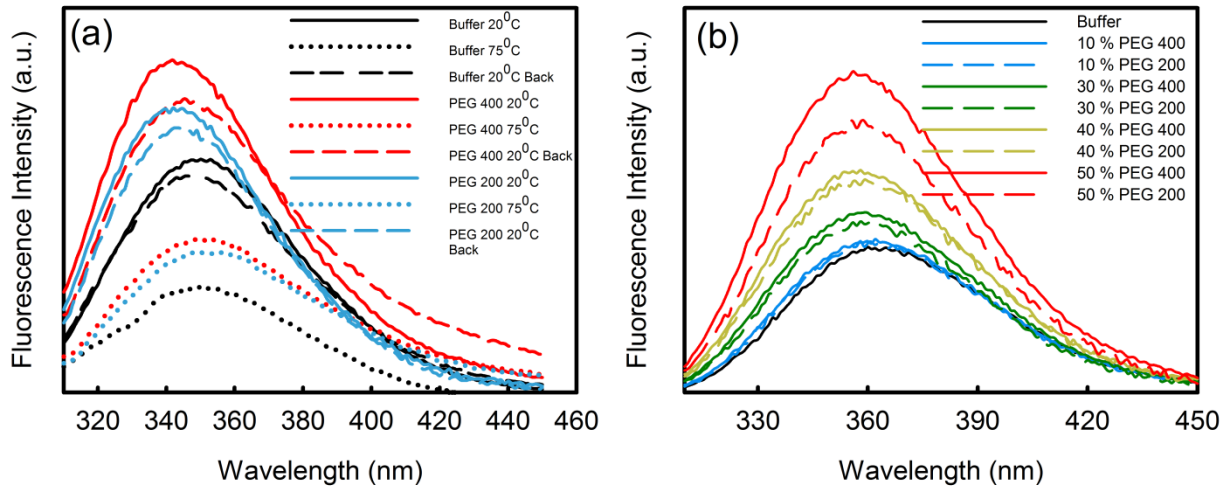

Figure 4.3.I.4. (a) Temperature dependent tryptophan fluorescence emission spectra of HSA (excited at 299 nm) in buffer and in different PEGs (at 30% concentration). (b) Emission spectra of tryptophan in buffer in presence of PEG 200 and PEG 400.

With the addition of PEG, the emission of Trp suffers a further blue shift, more prominently beyond 30% PEG with a concomitant increase in the fluorescence intensity. The observed blue shift of the emission profile is indicative of the relocation of the Trp moiety to a more hydrophobic environment compared to the native protein molecule. This observation is strengthened with the fact that Trp emission in bulk water suffers 4-5 nm blue shift on addition of PEG (figure 4.3.I.4.). Addition of PEG significantly modifies the hydration around the Trp moiety making it more compact with a greater hydrophobic exposure resulting in the observed blue shift of the emission maximum. A possible contribution of direct interaction of Trp with PEG molecules for the observed emission profile at higher PEG concentrations could also not be ruled out.

Thermal Denaturation of HSA:

Effect of temperature on HSA has previously been studied using different techniques [80-83]. One of the early studies[81] have concluded that the process follows multiple steps: native (N) → extended (E) → unfolded (U). In the extended form (E) (at ≤55°C), domains I and II move apart keeping the native conformation almost intact, whereas in the unfolded state (U) domain II starts to melt, disrupting the secondary and tertiary structure of the protein. The N→E transition is reversible whereas for the E→U transition the native state could not be retrieved upon decreasing the temperature. We measure the CD spectra of HSA in the absence and in the presence of PEG at different temperatures and it is found that in buffer the α-helical content decreases from 67% at 20^0C to 48% at 75^0C, which then recovers to 62% as the system is cooled down to 20^0C. Figure 4.3.I.1b depicts the temperature dependent CD spectra of HSA in presence of 30% PEG 400. It is observed that with increasing temperature, the secondary structure of the protein suffers considerable damage, signifying the onset of an unfolding process. The calculated α-helical content decreases from 71% at 20^0C to 50% at 75^0C, recovering to 63% at 20^0C upon refolding. Similar trend is also obtained with PEG 200. The refolding behaviour in the presence of small chain PEGs remains irreversible as that in the buffer solution. A similar irreversibility is also observed in the compressibility measurements in which ϕ_v and ϕ_k values do not retrieve the unfolding pathway. The phenomenon of thermal denaturation can more comprehensively be understood by considering a two state transition between the native and the unfolded states[74], and the corresponding equilibrium constant for the unfolding process (K_u) can analytically be expressed as,

$$K_u = \frac{Fraction\ of\ the\ unfolded\ protein}{Fraction\ of\ the\ native\ protein} \qquad (4.4)$$

where these fractions are related to the ellipticities for the unfolded ($[\theta]_u$) and native ($[\theta]_n$) states[74]. We estimate the native fraction of the protein as a function of temperature by measuring the CD signal at 222 nm at different temperatures and a representative illustration for PEG 200 at different concentrations is shown in figure 4.3.I.5.

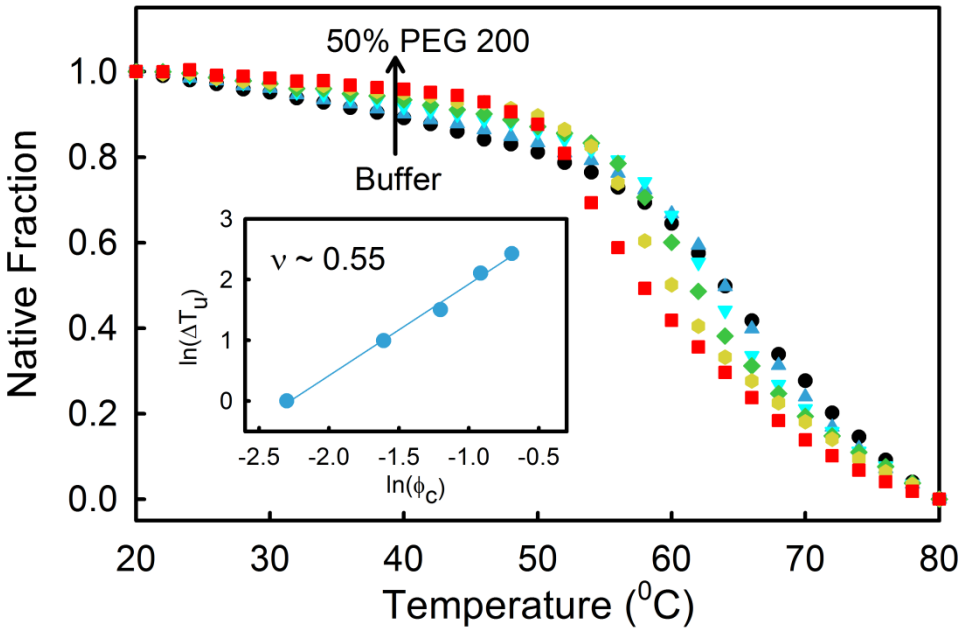

Figure 4.3.I.5. Temperature dependence of the native fraction of HSA as determined by CD measurements in presence of different concentrations of PEG 200. The corresponding plot for $\ln(\phi_c)$ vs. $\ln(\Delta T_u)$ is shown in the inset. The solid line corresponds to a linear fit.

The transition temperature at which the protein starts unfolding (T_u) has been estimated from the first derivative plot of the CD signal (at 222 nm wavelength) as a function of temperature and the obtained T_u values are plotted as a function of PEG concentration (figure 4.3.I.1b, inset). The unfolding temperature decreases with increasing PEG concentration, revealing that in presence of PEG the protein is more prone towards thermal denaturation.

Temperature dependent DLS measurements are shown in figure 4.3.I.2b. It can be observed that the size of the protein in buffer does not suffer considerable change up to 65^{0}C, and on further increase in temperature the size increases sharply indicating to an onset of the unfolding process.[84] In presence of PEG, the onset of the increase in the hydrodynamic size of the protein occurs at a lower temperature compared to that in buffer, and the considerable increase in the size clearly indicates a definite interaction of the unfolded protein with the polymer, which in turn stabilizes the unfolded protein and thereby decreasing the unfolding temperature as evidenced in CD and DSC measurements.

The temperature dependent unfolding of HSA has also been monitored using the intrinsic fluorophore Trp [figure 4.3.I.4.(a)]. In absence of any crowding agent, the emission of the unfolded HSA shows ~4 nm blue shift of the emission peak coupled with a decrease in the emission intensity.[49] A probable explanation for the observed blue shift could be brought

forward as: in the thermally unfolded HSA the Trp214 residue finds itself in a more hydrophobic environment compared to the native structure due to the exposure of the hydrophobic moieties to the protein surface[49]. In case of 30% PEG 400, however, a distinct 8-9 nm red shift of the emission peak is observed at elevated temperature and when the temperature is reverted back to 20^0C, the peak position retrieves to its native value with decreased intensity (figure 4.3.I.4a). A similar trend is also observed for PEG 200. The effect of PEG thus seems strikingly different relative to that in the buffer. As a control experiment we obtain the fluorescence spectra of bare Trp in PEG solutions; it has been found that addition of PEG itself induces a considerable blue shift in the room temperature emission spectra of Trp both in water and in protein (figure 4.3.I.4a). Thus the apparently opposite behaviour in PEG solution can be rationalized as: in buffer, the thermally unfolded protein finds its Trp moiety exposed towards more hydrophobic environment causing the observed blue shift, whereas the observed red shift in presence of PEG infers a rather hydrophilic exposure of Trp. The temperature dependent fluorescence study thus supports a direct interaction mechanism of the PEG molecules at the protein surface at high PEG concentrations, as has also been envisaged from DLS, densimetry and DSC measurements.

DSC Measurements:

Thermal unfolding of HSA in buffer and at different PEG concentrations is measured by DSC technique and a representative C_p vs. temperature curve is shown in figure 4.3.I.6.a. The transition temperature (T_m) for HSA in buffer is found to be 67.5^0C and it decreases gradually with increasing PEG concentration (figure 4.3.I.6b), a phenomenon much in accordance with that reported from the CD experiments (figure 4.3.I.1.b). The observed decreasing trend of T_m in the presence of PEG perhaps results from a preferential interaction of PEG with the thermally unfolded forms of the protein, shifting the folding to unfolding transition towards the forward direction. Another probable reason could be an enhanced electrostatic repulsion between the polar amino acid residues as HSA becomes more compact at higher PEG concentrations making the native state energetically less stable. Such an argument gets support from the study of Spitzer and Poolman[85], who suggested that electrostatics play a major role in cells, because the intracellular surface-to-surface distance between proteins is less than the Debye screening length. Moreover, according to Miklos et al.[12] the electrostatic interaction is a cause for protein destabilization by crowding agents. The enthalpy and entropy parameters obtained from DSC measurements have been summarized in Table 4.I.1 The estimated van't

Hoff enthalpy (ΔH_{vH}) value suffers a slight decrease (from 122.5 to 103.2 kcal mol^{-1}) with increasing PEG content (figure 4.3.I.6b), which is somewhat contrary to the thermal unfolding of lysozyme in which molecular weight and content of PEG does not offer significant change in the ΔH_{vH} values[21]. The ratio of the measured calorimetric enthalpy (ΔH_{cal})

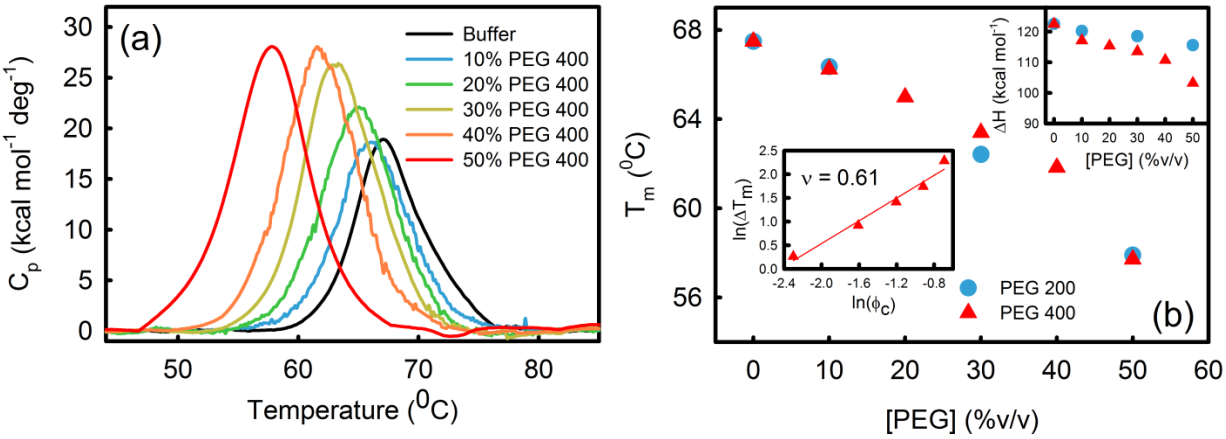

Figure 4.3.I.6. (a) C_p vs. temperature plot for HSA in buffer and different concentrations of PEG 400. (b) Melting temperature of HSA as a function of PEG concentration. The inset shows plot for $\ln(\phi_c)$ vs. $\ln(\Delta T_m)$ for PEG 400 system. The solid line is a linear fit. The corresponding van't Hoff enthalpy values are plotted as a function of PEG concentration in another inset.

and estimated van't Hoff enthalpy (ΔH_{vH}) for HSA is less than unity (Table 4.I.1) and decreases gradually with increasing PEG concentration as more than one transition states are involved for the conversion of native to unfolded states[86] indicating several domains of HSA undergo independent transitions. The progressive increment of ΔH_{cal} with increasing PEG concentration is due of the fact that more heat is required to break the additional H-bonds in the HSA-PEG aggregates. As small chain PEGs are sterically less hindered compared to the higher PEGs, the non-covalent attractive interaction plays major role during thermal unfolding. The decreasing trend in ΔH_{vH} and the increased entropy (ΔS) of unfolding with PEG concentration indicate that the hydrophobic side chains of the protein get exposed during the unfolding process to interact with the hydrophobic chains of PEG and making the free energy change more favourable. Contrary to our findings earlier studies have, however, evidenced progressive decrease in the conformational entropy in presence of crowding agents which in turn has destabilized the unfolded state making the T_m to increase[8].

The change in transition temperature on the content of crowding agent can be rationalized by using the changes in the free energy due to localization of volume[87]. The effect of macromolecular crowding on the thermal behaviour of proteins could theoretically be correlated as, $\Delta T_m \approx \chi \varphi_c^{\alpha/3}$ where ϕ_c is the volume fraction of PEG, χ is a constant and α is a parameter related to the Flory exponent (ν) according to the relation, $\nu = \frac{1}{\alpha} + \frac{1}{3}$ [5, 7, 8]. We plot $\ln(\Delta T_m)$ as a function of $\ln(\phi_c)$ and good linear fits are obtained (figure 4.3.I.6b) from which the value of the Flory exponent has been calculated to be 0.61. This value is in good agreement with those obtained for thermal denaturation of ubiquitin[7] and calcium binding protein (RC_L)[8] in the presence of Ficoll 70. A similar plot with the T_u data obtained from CD measurements (figure 4.3.I.5) offers a marginally smaller Flory exponent (ν=0.55). The difference in the estimated value of ν lies on the fact that the transition temperature estimated in CD measurements is more of a local origin (estimated as the change in the CD signal at 222 nm) compared to the global character of DCS measurements. However, the estimated ν values are well in accordance with the random coil conformation of the unfolded protein over an elongated coil structure[8]. The nonlinear behaviour of the unfolding process as a function of the concentration of the crowding agent affirms the possibility that the volume exclusion model is not solely responsible for the observed destabilization of the protein for the thermal unfolding process, rather the molecular interaction of the crowding agent with the protein surface should be taken into consideration.

Earlier studies have concluded that addition of high molecular weight PEG retards the thermal denaturation of DNase I[34], addition of Ficoll 70 increases the unfolding temperature of α/β flavodoxin[9] and apo-flavodoxin[6], while a recent study has revealed that addition of PEG 2000 significantly destabilizes the thermal stability of human α-lactalbumin (HLA).[88] On the other hand, small molecule like trimethylamine N-oxide (TMAO) has been reported to stabilize the native structure of proteins against urea denaturation.[89, 90] The group of G.D. Rose[91, 92] have introduced a molecular mechanism for the effect of both protecting and denaturing osmolytes (TMAO, betaine, sucrose, proline, urea etc.) on the stability of proteins. Extensive thermodynamics studies by the group of W. Bolen has shown that protecting osmolytes are preferentially excluded from the immediate vicinity of the protein surface, and this exclusion implies a solvophobic interaction between groups on the protein surface and the protecting osmolyte species.[93-95] The effect of several small and large molecular weight osmolytes on the biomolecular stability has theoretically been investigated by the group of

Record et al.[46, 96, 97] However, the exact mechanism of the stabilization (whether direct or indirect interaction) has not yet properly been understood for small polymer which also behaves as osmolyte.[98] Thus, it stands argumentative to predict on the thermal stability of a protein as a function of the crowding agents. Interaction of PEG with proteins can be described in the form of an optimization between two competing factors: the repulsive excluded volume interaction between PEG and protein (PEG acts as an inert osmolyte) and a direct attractive interaction (PEG non-specifically binds to the protein).[26] The first factor stabilizes the protein while a predominant non-specific interaction between PEG and protein exceeding the repulsive excluded volume interaction decreases the structural stability of the protein. It may be noted here that the unfolding of HSA is primarily a helix to random coil transition in which the random coil content increases by ~45% relative to the native state upon heating up to 70^0C. This observation is strongly corroborated from the measured Flory exponent values. In presence of PEG 400, the helix to coil transition occurs at a lower temperature and at 70^0C the random coil content is increased by ~72% compared to the native state. Addition of 30% PEG 400 increases the α-helix content of the native protein by ~6% compared to that in the buffer at the expense of the random coil content in order to stabilize the native protein, a phenomenon much anticipated for crowding agents in accordance to the 'volume exclusion principle'. However, upon unfolding the random coil structure gets stabilized due to strong interaction of the exposed hydrophobic moiety of the protein with the small PEG molecules at the protein surface and thereby facilitating the unfolding process. In presence of PEG 400, ~73% of the random coil recovers into the helical conformation upon refolding compared to ~86% recovery in case of the buffer. It thus stands pertained that stabilization of the native state of a protein in the potential energy surface by excluded volume model is not the sole parameter that governs the thermal unfolding phenomenon as the stabilization of the unfolded state also plays a decisive role in shifting the native to unfolded transition.

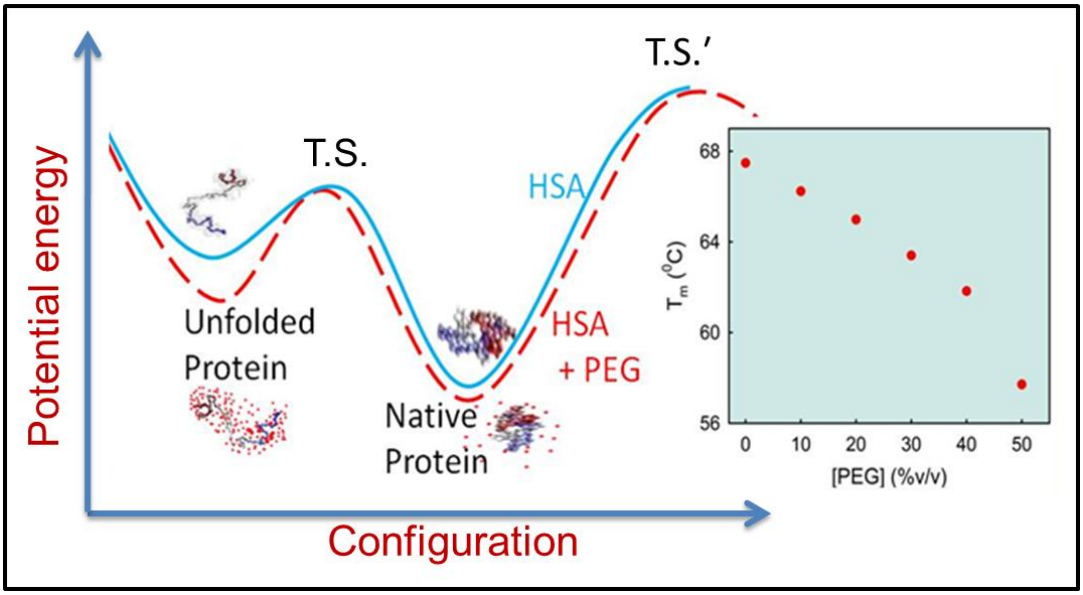

Scheme 4.3.I.1. A model to represent (not to the scale) the potential energy of native and denatured state of HSA in absence and in presence of the short chain PEGs.

Table 4.3.I. Thermodynamic parameters obtained from DSC during thermal denaturation of HSA in absence and presence of PEG 200 and PEG 400

System	T_u (1) (^{0}C)	T_m (2) (^{0}C)	ΔH_{cal} (kcal mol^{-1})	ΔH_{vH} (kcal mol^{-1})	ΔH_{VH} /ΔH_{cal}	ΔS_{Tm} (kcal mol^{-1} ^{0}C^{-1})
Buffer	65.4	67.5	137.5±0.6	122.5±0.7	0.89	2.04
PEG 200						
10%	64.4	66.4	140.5±0.8	120.2±0.8	0.85	2.12
20%	62.7	-	-	-	-	-
30%	60.9	62.4	196.3±0.5	118.5±0.4	0.60	3.15
40%	57.2	-	-	-	-	-
50%	54.1	57.9	226.8±1.0	115.6±0.6	0.51	3.93
PEG 400						
10%	64.9	66.2	144.8±0.3	117.1±0.3	0.81	2.19
20%	63.2	65.0	174.3±0.4	115.4±0.4	0.66	2.69
30%	62.0	63.4	210.6±0.6	113.5±0.4	0.54	3.33
40%	60.1	61.8	222.5±0.4	110.7±0.2	0.50	3.61
50%	56.2	57.7	234.8±0.7	103.2±0.4	0.44	4.08

(1) from CD measurements. (2) from DSC measurements.

4.3.II. Effect of Short Chain Polyethyleneglycols on the Hydration Structure and Dynamics around Human Serum Albumin

FIR-FTIR Measurements:

In order to understand whether the interaction of PEG with the protein surface modifies its collective hydration network we measure the FIR (30-450 cm^{-1}) FTIR spectra of hydrated HSA in presence of PEGs. The results are depicted in figure 4.3.II.2. In this frequency window water produces two characteristic peaks, one in the ~200 cm^{-1} region which is distinctly collective in nature and corresponds to the hindered longitudinal motion of water molecules along hydrogen bonds, while the other one appears at a higher frequency ~600 cm^{-1} which emanates from their librational (hindered rotational) modes.[52, 99-101] When we plot the FIR spectra of buffer and HSA at different concentrations in figure 4.3.II.1a, we observe a marginal decrease of absorption with increasing HSA concentration. Thus we conclude that the changes upon addition of HSA are below the detection limit of the FTIR spectrometer. In contrast, upon addition of PEG 400, we find a substantial change in the absorption, i.e. a considerable decrease in the intensity and a blue shift of the 200 cm^{-1} peak (figure 4.3.II.1b). PEG is found to have lower absorbance than water and produces an absorption band at ~225 cm^{-1}. The progressive blue shift of the 200 cm^{-1} band in the water- PEG mixture clearly indicates an influence on the hydrogen bond network in water.

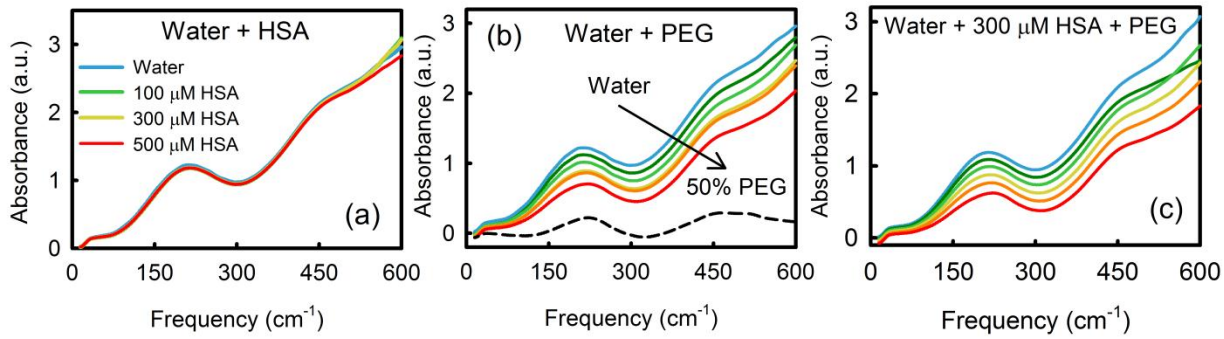

Figure 4.3.II.1. (a) FIR-FTIR of water and HSA at different concentrations. (b) FIR-FTIR of PEG 400 at different concentration. The absorption spectrum of pure PEG 400 is shown as a broken line. (c) FIR-FTIR of HSA in presence of different concentrations of PEG 400.

In figure 4.3.II.2a we plot the absorbance of 0.5 mM HSA-buffer solution in absence and in presence of 30% and 50% PEG 400. It can clearly be noticed that the change is small in 30% PEG solution while it is significant in 50% PEG. To exclude the contribution of the PEG

hydration from the observed spectra we calculate the difference absorbance (figure 4.3.II.2b) in which the spectrum of PEG solution is subtracted from that of HAS in presence of PEG (Diff. Abs. = Absorbance of solution with HSA – Absorbance of solution without HSA).

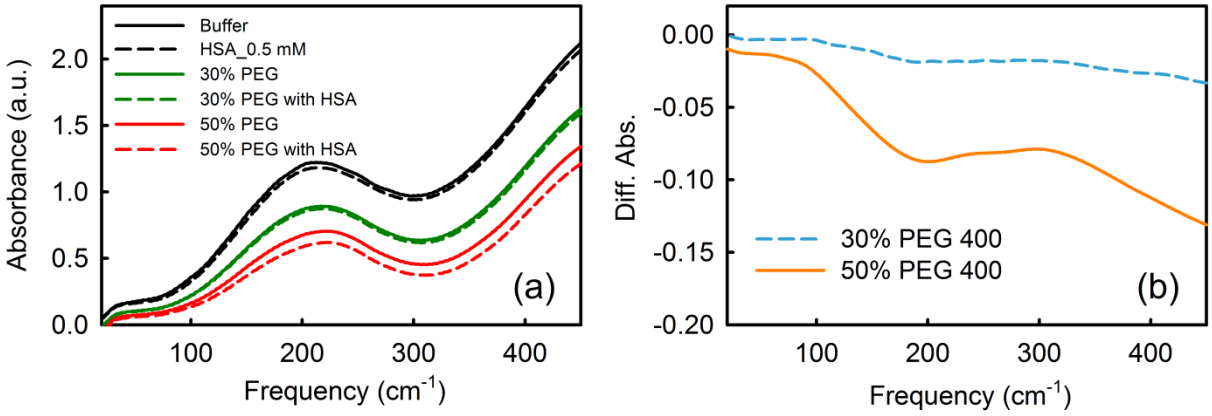

Figure 4.3.II.2. (a) FIR-FTIR absorbance spectra of the buffer, 30% and 50% PEG 400 in absence and in presence of 0.5 mM HSA. (b) Difference absorbance between the solution with0.5 mM HSA and without HSA.

This gives a precise idea of the changes in the absorbance of HSA hydration layer caused by the presence of PEG. It is distinctly evident from the figure that the change is nominal in case of 30% PEG, whereas considerable change is obtained in case of 50% PEG, especially in the 200 cm^{-1} region. This observation supports the conclusion derived from earlier acoustic measurements that a substantial modification of hydration structure at the HSA surface takes place at a high PEG concentration. The decrease in the intensity in the 200 cm^{-1}range indicates that the collective vibrational modes of the hydrogen bonded network of water associated at the HSA surface are affected, which is a manifestation of a direct interaction and/or overlap of PEG and protein hydration layers. A rough estimate of the dehydration at the HSA surface in presence of 30 % PEG can be made from the densimetric data reported in the previous study. The change in $\Delta\phi_v$ (apparent specific volume) can be written as:[67]

$$\Delta\phi_v = \Delta n_h\left(\frac{\bar{V}_h - \bar{V}_0}{M}\right) \qquad (4.5)$$

where, Δn_h is the change in hydration number at the protein surface, M is the molecular weight of the protein, $\bar{V}_h$and $\bar{V}_0$ are the partial molar volumes of water in the hydration shell and in the bulk, respectively. Considering $\bar{V}_h$~11$cm^3 \cdot mol^{-1}$ [102] we estimate a loss of ~950 and 1100 water molecules from the protein surface upon addition of the critical amount (30%) of PEG 200 and 400, respectively. Assuming a monolayer of closely packed hydration around the protein surface this number accounts for ~25% of the hydration shell.

Fluorescence Anisotropy and Lifetime Measurements:

The intrinsic fluorophore Trp214 has extensively been used to extract site specific information of domain IIA of HSA.[103, 104] We have measured the steady state anisotropy (r) (details in Chapter 2), which is a measure of the average angular displacement of a fluorophore in a solvent following the excitation, of HSA and free Trp in different PEG solutions. Figure 4.3.II.3b shows that the anisotropy of free Trp increases linearly with increasing PEG concentration. Anisotropy depends on the viscosity of the solvent as experienced by a fluorophore[76] and the observed linear increase in Trp anisotropy in PEG-buffer solutions is in accordance with the increasing viscosity of the solutions.[105] The anisotropy of Trp214 in HSA is increased by a factor of five compared to the anisotropy of bare Trp in the buffer. This increase is related to the location in a hydrophobic core where the free rotation of Trp214 is considerably restricted by surrounding amino acid residues. On contrary to the water-PEG solution the anisotropy of Trp214 in HSA does not increase linearly with increasing PEG concentration, rather it suffers a marginal decrease which infers that the solvent viscosity does not affect the rotational dynamics of Trp214 as it is not exposed to PEG. We measure the lifetime of Trp in buffer and in HSA; the results are depicted in figure 4.3.II.3d. Some representative emission transients are presented in figure 4.3.II.3c. The emission decay of Trp in buffer could be fitted bi-exponentially with time constants of 0.5 ns (17%) and 3.2 ns (83%), and with an average time constant $<\tau>(= \sum_i a_i \tau_i)$ of 2.73 ns.

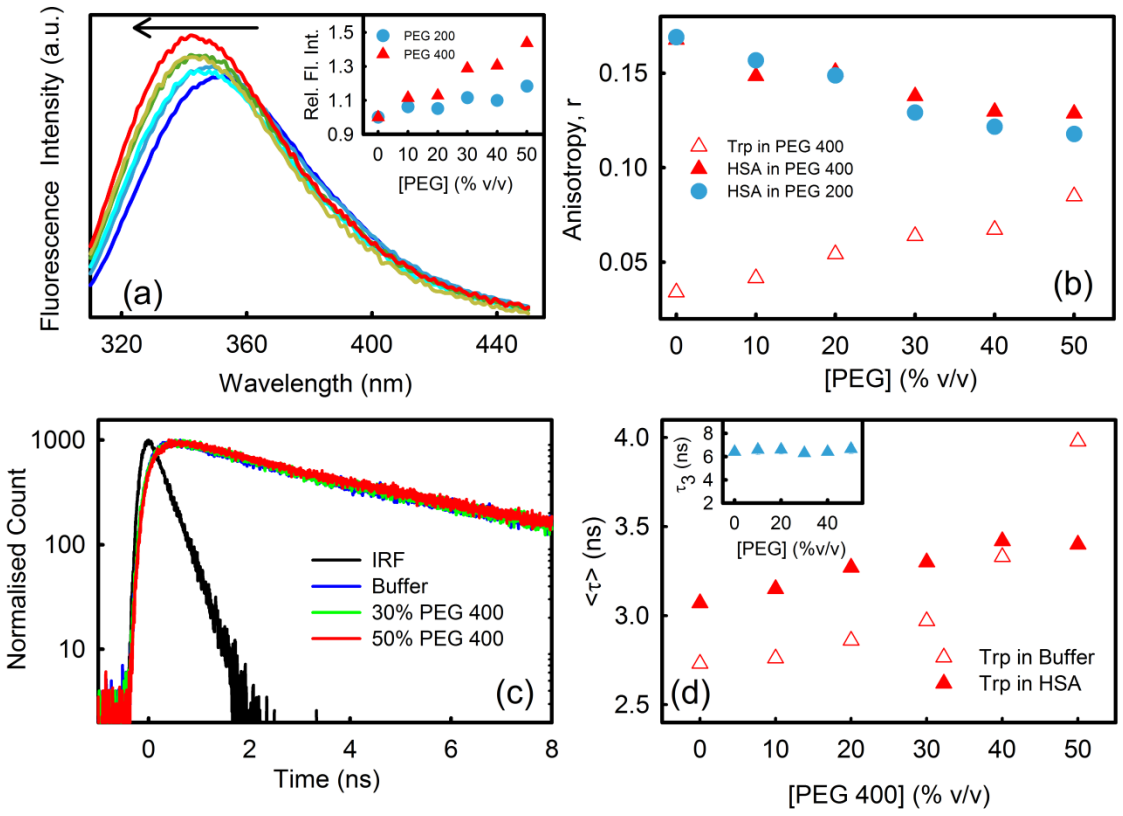

Figure 4.3.II.3. (a) Emission profile of Trp214 of HSA in buffer and in presence of PEG 400 at different concentrations. The arrow indicates increasing PEG concentration. The relative fluorescence intensity of Trp214 in HSA has been plotted in the inset as a function of PEG 200 and PEG 400 concentrations. (b) Steady state anisotropy (r) of Trp in bulk and in HSA is shown as a function of PEG concentration. (c) Temporal decay of Trp214 in HSA in absence and in presence of PEG 400. (d) Average time constant of temporal decay of Trp in buffer and Trp214 in HSA as a function of PEG 400 concentrations. The time constant τ_3 of HSA has been plotted as a function of PEG 400 concentration in the inset.

This result is in excellent agreement with that reported in earlier studies[106] and the two observed timescales originate from the two substructures formed by the tryptophan backbone in the excited state.[77] In PEG solutions, both time constants increase with increasing PEG content, c.f. in 50% PEG the time constants obtained are 1.6 ns (27%) and 4.9 ns (73%) with $\langle\tau\rangle$ of 4.0 ns (figure 4.3.II.3d). We conclude that the interaction of Trp with PEG stabilizes the excited state sub structures. In HSA, Trp emission decays more slowly and the transient could be fitted with time constants of 0.5 ns (28%), 2 ns (36%) and 6.4 ns (36%). The first two timescales are inherent to bare Trp emission while the longer timescale of ~6 ns is intrinsic for Trp in proteins and is associated with the interaction of the Trp residue and the surrounding amino acid residues present in the folded protein.[106, 107] It is interesting to observe that the average emission lifetime of Trp in HSA remains almost unchanged ($\langle\tau\rangle$ changes from 3.1-3.4 ns) in the presence of PEG, in contrast to the lifetime of Trp in buffer.

When we plot τ_3 (the time constant of Trp intrinsic to protein) as a function of PEG concentration (see the inset of figure 4.3.II.3.d), it is evident that it remains almost independent of the concentration of PEG. The time resolved fluorescence study thus excludes a direct interaction of the embedded amino acid residues with PEG.

THz Time Domain Measurements:

We study the hydration dynamics of PEG-water system using THz time domain (TTDS) measurements. TTDS probes the ps hydration dynamics around biomolecules.[57] We record the frequency dependent absorption coefficient, $\alpha(\nu)$ and refractive index, $n(\nu)$ of PEG-water systems at different PEG concentrations (figure 4.3.II.4b) and the deduced real and imaginary dielectric constants (ε_{re} and ε_{im}) are plotted in figure 4.3.II.4c.

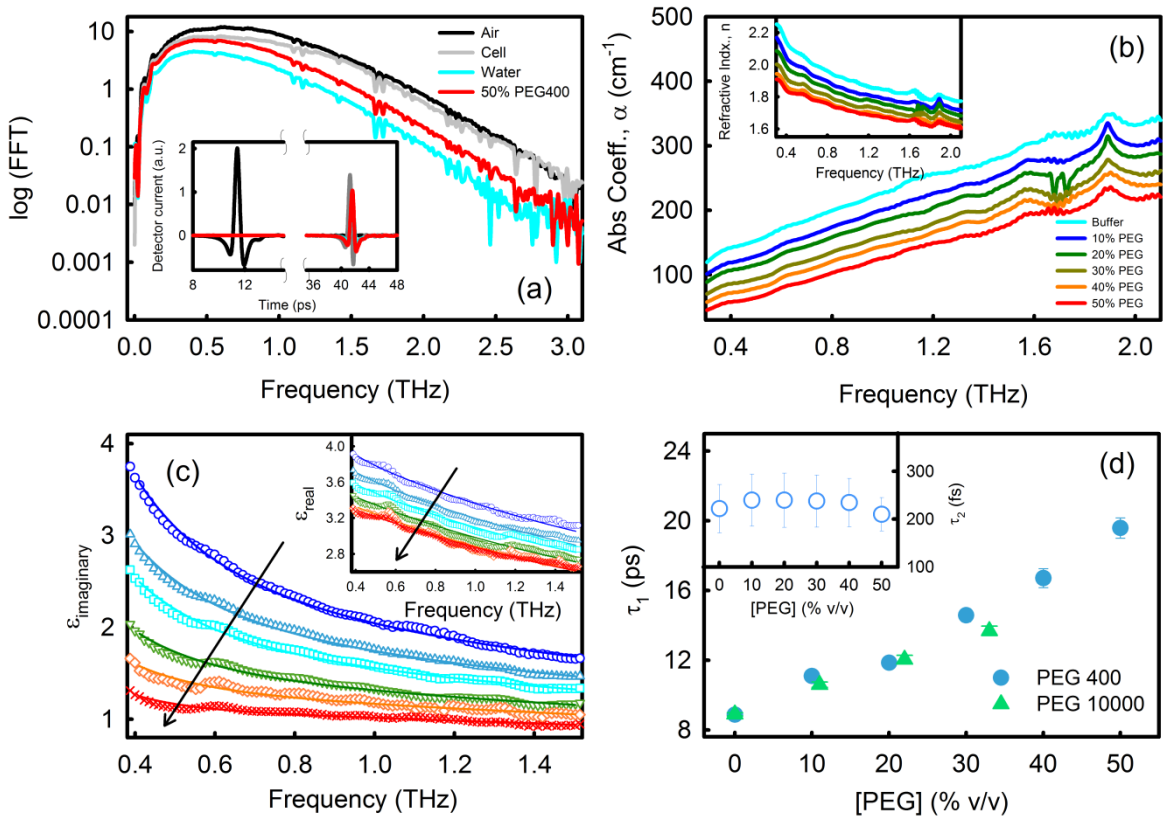

Figure 4.3.II.4. (a) Frequency domain and time domain (inset) THz signal (b) Frequency dependent THz absorption coefficient and refractive index of PEG 400 solutions. (c) Real (inset) and imaginary dielectric constant of buffer and PEG 400 solutions of concentration 10-50% (v/v) in THz frequency range. The arrow denotes increasing PEG concentration. The solid lines are multiple Debye relaxation fitting curves. (d) Debye relaxation timescales of PEG 400 and PEG 10000 solutions as a function of concentration. For PEG 10000, the concentration is given in term of w/v.

In accordance the previous studies[57, 108, 109] we deploy a triple Debye dielectric relaxation model to fit the curves (figure 4.3.II.4a), the fitted data are presented in table 4.3.II.1. In water, the Debye dielectric time constants are found to be τ_1=8.9 ps, τ_2=222 fs and τ_3=84 fs; these timescales are in excellent agreement with those reported in earlier studies.[57, 108] τ_1 and τ_2 are attributed to the cooperative rearrangement of the hydrogen bonded network and the rotational modes of individual polar water molecules, respectively[55, 110]and τ_3 is related to the 60 cm^{-1} vibrational band which is found to be associated with a concerted motion of the water molecules involving the second hydration shell.[111] As PEG is gradually added to water, τ_1 increases linearly while τ_2 changes within the experimental error limit (figure 4.3.II.4d).We reported a similar increase in τ_1 with another crowding agent, sucrose in aqueous solutions.[109] The increase in the τ_1 clearly indicates that the cooperative rearrangement of the hydrogen bonded water molecules gets restrained compared to that in bulk water as a result of the formation of structured hydration layer around PEG.

***p-Ge THz Study*:**

We measure the hydration dynamics of the extended solvation shell of HSA using a high intensity p-Ge THz laser which measures the absorption coefficient in the frequency range around 80 cm^{-1} (2.1-2.8 THz) region. This technique has previously been explored to determine the hydration dynamics around proteins and biologically important solute molecules.[47, 58, 112, 113]

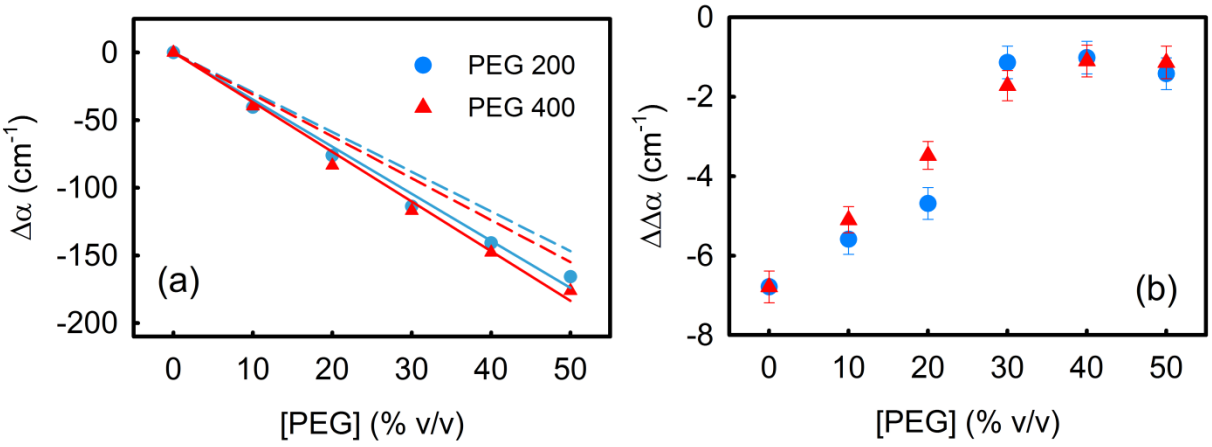

Figure 4.3.II.5. (a) Difference absorbance compared to PBS buffer of PEG-buffer solutions. The solid lines are linear fits. The broken lines represent a linear fit when neglecting further effects due to hydration of PEGs. (b) Change in the absorption coefficient of the protein solutions (0.5 mM HSA) compared to the respective buffers.

Figure 4.3.II.5 summarizes the results obtained from p-Ge measurements. We first investigate the hydration dynamics around PEG. Figure 4.3.II.5.a shows the difference absorbance of PEG 200 and 400 solutions as a function of PEG concentration. As observed from the figure, $\Delta\alpha$ decreases linearly with increasing PEG content, which is explained by the replacement of water molecules with PEG 200 or 400 which have decreased absorption coefficient compared to that of water (integrated absorption coefficients at the frequency range 2.1-2.8 THz of water, PEG 200 and PEG400: 424, 138 and 113 cm^{-1}, respectively). However, the slopes obtained from the experimental linear fits (solid lines) are found to be steeper than those obtained by considering a simple two component model involving water and PEG only (the broken lines in the figure). The experimental slopes can only be realized after considering a three component model by introducing a dynamical solvation shell around PEG having an absorption coefficient different from that of bulk water as has also been evidence from the TTDS measurements. We now consider the effect of PEG on the hydration dynamics of HSA. In order to understand the effects in a more comprehensive manner, we deduce a net change in the absorption coefficient $\Delta\Delta\alpha$ which exclusively reflects the changes in the hydration dynamics of the protein excluding the contribution in the PEG hydration (figure 4.3.II.5b). It can be noticed from the figure that at low PEG concentration, $\Delta\Delta\alpha$ increases linearly suggesting that the observed changes in the collective dynamics of protein hydration is related to the depletion of the protein hydration layer in presence of PEG with a concomitant increase in the α-helical content and the consequent compaction of the protein molecule in accordance with the 'exclusion volume principle'.[114] This also suggests that at this low PEG concentration the protein hydration can be treated separately from the PEG hydration. At the critical PEG concentration, however, the slope changes drastically, and the simple consideration of volume exclusion is insufficient to explain the behaviour.

To compare the observed perturbation of small PEGs, we study two additional crowding agents, namely sucrose and a long chain polymer, PEG 10000. The former one is known to be an indifferent additive toward proteins and sometimes stabilizes proteins to a moderate extent,[115, 116] while the later one stabilizes proteins in low concentrations.[117] We measure the CD spectra of HSA in presence of both the crowding agents (figure 4.3.II.6). It is observed that the CD signal does not suffer considerable structural changes even in the presence of 45% sucrose indicating that the protein suffers marginal perturbation in presence of sucrose. It is evident that at low concentration PEG 10000 marginally stabilizes the protein, however, at and beyond 30% PEG, the CD signal decreases drastically indicating a

considerable perturbation of HSA secondary structure. The observed loss in CD signal might originate from a PEG induced protein aggregation followed by precipitation (leading to a partial loss in the optical transparency of the solution) in presence of high concentration PEG 10000.

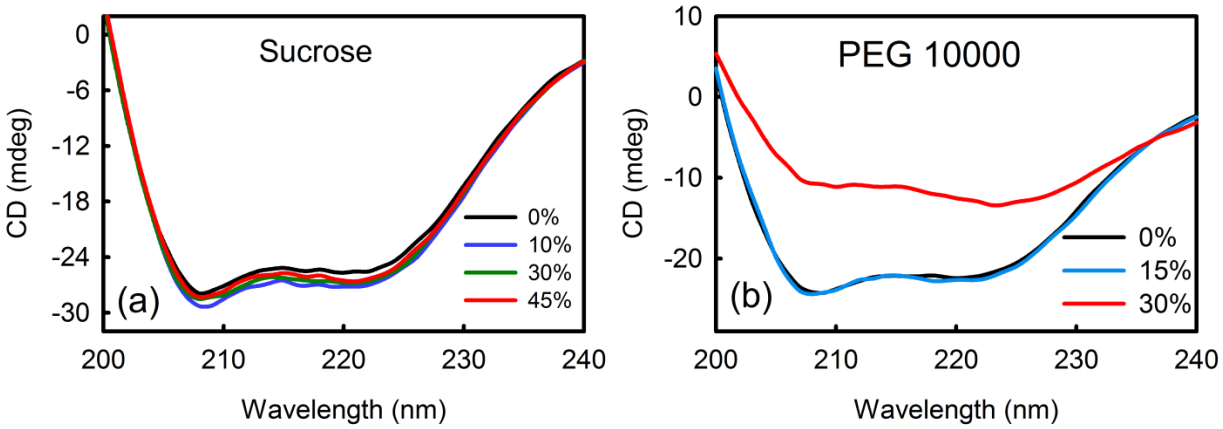

Figure 4.3.II.6. (a) Far-UV CD spectra of HSA at different concentrations of Sucrose. (b) Far-UV CD spectra of HSA at different concentrations of PEG 10000.

We study the dielectric relaxation of both these co-solutes using the TTDS measurements. In comparable agreement to PEG 400, both sucrose[109] and PEG 10000 (figure 4.3.II.7) show a near linear increase in the cooperative H-bond exchange dynamics (manifested by the time scale τ_1 in figure 4.3.II.4) which identifies the formation of structured water around these solutes. It is now interesting to study how these two crowders modulate the collective hydration dynamics around HSA in comparison to that of PEG 400. Figure 4.3.II.7 describes the p-Ge THz measurements of HSA in presence of sucrose and PEG 10000. As evident from the inset of figure 4.3.II.7, $\Delta\alpha$ of sucrose solution decreases linearly as has also been observed in case of PEG 400, however, the change in $\Delta\Delta\alpha$ (protein hydration) differs significantly from the observed change in case of PEG400. $\Delta\Delta\alpha$ shows a near linear increase as a function of sucrose concentration without any marked discontinuity which signifies that even at 50% sucrose concentration the hydration layers of sucrose and HSA acts independent of each other.

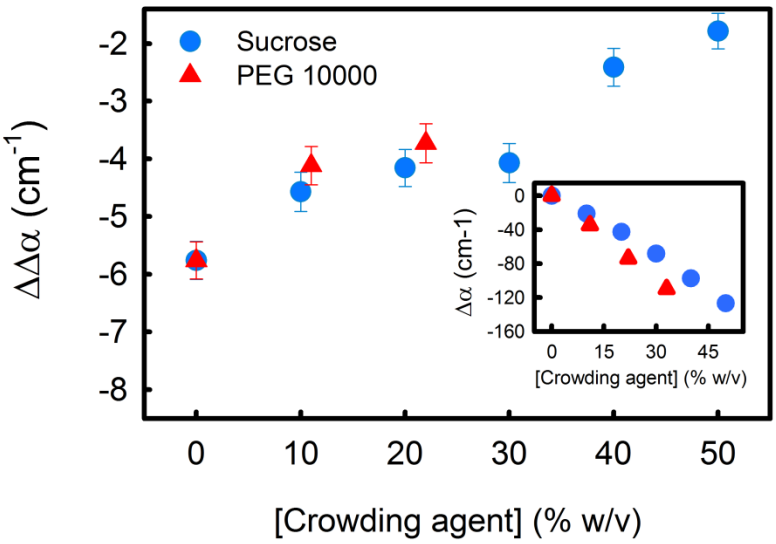

Figure 4.3.II.7. Change in the absorption coefficient of the protein solutions (0.5 mM HSA) at different concentration of sucrose and PEG 10000. Inset: Difference absorbance compared to PBS buffer of sucrose and PEG 10000 solutions.

For PEG 10000 also Δα produces a linear decrease (figure 4.3.II.7, inset) in the studied concentration regime (30% PEG). For the protein solution, however, we prefer to keep the concentration range up to 20% as beyond this concentration range HSA gets precipitated. The change in protein hydration dynamics (ΔΔα) shows a near-linear increase (figure 4.3.II.7), which is identical to that observed in sucrose. It thus concludes that the hydration behaviour of short chain PEGs beyond the critical concentration is distinctly different than the otherwise protein stabilizer co-solutes.

We also measure the temperature dependent THz response of HSA in presence of PEG 400. We increase the temperature up to 55˚C, wherein the protein shows a reversible native to extended state transition process.[118] Figure 4.3.II.8 shows change in the absorption coefficient of the protein solutions compared to the respective buffers (ΔΔα) as a function of temperature. Δα of the aqueous protein solution (in absence of PEG) decreases as the protein melts; perhaps an increased hydrophobic interaction of water with the protein surface brings about the observed decrease. For 10% PEG 400, the decrease in ΔΔα is moderate, which can be explained from the fact that at 10% PEG 400 the protein gets slightly stabilized following the "exclusion volume principle".[114] At 30% PEG, however, the decrease in ΔΔα is considerably sharp indicating an altogether different interaction mechanism between the polymer and the protein at this PEG concentration. It seems reasonable to a priori consider that beyond the critical PEG concentration protein hydration cannot be treated independently

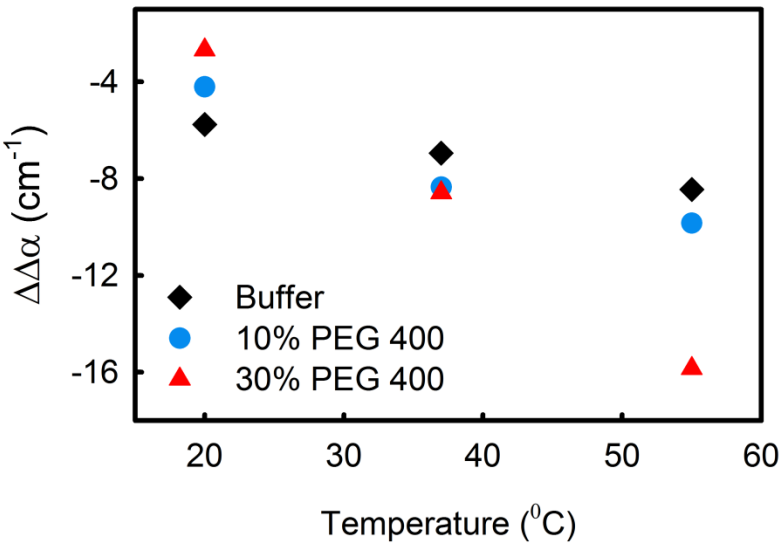

Figure 4.II.8. Temperature dependent change in the absorption coefficient of the protein solutions (0.5 mM HSA) compared to the respective buffers in absence and in presence of PEG 400.

of the PEG hydration as has previously been concluded by King et al.[28] Since the protein surface has more complex morphology compared to homogeneous PEG surface, the hydration structures in these two systems are presumably different. Near-UV CD measurements had affirmed that the protein's tertiary structure does not suffer any noticeable change in presence of smaller chain PEG,[114] and thus one can safely exclude the exposure of any embedded hydrophobic moiety of HSA to PEG. So the observed change in HSA hydration dynamics cannot be attributed to the change in the protein structure such as protein denaturation.[49] Based on the results of the study with an otherwise indifferent or protein stabilizing co-solute sucrose and PEG 10000 we conclude that in the studied concentration range the protein hydration is not significantly or "all the sudden" modified by their presence and it is the volume exclusion principle that governs the associated hydration dynamics. In this context, it seems also reasonable to consider the crowder induced protein aggregation phenomenon.[33] In case of PEG 10000, the protein 'depletion layer' is thicker than that of PEG 400, which makes the polymer assisted diffusion of the protein more feasible in the former environment allowing multiple collisions between the protein molecules leading to eventual precipitation as observed from the CD measurements (figure 4.3.II.6) and loss of optical transparency. For the smaller PEG 400, such aggregation is unfavourable at low crowder concentration. At high PEG concentration such interaction could lead to a modest fraction of protein molecules to aggregate and account for the changes observed in ΔΔα beyond the critical concentration. However, only a marginal change in the CD signals[114]

indicates only a fraction of the protein to undergo any such aggregation. It thus can be concluded that beyond a critical PEG concentration the hydration dynamics of HSA is not very straight forward as several factors may account for the observed changes and the hydration behaviour cannot be treated independently as the hydration layers of the HSA and short chain PEG overlap.

Table 4.3.II.1. Debye relaxation fitting parameters of aqueous solutions of PEG 400 at different concentrations

[PEG] (% v/v)	ε_∞	$^{(a)}\varepsilon_s$	ε_2	ε_3	τ_1 (ps)	τ_2 (fs)	τ_3 (fs)
0	2.13±0.03	75.13	3.92±0.06	3.49±0.10	8.86±0.2	222±65	84
10	2.01±0.03	71.73	3.81±0.06	3.31±0.07	11.08±0.2	239±54	84
20	1.99±0.02	65.67	3.69±0.06	3.20±0.08	11.85±0.2	239±57	84
30	1.90±0.03	58.76	3.57±0.06	3.07±0.08	14.58±0.4	237±54	83
40	1.82±0.03	51.48	3.48±0.06	2.96±0.08	16.70±0.5	234±54	83
50	1.86±0.02	44.65	3.43±0.03	2.90±0.08	19.59±0.6	210±34	84

(a) *Values are taken from Ind. J. Pure Appl. Phys. (2007) 45, 476-481.*

4.4. Conclusions

Our study aims to understand how small chain polymers affect the stability of Human serum albumin in its thermal unfolding. It is found that the primary nature of interaction of the polymer with the protein changes from a non-interacting or weakly repulsive (as an osmolyte) to interacting (as a non-specific ligand) mode with the increase in concentration of PEG. Addition of the polymer increases the compactness of the protein without adversely affecting the tertiary structure. At and beyond 30% PEG concentration the polymer interacts directly with the protein surface. Addition of PEG decreases the unfolding temperature of the protein making it more prone towards denaturation, which can be explained by considering the interaction of the unfolded protein with the polymer. We further investigate the hydration behaviour of HSA in presence of the PEGs. Combining acoustic and FIR-FTIR studies we conclude that the protein hydration is affected in a distinct way below and above the critical PEG concentration of 30% (v/v). Site specific fluorescence study exploiting the intrinsic fluorophore Trp214 of HSA affirms the hydrophobic moiety of domain II of HSA does not

directly interact with PEG. TTDS study unambiguously confirmed a retardation of the solvation dynamics by PEGs. The THz absorption coefficient measurements of HSA in PEG solutions confirms the independent behaviour of protein hydration at low PEG concentrations, and a noticeable interaction between protein and PEG hydration beyond the critical PEG concentration.

4.5. References

1. Zimmerman, S. B., and Minton, A. P. (1993) Macromolecular Crowding: biochemical, biophysical and physiological consequences, *Annu. Rev. Biophys. Biomol. Struct. 22*, 27-75.
2. Elcock, A. H. (2010) Models of macromolecular crowding effects and the need for quantitative comparisons with experiment, *Curr. Opin. Struct. Biol. 20*, 196-206.
3. Minton, A. P. (2000) Effect of a Concentrated "Inert" Macromolecular Cosolute on the Stability of a Globular Protein with Respect to Denaturation by Heat and by Chaotropes: A Statistical-Thermodynamic Model, *Biophys. J. 78*, 101-109.
4. Knoll, D., and Hermans, J. (1983) Polymer-protein interactions. Comparison of experiment and excluded volume theory, *J. Biol. Chem. 258*, 5710-5715.
5. Cheung, M. S., Klimov, D., and Thirumalai, D. (2005) Molecular crowding enhances native state stability and refolding rates of globular proteins, *Proc. Natl. Acad. Sci. USA 102*, 4753-4758.
6. Stagg, L., Zhang, S.-Q., Cheung, M. S., and Wittung-Stafshede, P. (2007) Molecular crowding enhances native structure and stability of α/β protein flavodoxin, *Proc. Natl. Acad. Sci. USA 104*, 18976-18981.
7. Waegele, M. M., and Gai, F. (2011) Power-law dependence of the melting temperature of ubiquitin on the volume fraction of macromolecular crowders *J. Chem. Phys. 134*, 095104.
8. Sotomayor-Pérez, A.-C., Subrini, O., Hessel, A., Ladant, D., and Chenal, A. (2013) Molecular Crowding Stabilizes Both the Intrinsically Disordered Calcium-Free State and the Folded Calcium-Bound State of a Repeat in Toxin (RTX) Protein, *J. Am. Chem. Soc. 135*, 11929-11934.
9. Perham, M., Stagg, L., and Wittung-Stafshede, P. (2007) Macromolecular crowding increases structural content of folded proteins, *FEBS Lett. 581*, 5065-5069.
10. Feig, M., and Sugita, Y. (2012) Variable Interactions between Protein Crowders and Biomolecular Solutes Are Important in Understanding Cellular Crowding, *J. Phys. Chem. B 116*, 599-605.
11. Sarkar, M., Li, C., and Pielak, G. J. (2013) Soft interactions and crowding, *Biophys. Rev. 5*, 187-194.
12. Miklos, A. C., Sarkar, M., Wang, Y., and Pielak, G. J. (2011) Protein Crowding Tunes Protein Stability, *J. Am. Chem. Soc. 133*, 7116-7120.
13. Sarkar, M., Smith, A. E., and Pielak, G. J. (2013) Impact of reconstituted cytosol on protein stability, *Proc. Nat. Acad. Sci. 110*, 19342-19347.
14. Schlesinger, A. P., Wang, Y., Tadeo, X., Millet, O., and Pielak, G. J. (2011) Macromolecular Crowding Fails To Fold a Globular Protein in Cells, *J. Am. Chem. Soc. 133*, 8082-8085.
15. Wang, Y., Sarkar, M., Smith, A. E., Krois, A. S., and Pielak, G. J. (2012) Macromolecular Crowding and Protein Stability, *J. Am. Chem. Soc. 134*, 16614−16618.

16. Kim, Y. C., and Mittal, J. (2013) Crowding Induced entropy-enthalpy compensation in protein association equilibria, *Phys. Rev. Lett. 110*, 208102.
17. Ebbinghaus, S., Dhar, A., McDonald, J. D., and Gruebele, M. (2010) Protein folding stability and dynamics imaged in a living cell, *Nature Methods 7*, 319-323.
18. Guzman, I., Gelman, H., Tai, J., and Gruebele, M. (2014) The extracellular protein VlsE is destabilized inside cells, *J. Mol. Biol. 426*, 11-20.
19. Minton, A. P. (2005) Models for Excluded Volume Interaction between an Unfolded Protein and Rigid Macromolecular Cosolutes: Macromolecular Crowding and Protein Stability Revisited, *Biophys. J. 88*, 971-985.
20. Miklos, A. C., Li, C., Sharaf, N. G., and Pielak, G. J. (2010) Volume Exclusion and Soft Interaction Effects on Protein Stability under Crowded Conditions, *Biochemistry 49*, 6984-6991.
21. Zielenkiewicz, W., Swierzewski, R., Attanasio, F., and G. Rialdi, G. (2006) Thermochemical, volumetric and spectroscopic properties of lysozyme–poly(ethylene) glycol system, *J. Therm. Anal. Cal. 83*, 587-595.
22. Farruggia, B., Nerli, B., Di Nuci, H., Rigatusso, R., and Picó, G. (1999) Thermal features of the bovine serum albumin unfolding by polyethylene glycols, *Int. J. Biol. Macromol. 26*, 23-33.
23. Ball, P. (2008) Water as an Active Constituent in Cell Biology, *Chem. Rev. 108*, 74-108.
24. Levy, Y., and Onuchic, J. N. (2006) Water mediation in protein folding and molecular recognition, *Annu. Rev. Biophys. Biomol. Struct. 35*, 389-415.
25. Zimmerman, S. B., and Trach, S. O. (1991) Estimation of macromolecule concentrations and excluded volume effects for the cytoplasm of Escherichia coli, *J. Mol. Biol. 222*, 599.
26. Zhou, H.-X., Rivas, G., and Minton, A. P. (2008) Macromolecular Crowding and Confinement: Biochemical, Biophysical, and Potential Physiological Consequences, *Annu. Rev. Biophys. 37*, 375-397.
27. Harada, R., Sugita, Y., and Feig, M. (2012) Protein Crowding Affects Hydration Structure and Dynamics, *J. Am. Chem. Soc. 134*, 4842 − 4849.
28. King, J. T., Arthur, E. J., Brooks, C. L., and Kubarych, K. J. (2014) Crowding Induced Collective Hydration of Biological Macromolecules over Extended Distances, *J. Am. Chem. Soc. 136*, 188 − 194.
29. Verma, P. K., Rakshit, S., Mitra, R. K., and Pal, S. K. (2011) Role of hydration on the functionality of a proteolytic enzyme α-chymotrypsin under crowded environment, *Biochimie. 93*, 1424-1433.
30. McGuffee, S. R., and Elcock, A. H. (2010) Diffusion, Crowding & Protein Stability in a Dynamic Molecular Model of the Bacterial Cytoplasm, *PLoS 6*, e1000694.
31. Tanizaki, S., Clifford, J., Connelly, B. D., and Feig, M. (2008) Conformational Sampling of Peptides in Cellular Environments, *Biophys. J. 94*, 747-759.
32. Senske, M., Törk, L., Born, B., Havenith, M., Herrmann, C., and Ebbinghaus, S. (2014) Protein Stabilization by Macromolecular Crowding through Enthalpy Rather Than Entropy, *J. Am. Chem. Soc. 136*, 9036-9041.
33. Kozer, N., Kuttner, Y. Y., Haran, G., and Schreiber, G. (2007) Protein-Protein Association in Polymer Solutions: From Dilute to Semidilute to Concentrated, *Biophys. J. 92*, 2139-2149.
34. Sasaki, Y., Miyoshi, D., and Sugimoto, N. (2007) Regulation of DNA nucleases by molecular crowding, *Nucleic Acids Res. 35*, 4086-4093.
35. Mora´n-Zorzano, M. T., Viale, A. M., Mun˜oz, F. J., Alonso-Casaju´s, N., Eydallı´n, G. G., Zugasti, B., Baroja-Ferna´ndez, E., and Pozueta-Romero, J. (2007) Escherichia

coli AspP activity is enhanced by macromolecular crowding and by both glucose-1,6-bisphosphate and nucleotide-sugars, *FEBS Lett. 581*, 1035-1040.

36. von Hippel, P. H., and Schleich, T. (1969) The Effect of Neutral Salts on the Structure and Conformational Stability of Macromolecules in Solution, In *Structure and Stability of Biological Macromolecules* (Timasheff, S. N., and Fasman, G. D., Eds.), pp 417-574, Marcel Dekker Inc., New York.
37. Tokuriki, N., Kinjo, M., Negi, S., M., H., Goto, Y., Urabe, I., and Yomo, T. (2004) Protein folding by the effects of macromolecular crowding, *Protein Sci. 13*, 125-133.
38. Kushare, S. K., Kolhapurkar, R. R., Dagade, D. H., and Patil, K. J. (2006) Compressibility Studies of Binary Solutions Involving Water as a Solute in Nonaqueous Solvents at T = 298.15 K, *J. Chem. Eng. Data 51*, 1617-1623.
39. Jarvis, T. C., Ring, D. M., Daube, S. S., and von Hippel, P. H. (1990) "Macromolecular Crowding": Thermodynamic Consequences for Protein-Protein Interactions within the T4 DNA Replication Complex, *J. Biol. Chem. 265*, 15160-15167.
40. Minton, A. P. (1983) The effect of volume occupancy upon the thermodynamic activity of proteins: some biochemical consequences., *Mol. Cell. Biochem. 55*, 119-140.
41. Winzor, D. J., and Wills, P. R. (2006) Molecular crowding effects of linear polymers in protein solutions., *Biophys. Chem. 119*, 186-195.
42. Delgado, C., Francis, G. E., and Fisher, D. (1992) The uses and properties of PEG-linked proteins, *Crit. Rev. Ther. Drug. Carrier Syst. 9*, 249-304.
43. Topchieva, I. N., Sorokina, E. M., Efremova, N. V., Ksenofontov, A. L., and Kurganov, B. I. (2000) Noncovalent adducts of poly(ethylene glycols) with proteins, *Bioconjug. Chem. 11*, 22-29.
44. Ragi, C., Sedaghat-Herati, M. R., Ouameur, A. A., and Tajmir-Riah, H. A. (2005) The effects of poly(ethylene glycol) on the solution structure of human serum albumin, *Biopolymers 78*, 231-236.
45. Atha, D. H., and Ingham, K. C. (1981) Mechanism of precipitation of proteins by polyethylene glycols. Analysis in terms of excluded volume, *J. Biol. Chem. 256*, 12108-12117.
46. Knowles, D. B., LaCroix, A. S., Deines, N. F., Shkel, I., and Record, J., M.T. (2011) Separation of preferential interaction and excluded volume effects on DNA duplex and hairpin stability *Proc. Natl. Acad. Sci. USA 108*, 12699-12704.
47. Ebbinghaus, S., Kim, S. J., Heyden, M., Yu, X., Heugen, U., Gruebele, M., Leitner, D. M., and Havenith, M. (2007) An extended dynamical hydration shell around proteins., *Proc. Natl. Acad.Sci.USA 104*, 20749-20752.
48. Heyden, M., and Havenith, M. (2010) Combining THz spectroscopy and MD simulations to study protein-hydration coupling *Methods 52*, 74-83.
49. Luong, T. Q., Verma, P. K., Mitra, R. K., and Havenith, H. (2011) Do Hydration Dynamics Follow the Structural Perturbation during Thermal Denaturation of a Protein: A Terahertz Absorption Study, *Biophys. J. 101*, 925-933.
50. Nibali, V. C., and Havenith, M. (2014) New Insights into the Role of Water in Biological Function: Studying Solvated Biomolecules Using Terahertz Absorption Spectroscopy in Conjunction with Molecular Dynamics Simulations, *J. Am. Chem. Soc. 136*, 12800-12807.
51. He, Y., Ku, P. I., Knab, J. R., Chen, J. Y., and Markelz, A. G. (2008) Protein Dynamical Transition Does Not Require Protein Structure, *Phys. Rev. Lett. 101*, 178103.

52. Heyden, M., Sun, J., Funkner, S., Mathias, G., Forbert, H., Havenith, M., and Marx, D. (2010) Dissecting the THz spectrum of liquid water from first principles via correlations in time and space *Proc. Natl. Acad.Sci.USA 107*, 12068-12073.
53. Privalov, P. L., and Khechinashvili, N. N. (1974) A thermodynamic approach to the problem of stabilization of globular protein structure: A calorimetric study, *J. Mol. Biol. 86*, 665-684.
54. Creighton, T. E., (Ed.) (1992) *Protein Folding*, Freeman, New York.
55. Kindt, J. T., and Schmuttenmaer, C. A. (1996) Far-infrared dielectric properties of polar liquids probed by femtosecond terahertz pulse spectroscopy, *J. Phys. Chem. 100*, 10373-10379.
56. Rønne, C., Åstrand, P. O., and Keiding, S. R. (1999) THz Spectroscopy of Liquid H2O and D2O, *Phys. Rev. Lett. 82*, 2888-2891
57. Polley, D., Patra, A., and Mitra, R. K. (2013) Dielectric relaxation of the extended hydration sheathe of DNA in the THz frequency region, *Chem. Phys. Lett. 586*, 143-147.
58. Bergner, A., Heugen, U., Bründermann, E., Schwaab, G., Havenith, M., Chamberlin, D. R., and Haller, E. E. (2005) New p-Ge THz laser spectrometer for the study of solutions: THz absorption spectroscopy of water, *Rev. Sci. Instr. 76*, 063110.
59. He, X. M., and Carter, D. C. (1992) Atomic structure and chemistry of human serum albumin, *Nature 358*, 209 - 215.
60. Mitra, R. K., Sinha, S. S., and Pal, S. K. (2007) Hydration in protein folding: Thermal unfolding/refolding of human serum albumin *Langmuir 23*, 10224-10229.
61. Naeem, A., Khan, A., and Hasan Khan, R. H. (2005) Partially folded intermediate state of concanavalin A retains its carbohydrate specificity *Biochem. Biophys. Res. Comm. 331*, 1284-1294.
62. Strickland, E. H. (1974) Aromatic contributions to circular dichroism spectra of proteins, *CRC Crit Rev Biochem. 2*, 113-175.
63. Woody, R. W., and Dunker, A. K. (1996) Aromatic and Cystine Side-chain Circular Dichroism in Proteins, In *Circular Dichroism and the Conformational Analysis of Biomolecules* (Fasman, G. D., Ed.), pp 109-157, Plenum Press, New York.
64. Carter, D. C., and Ho, J. X. (1994) Structure of Serum Albumin, *Adv. Protein Chem. 45*, 153-203.
65. Suo, X., Lu, X., Hu, T., Ma, G., and Su, Z. (2009) A solid-phase adsorption method for PEGylation of human serum albumin and staphylokinase: preparation, purification and biochemical characterization *Biotech. Lett. 31*, 1191-1196.
66. Chalikian, T. V., and Breslauer, K. J. (1996) Compressibility as a means to detect and characterize globular protein states, *Proc. Natl. Acad.Sci.USA 93*, 1012-1014.
67. Chalikian, T. V., Totrov, M., Abagyan, R., and Breslauer, K. J. (1996) The Hydration of Globular Proteins as Derived from Volume and Compressibility Measurements: Cross Correlating Thermodynamic and Structural Data, *J. Mol. Biol. 260*, 588-603.
68. Chalikian, T. V. (2003) Volumetric properties of proteins, *Ann. Rev. Biophys. Biomol. Str. 32*, 207-235.
69. Kushare, S. K., Terdale, S. S., Dagade, D. H., and Patil, K. J. (2007) Compressibility and volumetric studies of polyethylene-glycols in aqueous, methanolic, and benzene solutions at T = 298.15 K, *J. Chem. Thermodynamics 39*, 1125-1131.
70. Sasahara, K., Sakurai, M., and Nitta, K. (1999) The volume and compressibility changes of lysozyme associated with guanidinium chloride and pressure-assisted unfolding, *J. Mol. Biol. 291*, 693-701.

71. Gross, M., and Jaenicke, R. (1994) Proteins under pressure : The influence of high hydrostatic pressure on structure, function and assembly of proteins and protein complexes, *Eur. J. Biochem. 221*, 617-630.
72. Kharakoz, D. P., and Sarvazyan, A. P. (1993) Hydrational and intrinsic compressibilities of globular proteins, *Biopolymers 33*, 11-26.
73. Gekko, K., and Hasegawa, Y. (1986) Compressibility-structure relationship of globular proteins, *Biochemistry 25*, 6563-6571.
74. Tamura, Y., and Gekko, K. (1995) Compactness of thermally and chemically denatured ribonuclease A as revealed by volume and compressibility, *Biochemistry 34*, 1878-1884.
75. Kharakoz, D. P. (1997) Partial Volumes and Compressibilities of Extended Polypeptide Chains in Aqueous Solution: Additivity Scheme and Implication of Protein Unfolding at Normal and High Pressure, *Biochemistry 36*, 10276-10285.
76. Lakowicz, J. R. (2006) *Principles of fluorescence spectroscopy*, 3rd ed., Kluwer Academic/Plenum, New York.
77. Albani, J. R. (2009) Fluorescence Lifetimes of Tryptophan: Structural Origin and Relation with S o →1 L b and S o →1 L a Transitions, *J. Fluoresc. 19*, 1061-1071.
78. Curry, S., Mandelkow, H., Brick, P., and Franks, N. (1998) Crystal structure of human serum albumin complexed with fatty acid reveals an asymmetric distribution of binding sites *Nat. Struct. Biol. 5*, 827-835.
79. Zunszain, P. A., Ghuman, J., Komatsu, T., Tsuchida, E., and Curry, S. (2003) Crystal structural analysis of human serum albumin complexed with hemin and fatty acid, *BMC Str. Biol. 3*, 6.
80. Picó, G. (1997) Thermodynamic features of the thermal unfolding of human serum albumin, *Int. J. Biol. Macromol. 20*, 63-73.
81. Flora, K., Brennan, J. D., Baker, G. A., Doody, M. A., and Bright, F. V. (1998) Unfolding of Acrylodan-Labeled Human Serum Albumin Probed by Steady-State and Time-Resolved Fluorescence Methods, *Biophys. J. 75*, 1084-1096.
82. Wu, Y., Czarnik-Matusewicz, B., Murayama, K., and Ozaki, Y. (2000) Two-dimensional near-infrared spectroscopy study of human serum albumin in aqueous solutions, *J. Phys. Chem. B 104*, 5840-5847.
83. Michnik, A., Michalik, K., Kluczewska, A., and Drzazga, Z. (2006) Comparative DSC study of human and bovine serum albumin, *J. Thermal Analysis Calorimetry 84*, 113-117.
84. Sinha, S. S., Mitra, R. K., and Pal, S. K. (2008) Temperature-Dependent Simultaneous Ligand Binding in Human Serum Albumin, *J. Phys Chem. B 112*, 4884-4891.
85. Spitzer, J. J., and Poolman, B. (2005) Electrochemical structure of the crowded cytoplasm *Trends Biochem. Sci. 30*, 536-541.
86. Sasahara, K., McPhie, P., and Minton, A. P. (2003) Effect of Dextran on Protein Stability and Conformation Attributed to Macromolecular Crowding *J. Mol. Biol. 326*, 1227-1237.
87. de Gennes, P.-G. (1979) *Scaling Concepts in Polymer Physics*, Cornell University Press, New York.
88. Zhang, D.-L., Wu, L.-J., Chen, J., and Liang, Y. (2012) Effects of macromolecular crowding on the structural stability of human a-lactalbumin, *Acta Biochim. Biophys. Sinica 44*, 703-711.
89. Wang, A., and Bolen, D. W. (1997) A Naturally Occurring Protective System in Urea-Rich Cells: Mechanism of Osmolyte Protection of Proteins against Urea Denaturation, *Biochemistry 36*, 9101-9108.

90. Tseng, H.-C., and Graves, D. J. (1998) Natural Methylamine Osmolytes, Trimethylamine N-Oxide and Betaine, Increase Tau-Induced Polymerization of Microtubules, *Biochem. Biophys. Res. Comm. 250*, 726-730.
91. Street, T. O., Bolen, D. W., and Rose, G. D. (2006) A molecular mechanism for osmolyte-induced protein stability *Proc. Nat. Acad. Sci. 103*, 13997-14002.
92. Bolen, D. W., and Rose, G. D. (2008) *Structure and energetics of the hydrogen-bonded backbone in protein folding*.
93. Auton, M., and Bolen, D. W. (2005) Predicting the energetics of osmolyte-induced protein folding/unfolding, *Proc. Nat. Acad. Sci. 102*, 15065-15068.
94. Auton, M., Bolen, D. W., and Rosgen, J. (2008) Structural thermodynamics of protein preferential solvation: Osmolyte solvation of proteins, aminoacids, and peptides *Proteins 73*, 802-813.
95. Wu, P., and Bolen, D. W. (2006) Osmolyte-induced protein folding free energy changes, *Proteins 63*, 290-296.
96. Courtenay, E. S., Capp, M. W., Anderson, C. F., and Record, M. T. (2000) Vapor pressure osmometry studies of osmolyte-protein interactions: Implications for the action of osmoprotectants in vivo and for the interpretation of "osmotic stress" experiments in vitro, *Biochemistry 39*, 4455-4471.
97. Diehl, R. C., Guinn, E. J., Capp, M. W., Tsodikov, O. V., and Record, M. T. (2013) Quantifying Additive Interactions of the Osmolyte Proline with Individual Functional Groups of Proteins: Comparisons with Urea and Glycine Betaine, Interpretation of m-Values, *Biochemistry 52*, 5997-6010.
98. Zou, Q., Bennion, B. J., Daggett, V., and Murphy, K. P. (2002) The Molecular Mechanism of Stabilization of Proteins by TMAO and Its Ability to Counteract the Effects of Urea, *J. Am. Chem. Soc. 124*, 1192-1202.
99. Zelsmann, H. R. (1995) Temperature dependence of the optical constants for liquid H2O and D2O in the far IR region *J. Mol. Struct. 350*, 95-114.
100. Walrafen, G. E. (1990) Raman spectrum of water: transverse and longitudinal acoustic modes below .apprxeq.300 cm-1 and optic modes above .apprxeq.300 cm-1, *J. Phys. Chem. 94*, 2237-2239.
101. Ohmine, I., and Saito, S. (1999) Water Dynamics: Fluctuation, Relaxation, and Chemical Reactions in Hydrogen Bond Network Rearrangement, *Acc. Chem. Res. 32* 741-749.
102. Graziano, G. (2006) Non-intrinsic contribution to the partial molar volume of cavities in water *Chem. Phys. Lett. 429*, 420-424.
103. Mitra, R. K., Sinha, S. S., and Pal, S. K. (2007) Hydration in Protein Folding: Thermal Unfolding/Refolding of Human Serum Albumin, *Langmuir 23*, 10224-10229.
104. Singh, P., and Chowdhury, P. K. (2013) Crowding-Induced Quenching of Intrinsic Tryptophans of Serum Albumins: A Residue-Level Investigation of Different Conformations, *J. Phys. Chem. Lett. 4*, 2610 − 2617.
105. Han, F., Zhang, J., Chen, G., and Wei, X. (2008) Density, Viscosity, and Excess Properties for Aqueous Poly(ethylene glycol) Solutions from (298.15 to 323.15) K, *J. Chem. Eng. Data 53*, 2598-2601.
106. Albani, J. R. (2014) Origin of Tryptophan Fluorescence Lifetimes. Part 2: Fluorescence Lifetimes Origin of Tryptophan in Proteins, *J. Fluoresc. 24*, 105 - 117.
107. Helms, M. K., Petersen, C. E., Bhagavan, N. V., and Jameson, D. M. (1997) Time-resolved Fuorescence studies on site-directed mutants of human serum albumin, *FEBS Lett. 408*, 67-70.

108. Samanta, N., Das Mahanta, D., and Mitra, R. K. (2014) Collective hydration dynamics of guanidinium chloride solutions and its possible role in protein denaturation: a terahertz spectroscopic study, *Phys. Chem. Chem. Phys. 16*, 23308--23315.
109. Samanta, N., Das Mahanta, D., and Mitra, R. K. (2014) Does Urea Alter the Collective Water Structure: A Dielectric Relaxation Study in THz Region, *Chem. Asian J. 9*, 3457-3463.
110. Sato, T., and Buchner, R. (2004) Dielectric relaxation processes in ethanol/water mixtures, *J. Phys. Chem. A 108*, 5007-5015.
111. Walrafen, G. E., Chu, Y. C., and Piermarini, G. J. (1996) Low-Frequency Raman Scattering from Water at High Pressures and High Temperatures, *J. Phys. Chem. 100* 10363-10372.
112. Heugen, U., Schwaab, G., Bründermann, E., Heyden, M., Yu, X., Leitner, D. M., and Havenith, M. (2006) Solute-induced retardation of water dynamics probed directly by terahertz spectroscopy, *Proc. Natl. Acad.Sci.USA 103*, 12301-12306.
113. Heyden, M., Bründermann, E., Heugen, U., Niehues, G., Leitner, D. M., and Havenith, M. (2008) Long range influence of carbohydrates on the solvation dynamics of water - Answers from THz absorption measurements and molecular modeling simulations, *J. Am. Chem. Soc. 130*, 5773-5779.
114. Samanta, N., Das Mahanta, D., Hazra, S., G.S., K., and Mitra, R. K. (2014) Short chain polyethylene glycols unusually assist thermal unfolding of human serum albumin, *Biochimie 104*, 81-89.
115. Kendrick, B. S., Chang, B. S., Arakawa, T., Peterson, B., Randolph, T. W., Manning, M. C., and Carpenter, J. F. (1997) Preferential exclusion of sucrose from recombinant interleukin-1 receptor antagonist: Role in restricted conformational mobility and compaction of native state, *Proc. Natl. Acad.Sci.USA 94*, 11917-11922.
116. Timasheff, J. C. L. a. S. N. (1981) The stabilization of proteins by sucrose, *The Journal of biological chemistry 256*, 7193-7201.
117. Farruggia, B., Garcia, G., D'Angelo, C., and Picó, G. (1997) Destabilization of human serum albumin by polyethylene glycols studied by thermodynamical equilibrium and kinetic approaches, *International Journal of Biological Macromolecules 20*, 43-51.
118. Flora, K., Brennan, J. D., Baker, G. A., Doody, M. A., and Bright, F. V. (1998) Unfolding of Acrylodan-Labeled Human Serum Albumin Probed by Steady-State and Time-Resolved Fluorescence Methods, *Biophysical Journal 75*, 1084-1096.

Chapter 5

5. Understanding the Way of Protein Destabilisation/Stabilisation by Cosolutes

How protein folding or unfolding occurs in presence of stabilizing or denaturing agents is still a debatable issue. This chapter addresses a very fundamental question, whether urea and guanidinium chloride (GdmCl) act as water 'structure breakers'. Our study using THz time domain spectroscopy (TTDS) confirms that both these molecules perturb the extended solvation layer around themselves which supports the strongly debated "water structure breaker" notion of urea and GdmCl. This chapter also concerns about a detailed understanding of hydration of amino acids which are not only the building units of protein but also act as osmolytes. It is a key step to realize the overall solvation processes in proteins. A combined GHz (0.2-50) to THz (0.3-2.0) experimental spectroscopic study reveals the dynamics of water at room temperature in presence of different amino acids.

5.1 Introduction

Exact molecular mechanism of protein unfolding or stabilization by cosolutes is still remains a strongly debatable issue. It is believed to result either from their direct interaction with the protein backbone or as an indirect effect in which cosolutes perturbs the water network structure. The former argument has been supported by simulation and experiments; however, the later hypothesis has been debated in the past. While most of the earlier studies involved the dynamics of water limited to first 1-2 hydration layer, the cooperative H-bond network dynamics which extends up to 3rd or 4th hydration layer and leaves its imprint in the elusive THz frequency region, has rarely been investigated. The principal motive of the present investigation is to underline the effect of different cosolutes on the collective hydration dynamics of water.

Urea and its Derivatives: Urea is a neutral molecule having a size comparable to that of water and has historically been recognized to offer unique physicochemical properties like protein denaturation,[1] hydrocarbon solubilisation[2] etc., however, the exact molecular mechanism of the processes involved still remains a strongly debatable issue. The interaction

of urea with protein molecules during its denaturation process has been envisaged either as a result of its direct interaction with the protein backbone or as an indirect effect in which urea perturbs the water network structure.[3] One of the earlier discussions made on the mechanism of denaturation ability of urea was based on the water 'structure breaking' hypothesis[4] which encompasses the concept that incorporation of urea molecules breaks hydrogen bonded network in water. This hypothesis has, however, not received considerable support from experimental or simulation studies with only a few reports documented in the literatures.[5-11] Koga et al.[12] made detailed solution thermodynamics consideration and concluded that urea does form direct hydrogen bond and thereby perturbs the hydrogen bond network of water. Vanzi et al.[13] showed that the hydrogen bonded network of water predominates around the amine groups, however, the structure gets distorted around the carbonyl group. Simulation studies by Zou et al.[14] showed that the average number of hydrogen bonds per water molecule as well as the average water-water hydrogen bond lifetime decreases in the presence of urea. Molecular dynamic simulation study by Wei et al.[15] concluded that urea induces considerable reduction in the distances of the second hydration shell of hydrogen bonded network in water. The concept of urea being enacted as a water structure breaker has been challenged by a series of simulation and experimental studies.[16-18] Polarization resolved mid-infrared pump-probe spectroscopic experiment by Rezus et al.[16] clearly demonstrated that urea offers negligible effect on the hydrogen bond dynamics of water. They concluded that urea efficiently fits in the water network and thus does hardly affect its network structure. NMR studies of orientational relaxation and analysis of spin-lattice relaxation time of the ^{17}O nucleus of water molecules in urea/water system by Shimizu et al.[17] concluded water to remain mostly unaffected in the presence of urea. Similar observation has also been reported by mid-infrared (MIR) FTIR[19] and dielectric[20] measurements, as well as several simulation studies which unambiguously concluded the water structure to remain unaltered in urea solutions[21-24]. Some recent results have suggested a direct interaction of urea with protein backbone which eventually leads to its denaturation.[25, 26] According to the 'two stage denaturation process' as proposed by Hua et al.,[18] the process initiates with a preferential solvation of the globular protein by urea and exclusion of water from the protein solvation shell followed by solvation of the protein interior by both urea and water. Such direct mechanism, which manifests a causative interaction between urea and protein backbone finds support from earlier simulation studies.[27] The preferential solvation of urea is usually driven by Van der Waals interactions along with an additional solvent entropy gain as initially constrained water is displaced by urea.[28, 29] There has also been studies that even support the

electrostatic basis of urea activity.[30] The interaction of urea with protein thus still remains debatable and it is now commonly believed that the 'direct' interaction which involves Van der Waals attraction, hydrogen bonding and hydrophobic effect plays the key role in the protein denaturation process, however, the role of 'indirect' interaction through a possible water structure perturbation can not a priori to be neglected.[3]

There have been several experimental studies to understand the structure and dynamics of water around urea. Ultrafast optical Kerr effect spectroscopy of aqueous urea solution reveals several low frequency bands at 45-60, 80-100 and 175-200 cm^{-1} region.[31, 32] The lowest frequency band arises due to the vibrational motion of urea or water in a cage[31] or absorption of water.[32] The other two bands are related to the hydrogen bond interaction of water with urea and absorption of water, respectively. For pure water a prominent peak is observed at ~200 cm^{-1} which corresponds to the first-shell dynamics, whereas a concerted motion involving the second solvation shell contributes most significantly in the 80 cm^{-1} region.[33] Raman spectroscopic studies by Idrissi et al.[31] and Mazur et al.[32] have identified urea to act as a mild structure breaker. Recently Funkner et al.[34] studied the changes in the fast solvation dynamics of water around urea in the frequency range of 1.5 to 10 THz (50-350 cm^{-1}). Their study concluded the water structure to remain unperturbed in the thin hydration shell of urea. MIR pump-probe spectroscopic study by Rezus et al.[16] identified an unaltered hydration dynamics of water in presence of urea. It is, however, interesting to note here that most of these earlier studies are either concerned with the first solvation shell of urea in which water is strongly bound or with the bulk type water. The IR active modes of water in the MIR region is generally sensitive to the first solvation shell and thus unable to provide information on the extended solvation shell which extends up to 3-4 hydration layers.[33] The previous studies thus were not meant to detect any possible change in the dynamics of urea solution in its extended solvation sheathe. In the present investigation we have made an elaborate attempt to understand the ultrafast solvation dynamics of water by using a Debye type dielectric relaxation model in the THz (0.3-1.5 THz) frequency region using THz time domain spectroscopy (TTDS). Dielectric relaxation studies have previously been carried out in urea solution in the MHz to 40 GHz frequency range[20, 35] which identified strongly associated water exhibiting slower relaxation dynamics compared to that of bulk water, as has also been identified in MIR pump probe spectroscopic studies.[16] The GHz as well as MIR frequency range are limited to the intra-molecular stretching band of water and does not protrude into the global collective motion of water which extends to more than one hydration

layer.[33] Such global collective information can only be realized in the THz frequency domain.[36] To understand the nature of the usual hydration structure around conventional osmolytes, we initiate the measurements with a model solute sucrose which then is extended to urea. In order to achieve at a better insight, we have also investigated water dynamics in two derivatives of urea, namely thiourea (TU) and 1,1,3,3-tetramethylurea (TMU). We compare the results of urea with a well-known structure maker trimethylamine-N-oxide (TMAO) with the goal to understand the solvation behaviour as a consequence of the overwhelming protein stabilization behaviour of TMAO over urea.

Guanidinium Salts: Another denaturing agent guanidinium chloride (GdmCl) exhibits the remarkable ability of denaturing proteins.[37, 38] There has been substantial advancement in the studies of the denaturing effect on GdmCl, however, the exact mechanism involved in the phenomenon continues to be controversial and speculative.[39, 40] It has generally been believed that Gdm^+ interacts directly with proteins,[30, 41, 42] also the role of Gdm^+ in alteration of solution structure of water has also been argued,[43-46] which however, has received only limited support from experimental findings. Neutron scattering[41] and dielectric spectroscopy[47] experiments have concluded the non-existence of any strongly bound solvation shell around Gdm^+, primarily because of its low charge density,[41] however, MD simulation results have predicted a significant ordering of hydration layer around Gdm^+ ions depending upon its orientation.[44, 46] According to Scott et al.[45] Gdm^+ denatures protein by altering the water structure; their studies revealed that Gdm^+ drives the preferential formation of strong, linear H-bonds over weak, bent H-bonds. IR pump-probe study by Bekker et al.[48] has shown that the reorientation dynamics of water molecules suffers considerable alteration upon the addition of GdmCl. While GdmCl is known to be a strong protein denaturant, salts like NaCl or $MgCl_2$ mostly remain indifferent. This ambiguity certainly evokes the most pertained question that what drives these salts to act in opposite modes, and it remains mostly unanswered. Arakawa and Timasheff[49] have previously investigated the preferential interaction of bovine serum albumin (BSA) with guanidinium and sodium salts and tried to establish a possible correlation with their protein denaturation ability. The authors concluded that Gdm^+ behaves in a manner much comparable to that of the other cations, and shows a limited preferential interaction with BSA, which is otherwise also possible for normal salts. However, there exists a significant difference between the extent of the various interactions between Gdm^+ and Na^+ which probably brings about the remarkable denaturing ability for the former. In a later study Courtenay et al.[50] investigated the effect of GdmCl on BSA on the

basis of changes in the water-accessible surface area (WASA) of the protein in presence of the denaturant. The authors reported the existence of a strong favourable BSA-Gdm^+ interaction as compared to the water-Gdm^+ interaction which results in the accumulation of Gdm^+ at the negatively charged protein surface which might exert a variety of electrolyte effects on processes involving changes in the net charge density. While several earlier studies have concluded Gdm^+ to form hydrogen bond with peptide carbonyl[30, 51, 52] such possibility has strongly been opposed by Lim et al.[25] in a recent NMR study.

The above mentioned observations make it evident of the fact that the exact mechanism of the protein denaturation ability of GdmCl is debatable: it broadly is based on the fact that Gdm^+ shows preferential interaction with parts of proteins, which leads to its denaturation, while, the role of hydration of Gdm^+ on the denaturation phenomenon has hardly been critically addressed. It can be apprehended that the direct and indirect denaturation mechanisms are not mutually exclusive and might both the mechanisms be simultaneously active. In the present contribution we have investigated the collective hydrogen bond dynamics around GdmCl in aqueous solutions as well as in presence of a model globular protein human serum albumin (HSA) using terahertz (THz) time domain spectroscopy (TTDS) and to address the possible role, if any, of hydration dynamics in the denaturation process. In a recent study it was investigated that the change in the hydration dynamics of HSA during its thermal denaturation using THz spectroscopic technique and it was inferred that the exposure of hydrophobic moieties in the protein surface during thermal denaturation does indeed leave its imprint in the associated hydration dynamics.[53] We extend that study towards a more involved question related to the protein denaturation with GdmCl and have investigated the changes in hydration dynamics of both the protein and the salt during its chemical denaturation. Such denaturation study has previously been carried out using several experimental techniques,[54] however, the consequent changes in the corresponding hydration dynamics has hardly been considered. Since the proficiency of denaturation of proteins by ions partly depends upon the strength of their interaction with water it is of much importance to understand the hydration structure and dynamics of the heterogeneous solvation shell around Gdm^+. We have investigated the hydration dynamics of GdmCl in the THz frequency range (0.3-2.0 THz) using a multiple Debye dielectric relaxation (DR) model, which has extensively been used to underline the ultrafast dynamics of water associated with biomolecules.[55] Recently Hunger et al.[47] have studied the DR of GdmCl and $GdmCO_3$ in the 0.1-80 GHz frequency region; their study was mainly focused on

the possibility of the formation of large ion pairs. They unambiguously found to non-existent of such large ion pairs in the solution, however, some recent ab initio simulation studies have predicted the possible existence of contact ion pair in GdmCl.[56] The DR study by Hunger et al. has found striking resemblance in various solution properties as well as DR spectra of Gdm^+ and Na^+ salts, which evidently establishes no possible rationale behind the apparent opposing protein denaturation behaviour of these two salts. We, therefore, have attempted to compare the collective hydrogen bond dynamics in GdmCl and NaCl using TTDS technique and to establish the possibility of any such correlation. We have also compared the results with a more hydrophobic salt tetramethylguanidinium chloride (TMGdmCl). Finally, we have studied the effect of these salts on the stability of HSA and correspondingly on the hydration dynamics in absence and in presence of these salts. Our study is principally aimed to establish any possible correlation between the hydration dynamics of GdmCl and its ability to denature protein as well as the rationale behind the way this particular salt differs from the conventional monovalent cations.

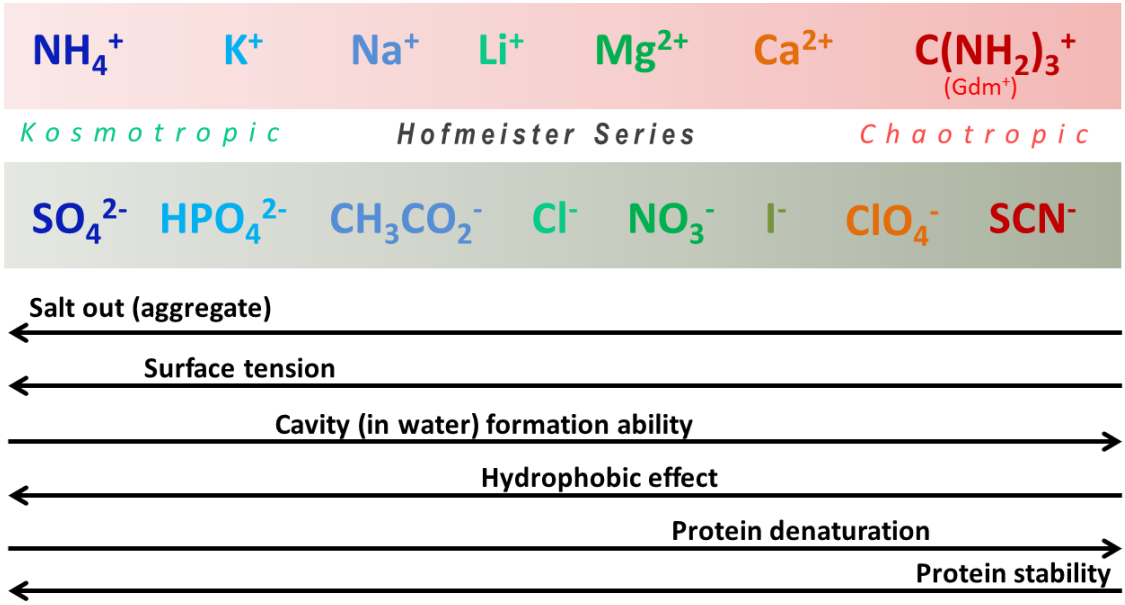

Scheme 5.1.1: Hofmeister series[57] to show the effect of different cation and anions to the protein/peptide in water.

Over 100 years ago Hofmeister (scheme 5.1.1) showed the effect of different cations and anions of salts to protein.[57] The denaturing ability of GdmCl is often believed to be due to direct interaction of Gdm^+ with the protein.[58, 59] Question arises when Gdm_2SO_4 was found to stabilize proteins.[60] In a very early study von Hippel and Wong reported that melting temperature of ribonuclease increase with the Gdm_2SO_4 concentration in contrast to

GdmCl.[61] But there is a lack of plausible mechanism behind this finding. Earlier studies showed that the protein denaturation ability is dependent on Gdm cation as well as the counter ion. In this notion we have further studied with guanidinium sulphate (Gdm_2SO_4) salt to observe the perturbation in water network structrure.

Amino Acid: Amino acids are not only the building blocks of proteins; they often also act as intermediates in metabolism as well as osmolytes that can stabilize proteins.[62-64] Depending upon the 'side group', amino acids are classified as hydrophilic or hydrophobic.[65, 66] Hydrophobicity of amino acids is believed to be a key parameter that regulates phenomena like protein folding-unfolding, aggregation, activity, protein-ligand binding and protein hydration in aqueous environments.[67-71] It has also been established that structure and activity of biomolecules are slaved by the associated hydration.[72] To unravel the heterogeneity in protein hydration it is of utmost importance to understand how individual amino acid hydrates. Hydration of a native protein changes substantially during structural unfolding process resulting in the exposure of some of the otherwise buried hydrophobic amino acid residues.[73, 74] While analysing the solvation of hydrophobic and hydrophilic parts of a protein separately one needs to take into consideration that the environment of amino acid residues are heterogeneous in nature as they are often composed of hydrophobic alkyl chains and hydrophilic groups. It is therefore essential to study the hydration of amino acids of various side chains in the exposure to solvents.

From a thermodynamic point of view a hydrophobic solute when exposed to water creates a void by breaking the H-bonds adjacent to its surface and the enthalpic penalty is minimised by ordering the water network in a more favourable direction.[75] There have been several experimental as well as theoretical studies carrying out addressing the hydrophobicity of the amino acids[65, 66, 76, 77] as well as structure, stability and solvent effect on different amino acids.[78-80] Aqueous solutions of amino acids have extensively been studied using different experimental techniques involving IR spectroscopy[81], NMR spectroscopy[82, 83], Raman spectroscopy[84], neutron diffraction[85] as well as using molecular dynamics simulation[86] technique. Recently Panuszko et al. have investigated the hydration structure in some amino acids using FTIR and MD simulation studies.[87] There have been a few dielectric relaxation (DR) studies in the MHz-GHz frequency domain to probe the dynamics of hydrated amino acids.[88-90] These studies reveal that the rotational dynamics of amino acid molecules take place in ~100 ps timescale. The cooperative reorientation motion of water molecules (~ 10 ps) as reported in these studies is an average effect of the solutes over the

whole hydration layer as this frequency window is unable to explicitly probe the ultrafast collective hydration dynamics. Sato et al.[88] have studied DR on a model amino acid glycine in the range of 0.1-89 GHz. They reported three time scales of ~ 40 ps for the rotational diffusive motion of glycine, ~ 9 ps and 1-2 ps for bulk water and localized free water or weakly hydrogen-bonded dynamics, respectively. Arteche et al.[89] carried out DR in a series of amino acids (glycine, alanine, threonine, histidine, proline, arginine, lysine) in 0.2-20 GHz frequency range and observed that the rotational motion of amino acids retards with size and concentration of the amino acids, however, water relaxation around amino acids vaguely changes from one amino acid to another. It is important to note here that DR in GHz region is unable to precisely probe the ultrafast cooperative water relaxation around small solutes as it is affected by the rotational relaxation of the solutes.

It thus stands pertained to understand that how the long-range collective water network around different amino acids changes; such changes leave their imprints in the elusive THz regime. Driving the solutes in the THz range associates fast and efficient coupling of water network which otherwise is not realized in the conventional IR spectroscopy, as it is more localized on the solute and little energy is transferred to the surrounding water. Niehues et al. studied the hydration of a series of amino acids in ~2.4 THz window and observed that α of hydrated amino acids can be correlated with the hydrophobicity and fraction of polar volume of amino acids. They have shown that glycine has the largest positive THz slope followed by serine whereas for the other amino acids the slope becomes gradually negative with increasing hydrophobicity.[91] They have simulated the hydration dynamics around hydrophobic and hydrophilic model particle using MD simulation technique. In a more recent report Shiraga et al.[92] have studied the hydration network around a fixed concentration of glycine and a series of analogous molecules in which hydrophobicity is progressively increased by adding methylene groups into the side chains. The authors found a correlation between the extent of H-bonding and the hydrophobicity of the solute. It is important to note that hydrophobic scales of amino acids, as introduced in previous literatures, are mostly theoretical in nature and are based on the gross calculation of the abundance of polar and nonpolar parts in the amino acids.[65, 66] The thus calculated hydration scale is often not the best interpretation of their complex structures. Solvent accessible surface area (SASA) is an important parameter that explicitly defines hydration behaviour in proteins.[93] Likewise, amino acids can also be assigned to different SASA values. It has been observed that SASA of hydrophobic solutes often describes hydrophobic hydration in a better

manner. Here we have used glycine (Gly) and the L- isomers of five different α-amino acids:, serine (Ser), aspartic acid (Asp), lysine (Lys), arginine (Arg) and tryptophan (Trp) of varying hydrophobicity and SASA and studied the DR up to their maximum water solubility in the frequency window of GHz-THz at neutral pH at 298 K. Our study is a preliminary step towards understanding the complex hydration behaviour of proteins, the organized assemblies of amino acids.

5.2 Materials and Methods

5.2.A. Materials & Sample Preparation:

Sucrose, urea (ultra-pure), thiourea, 1,1,3,3-tetramethylurea (TMU), and trimethylamine-N-oxide (TMAO), sodium chloride (NaCl), guanidinium chloride (GdmCl), 1,1,3,3-tetramethylguanidine (TMGdn), guanidinium sulphate (Gdm_2SO_4), human serum albumin (HSA) (M_w 66 kD) and amino acids (Glycine, L-Arginine, L-Serine, L-Tryptophan, L-Lysine, L-Aspartic acid) were purchased from Sigma Aldrich with a purity ~99% and used without further purification. 1,1,3,3-tetramethylguanidium chloride (TMGdmCl) was prepared by mixing a stoichiometric hydrochloric acid (HCl) with TMGdn. All the solutions were prepared in a 10 mM sodium phosphate buffer (pH=7.4) using deionized Milli-Q water.

5.2.B. Instruments & Methods:

TTDS measurements were carried out in a commercial THz spectrophotometer (*TERA K8, Menlo System*). (see *chapter 3 for details*).

Dielectric relaxation measurements in 0.2 -50 GHz regime were performed using a PNA-L network analyser (N5230C) with an open ended coaxial probe (85070E). Before the measurements it was calibrated using air, shorting block and water as open, short and load respectively and the details could be found elsewhere.[94-96] The sample solutions were taken in a glass cylindrical container of diameter greater than 1 cm. The solution in direct contact with the coaxial dielectric probe alters the magnitude as well as the phase of the reflected power observed by the network analyzer (NA). The real and imaginary dielectric constants were then obtained from the software directly after each frequency sweep.

Debye model (details provided in chapter 2) was used to describe the dynamics of water molecules in various cosolutes solutions. For Keeping in mind that a considerable fraction of water molecules in these concentrated solutions move rather slowly, we

introduced an additional Debye mode[48]; the following equation describes the frequency-dependent complex permittivity, $\tilde{\varepsilon}(\omega)$:

$$\tilde{\varepsilon}(\omega) = \varepsilon_\infty + \frac{S_{slow}}{1+i\omega\tau_{slow}} + \frac{S_1}{1+i\omega\tau_1} + \frac{S_2}{1+i\omega\tau_2} + \frac{S_3}{1+i\omega\tau_3} \qquad (5.1)$$

where S_i (i=slow, 1,2,3) is the relaxation strength of the i-th mode with relaxation time τ_i and ω is the angular frequency. The τ_{slow} values have been fixed using the literature data for urea[20], TU[35], TMU[97] and TMAO[98]. For ionic solution an additional term ($\sigma/i\omega\varepsilon_0$) is introduced in Debye equation where σ is dc conductivity (details in chapter 2).

5.3. Results and Discussions

5.3.I. Urea Alters the Collective Hydrogen Bond Dynamics in Water: A Dielectric Relaxation Study in the THz Frequency Region

We started with a rather inert biomolecule sucrose which is known to render protein stability[99] and often act as an osmolyte[100]. Figure 5.3.I.1(a) depicts a representative THz signal and the corresponding fast Fourier Transformation (FFT) spectra of sucrose solutions at different concentrations. The extracted frequency dependent optical parameters, viz. refractive index (n) and absorption coefficient (α) has been shown at different sucrose concentrations in figure 5.3.I.1 (b), (c). It can be observed that α decreases almost linearly with increasing sucrose concentration, which is consistent with earlier reports for another disaccharide, lactose in the 2.4-2.8 THz frequency region.[101, 102] The observed decrease in α can be rationalized as highly absorbing water molecules being replaced by comparatively less absorbing sucrose molecules. However, it should be taken into consideration that carbohydrate molecules are associated with a dynamic hydration shell which extends up to 5-7 Å from the solute surface and offers an absorption coefficient different from that of bulk water.[101] Thus the overall change in α(ν) is a collective contributions from the solvent, solute and the hydration water, which often makes the α(ν) profile to vary non-linearly with the solute concentration. We fit the obtained ε_{re} and ε_{im} in 0.3-1.5 THz frequency window considering a multiple Debye relaxation model and some representative fitted plots are shown in figure 5.3.I.1. (d). Dielectric relaxation of carbohydrate solutions in kHz to GHz region has previously been studied by several groups.[103-105] Broadband dielectric spectroscopic study by Kaminski et al. has concluded that aqueous sucrose solutions exhibit three different relaxation modes in the low frequency region, namely, α (~10^{-6} s), γ (~10^{-7} s) and β (~10^{-9} s) relaxation

mode.[106] A double Debye (and/or Cole-Cole) relaxation fitting of dielectric measurements in the 200 MHz-40 GHz region by Fuchs et al.[103] and Weingärtner et al.[104] have extracted two gross relaxation times, which are of the order of ~10 ps and ~35-45 ps for 1M sucrose solution, the former one being the rotation of water while the second one is sub-diffusive in nature.

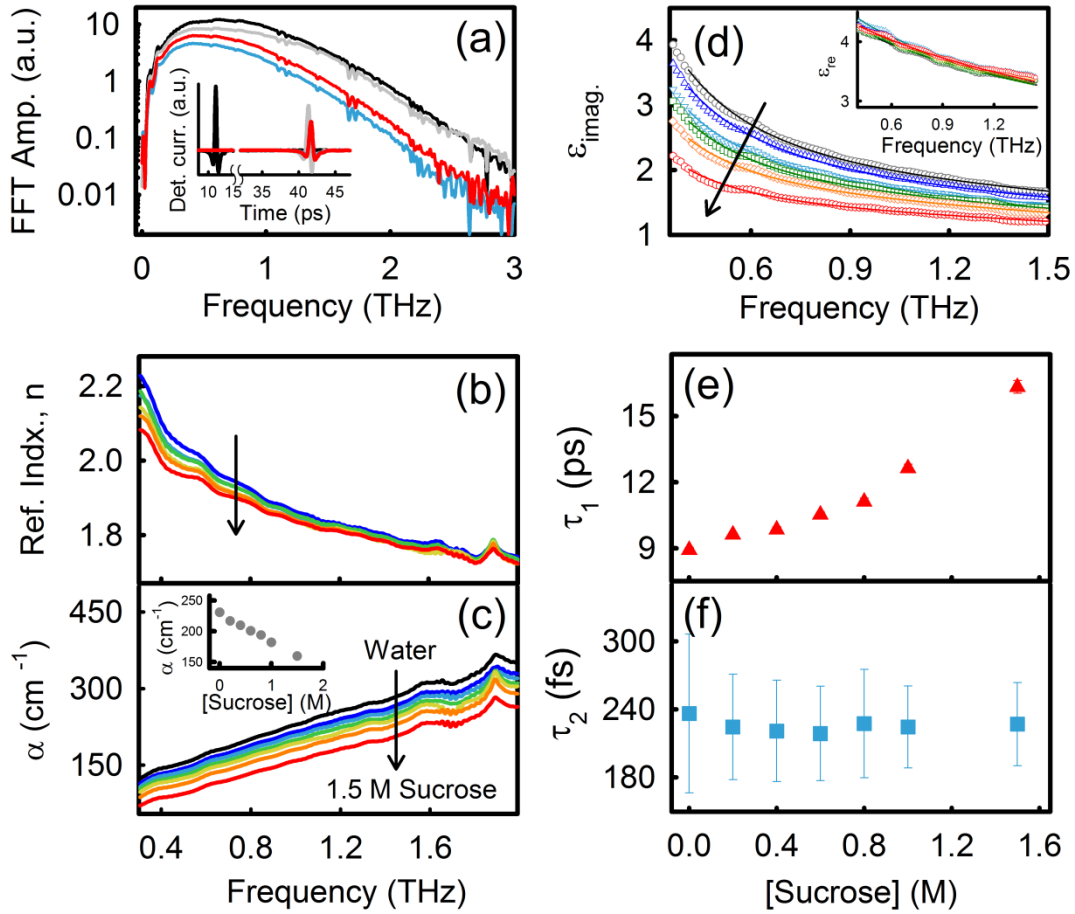

Figure 5.3.I.1. (a) Frequency dependent THz signals in air (*black line*), through the cell (*grey line*), the cell containing water (*blue line*) and 1.5 M sucrose (*red line*). Inset shows representative THz signal in time domain window. (b) Frequency dependent refractive index, n of aqueous sucrose solutions at different concentrations. The arrow indicates increasing sucrose concentration. (c) Frequency dependent absorption coefficient, α of aqueous sucrose solutions at different concentrations. The inset shows the absorption coefficient of sucrose solutions at 1 THz as a function of its concentration. (d) Frequency dependent real and imaginary dielectric constants of water and various sucrose solutions. The solid lines are the Debye relaxation fits. (e) and (f) show the time scales (τ_1 and τ_2) as a function of sucrose concentration.

The focus of our present investigation is the change in the ultrafast collective hydrogen bond dynamics which extends up to several hydration layers and leaves its imprint in the THz frequency region. Thus the timescale of ~30-40 ps is rather slow for the present frequency window to detect. It can be noted here that water exhibits a strong IR active mode at ~200 cm^{-1} which is due to the hydrogen bond stretching[107] and another very weak band at ~60 cm^{-1}

which emanates from hydrogen bond bending[33, 107] which does not contribute to the diffusive and re-orientatial relaxation processes. For water, the obtained times scales are ~ 9 ps, ~ 200 fs and ~80 fs, which are in excellent agreement with previous studies[108]. The ~9 ps and ~200 fs timescales are due to the well-known cooperative rearrangement of the hydrogen bonded network and the rotational modes of individual polar water molecules, respectively[109]. The ~80 fs timescale has its origin rooted to the 60 cm^{-1} vibrational band due to the hydrogen-bond bending and the related transverse acoustic phonons which propagate in a direction normal to the hydrogen bonds in between two neighbouring water molecules.[110, 111] It can be observed from figure 5.3.I.1. (e), (f) that the timescale τ_1 increases with increase in sucrose concentration, while τ_2 suffers only marginal change within the error limit. The increase in the τ_1 clearly indicates that the cooperative rearrangement of the hydrogen bonded water molecules gets restrained as compared to that in bulk water, which perhaps manifests the formation of highly structured hydration layer around sucrose. The DR study in sucrose thus affirms the formation of structured water around the solute following previous reports in the literature [101, 102].

The results of the urea measurements are shown in figure 5.3.I.2. Figure 5.3.I.2. (a) depicts the $\alpha(\nu)$ profile of urea differs from that of sucrose and does not show any near-linear dependency with urea concentration. An interesting phenomenon of intersection of $\alpha(\nu)$ curves of urea solutions with that of bulk water has also been observed. Appearance of such crossing point (CP) in aqueous solutions has significance in the THz frequency region as it indicates that at that particular frequency, the solution offers higher α compared to that of pure water. It is interesting to note that the $\alpha(\nu)$ profile has been reported to be rather regular in the 2.4-2.8 THz frequency region, with the hydration water showing higher $\alpha(\nu)$ compared to that of bulk water.[101, 102] In the frequency range of 0.1-2 THz instead, the hydration water offers lower $\alpha(\nu)$ at lower frequency and beyond the CP it overturns the bulk water values[112]. The location of a CP usually depends on the extent of hydrophobicity (or hydrophilicity) of the solute surface. The $\alpha(\nu)$ profile as observed in sucrose is rather featureless compared to that of urea and decreases gradually with increasing sucrose content indicating that the sucrose-water interaction results only in the formation of hydration layer. In figure 5.3.I.2(b), we have shown two representative $\alpha(\nu)$ intersections for 2M and 5M urea solution and the CP at different urea concentration has been plotted (figure 5.3.I.2.b, inset). It can be observed that the CP moves towards higher frequency as the concentration of urea increases, with a

considerable hike in the 5-6 M region. MD simulation studies have concluded that when water interacts with a hydrophilic surface, a CP is produced at a frequency blue shifted compared to that in case of a hydrophobic surface.[33] The observed blue shift thus infers that with increasing urea concentration, surface water experiences a more hydrophilic environment. We plot the measured α at 1 THz as a function of urea concentration (figure 5.3.I.2a, inset) and it is found that α suffers a smaller decrease with urea concentration compared to that of sucrose (figure 5.3.I.1). This observation qualitatively leads to infer that urea brings about change in the water structure, especially in the extended collective hydration layer which is markedly different from those offered by a rather indifferent or structure providing solute, sucrose.

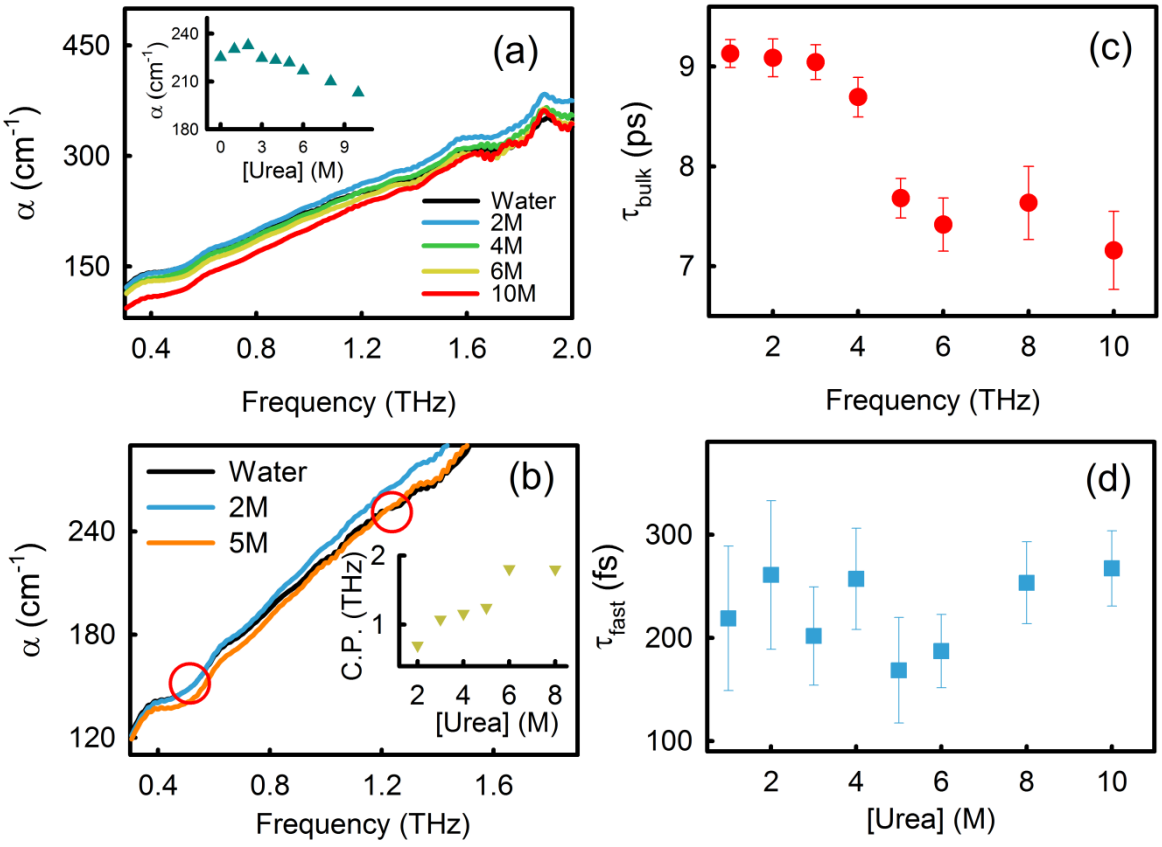

Figure 5.3.I.2. (a) Frequency dependent absorption coefficient, α of aqueous urea solutions at different concentrations. The inset shows the absorption coefficient of urea solutions at 1 THz as a function of urea concentration. (b) The circles demarcate the crossing point between the absorption coefficient of water and that of 2M and 5M urea solutions. The inset shows the crossing point (CP) as a function of urea concentration. (c) and (d) show the time scales (τ_1 and τ_2) as a function of urea concentration.

In order to obtain a more quantitative understanding, the ultrafast collective dynamics of water in the extended hydration layer of urea has been extracted using a multi exponential

Debye relaxation model (as discussed previously) after fixing the slower relaxation times arising out of the urea-water co-cluster interaction, following previous literatures.[20, 35] The results are depicted in figure. 5.3.I.2(c), (d) and table 5.3.I.1. Earlier studies have concluded that the slow relaxation dynamics of water-urea solution (~ 20-30 ps) which is associated with the rotation of water in the urea-water cluster suffers only marginal changes with urea concentration, however, the strength of this relaxation mode increases with increasing urea concentration.[20] In this context it is important to understand that our investigation is aimed more towards the water-water collective network dynamics and the timescales reported in this study are purely associated with the cooperative hydrogen bond rearrangement and hydrogen bond making-breaking dynamics in water. Thus we focus our attention on the changes in the timescales τ_1 and τ_2 as a function of urea concentration. It can be observed that τ_1 suffers a marginal change within the error limit up to a concentration of 4 M beyond which it decreases appreciably to a low value of 7.1 ps. This drastic decrease in τ_1 unambiguously points out towards a faster cooperative hydrogen bond rearrangement dynamics, which could have originated from a possible disruption in the extended hydration layer around urea. A similar change has also been observed in the τ_2 values wherein the timescale decreases sharply in the 4-6 M urea region. Since τ_2 is associated with the rotational modes of individual water diploes within the network, the observed decrease in τ_2 indicates towards an abundance of weakly bonded water molecules in the network. The observed decrease in τ_1 and τ_2 is in strong accordance with the simulation results by Zou et al.[14] which concluded a decrease in the average water-water hydrogen bond lifetime in presence of urea. Our study also experimentally verifies earlier MD simulation studies by Wei et al.[15] that concluded a slight collapse of the second water shell around a water molecule in urea solution relative to pure water; and also corroborates the results of Idrissi et al.[8] which concluded distortion of the tetrahedral distribution of water in the presence of urea. It is also interesting to note that the observed perturbation is more prominent in the 4-6 M region, which interestingly coincides with the threshold denaturing concentration of urea for most of the proteins.[113] It may be taken into consideration that TTDS technique is a useful tool to understand the dynamics of water molecules as it does not provide with a direct information on the structural aspects, thus our observation does not a priori render a direct support to the 'structure breaking' hypothesis of urea, however, the observed acceleration of the dynamics perhaps offers a direct manifestation of a perturbation of water structure in the extended hydration

sheathe of urea. The change in the water dynamics could be intuited to play a pivotal role in the protein denaturing ability of urea through the 'indirect mechanism'.

To further support the conclusions we study the relaxation dynamics of water in presence of two derivatives of urea, namely, thiourea (TU) and tetramethyl urea (TMU), which are also known to be protein denaturants.[48, 114, 115] The fitted parameters are depicted in figure. 5.3.I.3 and table 5.3.I.2, 5.3.I.3, respectively. TU has a lower water solubility compared to urea and the relaxation time constants also do not suffer appreciable changes within the error limit in the studied concentration range. It can be noted that TU only has the carbonyl oxygen of urea being replaced by a sulphur atom. The observed result is in excellent corroboration with the simulation results by Venzi et al.[13] which concluded that water structure remains unaltered around the amine groups, and gets perturbed only in the carbonyl part of urea.

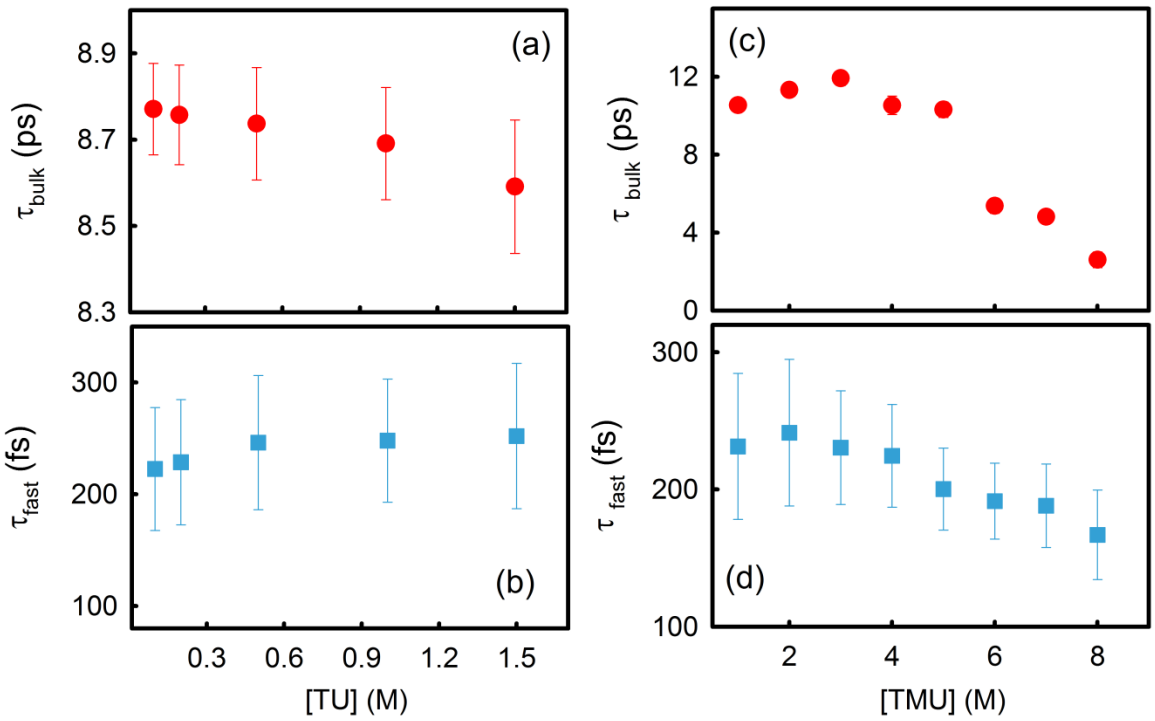

Figure 5.3.I.3. Time scales (τ_1 and τ_2) as a function of thiourea [(a) and (b)] and tetramethyl urea [(c) and (d)] concentration in aqueous solutions.

It thus appears that the interaction of the carbonyl oxygen of urea with water plays a predominant role in determining the dynamics of water in the extended hydration sheathe of urea. The Debye fitted parameters for TMU are provided in figure. 5.3.I.3(c),(d) and table 5.3.I.3. It can be observed that τ_1 increases mildly within the error limit up to 4 M concentration, beyond which it decreases sharply to 2.6 ps at 8 M concentration. The τ_2

values also offer a regular decrease beyond 4 M concentration. The observed change somewhat reciprocates the trend observed in case of urea (figure. 5.3.I.2.c, d). The decrease in the time constants clearly indicates a perturbation of the network water structure in presence of TMU. Such a tetrahedral network 'structure breaking' ability of TMU has previously been concluded on the basis of the change in the distribution function of the O-O-O angle of water molecules by TMU[15]. A detailed dielectric relaxation and polarization-resolved fs MIR pump-probe experiment on aqueous solution of TMU has been reported by the group of Bakker et al.[97, 116, 117] Their studies have identified immobilized water at the surface of the solute TMU which offers relaxation dynamics as slow as ~80 ps, the immobilization being significantly prominent with respect to that in urea. The authors concluded that water forms small clusters around TMU, in which the directly hydrogen bonded OH group stands responsible for the observed retardation of water dynamics, whereas those in the interior of the cluster can take part in the cooperative hydrogen bond exchange and show the fast dynamics. At high TMU concentration, however, there does exist certain unbound OH groups which are mobile and contribute to the fast dynamics.[117] The observed acceleration of τ_1 and τ_2 at a higher TMU concentration perhaps manifests the occurrence of the unbound OH groups.

In contrast to urea and its derivatives, TMAO is well known to bias the unfolded structure of proteins toward the folded state.[118, 119] The exact mechanism of the opposing effect of TMAO on urea denaturation is, however, still not clearly understood. It has experimentally been shown that TMAO does not directly interact with urea,[120] however, neutron scattering experiment have concluded the oxygen atom of TMAO to preferentially form hydrogen bond with urea.[121] There have been several counterintuitive proposals which include preferential exclusion of TMAO from protein[122] by altering the water structure[14] and preferential solvation of TMAO by water and urea.[123] In the present study we attempt to address the question that whether the water dynamics suffers any significant alteration when TMAO is added to urea solutions. Figure. 5.3.I.4(a), (b) shows the $n(\nu)$ and $\alpha(\nu)$ profiles of TMAO at different concentrations. It can be observed that $\alpha(\nu)$ decreases almost linearly with increasing TMAO concentration.

The Debye relaxation fitting parameters are depicted in figure. 5.3.I.4. (c), (d) and table 5.3.I.4. It can be observed that τ_1 increases rapidly with increasing TMAO

concentration, which clearly indicates that TMAO strengthens the collective hydrogen bonded network in water as has also been observed in case of sucrose.

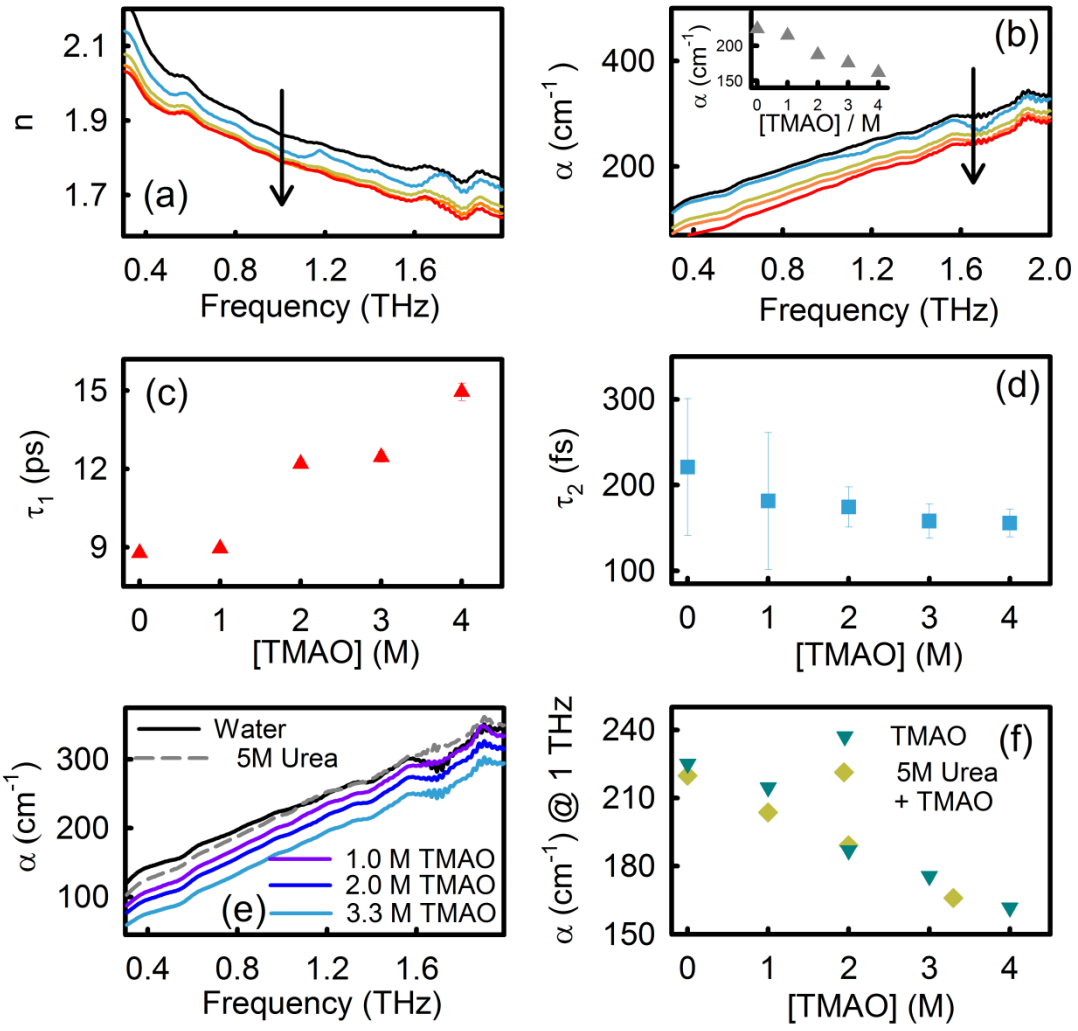

Figure 5.3.I.4. (a) Frequency dependent refractive index, n of aqueous TMAO solutions at different concentrations. The arrow indicates increasing TMAO concentration. (b) Frequency dependent absorption coefficient, α of aqueous TMAO solutions at different concentrations. The arrow indicates increasing TMAO concentration. The inset shows the absorption coefficient of TMAO solution at 1 THz as a function of its concentration. (b) and (d): Time scales (τ_1 and τ_2) as a function of TMAO concentration in aqueous solutions. (e) Absorption coefficient, α of 5 M urea solution in presence of 1.0, 2.0 and 3.3 M TMAO. (f) Absorption coefficient, α at 1 THz of TMAO and TMAO + 5M urea solutions as a function of TMAO concentration.

Such observation is in excellent agreement with previous IR study[124] as well as simulation results which concluded enhancement of water structure by TMAO.[15, 123, 125] The restricted dynamics is thus related to the structured water molecules at the TMAO surface. We then extend our study to the mixture of urea and TMAO solution. Figure. 5.3.I.4.(e) depicts the α(ν) profile of 5 M urea in the presence of different concentrations of TMAO. It is clearly evident that α(ν) decreases steadily with increasing TMAO concentration. In order to achieve

at a more comprehensive insight we plot the absorption coefficient of aqueous TMAO solution in absence and in presence of 5 M urea in figure. 5.3.I.4.(f). The striking comparability of the α values for the two systems unambiguously specifies that the dynamic property of water in the mixed system resembles that in the presence of TMAO itself irrespective of its possible disruption in presence of urea. This leads to infer that the stronger hydrogen bonding of water with TMAO overwhelms the effect of urea to govern the overall dynamics of water, which might have a possible influence on the observed stabilization effect of TMAO over the urea destabilization. In order to obtain additional support towards our findings, we extend our study to the mixture of urea and sucrose. Figure 5.3.I.5 shows the α(ν) profile of 5 M urea in absence and in presence of sucrose and also the α measured at 1 THz of 1.5 M sucrose in presence of different concentration of urea solutions.

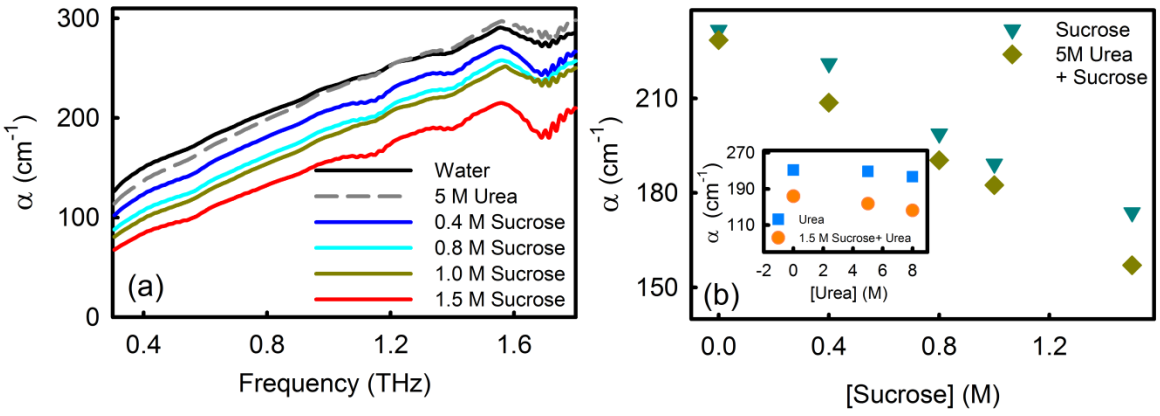

Figure 5.3.I.5. (a) Absorption coefficient, α of 5 M Urea solution in absence and presence of different concentrations of Sucrose solution. (b) Absorption coefficient, α at 1 THz of Sucrose and Sucrose + 5M Urea solutions as a function of Sucrose concentration. The inset shows the absorption coefficient, α at 1 THz of Urea and Urea + 1.5M Sucrose solutions as a function of Urea concentration.

From this comparative study it is evident that the absorption profile of the mixed system follows a trend similar to that of the sucrose itself rather than that of urea. This firmly suggests the water structure breaking ability of urea to be overwhelmed by the structure making ability of sucrose. This results is in excellent accordance with a previous study[126] that reports the ability of sucrose to reduce the protein denaturing ability of chaotropic agents, and thus render support to our notion that hydration of urea does play a pivotal role in the protein denaturation process.

To summarize, the remarkable ability of urea and its derivatives to denature proteins has received explanation on the basis of both ‘direct’ as well as ‘indirect’ interactions, the

later mechanism being involved with a possible ‘disruption’ of water structure, however, has not received much experimental support. In the present study we have made an attempt to understand the effect of urea on the relaxation dynamics of water, especially in the extended collective network regime using dielectric relaxation study in the THz frequency region using TTDS technique and its possible correlation on the hypothesis of water ‘structure breaking’. The advantage of TTDS over the conventional spectroscopic techniques is that it measures both the phase and the intensity of THz radiation which enables one to obtain various optical parameters of the solution. Also most of the ‘collective’ intermolecular rotational and vibrational modes of water leave their signature in the THz frequency range, and thus TTDS provides with the global dynamics of extended water network. The relaxation dynamics of small solutes as well as osmolytes is generally associated with strongly hydrogen bonded water molecules at the surface which relax at a timescale of tens to hundreds of ps. Such rotation is rather slow to be detected in the THz frequency range. Our study is more focused to extract the collective dynamics (e.g. the cooperative rearrangement of hydrogen bonds) which, in bulk water, occurs in ~9 ps and ~200 fs time scale. It is important to note here that our study does not disregard the formation of strongly hydrogen bonded solvation layer, the existence of which has been realized by several experimental and simulation studies. It rather complements these observations by extracting the relaxation dynamics in the extended solvation shell. As a model osmolyte we have studied the aqueous solution of sucrose which shows retardation in the dynamics correlating the formation of structured water around itself. In case of urea and TMU, however, the relaxation dynamic shows considerable acceleration beyond a threshold concentration. Such acceleration is possibly associated with a disruption of the tetrahedral water network structure. It seems also intriguing that the observed collapse occurs at a certain urea concentration which strikingly coincides with the denaturation concentration of urea for many proteins. Despite the fact that TTDS does not provide any direct information on the structure of the solvents and thus not directly supports the notion of urea being a ‘structure breaker’, the extracted dynamics essentially hints towards a perturbation in the extended hydrogen bonded network in water, and also possibly invokes the idea that the ‘indirect’ mechanism of water structure breaking perhaps has non-negligible role to play in the protein denaturation process.

Table 5.3.I.1. Debye relaxation fitting parameters of aqueous solutions of urea at different concentrations

[Urea] (M)	ε_∞	$^{(a)}S_{slow}$	$^{(a)}S_1$	S_2	S_3	$^{(a)}\tau_{slow}$ (ps)	τ_1 (ps)	τ_2 (fs)	τ_3 (fs)
0	2.15±0.02	-	71.6	0.41±0.1	1.18±0.19	-	8.86±0.1	224±73	84
1	1.99±0.04	08.94	67.3	0.37±0.1	1.44±0.16	21.30	9.13±0.1	218±83	88
2	2.00±0.03	18.12	60.2	0.46±0.04	1.63±0.12	21.30	9.09±0.2	260±81	89
3	2.10±0.04	25.49	53.5	0.70±0.12	1.28±0.20	21.30	9.04±0.2	201±48	89
4	2.06±0.03	35.11	45.2	0.65±0.04	1.47±0.10	21.30	8.69±0.2	257±49	88
5	2.13±0.08	47.02	37.4	0.71±0.26	1.25±0.36	21.30	7.68±0.2	168±51	88
6	2.22±0.04	61.40	26.8	0.95±0.15	1.12±0.25	21.60	7.42±0.3	187±36	88
8	2.11±0.03	71.62	20.1	0.85±0.04	1.57±0.11	24.80	7.63±0.4	253±40	88
10	2.15±0.03	76.25	16.1	0.90±0.03	1.65±0.09	28.26	7.16±0.4	267±36	88

(a) Values taken from: *J. Phys. Chem. B*, (2007) ***111*****,** 1076-1080.

Table 5.3.I.2. Debye relaxation fitting parameters of aqueous solutions of thiourea (TU) at different concentrations

[TU] (M)	ε_∞	$^{(c)}S_{slow}$	$^{(c)}S_1$	S_2	S_3	$^{(c)}\tau_{slow}$ (ps)	τ_1 (ps)	τ_2 (fs)	τ_3 (fs)
0	1.94±0.03	-	71.59	0.28±0.04	1.4±0.1	-	8.85±0.1	229±90	84
0.1	1.95±0.03	0.99	70.98	0.32±0.05	1.4±0.1	18.3	8.77±0.1	222±81	83
0.2	1.95±0.03	2.13	70.24	0.33±0.05	1.4±0.1	18.3	8.76±0.1	228±85	83
0.5	1.96±0.03	5.01	68.81	0.33±0.04	1.5±0.1	18.3	8.74±0.1	246±94	83
1.0	1.96±0.03	9.42	65.21	0.36±0.04	1.5±0.1	18.3	8.69±0.1	248±83	84
1.5	1.98±0.03	12.94	62.44	0.36±0.04	1.4±0.1	18.3	8.59±0.1	252±95	84

(c) Values taken from: *J. Phys. Chem.*, (1986) ***90*****,** 5464-5469.

Table 5.3.I.3. Debye relaxation fitting parameters of aqueous solutions of tetramethylurea (TMU) at different concentrations

[TMU] (M)	ε_∞	$^{(b)}S_{slow}$	$^{(b)}S_1$	S_2	S_3	$^{(b)}\tau_{slow}$ (ps)	τ_1 (ps)	τ_2 (fs)	τ_3 (fs)
0	1.89±0.03	-	71.50	0.28±0.04	1.5±0.1	-	8.71±0.1	234±97	84
1	1.92±0.03	12.28	58.98	0.43±0.04	1.3±0.1	28.50	10.53±0.2	231±53	83
2	1.82±0.03	19.1	44.01	0.46±0.03	1.3±0.1	38.92	11.32±0.3	241±53	83
3	1.83±0.03	32.60	30.24	0.52±0.03	1.0±0.1	50.00	11.92±0.4	230±41	82
4	1.75±0.03	39.56	18.34	0.55±0.04	0.9±0.1	62.59	10.53±0.5	224±37	82
5	1.71±0.03	40.45	10.59	0.62±0.06	0.65±0.1	71.60	9.90±0.6	200±30	83
6	1.69±0.03	41.00	5.00	0.64±0.07	0.56±0.1	80.09	5.37±0.4	192±28	83
7	1.54±0.03	41.03	4.1	0.56±0.07	0.59±0.1	88.58	4.81±0.4	188±30	82
8	1.44±0.02	41.15	1.05	0.50±0.11	0.40±0.2	50.01	2.61±0.4	167±33	82

(b) Values taken from: *J. Am. Chem. Soc.* (2010) *132*, 15671-15678; *Faraday discuss.* (*2013) 160*, 171-189.

Table 5.3.I.4 Debye relaxation fitting parameters of aqueous solutions of TMAO at different concentrations

[TMAO] (M)	ε_∞	$^{(d)}S_{slow}$	$^{(d)}S_1$	S_2	S_3	$^{(d)}\tau_{slow}$ (ps)	τ_1 (ps)	τ_2 (fs)	τ_3 (fs)
0	1.89±0.03	-	71.50	0.28±0.04	1.5±0.1	-	8.71±0.1	234±97	84
1	1.94±0.05	5.68	63.59	0.38±0.16	1.23±0.2	21.02	8.94±0.13	181±80	82
2	1.91±0.03	12.05	52.43	0.82±0.12	1.00±0.2	22.6	12.19±0.2	174±23	82
3	1.90±0.04	14.89	44.68	0.99±0.17	0.83±0.2	32.0	12.46±0.2	158±20	82
4	1.82±0.03	17.86	35.58	1.10±0.17	0.89±0.21	40.2	14.94±0.3	156±16	82

(d) Values taken from: *J. Phys. Chem. B*, (2012) *116*, 4783-4795.

5.3.II. Collective Hydration Dynamics of Guanidinium Chloride Solutions and its Possible Role in Protein Denaturation: A Terahertz Spectroscopic Study

The results of the GdmCl aqueous solutions measurements are depicted in figure 5.3.II.1 The frequency dependent profiles of absorption coefficient, α of GdmCl solutions at different concentrations are shown in figure 5.3.II.1.(b). α is found to increase with increasing frequency and the $\alpha(\nu)$ profile for the buffer shows good agreement with previously reported results.[108, 109] For a better comprehension, we plot the α values at 1 THz as a function of GdmCl concentration (inset of figure 5.3.II.1.(b). It is observed that α increases linearly up to a concentration of 2 M beyond which it does not change appreciably. The frequency dependent absorption coefficient of aqueous solutions in the THz frequency region provides with useful information as α essentially manifests the collective dynamics of water molecules in the THz frequency range.[33, 112] It is generally expected that when highly absorbing water is replaced with a low absorbing solute, $\alpha(\nu)$ decreases. The observed change in $\alpha(\nu)$ in GdmCl is not that straightforward as depicted in figure 5.3.II.1.(b). While explaining the behaviour of $\alpha(\nu)$ it should be taken into account that many solutes are generally associated with a dynamic hydration shell which might extend up to 5-7 Å from the solute surface and offers an absorption coefficient different from that of bulk water[101]. Thus the overall change in $\alpha(\nu)$ is a collective contributions from the solvent, solute and the hydration water, which often makes the $\alpha(\nu)$ profile to vary non-linearly.[36, 127] A careful observation of the $\alpha(\nu)$ profile reveals another interesting phenomenon as the $\alpha(\nu)$ curve of pure water (buffer) intersects the curves of the solutions. Appearance of such intersection or crossing point (CP) in aqueous solutions has significance as it indicates that beyond the corresponding frequency limit (ν_{CP}) the solution offers higher α compared to that of the buffer. A better representation of these intersections could be found in figure 5.3.II.1c, and it is evident that ν_{CP} shifts towards higher frequency with increasing GdmCl concentration. It is interesting to note that $\alpha(\nu)$ profile in the 2.4-2.8 THz frequency region shows consistently higher $\alpha(\nu)$ for hydration water compared to that of the bulk water.[101, 102] In the frequency range of 0.1-2 THz instead, the hydration water offers lower

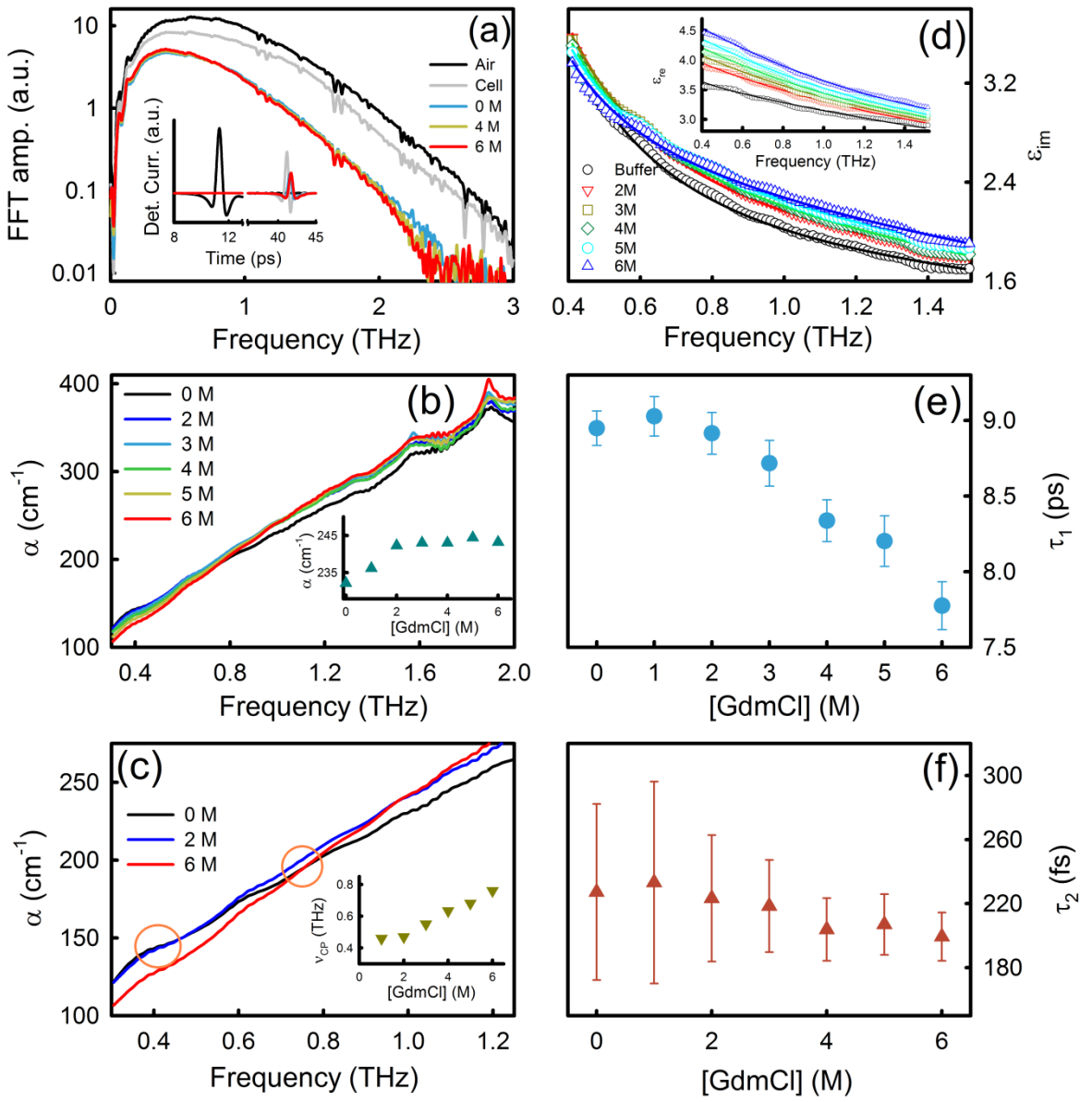

Figure 5.3.II.1. (a) The inset shows a representative THz signal in air (black), of the cell (grey) and the cell containing 6 M GdmCl (red). The corresponding FFT spectra are shown in the main figure. (b) Frequency dependent absorption coefficient, α of aqueous GdmCl solutions at different concentrations. The inset shows α at 1 THz as a function of GdmCl concentration. (c) Absorption coefficient of buffer and that of 2M and 6M GdmCl solutions. The circles demarcate the crossing points. The inset shows the crossing point as a function of GdmCl concentration. (d) Representative fittings of ε_r and ε_{im} for aqueous GdmCl solutions using multiple Debye relaxation model. (e) and (f) show the relaxation time scales (τ_1 and τ_2) as a function of GdmCl concentration.

α(ν) at lower frequency and beyond the ν_{CP} it overwhelms the bulk water values.[112] The value of ν_{CP} usually depends on the extent of hydrophobicity (or hydrophilicity) of the solute surface. We plot the ν_{CP} as a function of GdmCl concentration in figure 5.3.II.1c (inset) and it is observed that ν_{CP} increases linearly with GdmCl concentration similar to that of urea solution. In accordance to the earlier reported MD simulation studies [33] the observed blue

shift can be rationalized by the fact that with increasing GdmCl concentration, water molecules experience a more hydrophilic environment as well as a change in the in the water structure, especially in the extended collective hydration layer. A recent simulation study has predicted GdmCl to form like-ion pairs owing to its amphiphilic nature which eventually results in stacked structures.[56] Formation of such a structure perhaps leads the water molecules to get expelled from the surface and interact solely with the hydrophilic part of the salt aggregates, and induces ν_{CP} to suffer a blue shift.

The ultrafast collective dynamics of water in the extended hydration layer of GdmCl has been extracted using a multi exponential Debye relaxation model (as discussed previously). Some representative fitted curves are shown in figure 5.3.II.1.(d) and the fitting parameters are presented in table 5.3.II.1. We observe three time scales to fit the solvent (buffer) relaxation dynamics which are of the order of ~ 9 ps (τ_1), 200 fs (τ_2) and 80 fs (τ_3). These time scales are in excellent agreement with the previously reported results.[108] The ~9 ps timescale explicitly associates the spontaneous restructuring of the hydrogen bond network.[48, 107] The ~200 fs timescale emanates from either quick jumps of under-coordinated water[128] or interaction induced components in the water relaxation mechanism[129] or a small angular rotation preceding a large angle jump.[130] The ~80 fs timescale has its origin rooted to the 60 cm^{-1} vibrational band due to the hydrogen-bond bending and the related transverse acoustic phonons which propagate in a direction normal to the hydrogen bonds in between two neighbouring water molecules.[110, 111] It is important to note here that the essence of the present investigation lies on the modification of the cooperative hydrogen bond dynamics of water in presence of GdmCl and a consequent correlation on its protein denaturation ability. In that respect we focus our attention on the timescales τ_1 and τ_2 only, with major emphasis to τ_1 and the remaining discussion is made on the basis of these two timescales only. We plot these two timescales as a function of GdmCl concentration in figure 5.3.II.1.(e) and (f), respectively. It is observed that τ_1 does not change appreciably up to 2 M GdmCl, beyond which it decreases linearly to reach 7.7 ps at 6 M. On the other hand τ_2 decreases only marginally with GdmCl concentration. The observed decrease in τ_1 signifies acceleration in the hydrogen bond dynamics which correlates a possible rupture in the hydrogen bond network in the extended hydration sheathe of the solute. This observation corroborates the earlier notion of GdmCl to act as a water 'structure breaker'.[45, 131, 132] The FTIR measurements by Scott et al.[45] concluded the restructuring of the water H-bond network

which is also been strongly supported by the observed acceleration in the relaxation dynamics.

In order to understand the influence of the cation on the observed hydration dynamics, we extend our study to two other salts having the same anion (Cl^-) and with two different cations: a normal alkali metal ion Na^+ and a more hydrophobic counterpart of guanidinium, $TMGdm^+$. The results are depicted in figure 5.3.II.2. It is observed that $\alpha(\nu)$ decreases consistently with increasing TMGdmCl concentration (figure 5.3.II.2a), a phenomenon much in contrary to what has been observed in case of GdmCl. To obtain a more comprehensive comparison, we plot the difference in absorption coefficient, $\Delta\alpha=\alpha_{buffer}-\alpha_{solution}$ measured at 1 THz for all the three salts in figure 5.3.II.2.(b). The absorption behaviour of the hydrophobic salt is found to be strikingly opposite compared to that of GdmCl. The gradual increase in the $\Delta\alpha$ value in TMGdmCl indicates that the nature of hydration in TMGdmCl is dissimilar to that of GdmCl. On the other hand, NaCl shows an enhanced decreasing $\Delta\alpha$ trend, which confirms that, the hydration structure around NaCl is comparable to that in GdmCl, as has previously been concluded.[47] We also determine the Debye relaxation dynamics of water in presence of these two salts. It is important to note here that TMGdmCl offers a relatively slow relaxation dynamics,[48] comparable to that obtained previously in tetramethyl urea (TMU) solutions,[97] which is of the order of 20-40 ps and is otherwise too slow to be detected in the present frequency range. We therefore fit the relaxation dynamics with a modified version of Debye model (chapter 2) introducing a slow relaxation term (τ_{slow}). In the modified equation 5.1 the τ_{slow} and S_{slow} values are kept fixed in accordance with those obtained for TMU in reference[97] (see table 5.3.II.2). Although TMGdmCl is soluble in water, meaningful fittings can only be obtained up to 1.5 M solution. We therefore report the dynamics up to 1.5 M (figure 5.3.II.2c), which, provides with a definite trend to conclude that the dynamics gets considerably slower with increasing TMGdmCl solutions, while τ_2 does not change appreciably within the error limit. The result for NaCl has been depicted in figure 5.3.II.2d and table 5.3.II.3. NaCl shows a linear decrease in τ_1, while the change in τ_2 is only marginal. The decreasing trend in τ_1 is in accordance with that of GdmCl, however, the extent of change is greater in case of NaCl. It is also interesting to note that while for GdmCl, the decrease essentially occurs beyond a threshold concentration of 2 M; for NaCl, the decrease is rather linear. This difference in the trend is very much evident in the $\Delta\tau_1$ ($= \tau_{1,buffer}$ -

$\tau_{1,solution}$) vs. salt concentration profile (figure 5.3.II.2d, inset), which in turn is in good accordance

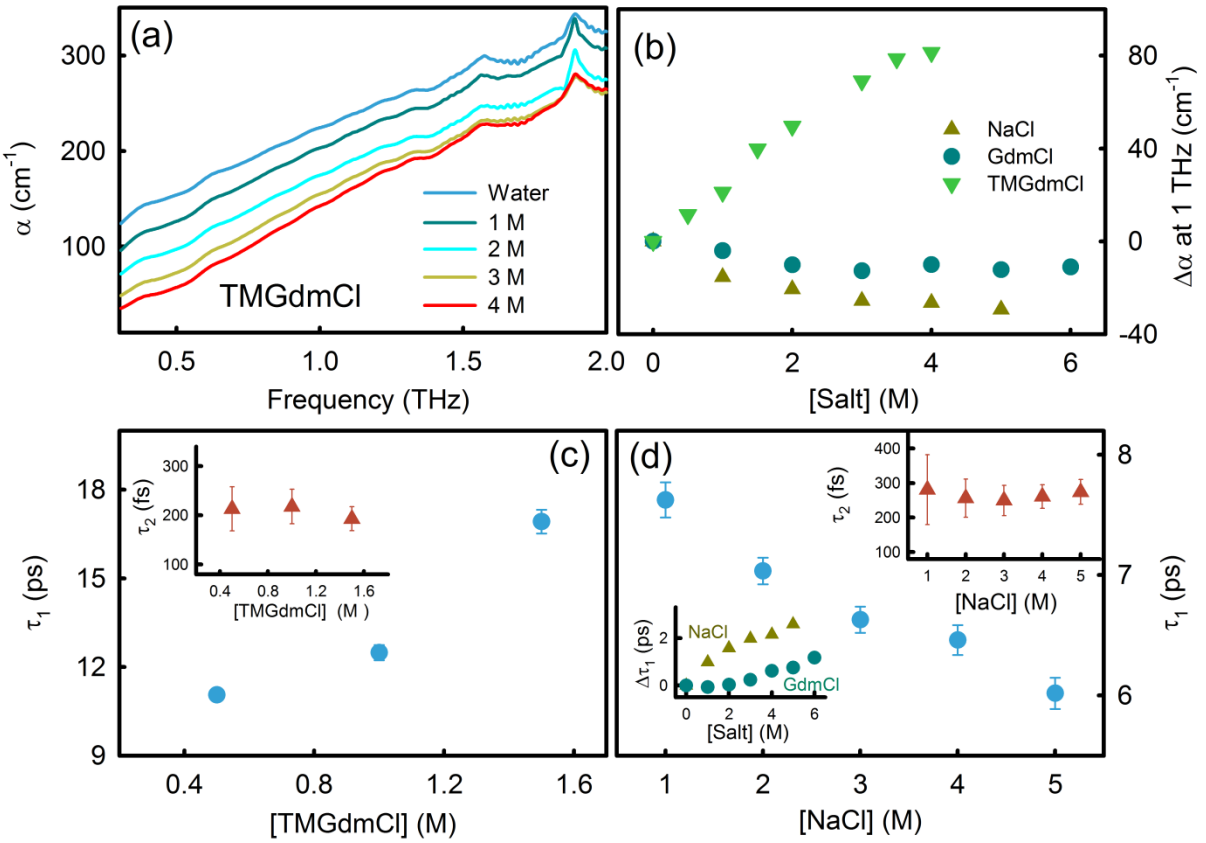

Figure 5.3.II.2. (a) Frequency dependent absorption coefficient, α of aqueous TMGdmCl solutions at different concentrations. (b) Difference absorption coefficient (Δα) at 1 THz for GdmCl, TMGdmCl and NaCl as a function of salt concentration. (c) Relaxation time scales (τ_1 and τ_2) as a function of TMGdmCl concentration. (d) Relaxation time scales (τ_1 and τ_2) as a function of NaCl concentration. The change in timescale ($\Delta\tau_1$) has been plotted as a function of salt (NaCl and GdmCl) concentration in the inset.

with the changes observed in the α(ν) profile indicating to the similarity in the ion-water interaction in these two salts. The DR study thus affirms that the collective hydrogen bond dynamics around GdmCl is somewhat similar to that of a conventional electrolyte, NaCl, with the extent of perturbation being more evident for the later. On the other hand, the dynamics is completely different in the hydrophobic TMGdmCl and the observed retardation in the cooperative hydrogen bond dynamics clearly indicates the formation of slow moving hydration layer in the vicinity of the salt. The observed retardation in TMGdmCl is in excellent corroboration to that reported by van der Post et al.[48] using fs-IR pump probe spectroscopy. It should be taken into consideration that in analogy to TMU[97, 133] there remains a possibility of aggregation of TMGdmCl molecules which can induce the observed retardation of the dynamics, however, on the other hand, such an aggregation is also expected

to be opposed by the electrostatic repulsion. The DR study thus concludes that water interacts with NaCl and GdmCl in a comparable manner, while it is markedly opposite for a more hydrophobic molecule TMGdmCl. It thus stands interesting to investigate whether such a trend reciprocates in their interaction with a globular protein, HSA.

We study the interaction of HSA with these salts using circular dichroism (CD) spectroscopy and the results are depicted in figure 5.3.II.3a. The CD signal for HSA-TMGdmCl appears to be very noisy and least meaningful.

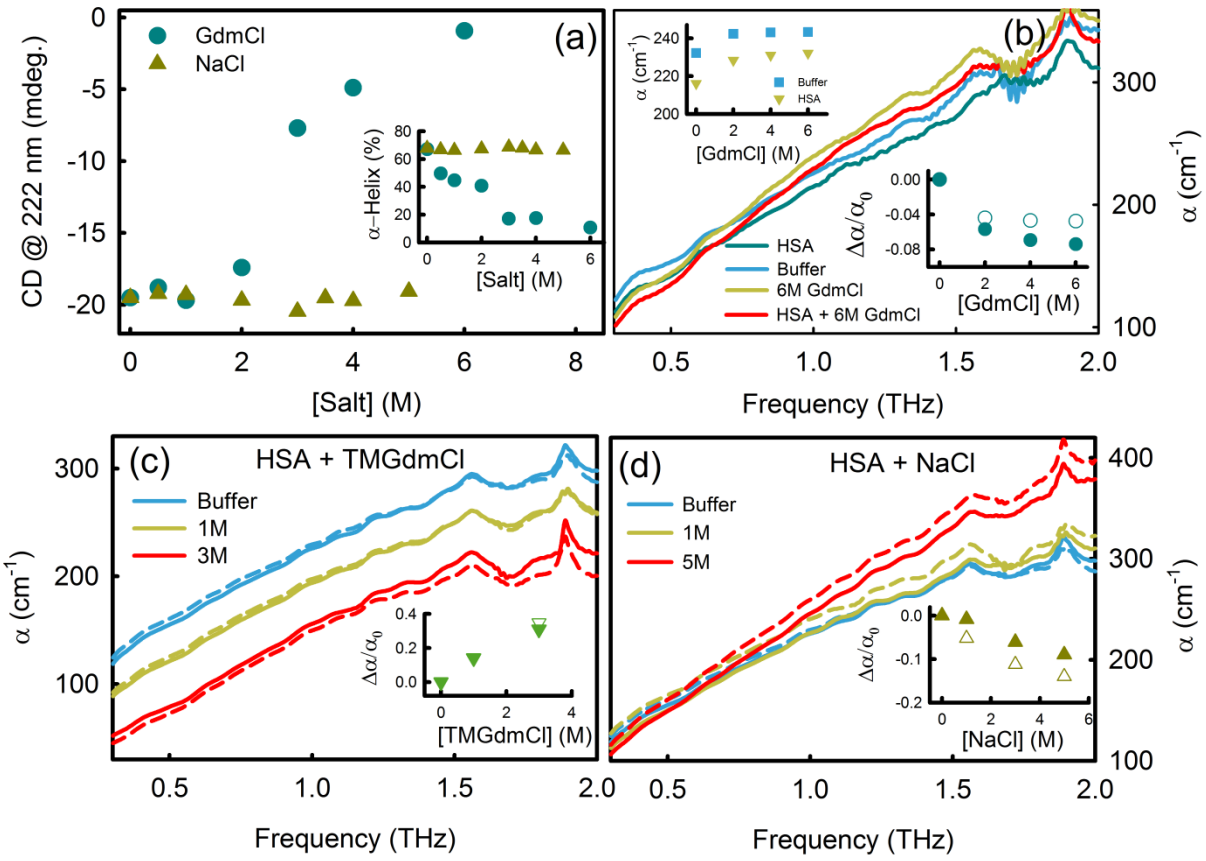

Figure 5.3.II.3. (a) CD at 222 nm for human serum albumin (HSA) as a function of GdmCl and NaCl concentrations. The inset shows the α helix content (in percentage) of the protein as a function of salt concentration. (b) Frequency dependent α of 1 mM HSA in buffer and in aqueous GdmCl solutions. The upper inset shows the value of α at 1 THz as a function of GdmCl concentration. The lower inset shows the relative change in α (see text) as a function of GdmCl concentration. The open symbols represent data without protein, the closed symbols are those in presence of the protein. (c) Frequency dependent α of 1 mM HSA in buffer and in aqueous TMGdmCl solutions. The broken lines represent the corresponding curves in absence of the protein. The inset shows the relative change in α as a function of TMGdmCl concentration. The open and the closed symbols represent data without and with protein, respectively. (d) Frequency dependent α of 1 mM HSA in buffer and in aqueous NaCl solutions. The broken lines represent the corresponding curves in absence of the protein. The inset shows the relative change in α as a function of NaCl concentration. The open and the closed symbols represent data without and with protein, respectively.

We therefore report the results of GdmCl and NaCl only and we plot the CD signal of HSA in presence of these salts at 222 nm (figure 5.3.II.3a) which is particularly sensitive towards the secondary structure of proteins.[134] It appears from the figure that the CD signal at 222 nm does not change appreciably for NaCl, however, a drastic change is observed in case of GdmCl, especially beyond a concentration of 2 M indicating the onset of unfolding of the protein, a phenomenon much consistent with earlier studies using the same protein.[54] The percentage of α helix content as a function of GdmCl and NaCl has been plotted in the same figure. It is found that NaCl has no effect on the α helix content; however, GdmCl decreases the α helix content drastically with a concomitant increase in the random coil conformation, especially beyond 2 M GdmCl. During the unfolding process the α helix to random coil transition eventually increases the extent of hydrophobic residues at the protein surface, which in turn is expected to interact with the GdmCl molecules making the denatured state stabilized. However, if the direct interaction with the hydrophobic residues would have been the sole reason for the observed denaturation, TMGdmCl should have been expected to act as a more efficient denaturing agent compared to GdmCl. On the contrary, it has been reported that TMGdmCl denatures proteins at a relatively higher concentration compared to the less hydrophobic GdmCl.[48] This leads to apprehend that hydration does have finite role to play and we investigate how the hydration dynamics of the water molecules associated with the protein changes in presence of the salts.

The α(ν) profile of HSA in absence and in presence of GdmCl is depicted in figure 5.3.II.3b. It can be observed that absorption coefficient of HSA solution is smaller than that of the buffer as has also been observed in earlier studies[53] and corroborates the fact that high absorbing water molecules being replaced by protein molecules. We plot α at 1 THz as a function of GdmCl concentration in absence and in presence of HSA in figure 5.3.II.3b, inset. It is found that HSA solution produces a smaller α compared to the buffer in all the studied concentrations of GdmCl. To appear at a more quantitative comparison we plot the relative change in α (given by $\Delta\alpha/\alpha_0$ where α_0 is the absorption coefficient of the buffer and $\Delta\alpha=\alpha_0 - \alpha$) as a function of GdmCl concentration. The relative change in α is found to be negative and becomes more prominent in presence of the protein (solid symbols), specially beyond 2M GdmCl which exactly coincides with the protein unfolding threshold. As discussed earlier, the measured value of α is an accumulation of several contributions arising from the buffer itself, the solutes and the hydration shell of the solutes. The relative change in α in presence

of the protein thus manifests a concomitant change in the collective dynamics in the hydration layer of the protein in the presence of the salt coupled with similar changes in the salt hydration (if any). It thus stands reasonable to argue that hydration at the GdmCl surface has some pivotal role to play during the denaturation process. Let us now consider the effect of the hydrophobic and less efficient denaturant, TMGdmCl (figure 5.3.II.3.(c)). The changes seem to be very marginal and the relative changes in α in absence and in presence of the protein are almost identical. As discussed earlier, unlike GdmCl the solvation dynamics of TMGdmCl supports a 'structure making' notion and $\Delta\alpha$ offers a positive value. However, the marginal changes in the $\Delta\alpha/\alpha_0$ values in absence and in presence of the protein strongly indicates that TMGdmCl does not alter the hydration dynamics of the protein in a significant manner, at least in the studied concentration range. We finally investigate the trend of an inert molecule, NaCl, which shows a relaxation dynamics comparable to that of GdmCl, however, the former has no ability to denature proteins. As observed from figure 5.3.II.3.(d), $\Delta\alpha/\alpha_0$ is negative as has also been observed in GdmCl, however, the trend in presence of the protein is completely opposite as the protein containing solution offers smaller changes compared to the buffer solutions. The observed difference in these two salts can be rationalized in the manner: NaCl is an inert salt which does not directly interact with the protein. Thus the changes observed in $\Delta\alpha$ can safely be considered as contributions from each component taken separately. It therefore is affirmed that the smaller negative change in $\Delta\alpha/\alpha_0$ in presence of the protein is due solely to the solvation dynamics associated with the protein. The scenario is altogether different in case of GdmCl, which denatures the protein and probably associates with a direct interaction at the protein surface. Thus the overall change in $\Delta\alpha$ in presence of the protein cannot be accounted for by taking the individual contributions separately. Denaturation of HSA essentially involves helix to coil transition, which eventually results in the exposure of a fraction of its hydrophobic moiety to the protein surface and consequently a considerable change in the hydration dynamics.[53] An additional change can also be envisaged at the GdmCl surface as it interacts with the protein surface. However, such a change is not very evident in case of TMGdmCl, which rather has a more structured hydration layer compared to GdmCl and incidentally offers a feebler denaturation power. This leads us to conclude that the denaturation of protein with GdmCl is essentially driven by a direct interaction, however, a certain role of the associated hydration dynamics could a priori not be overruled.

Table 5.3.II.1. Debye relaxation fitting parameters of aqueous solutions of GdmCl at different concentrations.

[GdmCl] (M)	ε_∞	[a]S_1	S_2	S_3	τ_1 (ps)	τ_2 (fs)	τ_3 (fs)	σ (S m^{-1})
0	1.76±0.03	71.16	0.34±0.04	1.54±0.10	8.94±0.1	227±70	74	0.20
1	1.91±0.03	62.70	0.46±0.07	1.47±0.06	9.02±0.1	233±63	86	8.02
2	1.93±0.03	54.29	0.69±0.07	1.45±0.06	8.91±0.1	222±39	86	14.63
3	1.94±0.03	46.38	0.92±0.08	1.39±0.06	8.72±0.2	218±29	84	19.20
4	2.07±0.03	38.59	1.17±0.07	1.17±0.06	8.33±0.1	204±19	86	22.82
5	2.05±0.03	33.06	1.29±0.07	1.27±0.06	8.20±0.16	207±19	86	25.22
6	2.09±0.03	27.75	1.46±0.07	1.26±0.06	7.77±0.2	200±15	86	26.01

(a) Values are taken from, *J Phys. Chem. B,* (2010) *114,* 13617-13627.

Table 5.3.II.2. Debye relaxation fitting parameters of aqueous solutions of TMGdmCl at different concentrations.

[TMGdmCl] (M)	ε_∞	[b]S_{slow}	[c]S_1	S_2	S_3	[b]τ_{slow} (ps)	τ_1 (ps)	τ_2 (fs)	τ_3 (fs)	σ (S m^{-1})
0.5	2.07±0.03	10.5	65.92	0.56±0.06	1.3±0.1	21.85	11.05±0.2	213±44	80	5.0
1	2.06±0.03	12.3	58.98	0.75±0.06	1.3±0.1	31.87	12.48±0.3	218±35	80	7.0
1.5	2.03±0.04	14.5	55.35	0.90±0.07	1.0±0.1	33.21	16.92±0.4	192±24	79	9.0

[b] Values taken from: *J. Am. Chem. Soc.* (2010) *132***,** 15671-15678.

Table 5.3.II.3. Debye relaxation fitting parameters of aqueous solutions of NaCl at different concentrations.

[NaCl] (M)	ε_∞	[c]S_1	S_2	S_3	τ_1 (ps)	τ_2 (fs)	τ_3 (fs)	σ (S m^{-1})
1	1.99	58.20	0.39±0.06	1.74±0.07	7.62±0.14	281±90	79	8.26
2	2.07	51.66	0.56±0.03	1.74± 0.08	7.04±0.11	256±55	79	11.96
3	2.05	44.97	0.67±0.03	1.86±0.08	6.63±0.10	249±43	80	16.02
4	2.07	36.58	0.86±0.03	2.05±0.06	6.46±0.12	261±33	81	21.60
5	2.05	32.83	0.89±0.03	2.30±0.06	6.01±0.04	274±35	79	22.29

[c] Values are taken from, *J. Chem. Phys.* (1948) *16***,** 1-20.

5.3.III. THz Spectroscopic Study Unravels why Chloride Salt of Guanidinium is a Protein Denaturing Agent while Sulphate Salt is not.

We studied the effect of GdmCl and Gdm_2SO_4 on the structure of a model protein BSA. Far UV CD spectra (figure 5.3.III.1(a)) of BSA reveal that in presence of GdmCl the protein is completely denatured while in Gdm_2SO_4 there is a marginal change in the spectra upto 6 M concentration. In presence of the two salts the full spectra are not available due to hike in voltage. The CD at 222 nm which is related to the α-helix content is shown in figure 5.3.III.1(b). The results unambiguously indicate that GdmCl denatures the structure of BSA whereas the Gdm_2SO_4 inhibits to denature.

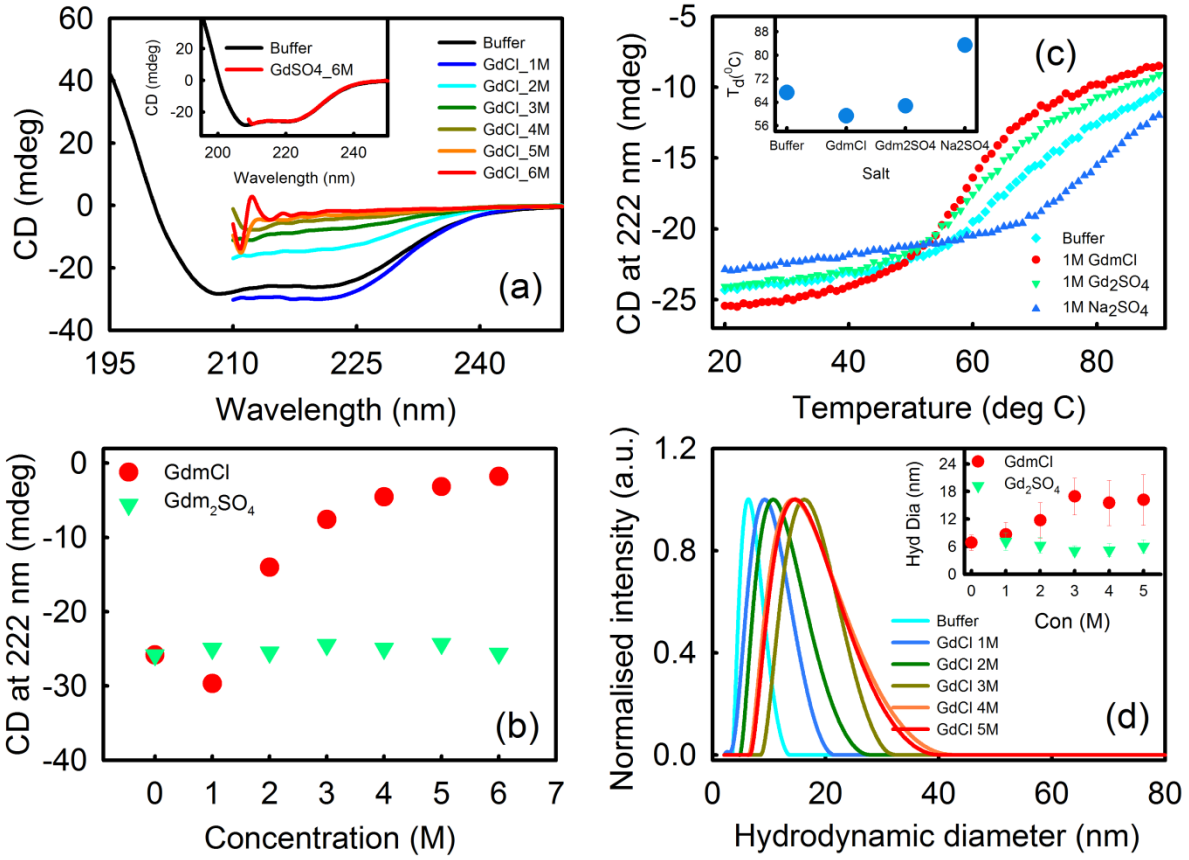

Figure 5.3.III.1: (a) Far UV-CD spectra of BSA in sodium phosphate buffer (pH ~7) at different concentration of GdmCl and (Inset) Gdm_2SO_4 solution at 20 ^{0}C. (b) CD at 222 nm of BSA as a function of GdmCl and Gdm_2SO_4 solution. (c) CD at 222 nm of BSA as a function of temperature in presence of 1M GdmCl, Gdm_2SO_4, Na_2SO_4 and in buffer. Inset shows denaturation temperature of BSA in those solutions. (d) Representative plot for scattering intensity distribution detected by DLS of BSA in GdmCl solution. Inset shows the hydrodynamic diameter of BSA as a function of concentration of GdmCl and Gdm_2SO_4.

Thermal denaturation study shows that denaturation temperature (T_d) decreases sharply for GdmCl salt while for Gdm_2SO_4 the change is only moderate. As control experiments we have

measured the T_d in Na_2SO_4 and found an increase in the T_d. Previously we reported marginal change in thermal denaturation temperature for BSA in presence of NaCl.[135] So it is the SO_4^{2-} ion which stabilizes the protein and protects to denature.

DLS study also supports the indifference of Gdm_2SO_4 in comparison to GdmCl towards protein denaturation. As depicted in figure 5.3.III.1(d)), in GdmCl salt solution the hydrodynamic diameter of BSA increases whereas in Gdm_2SO_4 it marginally decreases.

So it is clear that protein denaturation is not solely dependent on the interaction of Gdm^+ cation with the protein, there is a non-negligible role of the counter ions. In our previous results we have shown that there a definite role of water network structure and dynamics during protein denaturation by GdmCl. Hence it is intriguing to study the effect of Gdm_2SO_4 on the water network structure.

We investigate with MIR-FTIR (2300-2800 cm^{-1}) measurements to observe how water structure behaves in presence of GdmCl and Gdm_2SO_4 by measuring the O-D stretching

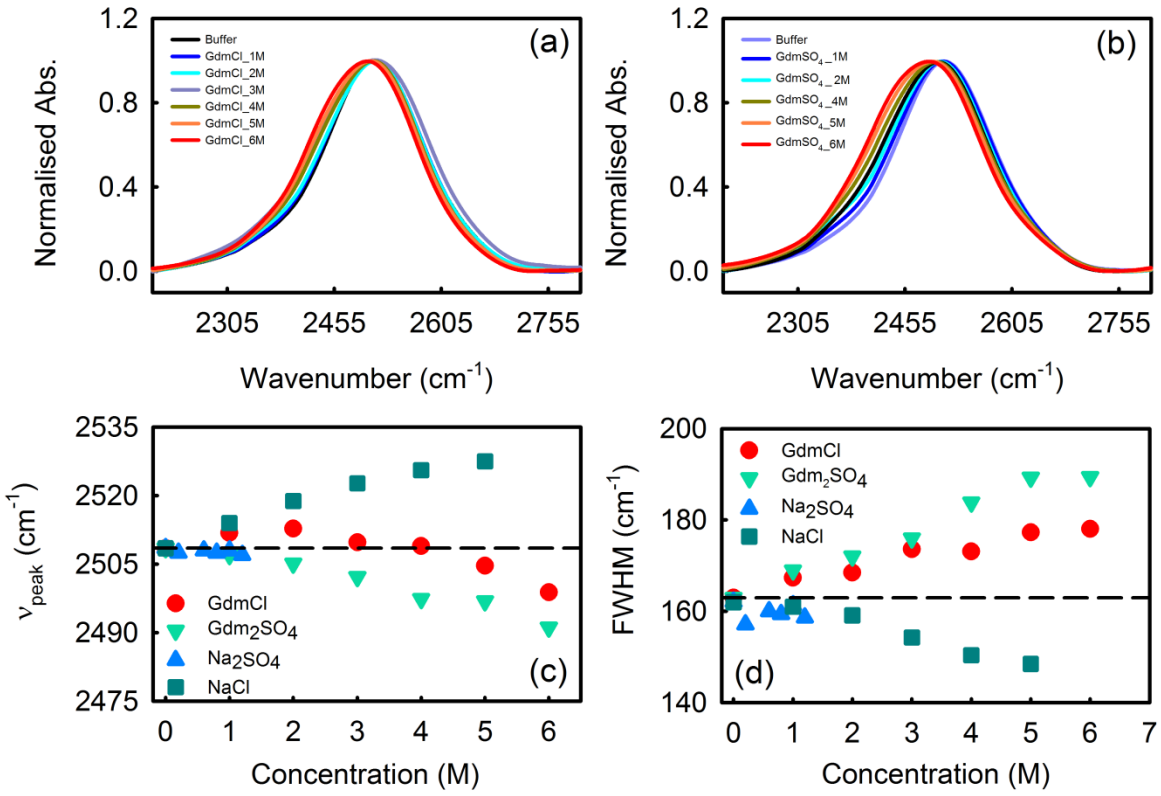

Figure 5.3.III.2: (a) MIR spectra of 4% D_2O in buffer, GdmCl and (b) Gdm_2SO_4 solution. (c) Peak frequency (ν_{peak}) and (d) full width at half maximum (FWHM) as a function of concentration of the salts.

spectra (figure 5.3.III.2). For comparison solutions of NaCl and Na_2SO_4 were also studied. We used 4% D_2O to study the O-D stretching in presence of the salts. As depicted in figure 5.3.III.2(c) in GdmCl solution the peak frequency (ν_{peak}) changes in a nonlinear manner which is contrasting to the changes observed in NaCl or Gdm_2SO_4 salts (marginal change for less soluble Na_2SO_4). For NaCl we found a gradual blue shift of the peak frequency and decrease in FWHM (i.e. narrower band) with increasing salt concentration.[135] This indicates the strengthening of the O-D bond due to the weakening of the water-water hydrogen bonds as the salts with high charge density ions are introduced. For GdmCl, it however suffers a marginal blue shift up to certain concentration and beyond that it is red shifted. At lower concentration blue shift occurs due to the weakening of water-water H-bond whereas at higher concentration, as bulk water concentration decreases contribution of water-Gdm^+ predominates resulting in the red shift due to the weakening of O-D bond (for the H-bonding with Gdm^+). For Gdm_2SO_4 it is throughout red shifted and the FWHM increases with concentration. The red shift emanates from the weakening of O-D bond due to the formation of strong H-bonds.

The long range effect of the salts has been studied by TTDS measurements. The absorption coefficient, α (ν) in THz regime provides information of the collective H-bond structure and dynamics of water (already discussed previously). As shown in figure 5.3.III.3, the frequency dependent absorption coefficient, α (ν) decreases with increasing concentration of Gdm_2SO_4 and the trend in α is solely different from that of GdmCl as found in the previous section (5.3.II).

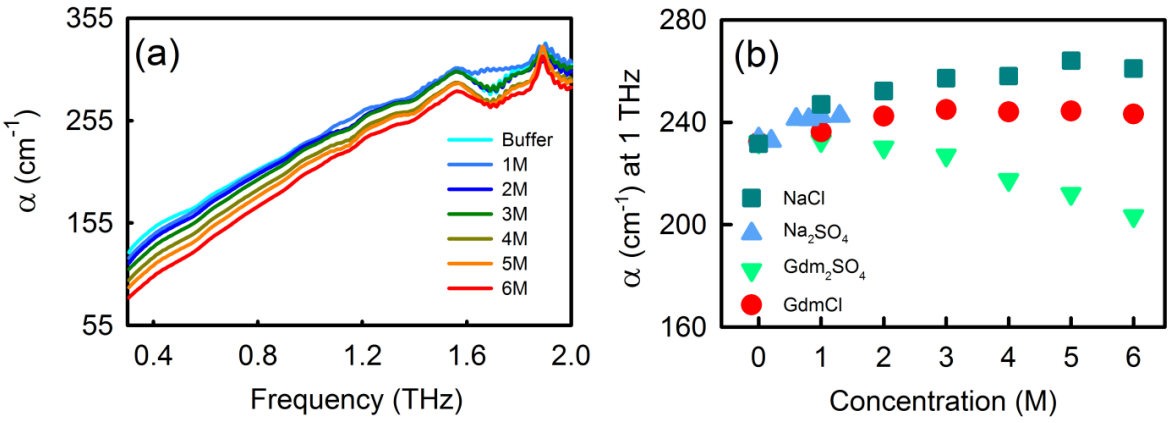

Figure 5.3.III.3: (a) Frequency dependent absorption coefficient (α) of Gdm_2SO_4 solution of different concentration. (b) Absorption coefficient at 1 THz as a function of NaCl, Na_2SO_4, Gdm_2SO_4 and GdmCl concentration.

For better understanding we have plotted α at 1 THz as a function of Gdm_2SO_4 concentration and for comparison other salts (GdmCl, NaCl, Na_2SO_4) are also plotted. As depicted in the figure for the water structure breaking salt[135] NaCl the α values at 1 THz increases gradually with concentration. For GdmCl α increases linearly upto ~2 M concentration and beyond that no appreciable change was observed whereas for Gdm_2SO_4 salt α decreases with concentration. This indicates that in presence of Gdm_2SO_4 more structured water forms i.e. strengthening of H-bond occur unlike GdmCl.

5.3.IV. Collective Hydration Dynamics in Some Amino Acid Solutions: A Combined GHz-THz Spectroscopic Study

GHz Measurement: The real and imaginary parts of the complex permittivity of the amino acid solutions in the 0.2-50 GHz frequency window are fitted in a double Debye model (discussed in chapter 2). Representative fitted plots for Gly in buffer are shown in figure 5.3.IV.1(a,b). Frequency dependent real and imaginary dielectric constants for other amino acids are shown in figure 5.3.IV.2. The fitting parameters are shown in the table 5.3.IV.3-8. The obtained time scales and dielectric constants are in good agreement with previously reported values involving similar amino acids.[88, 89] As shown in figure 5.3.IV.1(c) the static dielectric constants (ε_s) of the amino acids solutions increase with amino acid concentrations as water molecules are replaced by more dipolar zwitterions of the amino acids.

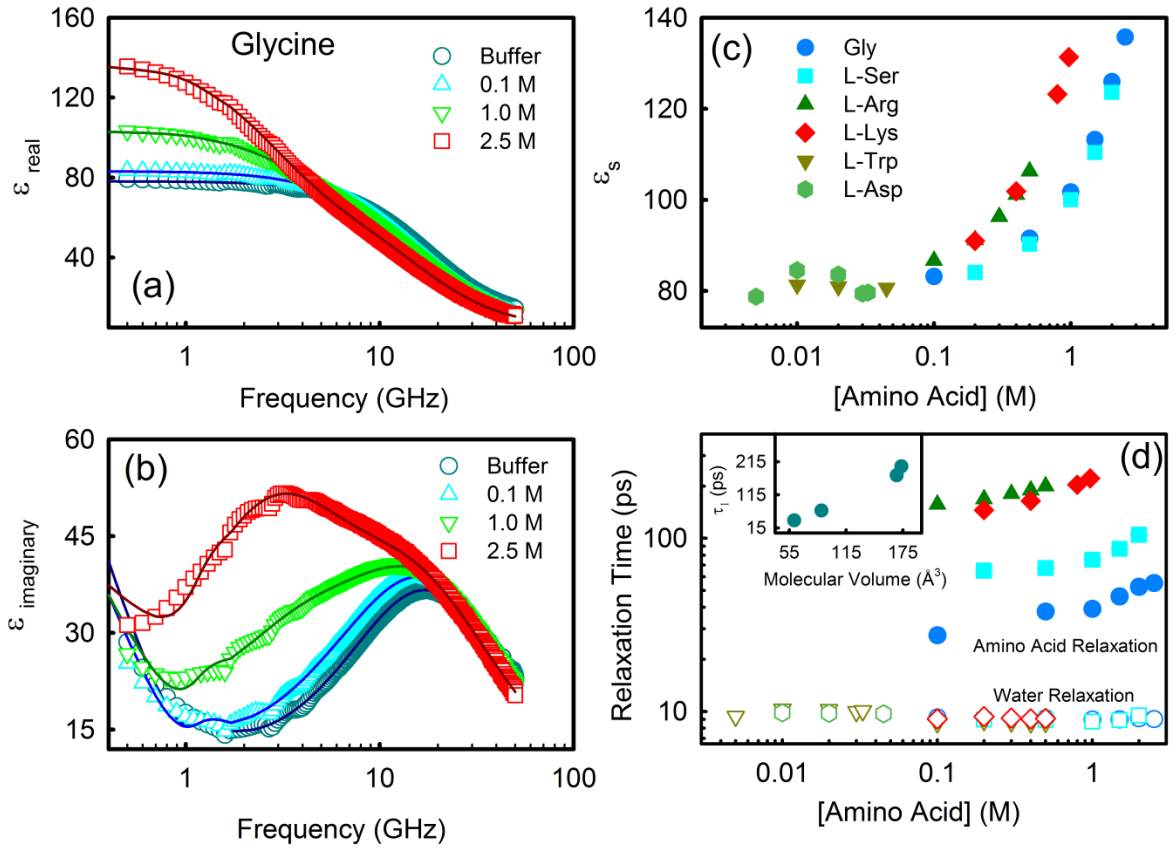

Figure 5.3.IV.1. (a) Real and (b) imaginary permittivity, (c) Static dielectric constants (ε_s) (d) relaxation time scale (obtained in Debye fitting of GHz data) of different amino acids in buffer (pH 7). The inset in (d) shows the τ_1 (= τ_{slow}) value as a function of the molecular volume of the amino acids at a fixed concentration of 0.5 M.

In this frequency window two relaxation processes are involved: (i) a slow process corresponding to the dipolar relaxation of the amino acid itself (τ_{slow}~ 100 ps) and (ii) a faster

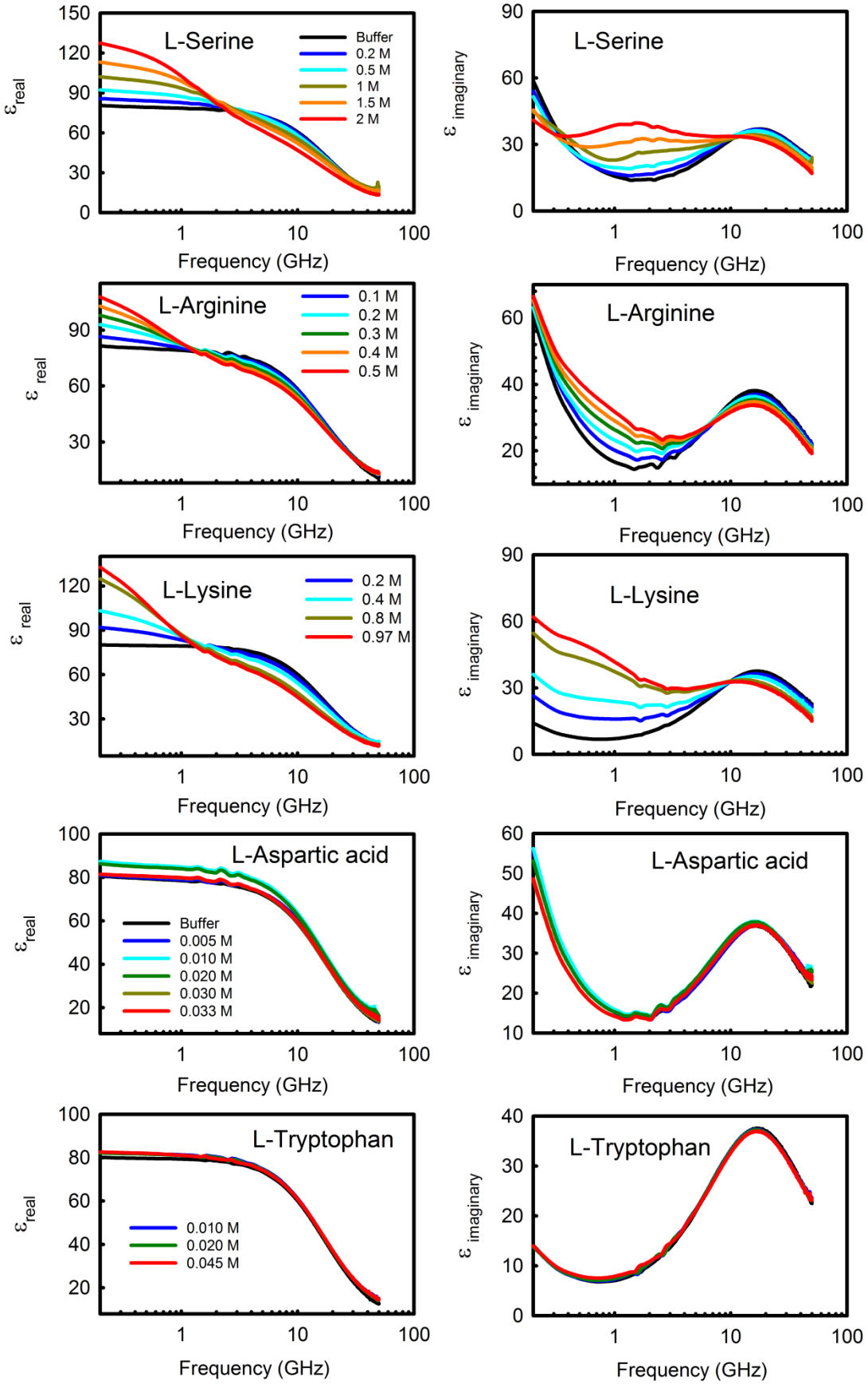

Figure 5.3.IV.2. Frequency dependent Real and imaginary permittivity in the GHz region.

one (~ 10 ps) originating near ~18 GHz responsible for the water dipole relaxation.[89] τ_{slow} increases with the size of the amino acids (figure 5.3.IV.1d, inset). The size dependent increase can be explained using the modified Stokes-Einstein model[136] which relates the microscopic relaxation time of amino acid molecules (τ'_{slow}) to the macroscopic dielectric relaxation time τ_{slow}. Both the time scales are related to viscosity (η) of the solution and effective volume (V_{eff}) of the solute according to the following relation,

$$\tau'_{slow} = \frac{2\varepsilon_s+\varepsilon_{\infty,1}}{3\varepsilon_s}\tau_{slow} = \frac{3V_{eff}\eta}{k_BT} \qquad (5.3.IV.1)$$

V_{eff} is related to the molecular volume (V_m) as, $V_{eff} = f_s C V_m$, where f_s is a geometrical parameter which accounts for the deviation of the shape of a molecule from sphere and C represents a friction parameter that correlates the macroscopic and microscopic viscosities. We use the τ_{slow} values obtained from the dielectric fittings (table 5.3.IV.3-8) and applying infinite dilution limit ($\tau'_{slow} \rightarrow \tau_{slow}$ i.e. $\eta \rightarrow \eta_{slow}$) in equation (3) and obtain the values of V_{eff} of the amino acids. From the V_{eff} values we determine the f_sC values and plot them in figure 5.3.IV.3 (inset). The ideal value of f_sC is 1 and it is found that for all the four amino acids it deviates from 1. For Lys (1.01) and Arg (1.15) the values are slightly greater than 1 while in Gly (0.65) and Ser (0.87) it is considerably smaller. It should be noted that these observed values are dependent on both the structure factor and the friction parameter. Gly being a nearly spherical molecule (f_s~1) the value of C is expected to be ~0.65, which is in good agreement with the previously reported values.[88] Similarly a near-spherical Ser also produces a value less than 1. This suggests that water structuring around these amino acids does influence its ideal rotation and is far from the stick limit.[137] Arg and Lys being more like an ellipsoid have the f_s values might deviate significantly from 1, however, the values of C change in a manner such that the overall f_sC value lies in the vicinity of the ideal value of 1.

The fitting of the GHz data produces a faster relaxation timescale of ~10 ps which corresponds to the cooperative rearrangement of water around the amino acids. We do not observe much variation in this timescale with concentration and amino acid type. It should be taken into consideration that this cooperative relaxation process occurs in ps to sub-ps timescale which is too fast to be precisely estimated in the GHz frequency region. We therefore do not discuss about this timescale, instead we carry out TTDS measurements to probe this relaxation process (see later).

In this context it is interesting to investigate whether the amino acid molecules aggregate, specially at high concentrations. We found a linear increase in the relaxation strength (S_1) for all the amino acids (figure 5.3.IV.3, inset). S_1 is related to the effective dipole moment of the solute due to the dipole-dipole alignments (parallel or antiparallel). Aggregation of amino acids would have been resulted in a nonlinear behaviour. Our results thus indicate that the amino acids hydrate individually even at high concentrations and the solute dipole-dipole interaction is screened by water molecules. For a quantitative apprehension we have used the Cavell equation[138] that relates the measured dielectric relaxation strength (S_j) of the j-th relaxation process with molar concentration (c_j) and effective dipole moment ($\mu_{eff,j}$) as:

$$\frac{\mu_{eff.,j}^2}{(1-a_j f_j)^2} = S_j \frac{3\{\varepsilon_s+(1-\varepsilon_s)A_j\}}{\varepsilon_s} \frac{k_B T \varepsilon_0}{N_A} \frac{1}{c_j} \qquad (5.3.IV.2)$$

where ε_s is the static permittivity of the solution, A_j is the shape parameter that accounts for the shape of the relaxing particle (assuming a sphere A_j=1/3), k_B is the Boltzmann constant, T is the temperature and ε_0 is the permittivity of vacuum. a_j and f_j are the molecular polarizability and reaction field factor, respectively.

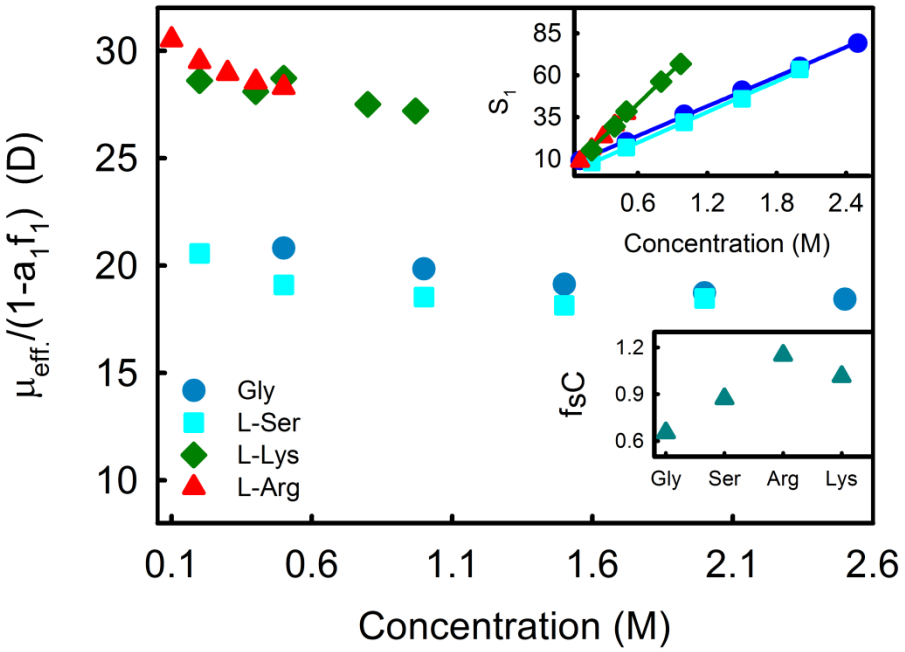

Figure 5.3.IV.3. μ_{eff} plotted as a function of amino acid concentration. The inset shows linear fits of relaxation strength (S_1) with amino acid concentrations. The other inset shows the f_cC values (see text for details) for different amino acids.

For the solute relaxation (j=1) we assume a_1 and f_1 to be independent of concentration. Effective dipole moment ($\mu_{eff,1}$) of the solute is related to the gas phase dipole moment ($\mu_{0,1}$) by the following relation,

$$\mu_{eff,1}^2 = g_1 \mu_{0,1}^2 \tag{5.3.IV.3}$$

where g_1 is an empirical factor the value of which correlates dipole-dipole orientation. $g_1 = 1$ implies no orientational correlation between the dipoles while $g_1 > 1$ indicates parallel alignment and $g_1 < 1$ indicates anti-parallel orientation between the dipoles.

$$\hat{\mu} \equiv \frac{\mu_{eff,1}}{1-a_1 f_1} = \frac{g_1^{1/2}\mu_{0,1}}{1-a_1 f_1} \tag{5.3.IV.4}$$

$\hat{\mu}$ changes only moderately with increasing concentration of amino acids (figure 5.3.IV.3). This indicates that hydrated amino acids approach each other at elevated concentrations and the dipoles align antiparallel, however, they do not aggregate.[89] We estimate the maximum value of the correlation factors g_1 by the following equation and the thus obtained values are shown in table 5.3.IV.1.

$$\frac{\hat{\mu}(c_{max})}{\hat{\mu}(c\to 0)} \approx \frac{g_1^{\frac{1}{2}}(c_{max})}{g_1^{\frac{1}{2}}(c\to 0)} = g_1^{\frac{1}{2}}(c_{max}) \tag{5.3.IV.5}$$

It can be noted that $g_1(c \to 0)$ =1, as at infinite dilution there exists no correlation between the amino acid dipoles. $\hat{\mu}(c \to 0)$ is obtained from the intercept (y-axis) of the linear fitting of the $\hat{\mu}$ vs. concentration plot. c_{max} is the maximum concentration (maximum solubility) of each amino acid. As the obtained g_1 values are less than unity and the deviation from the lowest concentration value (where aggregation hardly takes place) is less than 20%, we can unambiguously conclude that there only occurs short range antiparallel ordering of the dipoles rather than aggregation.

THz Measurement: We now discuss the TTDS results. As water molecules are replaced by less absorbing solutes, α(ν) changes as (assuming ideal mixing of the components)

$$\alpha^{id} = \alpha_w \varphi_w + \alpha_{AA} \varphi_{AA} \tag{5.3.IV.6}$$

where φ_w, φ_{AA} are the volume fractions of the buffer and amino acid, respectively. We calculate φ_{AA} using the molecular volume of the amino acids (table 5.3.IV.1)[139] and α_{AA} is the absorption coefficient of solid amino acids which is very small[140, 141] compared to that of

water. The difference in the absorption coefficient (assuming ideal mixing) could be obtained as,

$$\Delta\alpha^{id} = (\varphi_w - 1)\alpha_w + \alpha_{AA}\varphi_{AA} \qquad (5.3.IV.7)$$

We plot the difference in the absorption coefficient, measured at 1 THz, as a function of amino acid concentration (figure 5.3.IV.4a, solid symbols).

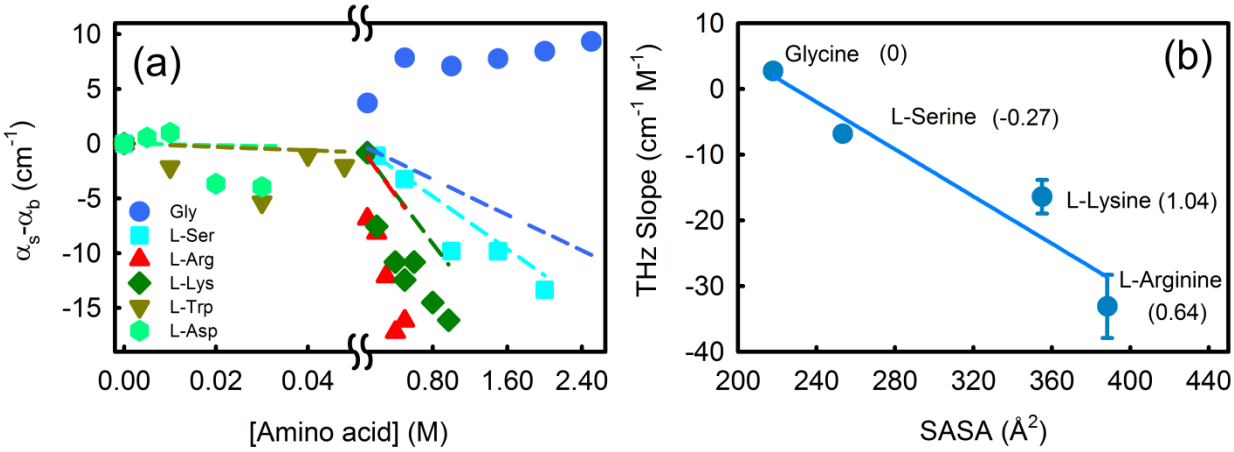

Figure 5.3.IV.4. (a) Difference in absorption coefficient of amino acids solutions with respect to that of buffer ($\Delta\alpha=\alpha_s-\alpha_b$) at 1 THz (closed symbols). The broken lines represent the values according to a two component model assuming no hydration at the amino acid interface (see equation 8). (b) THz slope as a function of the SASA of amino acids. The Frömmel hydrophobicity index for the corresponding amino acid are shown in the parenthesis.

The observed $\Delta\alpha$ values are found to deviate from the calculated $\Delta\alpha^{id}$ values (broken lines). It is therefore necessary to take into consideration a three component model where the absorption coefficient of a solution is given as[142]

$$\alpha = \alpha_w\varphi_w + \alpha_{AA}\varphi_{AA} + \alpha_h\varphi_h \qquad (5.3.IV.8)$$

In equation 5.3.IV.8, α_h and φ_h are the absorption coefficient and volume fraction of the solvation water associated with the solutes, respectively. Hydrated solutes associate a dynamic hydration shell which extends up to 5-7 Å from the solute surface and offers an absorption coefficient different from that of bulk water[101]. Thus the overall change in $\alpha(\nu)$ is a collective contributions from the solvent, solute and the hydration water, which makes the $\alpha(\nu)$ profile to deviate from $\alpha_{id}(\nu)$.[127] The difference in $\Delta\alpha$ thus manifests the absorption of the hydration layer around the amino acids. We notice that the extent of deviation varies with the type of amino acids indicating the specificity of amino acid hydration. For a better apprehension we fit $\Delta\alpha$ (at 1 THz) as a linear function of concentration and the obtained THz

slopes[143] are provided in table 5.3.IV.2. For Gly the slope is positive, while it is negative for Ser, Lys and Arg. Asp and Trp are only mildly soluble and the obtained $\Delta\alpha$ values are not strictly linear. Niehues et al. have previously reported a change in the THz slope (in the 2.4-2.7 THz range) according to the hydrophobicity scale (Frömmel) of amino acids.[91] We found that the THz slope does not exactly follow the Frömmel hydrophobicity scale[65] rather it is linear with the corresponding SASA as depicted in figure 5.3.IV.4(b). Our observation strongly corroborates Shiraga et al.[92] who reported a SASA dependent change in the H-bond ability of glycine and analogous solutes.

Change in absorption coefficient at 1 THz provides information on the hydration state of solutes[144]. In our earlier studies we have found that $\Delta\alpha$ is positive for the water structure breaker solutes, e.g. guanidinium chloride[145], alkaline metal cations[135] and urea,[146] whereas it is negative for the water structure makers and hydrophobic solutes[146, 147]. Thus a positive $\Delta\alpha$ for Gly strongly suggests that it breaks the collective water network owing to the preferential interaction of the amine group of Gly with water.[148] For the rest of the amino acids the observed negative $\Delta\alpha$ unambiguously indicating the formation of ordered water network structure around the amino acids, the extent of $\Delta\alpha$ being specific to the respective amino acids and is linear to their corresponding SASA (figure 5.3.IV.4b). The overall interaction of amino acids with water can be understood as a result of two different effects: (a) interaction with the $-COO^-$ group, which is believed to be a structure maker and (b) interaction with the $-NH_3^+$ group which is a structure breaker.[148, 149] Recent MD simulation studies[150, 151] also suggest that the hydrophilic hydration by –COOH dominates over the less hydrophilic $-NH_3^+$. The observed change in $\Delta\alpha$ as well as in the THz slope is an optimization between these two opposing factors coupled with the hydration of the side chain of the amino acids. With increase in SASA more water molecules get associated to hydrate the amino acids and depending upon the polarity of the accessible surface the water-water tetrahedral network gets stronger or weaker. This perhaps makes SASA a more accountable parameter to define hydration over hydrophobicity.

Gly, the simplest of all the amino acids, is yet reckoned as an unusual member of the amino acid family[152]. We identify an intriguing feature as the $\alpha(\nu)$ curve of the buffer intersects those of the Gly solutions (figure 5.3.IV.5). We plot the corresponding $\nu_{crossover}$[145] (frequency at which the curves intercept each other) as a function of Gly concentration [figure 5.3.IV.5 (inset)] and it is observed that $\nu_{crossover}$ shifts towards higher frequency with

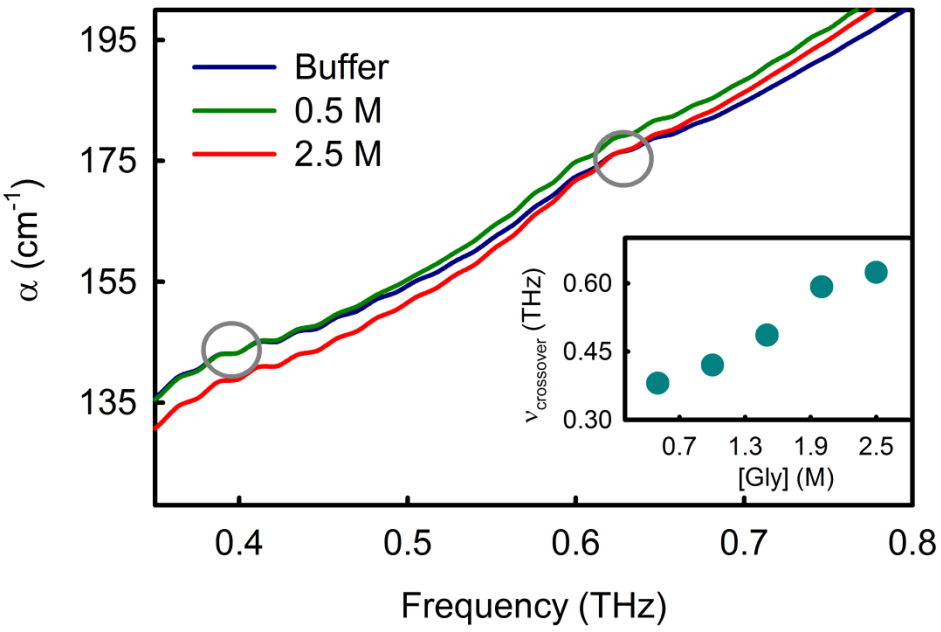

Figure 5.3.IV.5. Absorption coefficient (α) of glycine solution showing the crossover with buffer. The inset shows the crossover frequency ($\nu_{crossover}$) as a function of glycine concentration.

concentration. $\nu_{crossover}$ depends on the extent of hydrophobicity of the solute surface in interaction with solvents. Recently Heyden et al. computed the vibrational density of states of water molecules (in the FIR region) at the surface of a model protein $\lambda^*_{6\text{-}85}$-repressor and they found that the vibrational modes in contact to hydrophilic residues get 5-10 cm^{-1} blue-shifted leading to a decrease in the density of vibrational modes below 55 cm^{-1} and an increase in the density of states above 55 cm^{-1}.[153] In Gly also with increasing the concentration the amino acid zwitterions orient themselves so that the hydrophilic –COOH group experiences more water exposed. Such crossing, however, is not observed for the other amino acids, at least in the studied frequency range. Perhaps, the frequency is too much blue shifted as observed in the present measurement window. Arg is another interesting member in the amino acid family. It has considerable structural similarity to that of guanidinium (Gdm^+) cation, however, shows remarkably contrasting behaviour with proteins: while Gdm^+ denatures them, Arg modestly stabilizes.[154] This makes it worth comparing their hydration behaviour. Δα of GdmCl (at 1 THz) increases linearly up to a concentration of ~3 M beyond which it does not change appreciably, for Arg it rather decreases linearly with increasing concentration (figure 5.3.IV.6a). This result unambiguously concludes that while Arg is a structure maker, GdmCl is a water structure breaker. Gdm^+ consists of a delocalised positive charge that makes it highly polarisable. So water dipoles orient towards Gdm^+ breaking the intermolecular water-water H-bond network. On the other hand, for Arg the overall hydration

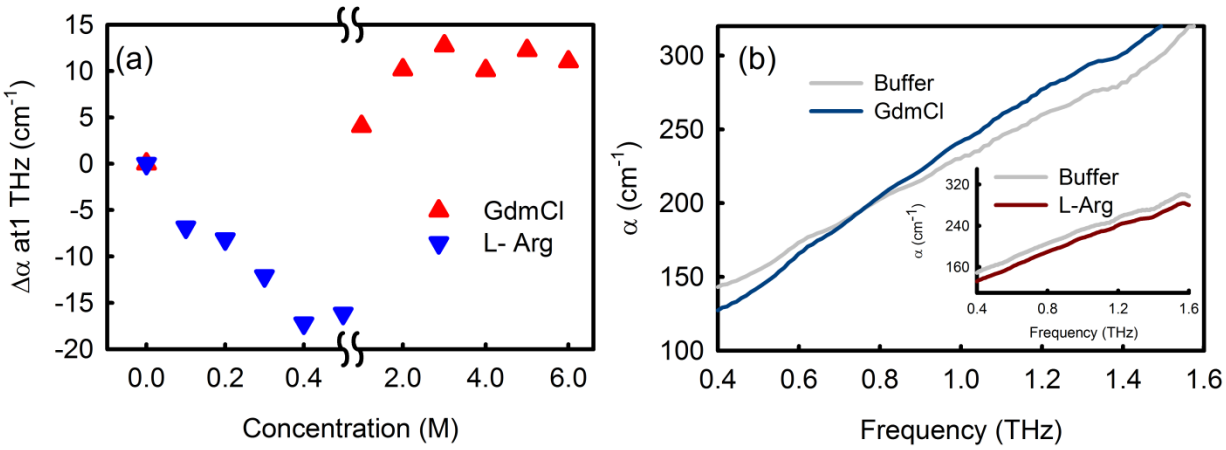

Figure 5.3.IV.6. (a) Δα measured at 1 THz of GdmCl and L-Arg solutions as a function of concentration. (b) Frequency dependent α at maximum concentration of GdmCl and L-Arg (inset) and that of the buffer.

depends on the individual contributions of the hydrophilic guanidine and acid units, and the hydrophobic methylene ($-(CH_2)_3-$) units. Unlike in GdmCl the guanidine unit of Arg is not charged (at pH 7) and it forms weaker hydrogen bonds with the under coordinated water, consequently it does not break the water network to the extent Gdm^+ does. Moreover, the hydrophobic methylene units are reluctant to interact with water molecules, consequently the water-water H-bond around this unit becomes relatively strong. The Gly-like remaining unit in its turn does break water network but not to the extent to overwhelm the hydrophobic effect, this eventually enables an overall structure making notion. We also notice a $\nu_{crossover}$ in GdmCl solution, however, in Arg solution it is not found within the studied frequency window (figure 5.3.IV.6b).

We fit the real and imaginary dielectric constants of water and amino acid solutions in a multiple Debye model (see Chapter 2) and the fitting parameters are presented in table 5.3.IV.9-14. For the buffer we obtain three timescales of ~ 8.7 ps, ~ 200 fs and ~80 fs, which are in good agreement with previous studies.[108] The ~8.7 ps timescale (designated as τ_2) is due to the cooperative rearrangement of the hydrogen bonded network while the component ~200 fs (designated as τ_3) emanates from either quick jump of under coordinated water or small angular rotation preceding a large angle jump.[109, 155] The ~80 fs (designated as τ_4) timescale has its origin near the 60 cm^{-1} vibrational band due to the hydrogen-bond bending and the related transverse acoustic phonons which propagate in a direction normal to the hydrogen bonds in between two neighbouring water molecules.[110, 111] Due to the limited

resolution of our setup we do not observe much variation in τ_4 and would therefore make the subsequent discussions on the other two timescales only. The results are depicted in figure 5.3.IV.7 and table 5.3.IV.9-14.

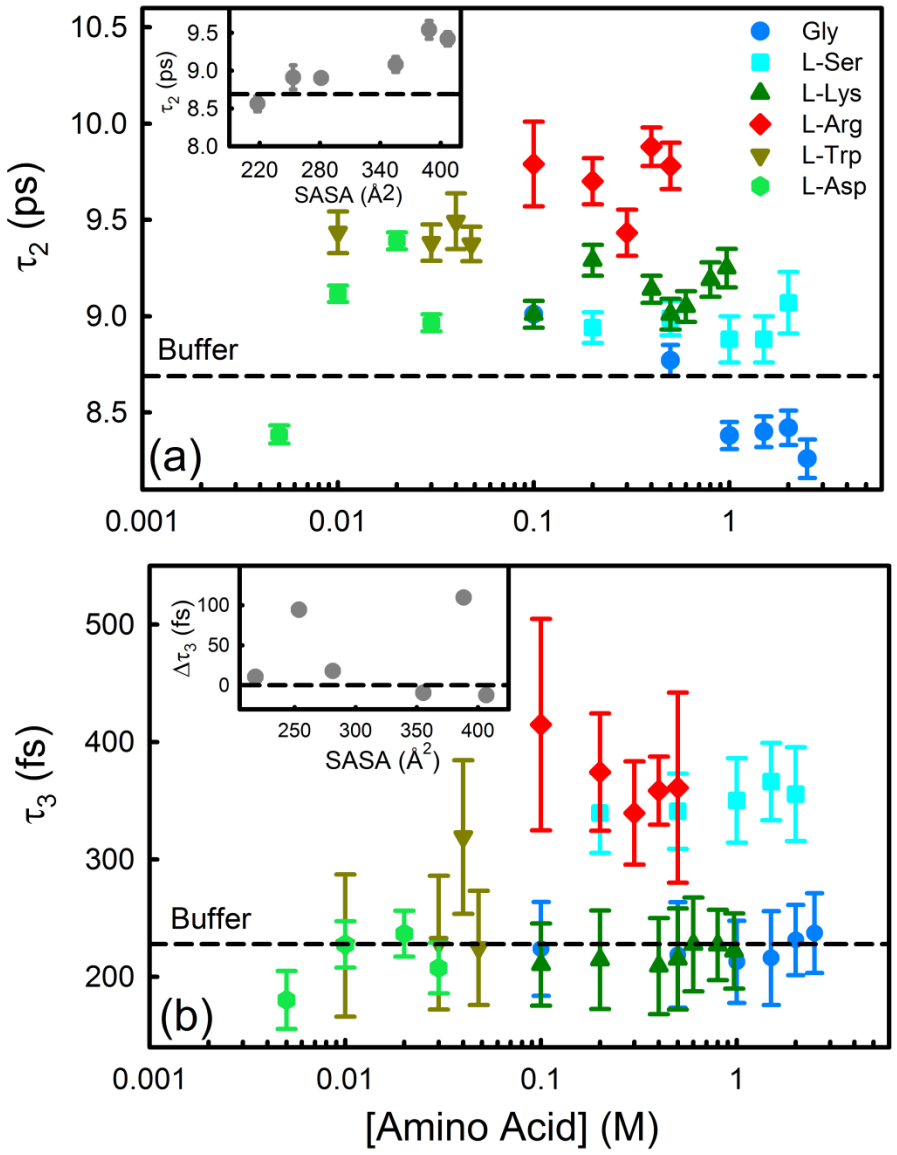

Figure 5.3.IV.7. (a) Cooperative hydrogen bond relaxation time constant (τ_2) of aqueous solutions of amino acids as a function of their concentration. The dotted line is the time constant for the buffer solution. The inset shows the change in τ_2 (measured at maximum amino acid concentration) as a function of the SASA of amino acid. (b) Relaxation time scale τ_3 corresponding to the jump orientation of water (obtained by Debye fitting of THz data) of different amino acids solutions. The dotted line is the time constant for that of the buffer. The inset shows the change in the timescale ($\Delta\tau_3=\tau_{solution}-\tau_{buffer}$) at the maximum concentration of the amino acids.

As evident from the figure the cooperative relaxation timescale (τ_2) is faster in Gly than that of bulk water, whereas for the other amino acids it is slower. For Gly zwitterion the water-

solute interaction is more favourable in comparison to the water-water interaction, this breaks the water-water H-bonds and eventually the cooperative relaxation dynamics gets accelerated. For the rest of the amino acids the increased hydrophobicity increases τ_2 corroborating the structure making notion as evidenced from the absorption coefficient measurements (figure 5.3.IV.4a). We observe a good correlation between the time scale τ_2 and the SASA of different amino acids (figure 5.3.IV.7a, inset). With increasing SASA higher number of water molecules get excluded from the nonpolar/hydrophobic surface area of amino acids and for thermodynamic stabilization they form stronger H-bonds with the neighbouring water molecules to avoid minimum interaction with the hydrophobic part. This eventually retards τ_2. The relatively faster component τ_3, which essentially depicts the jump reorientation dynamics, also shows solute specific trend (figure 5.3.IV.7b): we plot the difference in timescale $\Delta\tau_3$ ($=\tau_{3,AA} - \tau_{3,w}$) at the respective highest amino acid concentration in the inset of figure 6b. It is observed that for Gly, Ser and Arg it is increased compared to that of bulk water while for Lys, Asp and Trp, it is marginally accelerated. The quick jump motion responsible for this timescale is highly disfavoured in Ser and Arg, which form highly structured water around it (figure 5.3.IV.7.b), binding of water molecules with the hydroxyl and amine groups present in the side chains of Ser and Arg perhaps hinders this motion.

The timescales and the relaxation strengths obtained from the TTDS measurements can be used to estimate the overall hydration state in the solutions. We observe that the relaxation strength S_2 mostly tends to decrease with increasing concentration of amino acids (table 5.3.IV.9-14). This can be explained by three possible effects:[156] i) hydrogen bonded (HB) bulk water is replaced by amino acids, ii) HB hydration water around amino acids is dynamically retarded, and iii) amino acids perturb a fraction of water molecules by breaking hydrogen bonds and create non hydrogen bonded bulk water (NHB), which is manifested in the changes in the timescales τ_3 and τ_4. The molar concentration of bulk water (C_{bulk}) can be calculated by the relaxation terms obtained in Debye fitting using the following relation[92],

$$C_{bulk} = \frac{S_2^s + S_3^s + S_4^s}{S_2^w + S_3^w + S_4^w} \frac{\rho_w}{M_w} \qquad (5.3.IV.9)$$

where S_i^s and S_i^w represent the relaxation strengths in solution and water respectively, ρ_w is the density of water and M_w is the molecular weight of water. Molar concentration of hydrated water (C_{hyd}) is obtained by,

$$C_{hyd} = C_w - C_{bulk} \qquad (5.3.IV.10)$$

where C_w is the molar concentration of total water for a particular concentration (say, C) of the solute. The NHB water population is consequently obtained as,

$$C_{NHB} = \frac{S_3^S + S_4^S}{S_2^W + S_3^W + S_4^W} \frac{\rho_w}{M_w} \qquad (5.3.IV.11)$$

We plot the molar concentrations C_{hyd} and C_{NHB} for different amino acids in figure 5.3.IV.8.

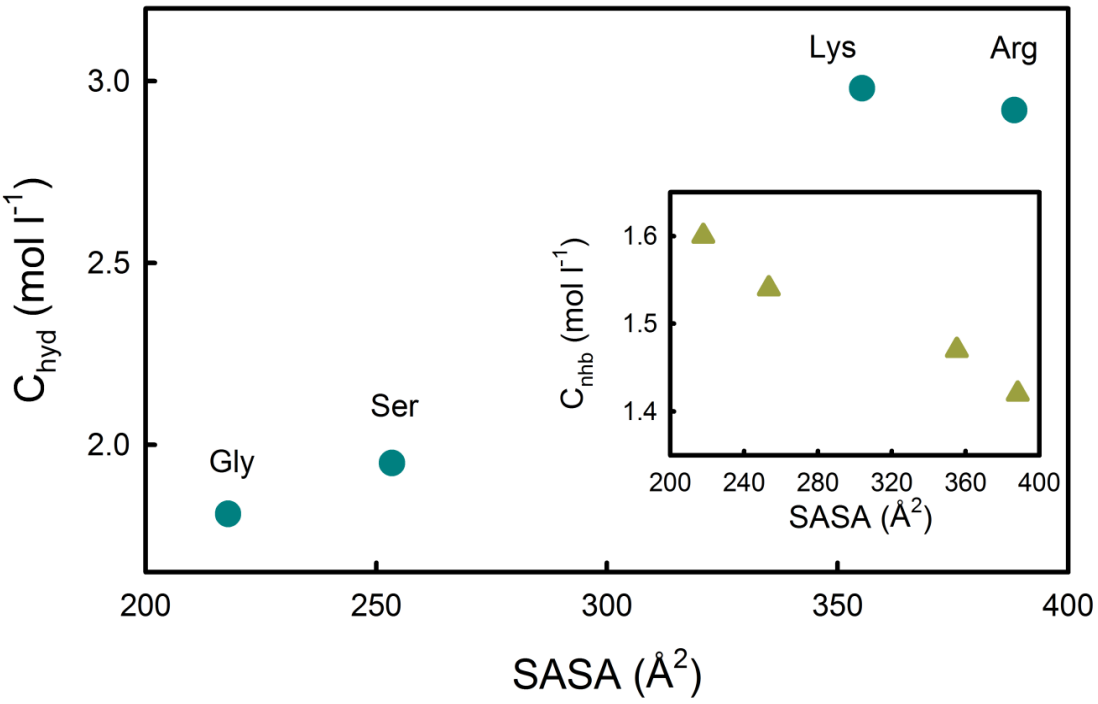

Figure 5.3.IV.8. Concentration of hydrated (C_{hyd}) and non-hydrogen bonded (C_{nhb}) water molecules of different amino acids.

We found an increase in the C_{hyd} as the SASA of the amino acid increases while the trend is opposite for C_{NHB}. The increase in the C_{hyd} with SASA is intuited as more water molecules interact with the side chains of the amino acids. The C_{hyd} obtained for Gly is in good agreement with previously reported value by Shiraga et al.[92] Gly contains the amino acid backbone only and its hydration is due only to the terminal NH_3^+ and COO^-. It has previously been observed that with increasing hydrophobic chain length in Gly, C_{hyd} increases. In our study, the amino acids used contain both hydrophilic as well as hydrophobic parts. Thus the linear increase in C_{hyd}, as observed by Shiraga et al.[92] for analogous amino acids, are not obvious in the present case. For example, the C_{hyd} for aminobutyric acid (Aba) and norvaline (n-Val) (with corresponding SASA of 275 and 306 Å) is higher compared to those of Lys and

Arg containing relatively higher SASA. The hydration in Aba and n-Val is purely hydrophobic in nature while in Lys and Arg it receives contribution from both, e.g. the polar SASA of Arg is higher than that of Lys and accordingly the latter has a slightly lower C_{hyd} compared to the former. C_{NHB} is higher for Gly, which corroborates with the α measurements showing the structure breaking notion of the amino acid. For the other amino acids, it decreases monotonously with increasing SASA. As described earlier, Lys and Arg contain a considerable portion of polar SASA which can induce structure in surrounding water, and is therefore can overwhelm the disruption of HB network by hydrophilic Gly.[157]

Table 5.3.IV.1. Molecular volume of amino acids

Amino acid	**Molecular volume ($Å^3$)#**	**τ_{slow} (ps)***	**g_1***
Gly	60.1	55.1	0.78
Ser	89.0	104.8	0.81
Arg	173.4	200.1	0.85
Lys	168.6	222.02	0.88

* Obtained at the maximum concentration of the amino acid.
*# Zamyatnin, A. A. Protein volume in solution. Progress in biophysics and molecular biology **1972,** 24, 107-23.*

Table 5.3.IV.2. The SASA and hydrophobicity according to Frömmel scale

Amino acid	**SASA ($Å^2$)**	**Hydrophobicity**	**THz slope**
Gly	217.9	0	2.7000
Ser	253.4	-0.27	-6.8400
Asp	281.2	0.28	–
Lys	355.3	1.04	-16.4200
Arg	388.3	0.64	-33.1200
Trp	406.9	2.55	–

Table 5.3.IV.3. Debye fitting parameters in the GHz region of Gly solutions

[Amino acid] (M)	ε_∞	S_{slow}	S_{water}	τ_1 (ps)	τ_2 (ps)	σ (S m^{-1})
0	5.41	-	71.88	-	8.98	0.64
0.1	3.90	8.96	70.31	27.49	9.36	0.63
0.5	4.41	20.1	67.03	37.69	9.23	0.62
1	4.68	36.55	60.49	39.00	9.10	0.72
1.5	3.94	51	58.3	46.08	9.12	0.60
2	4.98	65.13	55.84	52.43	9.26	0.49
2.5	4.66	78.97	52.12	55.11	9.15	0.57

Table 5.3.IV.4. Debye fitting parameters in the GHz region of Ser solutions

[Amino acid] (M)	ε_∞	S_{slow}	S_{water}	τ_1 (ps)	τ_2 (ps)	σ (S m^{-1})
0.2	6.10	7.84	70.11	65.05	8.98	0.58
0.5	6.69	16.91	66.65	67.31	8.92	0.54
1	8.60	31.86	59.6	75.24	8.74	0.51
1.5	8.08	45.88	56.42	86.86	8.91	0.44
2	7.14	63.38	53.08	104.76	9.47	0.36

Table 5.3.IV.5. Debye fitting parameters in the GHz region of Arg solutions

[Amino acid] (M)	ε_∞	S_{slow}	S_{water}	τ_1 (ps)	τ_2 (ps)	σ (S m^{-1})
0.10	5.15	8.64	71.25	157.23	9.43	0.67
0.20	5.73	16.16	69.33	168.44	9.72	0.64
0.30	6.11	23.35	66.87	180.65	9.54	0.64
0.40	5.70	30.26	65.19	189.75	9.46	0.63
0.50	6.46	37.19	62.69	200.14	9.51	0.62

Table 5.3.IV.6. Debye fitting parameters in the GHz region of Lys solutions

[Amino acid] (M)	ε_∞	S_{slow}	S_{water}	τ_1 (ps)	τ_2 (ps)	σ (S m^{-1})
0.20	5.79	15.19	70.01	145.78	9.44	0.25
0.40	6.51	29.31	66.04	164.54	9.74	0.32
0.5	6.62	38.31	63.5	176.64	9.52	0.38
0.80	6.75	56.23	60.23	203.72	10.63	0.44
0.97	7.02	66.73	57.59	222.02	11.05	0.47

Table 5.3.IV.7. Debye fitting parameters in the GHz region of Asp acid solutions

[Amino acid] (M)	ε_∞	S_1	S_2	τ_1 (ps)	τ_2 (ps)	σ (S m^{-1})
0.005	5.10	71.71	1.95	9.36	3.11	0.61
0.01	3.99	72.43	8.13	10.28	1.44	0.61
0.02	3.74	72.57	7.31	10.24	1.31	0.58
0.03	4.56	71.23	3.62	9.95	2.26	0.53
0.033	4.10	69.75	5.79	10.07	2.35	0.53

Table 5.3.IV.8. Debye fitting parameters in the GHz region of Trp solutions

[Amino acid] (M)	ε_∞	S_1	S_2	τ_1 (ps)	τ_2 (ps)	σ (S m^{-1})
0.01	4.00	73.04	4.3	9.83	1.50	0.15
0.02	4.01	73.21	3.74	9.76	1.27	0.15
0.045	3.97	72.7	3.97	9.71	1.24	0.16

Table 5.3.IV.9. Debye fitting parameters in the THz region of Gly solutions

[Amino acid] (M)	ε_∞	S_1	S_2	S_3	S_4	τ_1 (ps)	τ_2 (ps)	τ_3 (fs)	τ_4 (fs)
0	1.94±0.03		71.41	3.67±0.2	3.28±0.1		8.68±0.06	211.2±35	80
0.1	1.89±0.03	8.96	70.31	0.48±0.05	1.49±0.1	27.49	9.01±0.07	223.8±40	78
0.5	1.82±0.04	20.10	66.90	0.52±0.06	1.59± 0.1	37.69	8.77±0.08	218.7±45	78
1	1.86±0.03	36.55	60.49	0.55±0.06	1.50±0.1	39.00	8.38±0.07	212.8±35	77
1.5	1.83±0.03	51.00	58.30	0.57±0.06	1.52±0.12	46.08	8.40±0.08	216.0± 40	77
2	1.85±0.03	65.13	55.84	0.63±0.04	1.63±0.1	52.43	8.42±0.09	231.4±30	77
2.5	1.82±0.04	78.97	52.12	0.65±0.04	1.71±0.1	55.11	8.26±0.1	237.2±34	77

Table 5.3.IV.10. Debye fitting parameters in the THz region of Ser solutions

[Amino acid] (M)	ε_∞	S_1	S_2	S_3	S_4	τ_1 (ps)	τ_2 (ps)	τ_3 (fs)	τ_4 (fs)
0.2	2.06±0.02	7.84	70.11	0.72±0.04	1.09±0.04	65.05	8.94±0.08	339.4±34	80
0.5	2.07±0.02	16.91	66.50	0.89±0.04	1.15±0.04	67.31	8.99±0.09	341±32	80
1	2.14±0.02	31.86	59.6	0.87±0.05	1.20±0.05	75.24	8.88±0.12	350.3±36	80
1.5	2.09±0.02	45.88	56.42	0.96±0.05	1.26±0.05	86.86	8.88±0.12	366.3±33	80
2	2.03±0.02	63.38	53.08	0.97±0.06	1.27±0.06	104.76	9.07±0.16	355.6±0.04	80

Table 5.3.IV.11. Debye fitting parameters in the THz region of Lys solutions

[Amino acid] (M)	ε_∞	S_1	S_2	S_3	S_4	τ_1 (ps)	τ_2 (ps)	τ_3 (fs)	τ_4 (fs)
0.1	1.87±0.03	9.89	71.78	0.48±0.06	1.50±0.12	135.00	9.01±0.07	210.5±32	80
0.2	1.91±0.04	15.19	70.01	0.49±0.06	1.43±0.12	145.78	9.29±0.08	214.5±42	80
0.4	1.90±0.04	29.31	66.04	0.50±0.07	1.45±0.12	164.54	9.14±0.07	209.1±41	80
0.5	1.89±0.04	43.02	63.5	0.48±0.06	1.46±0.12	176.64	9.01±0.08	215.1±43	80
0.6	1.85±0.03	49.08	62.05	0.53±0.04	1.573±0.1	189.85	9.05±0.08	227.6±0.04	80
0.8	1.85±0.03	56.23	60.23	0.56±0.04	1.545±0.1	203.72	9.19±0.09	227.1±36	80
0.97	1.82±0.03	66.73	57.59	0.56±0.04	1.68±0.09	222.02	9.25±0.1	222±43	80

Table 5.3.IV.12. Debye fitting parameters in the THz region of Arg solutions

[Amino acid] (M)	ε_∞	S_1	S_2	S_3	S_4	τ_1 (ps)	τ_2 (ps)	τ_3 (fs)	τ_4 (fs)
0.1	1.84±0.03	10.13	71.39	0.71±0.12	1.28±0.06	193.70	9.79±0.22	414.8±90	81
0.2	1.88±0.02	16.16	69.33	0.72±0.05	1.28±0.04	168.44	9.70±0.12	374.4±50	81
0.3	1.93±0.02	23.35	66.87	0.66±0.04	1.19±0.05	180.65	9.43±0.12	339.5±44	81
0.4	2.00±0.02	30.26	65.19	0.86±0.04	1.16±0.04	189.75	9.88±0.1	358.5±29	81
0.5	1.90±0.02	37.19	62.69	0.71±0.04	1.17±0.04	200.14	9.78±0.12	361.1±81	81

Table 5.3.IV.13. Debye fitting parameters in the THz region of Trp solutions

[Amino acid] (M)	ε_∞	S_1	S_2	S_3	τ_1 (ps)	τ_2 (fs)	τ_3 (fs)
0.01	1.90±0.1	74.45	0.80±0.02	0.99±0.5	9.43±0.10	144.66±60	82
0.03	1.96±0.09	74.17	0.73±0.03	1.03±0.5	9.38±0.09	147.17±54	82
0.04	1.74±0.09	73.89	0.32	1.90	9.53±0.20	265.54±56	82
0.048	1.89±0.09	73.79	0.82	1.00	9.37±0.09	142.60±56	82

Table 5.3.IV.14. Debye fitting parameters in the THz region of Asp solutions

[Amino acid] (M)	ε_∞	S_1	S_2	S_3	τ_1 (ps)	τ_2 (fs)	τ_3 (fs)
0.005	2.07±0.03	71.58	0.70±0.02	0.77±0.03	8.50±.04	192.32±14	80
0.010	2.22±0.05	77.55	0.98±0.01	0.45±0.2	9.12±0.04	157.59±19	80
0.020	2.16±0.04	76.91	0.89±0.1	0.53±0.1	9.39±0.04	166.77±19	80
0.030	2.19±0.06	73.29	1.20±0.1	0.12	8.97±0.04	137.48±21	82

5.4. Summary

We studied the collective hydration of water in the vicinity of various 'protein denaturing agents' (urea, GdmCl and their derivatives) in the 0.3-2.0 THz frequency range and found a distinct change in comparison to the stabilizing agents. By fitting the real and imaginary parts of the complex dielectric constants in Debye relaxation model, it was found that the cooperative relaxation dynamics of water gets faster beyond a 'threshold' salt concentration where almost all globular protein denaturation occurs. This indicates that water network has a pivotal contribution to the denaturing process of proteins.

How different amino acids modify the water network has been revealed by combined GHz-THz frequency spectroscopic investigation. From GHz study we observe that the molecular rotation of amino acids correlates their respective molecular volume. Also it is concluded that amino acids do not usually aggregate even at high concentrations. From THz study we found that Gly is a water structure breaker while the other amino acids are structure makers. Consequently Gly accelerates cooperative hydration, while the others retard. Our results establish that hydration of amino acids depends both on its hydrophobic as well as its hydrophilic nature of side chains. The present study to understanding individual hydration of amino acids is a step forward towards rationalizing the complex hydration behaviour of proteins. Our study will pave the key understanding of how individual hydration contributes towards to overall hydrophobic hydration of small poly-peptides and proteins.

5.5. References

1. Brandts, J. F., and Hunt, L. (1967) Thermodynamics of protein denaturation. III. Denaturation of ribonuclease in water and in aqueous urea and aqueous ethanol mixtures, *J. Am. Chem. Soc. 89*, 4826-4838.
2. Watlaufer, D. B., Malik, S. K., Stoller, L., and Coffin, R. L. (1964) Nonpolar Group Participation in the Denaturation of Proteins by Urea and Guanidinium Salts. Model Compound Studies, *J. Am. Chem. Soc. 86*, 508-514.
3. Rossky, P. J. (2008) Protein denaturation by urea: Slash and bond, *Proc. Nat. Acad. Sci. 105*, 16825-16826.
4. Frank, H. S., and F., F. (1968) Structural Approach to the Solvent Power of Water for Hydrocarbons; Urea as a Structure Breaker, *J. Chem. Phys. 48*, 4746-4757.
5. Walrafen, G. E. (1966) Raman Spectral Studies of the Effects of Urea and Sucrose on Water Structure, *J. Chem. Phys. 44*, 3726-3727.
6. Finer, E. G., Franks, F., and Tait, M. J. (1972) Nuclear magnetic resonance studies of aqueous urea solutions, *J. Am. Chem. Soc. 94*, 4424-4429.

7. Idrissi, A., Cinar, E., Longelin, S., and Damay, P. (2004) The effect of temperature on urea-urea interactions in water: a molecular dynamics simulation, *J. Mol. Liq. 110*, 201-208.
8. Idrissi, A., Gerard, M., Damay, P., Kiselev, M., and Puhovsky, Y. (2010) The Effect of Urea on the Structure of Water: A Molecular Dynamics Simulation, *J. Phys. Chem. B 114*, 4731-4738.
9. Herskovits, T. T., and Kelly, T. M. (1973) Viscosity studies of aqueous solutions of alcohols, ureas, and amides, *J. Phys. Chem. 77*, 381-388.
10. Sacco, A., and Holz, M. (1997) NMR studies on hydrophobic interactions in solution Part 2.-Temperature and urea effect on the self-association of ethanol in water *J. Chem. Soc., Faraday Trans. 93*, 1101-1104.
11. Das, A., and Mukhopadhyay, C. (2009) Urea-Mediated Protein Denaturation: A Consensus View, *J. Phys. Chem. B 113*, 12816-12824.
12. Koga, Y., Miyazaki, Y., Nagano, Y., and Inaba, A. (2008) Mixing Schemes in a Urea-H2O System: A Differential Approach in Solution Thermodynamics, *J. Phys. Chem. B 112*, 11341-11346.
13. Vanzi, F., Madan, B., and Sharp, K. (1998) Effect of the Protein Denaturants Urea and Guanidinium on Water Structure: A Structural and Thermodynamic Study, *J. Am. Chem. Soc. 120*, 10748-10753.
14. Zou, Q., Bennion, B. J., Daggett, V., and Murphy, K. P. (2002) The Molecular Mechanism of Stabilization of Proteins by TMAO and Its Ability to Counteract the Effects of Urea, *J. Am. Chem. Soc. 124*, 1192-1202.
15. Wei, H., Fan, Y., and Gao, Y. Q. (2010) Effects of Urea, Tetramethyl Urea, and Trimethylamine N-Oxide on Aqueous Solution Structure and Solvation of Protein Backbones: A Molecular Dynamics Simulation Study, *J. Phys. Chem. B 114*, 557-568.
16. Rezus, Y. L. A., and Bakker, H. J. (2006) Effect of urea on the structural dynamics of water, *Proc. Natl. Acad. Sci. USA 103*, 18417-18420.
17. Shimizu, A., Fumino, K., Yukiyasu, K., and Taniguchi, Y. (2000) NMR studies on dynamic behavior of water molecule in aqueous denaturant solutions at 25 °C: Effects of guanidine hydrochloride, urea and alkylated ureas, *J. Mol. Liq. 85*, 269-278.
18. Hua, L., Zhou, R., Thirumalai, D., and Berne, B. J. (2008) Urea denaturation by stronger dispersion interactions with proteins than water implies a 2-stage unfolding, *Proc. Nat. Acad. Sci. 105*, 16928-16933.
19. Grdadolnik, J., and Maréchal, Y. (2002) Urea and urea-water solutions-an infrared study, *J. Mol. Struct. 615*, 177-189.
20. Hayashi, Y., Katsumoto, Y., Omori, S., Kishii, N., and Yasuda, A. (2007) Liquid Structure of the Urea−Water System Studied by Dielectric Spectroscopy, *J. Phys. Chem. B 111*, 1076-1080.
21. Kuffel, A., and Zielkiewicz, J. (2010) The hydrogen bond network structure within the hydration shell around simple osmolytes: Urea, tetramethylurea, and trimethylamine-N-oxide, investigated using both a fixed charge and a polarizable water model, *J. Chem. Phys. 133*, 035102.
22. Smith, L. J., Berendsen, H. J. C., and van Gunsteren, W. F. (2004) Computer Simulation of Urea−Water Mixtures: A Test of Force Field Parameters for Use in Biomolecular Simulation, *J. Phys. Chem. B 108*, 1065-1071.
23. Kokubo, H., Rösgen, J., Bolen, D. W., and Pettitt, B. M. (2007) Molecular Basis of the Apparent Near Ideality of Urea Solutions *Biophys. J. 93*, 3392-3407.

24. Sarma, R., and Paul, S. (2013) Exploring the Molecular Mechanism of Trimethylamine-N-oxide's Ability to Counteract the Protein Denaturing Effects of Urea, *J. Phys. Chem. B 117*, 5691-5704.
25. Lim, W. K., Rösgen, J., and Englander, S. W. (2009) Urea, but not guanidinium, destabilizes proteins by forming hydrogen bonds to the peptide group, *Proc. Nat. Acad. Sci. 106*, 2595-2600.
26. Zangi, R., Zhou, R., and Berne, B. J. (2009) Urea's Action on Hydrophobic Interactions, *J. Am. Chem. Soc. 131*, 1535-1541.
27. Bennion, B. J., and Daggett, V. (2003) The molecular basis for the chemical denaturation of proteins by urea, *Proc. Nat. Acad. Sci. 100*, 5142-5147.
28. Stumpe, M. C., and Grubmüller, H. (2007) Interaction of Urea with Amino Acids: Implications for Urea-Induced Protein Denaturation, *J. Am. Chem. Soc. 129*, 16126-16131.
29. Kuharski, R. A., and Rossky, P. J. (1984) Solvation of hydrophobic species in aqueous urea solution: a molecular dynamics study, *J. Am. Chem. Soc. 106*, 5794-5800.
30. O'Brien, E. P., Dima, R. I., Brooks, B., and Thirumalai, D. (2007) Interactions between Hydrophobic and Ionic Solutes in Aqueous Guanidinium Chloride and Urea Solutions: Lessons for Protein Denaturation Mechanism, *J. Am. Chem. Soc. 129*, 7346-7353.
31. Idrissi, A., Bartolini, P., Ricci, M., and Righini, R. (2003) Temperature dependence of the reorientational dynamics and low-frequency response of aqueous urea solutions investigated by femtosecond optical Kerr-effect spectroscopy and molecular-dynamics simulation, *Phys. Chem. Chem. Phys. 5*, 4666-4671.
32. Mazur, K., Heisler, I. A., and Meech, S. R. (2011) THz Spectra and Dynamics of Aqueous Solutions Studied by the Ultrafast Optical Kerr Effect, *J. Phys. Chem. B 115*, 2563-2573.
33. Heyden, M., Sun, J., Funkner, S., Mathias, G., Forbert, H., Havenith, M., and Marx, D. (2010) Dissecting the THz spectrum of liquid water from first principles via correlations in time and space *Proc. Natl. Acad.Sci.USA 107*, 12068-12073.
34. Funkner, S., Havenith, M., and Schwaab, G. (2012) Urea, a Structure Breaker? Answers from THz Absorption Spectroscopy, *J. Phys. Chem. B 116*, 13374-13380.
35. Kaatze, U., Gerke, H., and Pottel, R. (1986) Dielectric relaxation in aqueous solutions of urea and some of its derivatives, *J. Phys. Chem. 90*, 5464-5469.
36. Ebbinghaus, S., Kim, S. J., Heyden, M., Yu, X., Heugen, U., Gruebele, M., Leitner, D. M., and Havenith, M. (2007) An extended dynamical hydration shell around proteins., *Proc. Natl. Acad.Sci.USA 104*, 20749-20752.
37. England, J. L., and Haran, G. (2011) Role of solvation effects in protein denaturation: From thermodynamics to single molecules and back, *Ann. Rev. Phys. Chem. 62*, 257-277.
38. Chang, J.-Y. (2009) Structural Heterogeneity of 6 M GdmCl-Denatured Proteins: Implications for the Mechanism of Protein Folding, *Biochemistry 48*, 9340-9346.
39. Tanford, C. (1970) Theoretical models for the mechanisms of protein denaturation, *Adv. Prot. Chem. 24*, 1-95.
40. Schellman, J. A. (2002) Fifty years of solvent denaturatio, *Biophys. Chem. 96*, 91-101.
41. Mason, P. E., Neilson, G. W., Dempsey, C. E., Barnes, A. C., and Cruickshank, J. M. (2003) The hydration structure of guanidinium and thiocyanate ions: Implications for protein stability in aqueous solution, *Proc. Natl. Acad. Sci. USA 100*, 4557-4561.

42. Timasheff, S. (1992) Water as ligand: Preferential binding and exclusion of denaturants in protein unfolding, *Biochemistry 31*, 9857-9864.
43. Mountain, R. D., and Thirumalai, D. (2004) Alterations in Water Structure Induced by Guanidinium and Sodium Ions, *J. Phys. Chem. B 108*, 19711–19716.
44. Mason, P. E., Neilson, G. W., Enderby, J. E., Saboungi, M.-L., Dempsey, C. E., MacKerell, J., A.D. , and Brady, J. W. (2004) The Structure of Aqueous Guanidinium Chloride Solutions, *J. Am. Chem. Soc. 126*, 11462-11470.
45. Scott , J. N., Nucci, N. V., and Vanderkooi, J. M. (2008) Changes in Water Structure Induced by the Guanidinium Cation and Implications for Protein Denaturation, *J. Phys. Chem. A 112*, 10939-10948.
46. Wernersson, E., Heyda, J., Vazdar, M., Lund, M., Mason, P. E., and Jungwirth, P. (2011) Orientational Dependence of the Affinity of Guanidinium Ions to the Water Surface, *J. Phys. Chem. B 115*, 12521-12526.
47. Hunger, J., Niedermayer, S., and Buchner, R. (2010) Are Nanoscale Ion Aggregates Present in Aqueous Solutions of Guanidinium Salts?, *J. Phys. Chem. B 114*, 13617–13627.
48. van der Post, S. T., Tielrooij, K.-J., Hunger, J., Backus, E. H. G., and Bakker, H. J. (2013) Femtosecond study of the effects of ions and hydrophobes on the dynamics of water, *Faraday Discuss. 160*, 171-189.
49. Arakawa, T., and Timasheff, S. N. (1984) Protein stabilization and destabilization by guanidinium salts, *Biochemistry 23*, 5924-5929.
50. Courtenay, E. S., Capp, M. W., and Record, J., M.T. (2001) Thermodynamics of interactions of urea and guanidinium salts with protein surface: Relationship between solute effects on protein processes and changes in water-accessible surface area, *Protein Sci. 10*, 2485–2497.
51. Mason, P. E., Brady, J. W., Neilson, G. W., and Dempsey, C. E. (2007) The Interaction of Guanidinium Ions with a Model Peptide, *Biophys. J. 93*, L04-L06.
52. Makhatadze, G., and Privalov, P. (1992) Protein interactions with urea and guanidinium chloride : A calorimetric study, *J. Mol. Biol. 226*, 491-505.
53. Luong, T. Q., Verma, P. K., Mitra, R. K., and Havenith, H. (2011) Do Hydration Dynamics Follow the Structural Perturbation during Thermal Denaturation of a Protein: A Terahertz Absorption Study, *Biophys. J. 101*, 925-933.
54. Ahmad, B., Ahmed, M. Z., Haq, S. K., and Khan, R. H. (2005) Guanidine hydrochloride denaturation of human serum albumin originates by local unfolding of some stable loops in domain III, *Biochimica et Biophysica Acta (BBA)-Proteins and Proteomics 1750*, 93-102.
55. Nandi, N., Bhattacharyya, K., and Bagchi, B. (2000) Dielectric relaxation and solvation dynamics of water in complex chemical and biological systems, *Chem. Rev. 100*, 2013-2045.
56. Vazdar, M., Uhlig, F., and Jungwirth, P. (2012) Like-Charge Ion Pairing in Water: An Ab Initio Molecular Dynamics Study of Aqueous Guanidinium Cations, *J. Phys. Chem. Lett. 3*, 2021-2024.
57. F., H. (1888) *Arch. Exp. Pathol. Pharmacol. 24*, 247-260.
58. O'Brien, E. P., Dima, R. I., Brooks, B., and Thirumalai, D. (2007) Interactions between Hydrophobic and Ionic Solutes in Aqueous Guanidinium Chloride and Urea Solutions: Lessons for Protein Denaturation Mechanism, *Journal of the American Chemical Society 129*, 7346-7353.
59. Godawat, R., Jamadagni, S. N., and Garde, S. (2010) Unfolding of Hydrophobic Polymers in Guanidinium Chloride Solutions, *The Journal of Physical Chemistry B 114*, 2246-2254.

60. Graziano, G. (2011) Contrasting the denaturing effect of guanidinium chloride with the stabilizing effect of guanidinium sulfate, *Physical Chemistry Chemical Physics 13*, 12008-12014.
61. TRAKSITION, T. R., and VON HIPPEL, P. H. (1965) On the conformational stability of globular proteins, *The Journal of Biological Chemistry 240*, 3909-3923.
62. Jamal, S., Poddar, N. K., Singh, L. R., Dar, T. A., Rishi, V., and Ahmad, F. (2009) Relationship between functional activity and protein stability in the presence of all classes of stabilizing osmolytes, *The FEBS journal 276*, 6024-6032.
63. Stambolic, V., and Woodgett, J. R. (1994) Mitogen inactivation of glycogen synthase kinase-3β in intact cells via serine 9 phosphorylation, *Biochemical Journal 303*, 701-704.
64. Shiraki, K., Kudou, M., Fujiwara, S., Imanaka, T., and Takagi, M. (2002) Biophysical effect of amino acids on the prevention of protein aggregation, *Journal of biochemistry 132*, 591-595.
65. Frommel, C. (1984) The apolar surface area of amino acids and its empirical correlation with hydrophobic free energy, *Journal of theoretical biology 111*, 247-260.
66. Kyte, J., and Doolittle, R. F. (1982) A simple method for displaying the hydropathic character of a protein, *Journal of Molecular Biology 157*, 105-132.
67. Zhou, R., Huang, X., Margulis, C. J., and Berne, B. J. (2004) Hydrophobic Collapse in Multidomain Protein Folding, *Science 305*, 1605.
68. Cheung, M. S., García, A. E., and Onuchic, J. N. (2002) Protein folding mediated by solvation: water expulsion and formation of the hydrophobic core occur after the structural collapse, *Proceedings of the National Academy of Sciences 99*, 685-690.
69. Chandler, D. (2005) Interfaces and the driving force of hydrophobic assembly, *Nature 437*, 640-647.
70. Estell, D. A., Graycar, T. P., Miller, J. V., Powers, D. B., Wells, J. A., Burnier, J. P., and Ng, P. G. (1986) Probing Steric and Hydrophobic Effects on Enzyme-Substrate Interactions by Protein Engineering, *Science 233*, 659.
71. Breydo, L., Sales, A. E., Frege, T., Howell, M. C., Zaslavsky, B. Y., and Uversky, V. N. (2015) Effects of Polymer Hydrophobicity on Protein Structure and Aggregation Kinetics in Crowded Milieu, *Biochemistry 54*, 2957-2966.
72. Biedermannová, L., and Schneider, B. (2016) Hydration of proteins and nucleic acids: Advances in experiment and theory. A review, *Biochimica et Biophysica Acta (BBA) - General Subjects 1860*, 1821-1835.
73. Denisov, V. P., Jonsson, B.-H., and Halle, B. (1999) Hydration of denatured and molten globule proteins, *Nat Struct Mol Biol 6*, 253-260.
74. Luong, T. Q., Verma, P. K., Mitra, R. K., and Havenith, M. (2011) Do hydration dynamics follow the structural perturbation during thermal denaturation of a protein: A terahertz absorption study, *Biophysical journal 101*, 925-933.
75. Blokzijl, W., and Engberts, J. B. F. N. (1993) Hydrophobic Effects. Opinions and Facts, *Angewandte Chemie International Edition in English 32*, 1545-1579.
76. Nozaki, Y., and Tanford, C. (1971) The Solubility of Amino Acids and Two Glycine Peptides in Aqueous Ethanol and Dioxane Solutions: ESTABLISHMENT OF A HYDROPHOBICITY SCALE, *Journal of Biological Chemistry 246*, 2211-2217.
77. Acharya, H., Vembanur, S., Jamadagni, S. N., and Garde, S. (2010) Mapping hydrophobicity at the nanoscale: Applications to heterogeneous surfaces and proteins, *Faraday discussions 146*, 353-365.

78. Jensen, J. H., and Gordon, M. S. (1995) On the Number of Water Molecules Necessary To Stabilize the Glycine Zwitterion, *Journal of the American Chemical Society 117*, 8159-8170.
79. Gontrani, L., Mennucci, B., and Tomasi, J. (2000) Glycine and alanine: a theoretical study of solvent effects upon energetics and molecular response properties, *Journal of Molecular Structure: THEOCHEM 500*, 113-127.
80. Gordon, M. S., and Jensen, J. H. (1996) Understanding the Hydrogen Bond Using Quantum Chemistry, *Accounts of Chemical Research 29*, 536-543.
81. Hecht, D., Tadesse, L., and Walters, L. (1993) Correlating hydration shell structure with amino acid hydrophobicity, *Journal of the American Chemical Society 115*, 3336-3337.
82. Ide, M., Maeda, Y., and Kitano, H. (1997) Effect of Hydrophobicity of Amino Acids on the Structure of Water, *The Journal of Physical Chemistry B 101*, 7022-7026.
83. Qvist, J., and Halle, B. (2008) Thermal Signature of Hydrophobic Hydration Dynamics, *Journal of the American Chemical Society 130*, 10345-10353.
84. Balabin, R. M. (2010) The First Step in Glycine Solvation: The Glycine−Water Complex, *The Journal of Physical Chemistry B 114*, 15075-15078.
85. McLain, S. E., Soper, A. K., Terry, A. E., and Watts, A. (2007) Structure and Hydration of l-Proline in Aqueous Solutions, *The Journal of Physical Chemistry B 111*, 4568-4580.
86. Pacios, L. F. (2001) Distinct Molecular Surfaces and Hydrophobicity of Amino Acid Residues in Proteins, *Journal of Chemical Information and Computer Sciences 41*, 1427-1435.
87. Panuszko, A., Adamczak, B., Czub, J., Gojło, E., and Stangret, J. (2015) Hydration of amino acids: FTIR spectra and molecular dynamics studies, *Amino Acids 47*, 2265-2278.
88. Sato, T., Buchner, R., Fernandez, Š., Chiba, A., and Kunz, W. (2005) Dielectric relaxation spectroscopy of aqueous amino acid solutions: dynamics and interactions in aqueous glycine, *Journal of molecular liquids 117*, 93-98.
89. Rodríguez-Arteche, I., Cerveny, S., Alegría, Á., and Colmenero, J. (2012) Dielectric spectroscopy in the GHz region on fully hydrated zwitterionic amino acids, *Physical Chemistry Chemical Physics 14*, 11352-11362.
90. Suzuki, M., Shigematsu, J., Fukunishi, Y., and Kodama, T. (1997) Hydrophobic Hydration Analysis on Amino Acid Solutions by the Microwave Dielectric Method, *The Journal of Physical Chemistry B 101*, 3839-3845.
91. Niehues, G., Heyden, M., Schmidt, D. A., and Havenith, M. (2011) Exploring hydrophobicity by THz absorption spectroscopy of solvated amino acids, *Faraday Discussions 150*, 193-207.
92. Shiraga, K., Suzuki, T., Kondo, N., and Ogawa, Y. (2014) Hydration and hydrogen bond network of water around hydrophobic surface investigated by terahertz spectroscopy, *The Journal of Chemical Physics 141*, 235103.
93. Shaytan, A. K., Shaitan, K. V., and Khokhlov, A. R. (2009) Solvent Accessible Surface Area of Amino Acid Residues in Globular Proteins: Correlation of Apparent Transfer Free Energies with Experimental Hydrophobicity Scales, *Biomacromolecules 10*, 1224-1237.
94. Blackham, D. V., and Pollard, R. D. (1997) An improved technique for permittivity measurements using a coaxial probe, *IEEE Transactions on Instrumentation and Measurement 46*, 1093-1099.
95. Venkatesh, M., and Raghavan, G. (2005) An overview of dielectric properties measuring techniques, *Canadian biosystems engineering 47*, 15-30.

96. (May 9, 2003) Technical Overview, Agilent 85070E Dielectric Probe Kit 200 MHz to 50 GHz, Agilent.
97. Tielrooij, K.-J., Hunger, J., Buchner, R., Bonn, M., and Bakker, H. J. (2010) Influence of Concentration and Temperature on the Dynamics of Water in the Hydrophobic Hydration Shell of Tetramethylurea, *J. Am. Chem. Soc. 132*, 15671-15678.
98. Hunger, J., Tielrooij, K.-J., Buchner, R., Bonn, M., and Bakker, H. J. (2012) Complex Formation in Aqueous Trimethylamine-N-oxide (TMAO) Solutions, *J. Phys. Chem. B 116*, 4783-4795.
99. Lee, J. C., and Timasheff, S. N. (1981) The stabilization of proteins by sucrose, *J. Biol. Chem. 256*, 7193-7201.
100. Kim, Y. S., Jones, L. S., Dong, A. C., Kendrick, B. S., Chang, B. S., Manning, M. C., Randolph, T. W., and Carpenter, J. F. (2003) Effects of sucrose on conformational equilibria and fluctuations within the native-state ensemble of proteins *Protein Sci. 12*, 1252-1261.
101. Heyden, M., Bründermann, E., Heugen, U., Niehues, G., Leitner, D. M., and Havenith, M. (2008) Long range influence of carbohydrates on the solvation dynamics of water - Answers from THz absorption measurements and molecular modeling simulations, *J. Am. Chem. Soc. 130*, 5773-5779.
102. Heugen, U., Schwaab, G., Bründermann, E., Heyden, M., Yu, X., Leitner, D. M., and Havenith, M. (2006) Solute-induced retardation of water dynamics probed directly by terahertz spectroscopy, *Proc. Natl. Acad.Sci.USA 103*, 12301-12306.
103. Fuchs, K., and Kaatze, U. (2002) Dielectric spectra of mono- and disaccharide aqueous solutions, *J. Chem. Phys. 116*, 7137-7144.
104. Weingärtner, H., Knocks, A., Boresch, S., Höchtl, P., and Steinhauser, O. (2001) Dielectric spectroscopy in aqueous solutions of oligosaccharides: Experiment meets simulation, *J. Chem. Phys. 115*, 1463-1472.
105. Kaminski, K., Kaminska, E., Hensel-Bielowka, S., Chelmecka, E., Paluch, M., Ziolo, J., Wlodarczyk, P., and Ngai, K. L. (2008) Identification of the Molecular Motions Responsible for the Slower Secondary (b) Relaxation in Sucrose, *J. Phys. Chem. B 112*, 7662-7668.
106. Kaminski, K., Adrjanowicz, K., Zakowiecki, D., Kaminska, E., Wlodarczyk, P., Paluch, M., Pilch, J., and Tarnacka, M. (2012) Dielectric Studies on Molecular Dynamics of Two Important Disaccharides: Sucrose and Trehalose, *Mol. Pharmaceutics 9*, 1559-1569.
107. Fukasawa, T., Sato, T., Watanabe, J., Hama, Y., Kunz, W., and Buchner, R. (2005) Relation between Dielectric and Low-Frequency Raman Spectra of Hydrogen-Bond Liquids, *Phys. Rev. Lett. 95*, 197802.
108. Polley, D., Patra, A., and Mitra, R. K. (2013) Dielectric relaxation of the extended hydration sheathe of DNA in the THz frequency region, *Chem. Phys. Lett. 586*, 143-147.
109. Kindt, J. T., and Schmuttenmaer, C. A. (1996) Far-infrared dielectric properties of polar liquids probed by femtosecond terahertz pulse spectroscopy, *J. Phys. Chem. 100*, 10373-10379.
110. Walrafen, G. E., Chu, Y. C., and Piermarini, G. J. (1996) Low-Frequency Raman Scattering from Water at High Pressures and High Temperatures, *J. Phys. Chem. 100* 10363-10372.
111. Vij, J. K., Simpson, D. R. J., and Panarina, O. E. (2004) Far infrared spectroscopy of water at different temperatures: GHz to THz dielectric spectroscopy of water *J. Mol. Liq. 112*, 125-135.

112. Heyden, M., and Havenith, M. (2010) Combining THz spectroscopy and MD simulations to study protein-hydration coupling *Methods 52*, 74-83.
113. Tanford, C. (1968) Protein denaturtion, *Adv. Prot. Chem. 23*, 121-282.
114. Gordon, J. A., and Warren, J. R. (1968) Denaturation of globular proteins. I. The interaction of urea and thiourea with bovine plasma albumin, *J. Biol. Chem. 243*, 5663-5669.
115. Sagle, L. B., Zhang, Y., Litosh, V. A., Chen, X., Cho, Y., and Cremer, P. S. (2009) Investigating the Hydrogen-Bonding Model of Urea Denaturation, *J. Am. Chem. Soc. 131*, 9304-9310.
116. Rezus, Y. L. A., and Bakker, H. J. (2007) Observation of Immobilized Water Molecules around Hydrophobic Groups, *Phys. Rev. Lett. 99*, 148301.
117. Rezus, Y. L. A., and Bakker, H. J. (2008) Strong Slowing Down of Water Reorientation in Mixtures of Water and Tetramethylurea, *J. Phys. Chem. A 112* 2355-2361.
118. Lin, T.-Y., and Timasheff, S. N. (1994) Why do some organisms use a urea-methylamine mixture as osmolyte? Thermodynamic compensation of urea and trimethylamine N-oxide interactions with protein, *Biochemistry 33*, 12695-12701.
119. Auton, M., and Bolen, D. W. (2005) Predicting the energetics of osmolyte-induced protein folding/unfolding, *Proc. Nat. Acad. Sci. 102*, 15065-15068.
120. Mello, C. C., and Barrick, D. (2003) Measuring the stability of partly folded proteins using TMAO, *Protein Sci. 12*, 1522-1529.
121. Meersman, F., Bowron, D., Soper, A. K., and Koch, M. H. J. (2009) Counteraction of Urea by Trimethylamine N-Oxide Is Due to Direct Interaction, *Biophys. J. 97*, 2559-2566.
122. Wang, A., and Bolen, D. W. (1997) A Naturally Occurring Protective System in Urea-Rich Cells: Mechanism of Osmolyte Protection of Proteins against Urea Denaturation, *Biochemistry 36*, 9101-9108.
123. Paul, S., and Patey, G. N. (2007) Structure and Interaction in Aqueous Urea−Trimethylamine-N-oxide Solutions, *J. Am. Chem. Soc. 129*, 4476-4482.
124. Freda, M., Onori, G., and Santucci, A. (2001) Infrared Study of the Hydrophobic Hydration and Hydrophobic Interactions in Aqueous Solutions of tert-Butyl Alcohol and Trimethylamine-n-oxide, *J. Phys. Chem. B 105*, 12714-12718.
125. Sarma, R., and Paul, S. (2013) Exploring the Molecular Mechanism of Trimethylamine-N-oxide's Ability to Counteract the Protein Denaturing Effects of Urea, *J. Phys. Chem. B 117*, 5691-5704.
126. Taylor, L. S., York, P., Williams, A. C., Edwards, H. G., Mehta, V., Jackson, G. S., Badcoe, I. G., and Clarke, A. R. (1995) Sucrose reduces the efficiency of protein denaturation by a chaotropic agen, *Biochim Biophys Acta. 1253*, 39-46.
127. Born, B., Kim, S. J., Ebbinghaus, S., Gruebele, M., and Havenith, M. (2009) The terahertz dance of water with the proteins: the effect of protein flexibility on the dynamical hydration shell of ubiquitin *Faraday Discuss.*, 161-173.
128. Laage, D., and Hynes, J. T. (2006) A Molecular Jump Mechanism of Water Reorientation *Science 311*, 832-835.
129. Fecko, C. J., Eaves, J. D., and Tokmakoff, A. (2002) Isotropic and anisotropic Raman scattering from molecular liquids measured by spatially masked optical Kerr effect spectroscopy, *J. Chem. Phys. 117*, 1139-1154.
130. Zasetsky, A. Y. (2011) Dielectric Relaxation in Liquid Water: Two Fractions or Two Dynamics? , *Phys. Rev. Lett. 107*, 117601.
131. Alonso, D. O. V., and Dill, K. A. (1991) Solvent denaturation and stabilization of globular proteins, *Biochemistry 30*, 5974-5985.

132. Breslow, R., and Guo, T. (1990) Surface tension measurements show that chaotropic salting-in denaturants are not just water-structure breakers, *Proc. Nat. Acad. Sci. 87*, 167-169.
133. Stirnemann, G., Sterpone, F., and Laage, D. (2011) Dynamics of Water in Concentrated Solutions of Amphiphiles: Key Roles of Local Structure and Aggregation, *J. Phys. Chem. B 115*, 3254-3262.
134. Woody, R. W., and Tinoco Jr., I. (1967) Optical Rotation of Oriented Helices. III. Calculation of the Rotatory Dispersion and Circular Dichroism of the Alpha- and 310-Helix, *J. Chem. Phys. 46*, 4927-4945.
135. Das Mahanta, D., Samanta, N., and Mitra, R. K. (2016) The effect of monovalent cations on the collective dynamics of water and on a model protein, *Journal of Molecular Liquids 215*, 197-203.
136. Böttcher, C. J. F. (1973) Theory of Electric Polarization, 2 ed., Elsevier, Amsterdam.
137. Dote, J. L., Kivelson, D., and Schwartz, R. N. (1981) A molecular quasi-hydrodynamic free-space model for molecular rotational relaxation in liquids, *The Journal of Physical Chemistry 85*, 2169-2180.
138. Cavell, E. A. S., Knight, P. C., and Sheikh, M. A. (1971) Dielectric relaxation in non aqueous solutions. Part 2.-Solutions of tri(n-butyl)ammonium picrate and iodide in polar solvents, *Transactions of the Faraday Society 67*, 2225-2233.
139. Zamyatnin, A. A. (1972) Protein volume in solution, *Prog Biophys Mol Biol 24*, 107-123.
140. Korter, T. M., Balu, R., Campbell, M. B., Beard, M. C., Gregurick, S. K., and Heilweil, E. J. (2006) Terahertz spectroscopy of solid serine and cysteine, *Chemical Physics Letters 418*, 65-70.
141. Dexheimer, S. L. (2007) *Terahertz spectroscopy: principles and applications*, CRC press.
142. Ebbinghaus, S., Kim, S. J., Heyden, M., Yu, X., Heugen, U., Gruebele, M., Leitner, D. M., and Havenith, M. (2007) An extended dynamical hydration shell around proteins, *Proceedings of the National Academy of Sciences 104*, 20749-20752.
143. Funkner, S., Niehues, G., Schmidt, D. A., and Bründermann, E. (2014) Terahertz absorption of chemicals in water: ideal and real solutions and mixtures, *Journal of Infrared, Millimeter, and Terahertz Waves 35*, 38-52.
144. Bye, J. W., Meliga, S., Ferachou, D., Cinque, G., Zeitler, J. A., and Falconer, R. J. (2014) Analysis of the Hydration Water around Bovine Serum Albumin Using Terahertz Coherent Synchrotron Radiation, *The Journal of Physical Chemistry A 118*, 83-88.
145. Samanta, N., Mahanta, D. D., and Mitra, R. K. (2014) Collective Hydration Dynamics of Guanidinium Chloride Solutions and its Possible Role in Protein Denaturation: A Terahertz Spectroscopic Study, *Physical Chemistry Chemical Physics 16*, 23308-23315.
146. Samanta, N., Mahanta, D. D., and Mitra, R. K. (2014) Does Urea Alter the Collective Hydrogen Bond Dynamics in Water: A Dielectric Relaxation Study in the THz Frequency Region, *Chemistry - An Asian Journal 9*, 3457-3463.
147. Samanta, N., Luong, T. Q., Mahanta, D. D., Mitra, R. K., and Havenith, M. (2016) The Effect of Short Chain Polyethyleneglycols on the Hydration Structure and Dynamics around Human Serum Albumin, *Langmuir 32*, 831-837.
148. Okouchi, S., Moto, T., Ishihara, Y., Numajiri, H., and Uedaira, H. (1996) Hydration of amines, diamines, polyamines and amides studied by NMR, *Journal of the Chemical Society, Faraday Transactions 92*, 1853-1857.

149. Uedaira, H. (1977) Activity Coefficients of Glycylglycine and α-Aminobutyric Acid in Aqueous Sucrose Solutions, *Bulletin of the Chemical Society of Japan 50*, 1298-1304.
150. Wood, I., Martini, M. F., and Pickholz, M. (2013) Similarities and differences of serotonin and its precursors in their interactions with model membranes studied by molecular dynamics simulation, *Journal of Molecular Structure 1045*, 124-130.
151. Campo, M. G. (2006) Molecular dynamics simulation of glycine zwitterion in aqueous solution, *The Journal of chemical physics 125*, 114511.
152. Uversky, V. N. (2005) A GLYmmer of Insight into Fibril Formation, *Structure 13*, 1090-1092.
153. Heyden, M., and Havenith, M. (2010) Combining THz spectroscopy and MD simulations to study protein-hydration coupling, *Methods 52*, 74-83.
154. Shah, D., and Shaikh, A. R. (2016) Interaction of arginine, lysine, and guanidine with surface residues of lysozyme: implication to protein stability, *Journal of Biomolecular Structure and Dynamics 34*, 104-114.
155. Mahanta, D. D., Patra, A., Samanta, N., Luong, T. Q., Mukherjee, B., and Mitra, R. K. (2016) Non-monotonic dynamics of water in its binary mixture with 1, 2-dimethoxy ethane: A combined THz spectroscopic and MD simulation study, *The Journal of Chemical Physics 145*, 164501.
156. Cametti, C., Marchetti, S., Gambi, C. M. C., and Onori, G. (2011) Dielectric Relaxation Spectroscopy of Lysozyme Aqueous Solutions: Analysis of the δ-Dispersion and the Contribution of the Hydration Water, *The Journal of Physical Chemistry B 115*, 7144-7153.
157. Godec, A., Smith, J. C., and Merzel, F. (2011) Increase of both order and disorder in the first hydration shell with increasing solute polarity, *Physical review letters 107*, 267801.

Chapter 6

6. Effect of Cosolutes on Protein Activity

This chapter reveals the effect of polyethylene glycols (PEG) of different chain lengths (M_n 400 and 4000) and their monomer ethylene glycol (EG) on the enzyme efficiency of a model protein hen egg white lysozyme (HEWL) at pH 7 and 20 °C. Micrococcus lysodeikticus (M. Lys.) cell has been used as a substrate. We have found a critical concentration of the osmolytes up to which the enzyme efficiency enhances and beyond that concentration it loses its activity. The structure and the local environment of the active site of lysozyme have been detected in presence of the osmolytes by using CD, fluorescence measurements. We have observed an interesting correlation between the thermal unfolding temperature (T_u) and the enzyme activity and found a minimal activation energy barrier for the critical concentration by analysing the catalytic parameters. There is a competition between excluded volume effect and soft interaction with HEWL and PEG and we found a reflection to the enzyme efficiency.

6.1. Introduction

Proteins and their functions are endlessly fascinating in living cell where upto 40% (w/v) volume is occupied by different macromolecules, e.g., ribosome, microtubules, intermediate filaments, nucleic acids etc. as well as some small cosolutes like glucose, salts, amino acids etc.[1, 2] It excites the curiosity to study protein in such crowded environment and to mimic such intracellular as well as extracellular compartments some synthetic polymers (e.g. dextran, ficoll, polyethylene glycol), and small molecules (e.g. sucrose, glycerol, TMAO) as well as proteins are often used to investigate how the structure, thermal stability, hydration and function or activity of proteins are modified under crowded environments.[3-6] Until recently such studies were mainly been concerned with the *excluded volume effect* which can explain the compaction of protein due to minimize steric overlaps.[7-9] In terms of thermodynamics, *excluded volume effect* results in a loss of configurational entropy of a protein under crowded environment.[10] However, this theory finds incompetency rationalate several *in vitro* studies which involve protein-crowder (or cosolutes) interactions which are still believed to be nonspecific in nature.[11] Recent studies have revealed that protein stabilization in presence of cosolutes is governed mainly by enthalpy rather than entropy, indicating specific interactions with proteins to govern predominate beyond the hard core repulsion.[12, 13] In an exciting recent study it is revealed that injected macromolecules inside a

cell did not show compactness in accordance to the excluded volume notion.[14] The authors concluded that in real cellular environment it is the attractive, nonspecific interactions that counteract the excluded-volume effect. In this notion study of enzyme activity in crowded milieu has expressed as a fascinating topic of research.[15, 16] It is not very trivial to predict the effect of different crowding agents or cosolutes on the activities of enzymes which eventually is example specific in nature. For amphiphilic crowders there remains always a competition between preferential hydration and preferential binding with protein residues.[17] In a previous study[18] the catalytic activity of α-chymotrypsin found to be retarded in presence of PEG 400 and terms of both catalytic parameters K_M and k_{cat} reduced. The phenomenon is believed to be governed by the osmolytic effect exerted by PEG causing a depletion of hydration shell and a consequence loss of water activity. Recently Shahid et al[19] reported that lysozyme is stabilized in presence of dextran 70 and ficoll 70 while its activity on M. lysodeikticus decreases with the increasing concentration of both the crowders. They ascribed the retarded activity in terms of the volume exclusion and increase in the viscosity which regulates the diffusion or encounter rates of enzymes and substrates. The authors also found that K_m does not depend on the shape and size of the crowders while that of K_{cat} does. A similar decrease in the catalytic activity of alkaline molten globular 5-aminolevulinate synthase in presence of osmolytes and macromolecular crowders (TMAO, glycerol, dextran 200, ficoll 400) has recently been reported.[20]

Unlike conventional crowding agents PEGs are of special mention as they can exert either or both *soft interaction* (H-bonding, van der Waals force or hydrophobic interaction) as well as *excluded volume effect*. The mode of interaction switches depending on the chain length and concentration of the PEG as well as the nature of protein. Senske et al. observed that in (wild type) ubiquitine the excess enthalpy of unfolding ($\Delta\Delta H_u$) increases (similar to glucose, dextran) while its melting temperature (T_m) decreases (similar to urea) in presence of PEG 20. This observation leads to the conclusion that PEG behaves as an intermediate between being a stabilizing osmolyte (preferential hydration) and a denaturant (preferential binding).[13] In our previous study we also noticed an unusual thermal destabilization of human serum albumin in presence of PEG 200 and 400. We found a PEG induced decrease in the vant Hoff enthalpy and an increase in entropy of unfolding (ΔS).[21] We proposed a polymer-protein interaction to switch from being non-interacting or weakly repulsive (as osmolyte) to interacting (as a non-specific ligand) with progressive increasing of PEG.[21, 22] This result intrigues to study how the enzyme activity changes with the chain lengths of PEGs. We

therefore take up the study to investigate the activity of a model enzyme lysozyme on Micrococcus lysodeikticus (M. lys.) cell in presence of the monomer EG and polyethylene glycols of varying chain lengths (400, 4000) in dilute to high concentration regions.

Hen egg white lysozyme (HEWL) is a single chain polypeptide of 129 amino acids cross-linked with four disulphide bridges (see details in chapter 2).[23] Substrates bind in this cleft and are hydrolyzed under the action of key residues Glu35 and Asp52 (Trp62, Trp63, Asp101, Trp108 are involved in substrate binding)[24], in the active site of the protein. Lysozyme catalyses the hydrolysis of β (1→4) glycosidic bond between N-acetyl glucosamine (NAG) and N-acetyl muramic acid (NAM) which form the backbone of many bacterial cell walls.[25] In the initial step lysozyme attaches to the large surface cell wall mostly driven by electrostatic interaction.[26] The mechanism shown in the scheme is proposed by D. J. Vocadlo et al.[27]

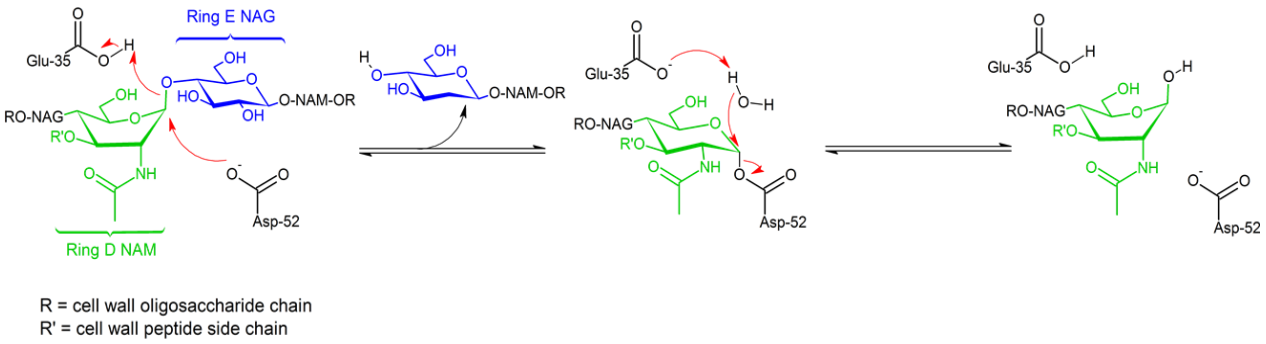

Scheme 6.1: Mechanism of lysozyme function as proposed by *D. J. Vocadlo et al. [Source: Wikipedia]*

In a previous study Malzert et al. have reported that lysozyme activity on M. Lys. cell wall hardly changes in presence of PEG 400, 2000, 5000 upto 0.02% (w/v).[28] However the authors measured the activity after incubating lysozyme and the cell solution for 4 hrs at 37 °C., thus information on real time changes is not evident in the study. It therefore stands concerned here the addition of PEG changes the real time activity of lysozyme.

6.2. Materials and Methods

Ethylene glycol (EG), polyethylene glycol (PEG 400 and 4000), lyophilised powder of hen egg white lysozyme (HEWL) [M_w 14.31 kDa[29], molar extinction coefficient[30], ε_{280nm}=36000 $M^{-1}cm^{-1}$], lyophilized Micrococcus lysodeikticus (M. lys.) cell were purchased from Sigma-Aldrich and used without further purification. The samples were dissolved in 10 mM sodium phosphate buffer of pH ~7.4. Enzyme activity measurements were performed by turbid

metric method using UV visible spectroscopy (Shimadzu UV-2450 spectrophotometer). The absorption at 450 nm of the turbid solution of M. lys. cell was recorded with time immediately after mixing with lysozyme. The structure of lysozyme was measured by circular dichroism spectroscopy (JASCO J-815) both in Far and near UV range to probe the secondary as well as tertiary structure of the enzyme respectively. Steady-state emission was measured using a quartz cuvette with 1 cm path length in Fluorolog fluorimeter (Horiba-Jobin Yvon, Edison, NJ) with a Peltier attachment (MODEL LFI-3751) to control the temperature. To rule out the emission of tyrosine or phenylalanine lysozyme was excited at 299 nm to study the tryptophan (Trp) emission only.

Following is the simplest mechanism to show enzyme (E) kinetic reaction on a substrate (S) to form a product (P):

$$E + S \leftrightarrows ES \rightarrow ES^{\#} \longrightarrow E + P \qquad (6.1)$$

where *ES* is the enzyme-substrate complex and $ES^{\#}$ is an intermediate transition state before product formation. At a fixed lysozyme concentration (0.1 µM) we measured the initial rate (V_0) varying concentration of substrate (S) and found that it follows the Michaelis-Menten equation (details are found in chapter 2). We have plotted enzyme catalytic efficiency (k_{cat}/K_M) as a function of crowding agent concentration.

6.3. Results and Discussions

Lysozyme Activity Measurement

The rate of hydrolysis catalysed by the HEWL is found to be dependent on the concentration of the added EG, PEG 400 and PEG 4000 (figure 6.3.1a). The initial rate of hydrolysis (V_0) increases in the low concentration region (~2% w/v) of all the cosolutes, however it decreases at higher concentration (figure 6.3.1b). We have previously reported such enhancement in activity of α-chymotrypsin (CHT) in presence of low concentration dodecyl-trimethylammonium bromide (DTAB) solution.[31] 6% enhancement in enzyme activity has been reported by Pancera *et al.*[32] However the activity has been found to lower in presence of PEG 1500 and 4000. A 20% increase in the activity of glucose-6-phosphate dehydrogenase was reported to by Pancera *et al.* in presence of 20 % (w/v) PEG 400 and 4000 solutions.[33] The present bell shaped activity profile is intriguing and we try to investigate the factors responsible for such concentration dependency.

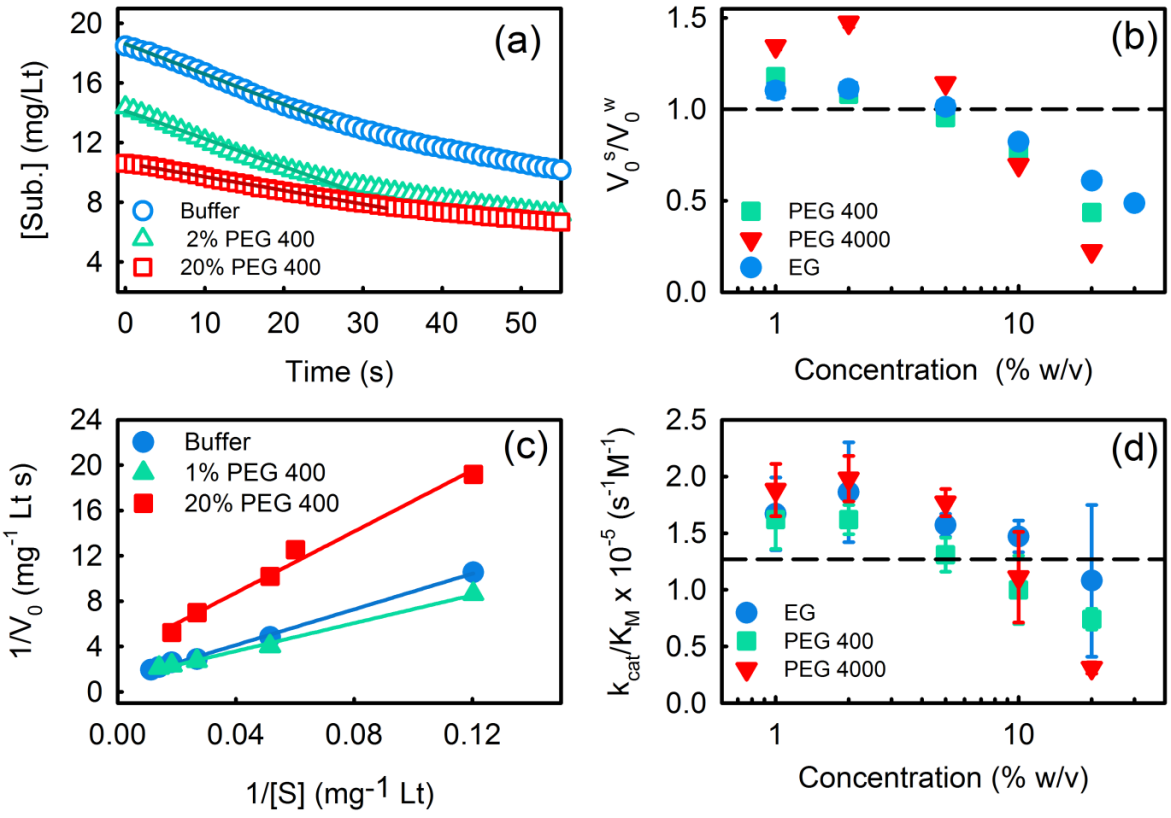

Figure 6.3.1. (a) A representative plot of lysozyme (0.1 µM) catalysed substrate (M. Lys. cell) concentration (obtained from O.D. at 450 nm) as a function of time in presence of PEG 400 in buffer of pH 7 at 20 °C. The linear fit has been shown by solid line. (b) Representative Lineweaver Burk (LB) plot in different concentration of PEG 400. (c) Initial relative rate of hydrolysis of M. Lys. cell wall in presence of different concentration of EG, PEG 400 and PEG 4000 at room temperature (pH 7). (d) Enzyme efficiency (k_{cat}/K_M) in presence of different concentration of EG, PEG 400 and PEG 4000.

For a quantitative understanding of the activity we measure substrate concentration (8-120 mg l^{-1}) dependent rate of reaction at a fixed lysozyme concentration (0.1 µM) in absence and in presence of the PEGs and EG (1-20% w/v). The kinetics is found to follow the Michaelis-Menten mechanism[34] in the entire concentration region. The double reciprocal LB plots show good linear fits (figure 6.1.1c) and from the slope and intercept of this fitting we calculate the catalytic parameters (Table 6.3.1). The obtained K_M (80.88±9.67 mg l^{-1}) and k_{cat} ((1.03± 0.12)×10^7 mg l^{-1} s^{-1} M^{-1} in buffer solution are in good agreement with earlier report[19]. The enzyme efficiency as defined by the ratio k_{cat}/K_M, increases initially to reach a maximum value at ~2% (w/v) beyond which it decreases with increasing concentration of both the PEGs and EG (figure 6.3.1.d). The value of K_M associates with the dissociation constant of the enzyme-substrate (ES) complex; larger is the value of K_M, weaker is the binding. In presence of EG K_M decreases upto 2% concentration indicating a strong E-S complex

formation which eventually weakens at higher EG concentration as K_M also increases (table 6.3.1). The k_{cat} value is higher than that in buffer and exhibits a rather non-regular trend. In PEG 400 and 4000 also smaller K_M values infer stronger *E-S* binding; at higher concentration k_{cat} decreases overwhelmingly which consequently decreases the overall enzyme activity (k_{cat}/K_M).

Secondary and Tertiary Structure from CD Spectra

Crucial to the understanding of enzyme activity is its structure and conformation, although this is not the sole factor to govern the overall activity. The far UV (190-260 nm) CD spectra

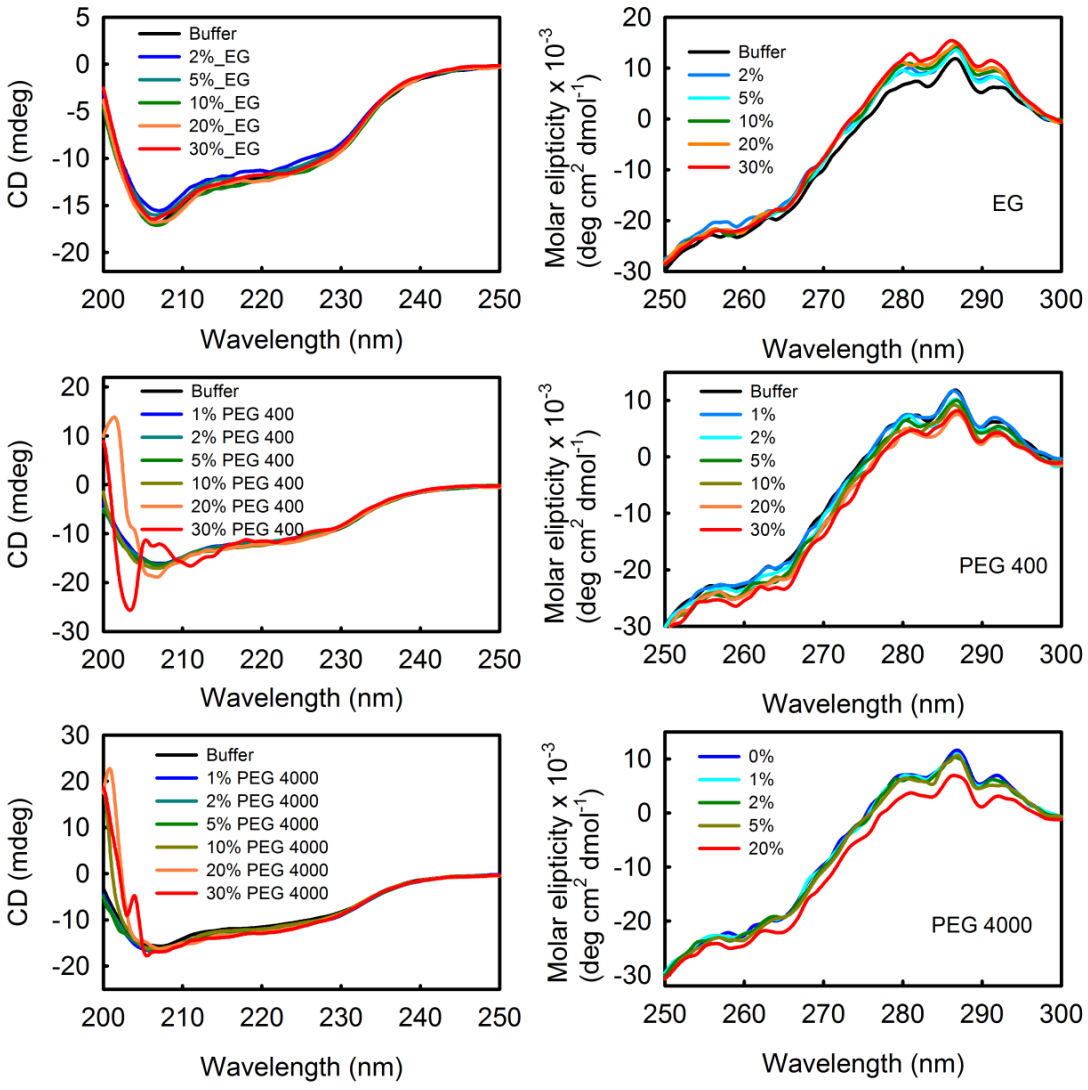

Figure 6.3.2. Far (left) and near UV CD spectra (right) of lysozyme in presence of EG, PEG 400 and 4000 at 20 C, pH 7.4.

(figure 6.3.2 & 6.3.3.a) of HEWL reveal only minimal change in the spectral feature in presence of EG, PEG 400 and 4000. At 20 °C the native structure of HEWL contains 32% α-

helix, 19% β-sheet, 18% β-turn and 31% random coil conformation[35]. In presence of EG and PEG 400 a marginal change in the α-helix content is observed whereas in presence of PEG 4000 the α-helix content is increased by 5%. This result can be explained on the basis of the excluded volume model. As lysozyme (hydrodynamic diameter, d_H ~4 nm) is comparable in size with PEG 4000 (d_H ~3.3 nm) while PEG 400 (~0.9 nm) and EG are comparatively smaller, the native protein is excluded from the PEG 4000 whereas smaller EG and PEG 400 interacts preferentially with lysozyme.[36, 37]

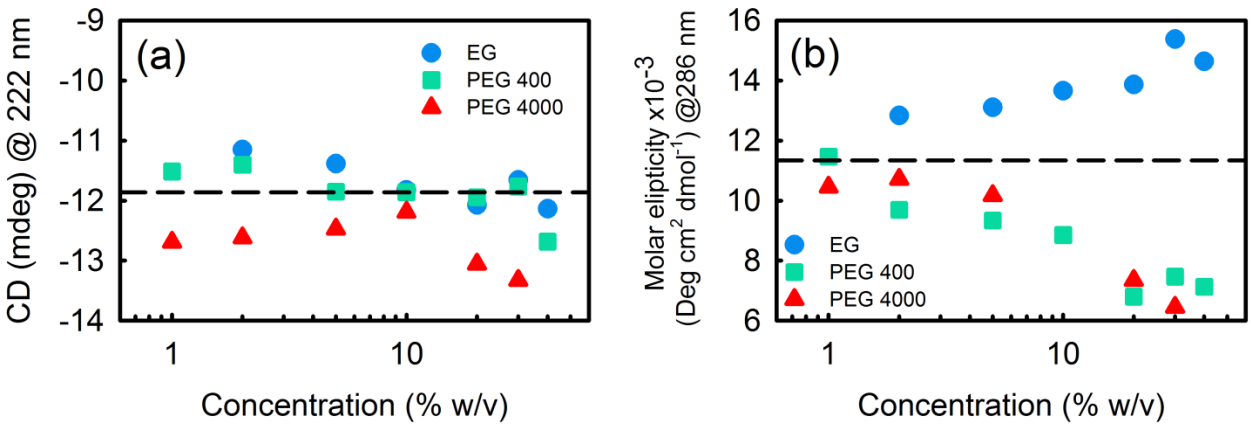

Figure 6.3.3. (a) CD at 222 nm (b) Molar elipticity at 286 nm of Lysozyme (in buffer of pH 7, 20 C) in presence of different concentration of EG, PEG 400 and PEG 4000.

The near UV CD region (250-300 nm) is the 'fingerprint' domain to determine protein's tertiary structure.[38] The CD peaks in this region are associated with the aromatic residues, usually, phenylalanine (254, 256,262, 267 nm), tyrosine (276, 283 nm), tryptophan (280-295 nm) disulfide bonds.[39] The band observed near 292 nm (figure 6.3.2) is due to *Trp108* which provides with direct insight into the active site of lysozyme.[40] Figure 6.3.2 shows that as EG, PEGs are introduced into the lysozyme solution the overall spectral features do not change abruptly compared to that in the buffer solution. This indicates that the global tertiary structure of the lysozyme remains almost intact in presence of the cosolutes at least in the studied concentration range. We measure the molar ellipticity of the enzyme and plot it as a function of cosolutes concentration (figure 6.3.3b). We found that while in EG the molar ellipticity increases in the PEGs it decreases gradually. This indicates that EG acts as a stabilizer whereas PEGs marginally destabilize the tertiary structure of the protein.

CD measurements thus affirm that the structure of the enzyme is not abruptly perturbed within the studied PEG concentration region; however, there occurs a definite

modification in the conformation and or flexibility/rigidity of lysozyme that could in its turn affect the enzyme activity. It is however difficult to specifically correlate this modification in structure with the enzyme activity.

Intrinsic Fluorescence Measurement to Probe Local Environment

HEWL contains six intrinsic Trp residues among which Trp62, Trp63 and Trp108 are present in the active site to bind the substrate while Trp28, Trp111 are present in the hydrophobic core therefore being less solvent sensitive. Trp123 is mostly exposed to the solvent. Almost 80% fluorescence of lysozyme is due to the Trp62 and Trp108 residues since the emission of Trp63, Trp111, Trp123 residues are quenched by the nearby disulphide linkages of Cys76-Cys94 and Cys6-Cys127.[41]

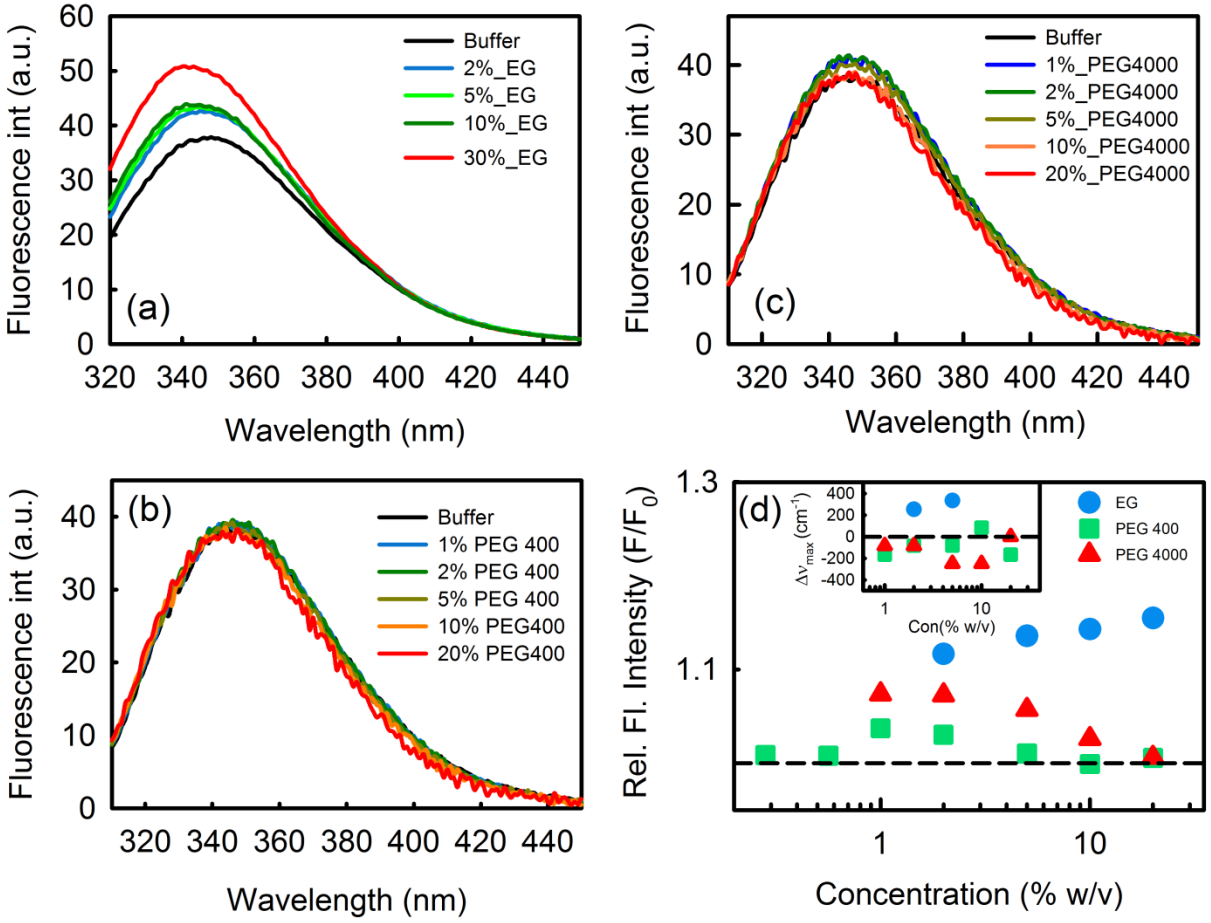

Figure 6.3.4. (a) Fluorescence emission spectra (excited at 299 nm) of HEWL (0.4 µM) in presence of EG, (b) PEG 400 and (c) PEG 4000. (d) Relative fluorescence intensity at 347 nm as a function of concentration of EG, PEG 400 and PEG 4000. (Inset) Change in emission peak ($\Delta\nu_{max}$) with respect to buffer as a function of concentration of EG, PEG 400 and PEG 4000.

As shown in figure 6.3.4(d) the relative fluorescence intensity (F/F_0) increases with increasing concentration of EG whereas a nonlinear trend in the intensity is observed for PEG 400 and 4000 solutions. In a recent study Singh *et al* have explained the fluorescence quenching of Trp-HEWL in presence of Dextran (6, 40, and 70), Ficoll 70, and PEG 8000.[42] On the basis of the *excluded volume effect* that modifies the protein to be conformationally more compact in a way that the neighbouring amino acids gets in close vicinity to the Trp residues (mainly Trp62, 108). The authors also reported nominal quenching for PEG 8000 as it exerts lower *excluded volume effect* in comparison to the other crowding agents (dextran, ficoll). In the present study also we have found a marginal increase in the fluorescence intensity upto ~2% (w/v) concentration of PEG 400 and 4000 and then it decreases with increasing concentration. The observation can be explained in the manner that shorter chain PEGs exerts relatively lower excluded volume effect. In PEG solution several counter interacting effects coexist i) excluded volume effect ii) nonspecific interaction with protein and iii) lowering of the local solvent polarity or dielectric constant as experienced by the probe. The latter two factors are likely to increase the fluorescence intensity.[22] In the low concentration region the lowering of solvent polarity factor acts predominantly whereas at higher concentrations the excluded volume effect overwhelms. For the EG the excluded volume effect is minimal and consequently we observe increase in the fluorescence intensity (figure 6.3.4d). This result corroborates the near UV-CD study (figure 6.3.3) where we have found contrasting spectral change in EG and PEGs.

Thermal Stability of Lysozyme

Study of the thermal denaturation process of a protein is reliant on the structural conformation and interaction of the protein with cosolutes.[43, 44] Mann et al. have reported that lysozyme activity gets enhanced significantly in presence of ethanolammonium formate (EtAF) which induces with thermal stability of the protein.[39] We measure temperature dependent (20-90 ^{0}C) fluorescence spectra of lysozyme in absence and in presence of the cosolutes. From the first derivative plot of the change in intensity (at 350 nm) we obtain unfolding temperature T_u (figure 6.3.5). The value in buffer solution (table 6.3.4) is in good agreement with the previous literature.[45]

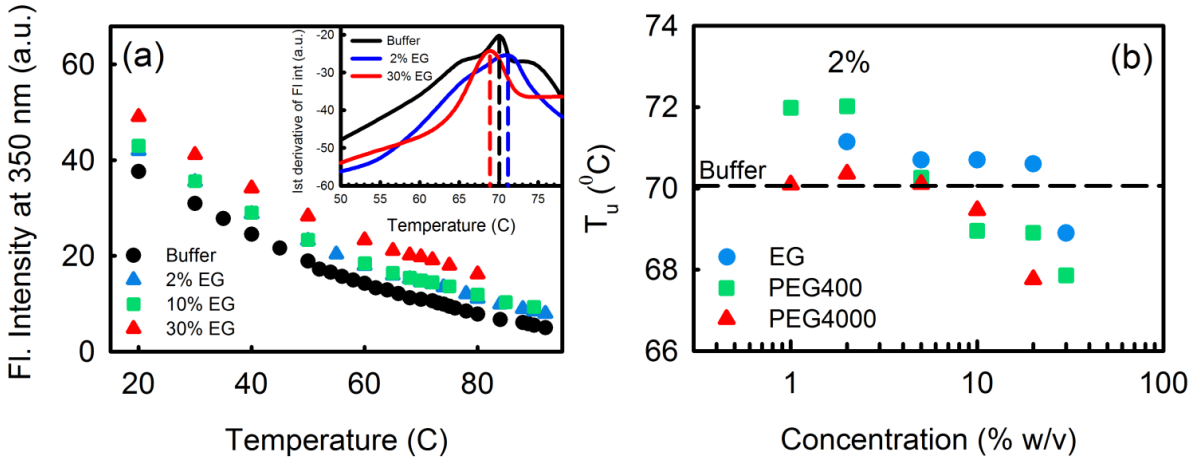

Figure 6.3.5. (a) Representative plot for fluorescence intensity of lysozyme at 350 nm (excited at 299 nm) as a function of temperature in presence of different EG solutions. Inset shows first derivative plot.

We observe a noticeable increase in T_u upto ~2% (w/v) concentrations in all the cosolutes followed by a drop in T_u (figure 6.3.5). Such nonlinear bell shaped trend in T_u in lysozyme and ribonuclease A has previously been reported in presence of betaine [46]. The observed result can be rationalized on the basis of a trade-off between preferential hydration and preferential binding, and an optimization between the associated enthalpy and entropy changes. EG, PEG 400, PEG 4000 can act as both H-bond donor as well as acceptor to both protein and water due to the presence of –OH group and ethereal oxygen (-O-). On the other hand their hydrcarbon moiety can interact with the hydrophobic residues of the protein. At lower concentration PEGs render modest thermal stability to lysozyme following the excluded volume effect while at higher concentration the PEGs might offer favourable preferential interaction with the unfolded form of the protein and thereby decreasing the Tu.[44] The excluded volume effect diminishes as the hydrophobic side chains of protein get exposed upon unfolding and interact favourably with the hydrophobic part of the polymer rather than water interaction. The trend in T_u extracted from the active site emission mostly corroborates well with the change in enzyme activityas shown in the previous section.

For a better insight we consider a two state denaturation process of the protein according to the following equilibrium,

$N \rightleftarrows D$ where N and D stands for native and denatured state of protein respectively. The equilibrium constant (K) of the process is related to the native fraction (f_N) by the following equation,

$$K = \frac{f_D}{f_N} = \frac{1-f_N}{f_N} \tag{6.2}$$

$$f_N = \frac{F_T - F_D}{F_N - F_D} \tag{6.3}$$

where F_T, F_N and F_D represent the fluorescence intensity at temperature T, in native state and complete denaturation state, respectively. The Gibbs free energy change for the unfolding process is given by, $\Delta G_u = -RTlnK$, where R is the gas constant.

The vant Hoff enthalpy change (ΔH) for the process is obtained from the following equation,

$$\frac{\partial(\Delta G_u/T)}{\partial(1/T)} = \Delta H \tag{6.4}$$

The corresponding entropy change (ΔS) is obtained as,

$$\Delta G_u = \Delta H - T\Delta S \tag{6.5}$$

Vant Hoff enthalpy is often obtained from calorimetric measurement which reckons the global unfolding of the protein.[21, 47]

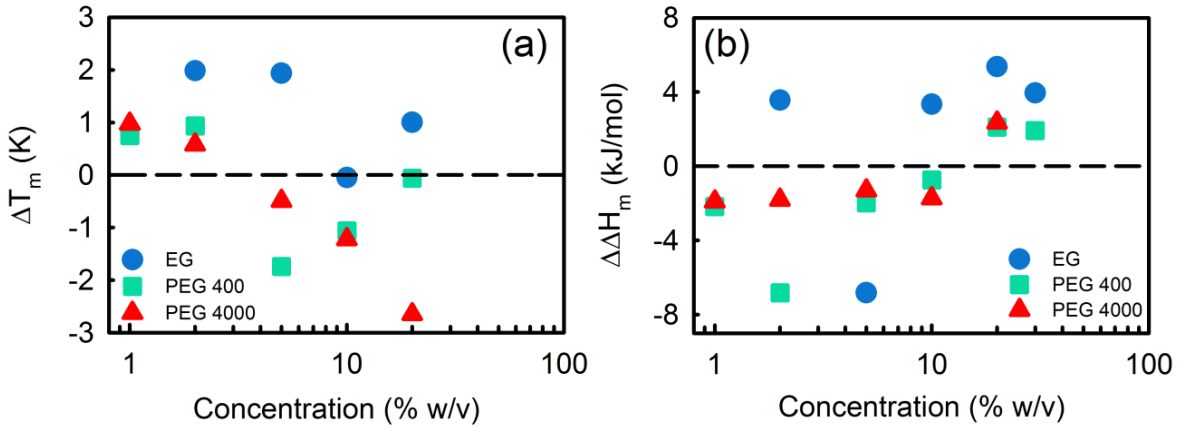

Figure 6.3.6. (a) ΔT_m and (b) ΔH_m, (as defined in the text) as a function of EG, PEG 400 and PEG 4000 concentration during thermal unfolding of HEWL. Dashed line represents for buffer.

The calculated van't Hoff enthalpy change (ΔH) for the unfolding process (at T_m where ΔG_u is zero) are shown in figure 6.3.6 for different concentration of EG and PEGs. We observe a lowering of ΔH in the lower concentration region while increase at higher concentration of the cosolutes. During thermal denaturation of protein in buffer solution we find positive value of 61.63±3 kJ/mol which is quite expected as the H-bonds between amino acids (besides the other weak interaction) break we would expect a positive value of ΔH. Now while

introducing the cosolutes we observe (figure 6.3.6) a less positive value of ΔH than that in buffer (i.e., ΔΔH <0, $\Delta\Delta H = \Delta H_{solution} - \Delta H_{buffer}$) This indicates that less number of intra H-bonds breaking occurs due to the cosolute effect. In the low concentration region *preferential hydration* dominates over *preferential binding*, as a consequence there is a very little contribution in enthalpy due to the formation of protein-cosolute inter H-bonds. For the higher concentration regime of the cosolutes the scenario becomes just opposite. Then the protein's intra H-bonds breaking occurs more on account of the *preferential binding* of the cosolutes with the protein. As a result, ΔΔH becomes positive with respect to buffer. Simon et al. group previously found such positive value of ΔΔH (with lowering of T_m) in 10-20% PEG solution for the ubiquitin protein.[13]

Energetics for the Enzyme Catalysis Reaction

The conventional *lock and key model* of enzyme catalysis has been modified by an *induced-fit model* which suggests that the enzyme (*E*) is putatively not rigid; rather it can adapt its structure to fit the substrate (*S*). When the substrate binds, the energy of binding causes the enzyme to alter its conformation to form catalytically competent state ($ES^{\#}$). The dissociation constant (K_d) of the complex *ES*, can be equated to the K_M. The corresponding free energy change can be written as[48]

$$\Delta G_M = -RTln(1/K_d) \approx RTlnK_M \qquad (6.6)$$

ΔG_M relates to the '*entrance channel*', which controls the access of substrate and solvent towards the active site of enzyme[49] as *E* and *S* react to form the *ES* complex. For the favorable interaction of *E* and *S*, the value of ΔG_M becomes negative. *ES* then reaches $ES^{\#}$ at the expense of a free energy change $\Delta G^{\#}$ given as,

$$\Delta G^{\#} = -RTln(\frac{h}{k_B T} k_{cat}) \qquad (6.7)$$

where k_B is the Boltzman constant and *h* is the plank constant. The formation of $ES^{\#}$ indicates an "exit channel", which controls the release pathway of unreacted substrate and product formed after the reaction, as $ES^{\#}$ is cleaved to form the products. The net free energy change for the formation of $ES^{\#}$ is given by,

$$\Delta G_t^{\#} = -RTln(\frac{h}{k_B T}\frac{k_{cat}}{K_M}) \qquad (6.8)$$

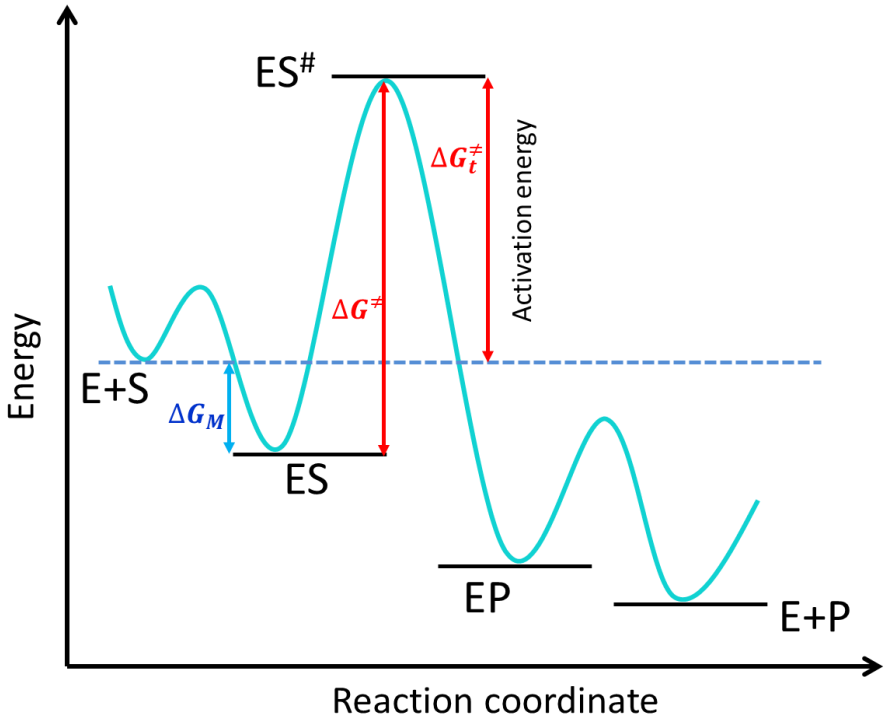

Scheme 6.2: Representative plot showing free energy change of lysozyme (Enzyme, E)-substrate (S) reaction.

We notice that in EG, ΔG_M becomes more negative upto 2% (w/v) concentration beyond which it increases indicating disfavoured with respect to buffer (figure 6.3.7).

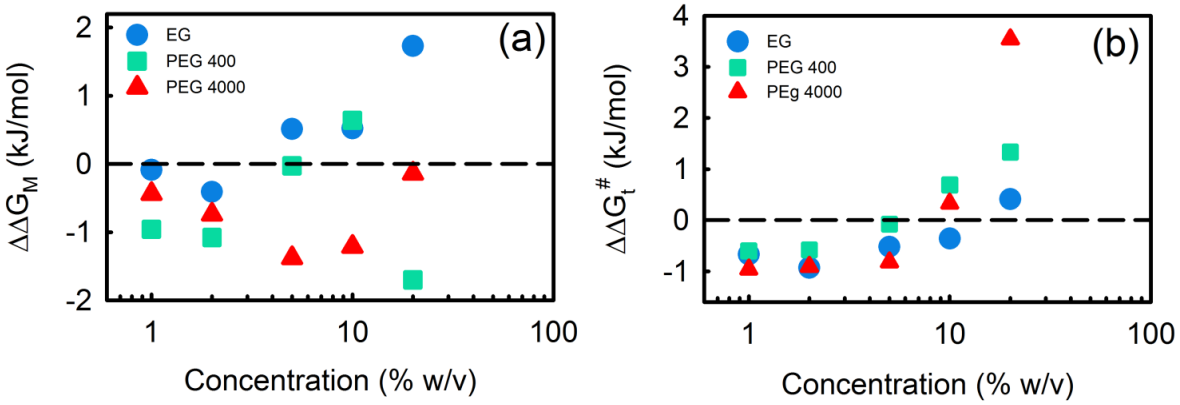

Figure 6.3.7. (a) $\Delta\Delta G_M = \Delta G_M^{solution} - \Delta G_M^{buffer}$ (as defined in text) (b) $\Delta\Delta G_t^{\#}$ as a function of cosolutes concentration.

This signifies that the entrance channel (ES complex formation) is favoured in dilute concentration region while it is disfavoured at higher concentration. The exit channel is quantified by the value of $\Delta G^{\neq}$ (eq^n 6.7) and feasibility of the overall reaction is governed by

the difference in the energy ($\Delta G_t^{\neq}$) which is equivalent to the activation energy. For higher concentration of the PEGs exit channel is disfavored (more positive value of $\Delta G^{\neq}$) as discussed in the previous section may be due to growing *preferential binding.* The net activation energy change ($\Delta\Delta G_t^{\neq}$) with respect to that in buffer decrease upto ~2% concentration and beyond that it increases for all the three cosolutes (figure 6.3.7b).

Table 6.3.1: Catalytic parameters of lysozyme in buffer, EG, PEG 400 and PEG 4000 at pH 7.

% w/v	K_M (mg Lt^{-1})	$k_{cat} \times 10^{-7}$ (mg Lt^{-1} s^{-1}M^{-1})	$k_{cat}/K_M \times 10^{-5}$ (s^{-1}M^{-1})
0	80.88±10	1.03±0.1	1.27±0.2
EG			
1	77.91±11	1.30±0.2	1.67±0.3
2	68.45±11	1.27±0.2	1.86±0.4
5	99.52±5	1.56±0.1	1.57±0.1
10	99.89±7	1.47±0.1	1.47±0.1
20	163.40±70	1.76±0.8	1.08±0.7
PEG 400			
1	54.75±6	0.89±0.1	1.62±0.3
2	52.14±3	0.84±0.1	1.62±0.1
5	79.80±6	1.05±0.1	1.31±0.2
10	104.94±33	1.01±0.3	1.00±0.4
20	40.52±8	0.30±0.1	0.74±0.1
PEG 4000			
1	67.49±6	1.27±0.1	1.88±0.2
2	59.83±4	1.10±0.1	1.98±0.2
5	46.20±2	0.82±0.1	1.77±0.1
10	49.39±14	0.55±0.1	1.11±0.4
20	76.34±10	0.23±0.1	0.31± 0.1

Table 6.3.2: Secondary structure content of HEWL in EG, PEG 400 and PEG 4000 solutions in buffer (pH 7) at 20 C as obtained by CDNN software.

% w/v	α-Helix (%)	Antiparallel β sheet (%)	Parallel β sheet (%)	β-Turn (%)	Random Coil (%)
0	32.11	9.71	8.90	18.00	31.29
EG					
2	29.94	10.08	9.38	18.04	32.66
5	30.60	10.03	9.22	18.03	32.22
10	29.33	13.71	8.97	18.15	29.74
20	32.55	9.62	8.80	17.91	31.22
30	31.98	9.67	8.96	17.92	31.57
PEG 400					
1	31.07	9.85	9.04	17.97	31.98
2	31.03	9.97	9.05	18.11	31.84
5	31.40	9.89	8.97	18.04	31.70
10	33.23	9.44	8.62	17.85	30.77
20	36.29	7.46	8.37	16.53	31.45
PEG 4000					
1	35.41	7.55	8.55	16.60	31.99
2	34.94	7.63	8.63	16.57	32.13
5	34.84	7.63	8.63	16.57	32.23
20	35.61	7.55	8.45	16.50	31.89

Table 6.3.3: Calculated hydrodynamic diameter of the PEGs.

Macromolecules	Hydrodynamic diameter (nm)
PEG 400	~ 0.9
PEG 4000	~ 3.3

Hydrodynamic diameter (d_H) of PEGs of different molecular mass are calculated from their molecular masses using the following equation:

[Ref: Asymptotic Behavior and Long-Range Interactions in Aqueous Solutions of Poly(ethy1ene oxide), Macromolecules 1991,24, 5943-5947]

$$d_H = 2 \times 0.145 \times M_w^{0.571 \pm 0.009} \text{Å}$$

Table 6.3.4: Thermal denaturation temperature (T_u) of lysozyme in buffer, EG, PEG 400 and PEG 4000 solutions.

% w/v	EG	PEG 400	PEG 4000
0	70.06	70.06	70.06
1	-	71.98	70.09
2	71.17	72.02	70.36
5	70.7	70.26	70.11
10	70.75	68.96	69.46
20	70.6	68.91	67.76
30	68.9	67.86	-

Table 6.3.5: Thermodynamic parameters obtained from temperature dependent fluorescence study.

[Cosolutes] (%) w/v	**At T_m**	
	ΔH_m (kJ mol^{-1})	**ΔS_m (kJ mol^{-1}K^{-1})**
0	61.63±3	0.19±0.01
EG		
2	62.79±2	0.20±0.01
5	52.41±2	0.16±0.01
10	62.57±3	0.197±0.01
20	64.59±3	0.20±0.01
30	63.18±3	0.20±0.01
PEG 400		
1	59.45±2	0.19±0.01
2	54.80±4	0.17±0.01
5	59.65±3	0.19±0.01
10	60.87±1	0.19±0.01
20	63.74±3	0.20±0.01
PEG 4000		
1	59.72±3	0.19±0.01
2	59.82±2	0.19±0.01
5	60.32±2	0.19±0.01
10	59.90±1	0.19±0.01
20	63.97±3	0.20±0.01

Table 6.3.6: Energetics for the Enzyme Catalysis Reaction

	ΔG_M (kJ/mol)	$\Delta G^{\neq}$ (kJ/mol)	$\Delta G_t^{\neq}$ (kJ/mol)
Buffer	-6.19	83.73	77.55
EG			
1	-6.28	83.16	76.88
2	-6.60	83.22	76.62
5	-5.68	82.71	77.03
10	-5.67	82.86	77.19
20	-4.46	82.42	77.96
PEG 400			
1	-7.15	84.09	76.95
2	-7.27	84.24	76.97
5	-6.22	83.69	77.47
10	-5.55	83.78	78.24
20	-7.89	86.77	78.88
PEG 4000			
1	-6.63	83.22	76.59
2	-6.93	83.57	76.64
5	-7.57	84.30	76.73
10	-7.40	85.28	77.88
20	-6.33	87.42	81.09

6.4. Summary

Enzyme activity in general depends upon several factors e.g., structure and conformation of the enzyme, local environment (*viz.* dielectric constant, ionic strength, viscosity of the medium) at the active site, and water activity. Our study elucidates an initial enhancement in activity which then decreases with the increase in cosolute concentration. The change can be rationalized on account of the following considerations:

Firstly, the electrostatic interaction between the positively charged lysozyme (at pH ~7) and the oppositely charged M.Lys cell wall vary inversely with the dielctric constant (ε) of the solution. As water is replaced by lower dielectric material (EG, PEGs)[50, 51], attractive interaction between lysozyme and the substrate increases, thus favouring the entrance channel. With increasing concentration of the cosolutes, due to the growing viscosity[52-54], the diffusion motion of both the enzyme and the substrate eventually gets retarded. As a

consequence the encounter rate between enzyme-substrate decreases and perhaps enacts to decrease the enzyme activity at higher concentration of the cosolutes.

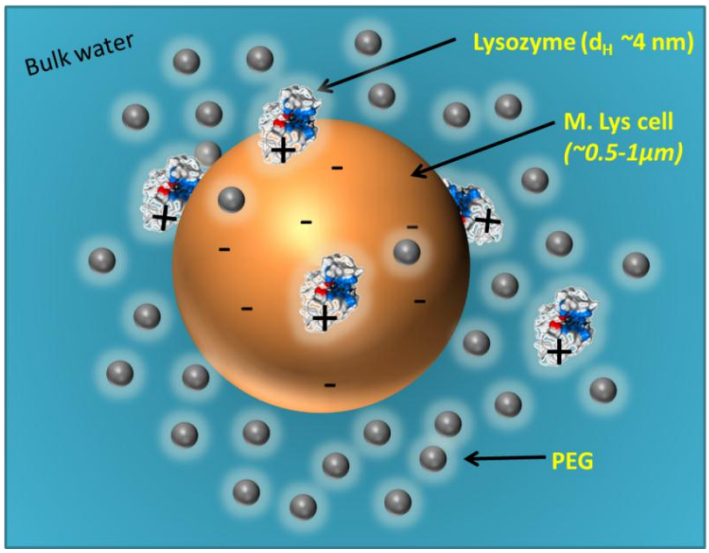

Scheme 6.3: Representation for lysozyme-substrate (Micrococcus lysodeikticus, M. Lys. cell) interaction in PEG solution.

In accordance with the results obtained by Wijaya et al.[45] the enhanced activity can also be explained in terms of favorable interaction of hydroxyl group (-OH) of EG and PEGs with lysozyme in dilute concentration regime. Also the study by Mann et al reported that lysozyme activity gets prominently enhanced in ethanolammonium formate (EtAF), which contain –OH group and also interestingly EtAF provides thermal stability to lysozyme.[39] This result corroborates our understanding that cosolutes dependent thermal stability of the enzyme is correlated with its activity trend. The decrease in activity at higher concentration of cosolutes is quite expected as obtained by previous studies and this can be explained by excluded volume effect or decrease in water activity or may be due to the lowering of enzyme substrate encounter rate in presence of higher number of EG and PEGs.

6.5. References

1. Fulton, A. B. (1982) How crowded is the cytoplasm?, *Cell 30*, 345-347.
2. Zimmerman, S. B., and Trach, S. O. (1991) Estimation of macromolecule concentrations and excluded volume effects for the cytoplasm of Escherichia coli, *Journal of molecular biology 222*, 599-620.
3. Stagg, L., Zhang, S.-Q., Cheung, M. S., and Wittung-Stafshede, P. (2007) Molecular crowding enhances native structure and stability of α/β protein flavodoxin, *Proceedings of the National Academy of Sciences 104*, 18976-18981.
4. Perham, M., Stagg, L., and Wittung-Stafshede, P. (2007) Macromolecular crowding increases structural content of folded proteins, *FEBS letters 581*, 5065-5069.
5. Ellis, R. J. (2001) Macromolecular crowding: obvious but underappreciated, *Trends in Biochemical Sciences 26*, 597-604.
6. Verma, P. K., Kundu, A., Ha, J.-H., and Cho, M. (2016) Water Dynamics in Cytoplasm-Like Crowded Environment Correlates with the Conformational Transition of the Macromolecular Crowder, *Journal of the American Chemical Society 138*, 16081-16088.
7. Minton, A. P., and Wilf, J. (1981) Effect of macromolecular crowding upon the structure and function of an enzyme: glyceraldehyde-3-phosphate dehydrogenase, *Biochemistry 20*, 4821-4826.
8. Minton, A. P. (2005) Models for Excluded Volume Interaction between an Unfolded Protein and Rigid Macromolecular Cosolutes: Macromolecular Crowding and Protein Stability Revisited, *Biophysical Journal 88*, 971-985.
9. Hermans, J. (1982) Excluded-volume theory of polymer–protein interactions based on polymer chain statistics, *The Journal of Chemical Physics 77*, 2193-2203.
10. Zhou, H.-X., Rivas, G., and Minton, A. P. (2008) Macromolecular crowding and confinement: biochemical, biophysical, and potential physiological consequences, *Annu. Rev. Biophys. 37*, 375-397.
11. Kuznetsova, I. M., Zaslavsky, B. Y., Breydo, L., Turoverov, K. K., and Uversky, V. N. (2015) Beyond the excluded volume effects: mechanistic complexity of the crowded milieu, *Molecules 20*, 1377-1409.
12. Sukenik, S., Sapir, L., and Harries, D. (2013) Balance of enthalpy and entropy in depletion forces, *Current opinion in colloid & interface science 18*, 495-501.
13. Senske, M., Törk, L., Born, B., Havenith, M., Herrmann, C., and Ebbinghaus, S. (2014) Protein stabilization by macromolecular crowding through enthalpy rather than entropy, *Journal of the American Chemical Society 136*, 9036-9041.
14. Gnutt, D., Gao, M., Brylski, O., Heyden, M., and Ebbinghaus, S. (2015) Excluded-Volume Effects in Living Cells, *Angewandte Chemie International Edition 54*, 2548-2551.
15. Laurent, T. C. (1971) Enzyme reactions in polymer media, *European Journal of Biochemistry 21*, 498-506.
16. Totani, K., Ihara, Y., Matsuo, I., and Ito, Y. (2008) Effects of Macromolecular Crowding on Glycoprotein Processing Enzymes, *Journal of the American Chemical Society 130*, 2101-2107.

17. Attri, P., Venkatesu, P., and Lee, M.-J. (2010) Influence of Osmolytes and Denaturants on the Structure and Enzyme Activity of α-Chymotrypsin, *The Journal of Physical Chemistry B 114*, 1471-1478.
18. Verma, P. K., Rakshit, S., Mitra, R. K., and Pal, S. K. (2011) Role of hydration on the functionality of a proteolytic enzyme α-chymotrypsin under crowded environment, *Biochimie 93*, 1424-1433.
19. Shahid, S., Ahmad, F., Hassan, M. I., and Islam, A. (2015) Relationship between protein stability and functional activity in the presence of macromolecular crowding agents alone and in mixture: An insight into stability-activity trade-off, *Archives of biochemistry and biophysics 584*, 42-50.
20. Stojanovski, B. M., Breydo, L., Uversky, V. N., and Ferreira, G. C. (2016) Macromolecular crowders and osmolytes modulate the structural and catalytic properties of alkaline molten globular 5-aminolevulinate synthase, *RSC Advances 6*, 114541-114552.
21. Samanta, N., Mahanta, D. D., Hazra, S., Kumar, G. S., and Mitra, R. K. (2014) Short chain polyethylene glycols unusually assist thermal unfolding of human serum albumin, *Biochimie 104*, 81-89.
22. Samanta, N., Luong, T. Q., Mahanta, D. D., Mitra, R. K., and Havenith, M. (2016) Effect of Short Chain Polyethyleneglycols on the Hydration Structure and Dynamics around Human Serum Albumin, *Langmuir 32*, 831–837.
23. Jollès, P. (1969) Lysozymes: A Chapter of Molecular Biology, *Angewandte Chemie International Edition in English 8*, 227-239.
24. Blake, C., Koenig, D., Mair, G., North, A., Phillips, D., and Sarma, V. (1965) Structure of hen egg-white lysozyme: a three-dimensional Fourier synthesis at 2 Å resolution, *Nature 206*, 757-761.
25. Gorin, G., Wang, S.-F., and Papapavlou, L. (1971) Assay of lysozyme by its lytic action on M. lysodeikticus cells, *Analytical biochemistry 39*, 113-127.
26. Davies, R., Neuberger, A., and Wilson, B. (1969) The dependence of lysozyme activity on pH and ionic strength, *Biochimica et Biophysica Acta-Enzymology 178*, 294-305.
27. Vocadlo, D. J., Davies, G. J., Laine, R., and Withers, S. G. (2001) Catalysis by hen egg-white lysozyme proceeds via a covalent intermediate, *Nature 412*, 835-838.
28. Malzert, A., Boury, F., Renard, D., Robert, P., Lavenant, L., Benoıt, J., and Proust, J. (2003) Spectroscopic studies on poly (ethylene glycol)–lysozyme interactions, *International journal of pharmaceutics 260*, 175-186.
29. Canfield, R. E. (1963) The Amino Acid Sequence of Egg White Lysozyme, *Journal of Biological Chemistry 238*, 2698-2707.
30. Davies, R. C., Neuberger, A., and Wilson, B. M. (1969) The dependence of lysozyme activity on pH and ionic strength, *Biochimica et Biophysica Acta (BBA) - Enzymology 178*, 294-305.
31. Patra, A., Samanta, N., Das, D. K., and Mitra, R. K. (2017) Enhanced Catalytic Activity of α-Chymotrypsin in Cationic Surfactant Solutions: The Component Specificity Revisited, *The Journal of Physical Chemistry B 121*, 1457-1465.
32. Pancera, S., Petri, D., and Itri, R. (2004) The effect of poly (ethylene glycol) on the activity, structural conformation and stability of yeast hexokinase, *Surface and Colloid Science*, 301-334.
33. Pancera, S. M., da Silva, L. H., Loh, W., Itri, R., Pessoa, A., and Petri, D. F. (2002) The effect of poly (ethylene glycol) on the activity and structure of glucose-6-phosphate dehydrogenase in solution, *Colloids and Surfaces B: Biointerfaces 26*, 291-300.

34. Berg, J. M., Tymoczko, J. L., and Stryer, L. (2002) *Biochemistry*, W.H. Freeman & Company, New York.
35. Knubovets, T., Osterhout, J. J., Connolly, P. J., and Klibanov, A. M. (1999) Structure, thermostability, and conformational flexibility of hen egg-white lysozyme dissolved in glycerol, *Proceedings of the National Academy of Sciences 96*, 1262-1267.
36. Chen, C., Loe, F., Blocki, A., Peng, Y., and Raghunath, M. (2011) Applying macromolecular crowding to enhance extracellular matrix deposition and its remodeling in vitro for tissue engineering and cell-based therapies, *Advanced Drug Delivery Reviews 63*, 277-290.
37. Kuznetsova, I. M., Turoverov, K. K., and Uversky, V. N. (2014) What macromolecular crowding can do to a protein, *International journal of molecular sciences 15*, 23090-23140.
38. Havel, H. A. (1996) *Spectroscopic methods for determining protein structure in solution*, VCH, New York.
39. Mann, J. P., McCluskey, A., and Atkin, R. (2009) Activity and thermal stability of lysozyme in alkylammonium formate ionic liquids—Influence of cation modification, *Green Chemistry 11*, 785-792.
40. Fasman, G. D. (1996) *Circular dichroism and the conformational analysis of biomolecules*, Springer, New York.
41. Kuznetsova, I. M., Biktashev, A. G., Lubov'N, M., and Bushmarina, N. A. (2000) UNDERSTANDING THE CONTRIBUTION OF INDIVIDUAL TRYPTOPHAN RESIDUES TO INTRINSIC LYSOZYME, *Protein & Peptide Letters 7*, 411-420.
42. Singh, P., and Chowdhury, P. K. (2017) Unravelling the Intricacy of the Crowded Environment Through Tryptophan Quenching in Lysozyme, *The Journal of Physical Chemistry B*.
43. Lee, L. L., and Lee, J. C. (1987) Thermal stability of proteins in the presence of poly (ethylene glycols), *Biochemistry 26*, 7813-7819.
44. Zielenkiewicz, W., Swierzewski, R., Attanasio, F., and Rialdi, G. (2006) Thermochemical, volumetric and spectroscopic properties of lysozyme–poly (ethylene) glycol system, *Journal of thermal analysis and calorimetry 83*, 587-595.
45. Wijaya, E. C., Separovic, F., Drummond, C. J., and Greaves, T. L. (2016) Activity and conformation of lysozyme in molecular solvents, protic ionic liquids (PILs) and salt–water systems, *Physical Chemistry Chemical Physics 18*, 25926-25936.
46. Santoro, M. M., Liu, Y., Khan, S. M., Hou, L. X., and Bolen, D. (1992) Increased thermal stability of proteins in the presence of naturally occurring osmolytes, *Biochemistry 31*, 5278-5283.
47. Zielenkiewicz, W., Swierzewski, R., Attanasio, F., and Rialdi, G. (2006) Thermochemical,volumetric and spectroscopic properties of lysozyme–poly(ethylene) glycolsystem, *Journal of Thermal Analysis and Calorimetry 83*, 587-595.
48. Fersht, A. (1974) Catalysis, binding and enzyme-substrate complementarity, *Proceedings of the Royal Society of London B: Biological Sciences 187*, 397-407.
49. Gora, A., Brezovsky, J., and Damborsky, J. (2013) Gates of Enzymes, *Chem. Rev. 113*, 5871-5923.
50. Shinyashiki, N., Sudo, S., Abe, W., and Yagihara, S. (1998) Shape of dielectric relaxation curves of ethylene glycol oligomer–water mixtures, *The Journal of chemical physics 109*, 9843-9847.
51. Mali, C., Chavan, S., Kanse, K., Kumbharkhane, A., and Mehrotra, S. (2007) Dielectric relaxation of poly ethylene glycol-water mixtures using time domain technique, *Indian Journal of Pure & Applied Physics 45*, 476-481.

52. Jerome, F. S., Tseng, J. T., and Fan, L. T. (1968) Viscosities of aqueous glycol solutions, *Journal of Chemical & Engineering Data 13*, 496-496.
53. Han, F., Zhang, J., Chen, G., and Wei, X. (2008) Density, viscosity, and excess properties for aqueous poly (ethylene glycol) solutions from (298.15 to 323.15) K, *Journal of Chemical & Engineering Data 53*, 2598-2601.
54. Silva, R. M. M., Minim, L. A., Coimbra, J. S. R., Rojas, E. E. G., da Silva, L. H. M., and Minim, V. P. R. (2007) Density, Electrical Conductivity, Kinematic Viscosity, and Refractive Index of Binary Mixtures Containing Poly(ethylene glycol) 4000, Lithium Sulfate, and Water at Different Temperatures, *Journal of Chemical & Engineering Data 52*, 1567-1570.

Chapter 7

7. Summary and Future Perspective

7.I. Summary

In the present thesis we have investigated the effects of crowding agents on protein structure, thermal stability and hydration dynamics. We have studied human serum albumin (HSA) as a model globular protein in presence of some synthetic polymers (PEGs of different chain length) which serve to mimic the crowded cellular environments. The secondary and tertiary structures of proteins have been detected by CD spectroscopy. Thermal stability of the protein has been studied by temperature dependent CD and DSC measurements. Both spectroscopic and thermodynamic studies reveal an unusual thermal stability of HSA in presence of short chain PEG 200 and 400. We find an unusual behaviour in the hydration of the protein which cannot be explained only by considering so called the *excluded volume theory* rather one has to consider some weak attractive interactions between the protein and the PEGs. The results show the dual characters (osmolytic effect as well as soft interactions) of the PEGs. We have studied the hydration of the protein from short range (by DLS and densimetry) to long range (by far IR-FTIR and THz spectroscopy) in presence of the PEGs. The measurements affirm a noticeable interaction between protein and short chain PEG hydration beyond a critical concentration (~30% w/v).

Our next study aims to understand the process of protein stabilization and denaturation by different cosolutes. We have tried to address a debatable issue whether protein denaturation (or stabilization) occurs due to the modification of water network by using some well-known denaturing agents (urea, GdmCl) and osmolytes (sucrose, TMAO, amino acids). Our finding using terahertz (THz) spectroscopy reveals an interesting correlation between protein stabilization or denaturation with the modification in collective hydrogen bond dynamics of water.

Finally, we check the activity of a protein in presence of cosolutes. We have studied the enzyme activity of a model protein lysozyme on bacteria (M. Lys.) cell wall in presence of PEG 400 and 4000. We have also studied the same in ethylene glycol to understand the monomeric effect. We have found an unusual enhancement of activity in very dilute concentration region of cosolutes whereas activity decreases at higher concentration region. We take into consideration various factors to address the activity trend and found a plausible mechanism.

In a nutshell, this thesis reveals detailed investigation of water soluble globular protein structure, conformation, hydration and activity in presence of different types of cosolutes (e.g. macromolecules, osmolytes, chemical denaturants) at physiological condition.

7.II. Future Perspective

The basic studies done during my PhD could imprint implications for the study of protein stability, which is crucial to understand some rising neurodegenerative diseases viz. Alzheimer's diseases, Parkinson's disease, Type II diabetes, mad cow disease, transthyretin amyloidosis disease etc.[1, 2] In certain physiological condition the concerning proteins (e.g. amyloid β, tau protein, α-synuclein, prions, transthyretin etc.) form fibrillar aggregation which eventually results in the diseases. For the progress of invention of effective therapeutic agents to prevent these diseases it is essential to study in details the structure, hydration of the related proteins and the process of fibrillar aggregate formation. Macromolecular crowders and osmolytes can modulate the aggregation/fibrillation pathways. Earlier studies have shown that the fibril/aggregate formation rate could be enhanced by crowding agents.[3, 4] There are, however, few studies which report that osmolytes, synthetic polymer could also inhibit the rate of fibrilation of oligomeric proteins in *in vitro* studies.[5]

With this perspective in view we plan to study the fibril formation of protein in crowded environments. How the rate of fibril formation/aggregation is modified by crowding will be studied. We also plan to study the enzyme activity of a native protein in presence of fibrilar proteins and consequently the effect of the crowders on it. We will use circular dichroism (CD), dynamic light scattering, and fluorescence spectroscopy to investigate the structure of the protein. To study the kinetics we would use the stopped flow technique and UV spectrophotometer. We design to study the effect of amyloid fibril on water network structure by using THz spectroscopy. The effect on ps to sub-ps dynamics of water will be measured by dielectric relaxation study. We expect inhibition of fibril formation in presence

of some suitable osmolytes or crowding agents for a specific protein depending upon the interactions.

The experimental scheme has been shown below:

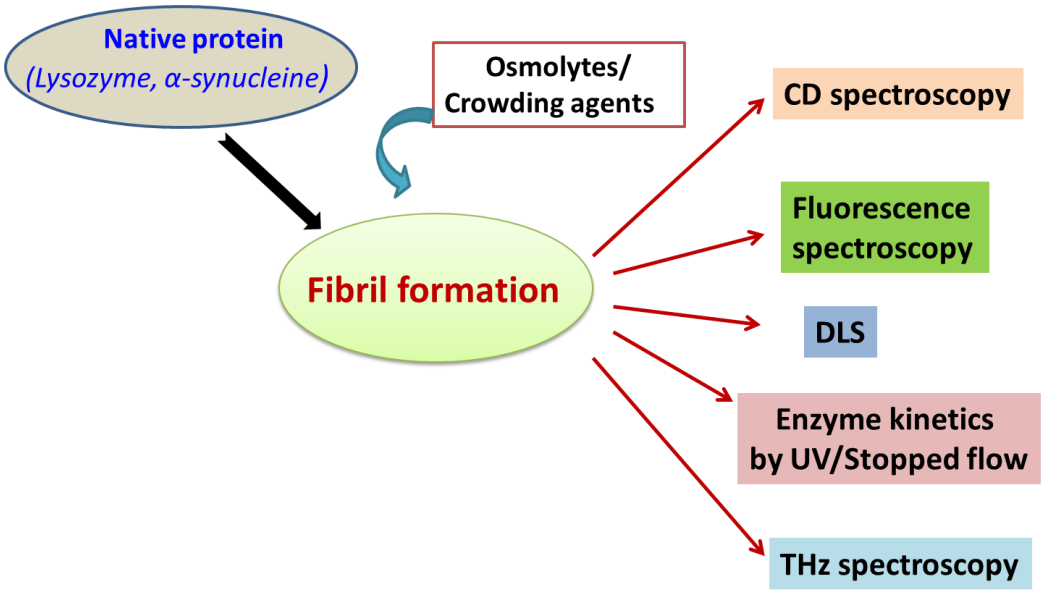

References

1. Uversky, V. N., Oldfield, C. J., Midic, U., Xie, H., Xue, B., Vucetic, S., Iakoucheva, L. M., Obradovic, Z., and Dunker, A. K. (2009) Unfoldomics of human diseases: linking protein intrinsic disorder with diseases, *BMC genomics 10*, S7.
2. Habchi, J., Tompa, P., Longhi, S., and Uversky, V. N. (2014) Introducing protein intrinsic disorder, *Chemical reviews 114*, 6561-6588.
3. Uversky, V. N., M. Cooper, E., Bower, K. S., Li, J., and Fink, A. L. (2002) Accelerated α-synuclein fibrillation in crowded milieu, *FEBS Letters 515*, 99-103.
4. Zhou, Z., Fan, J.-B., Zhu, H.-L., Shewmaker, F., Yan, X., Chen, X., Chen, J., Xiao, G.-F., Guo, L., and Liang, Y. (2009) Crowded cell-like environment accelerates the nucleation step of amyloidogenic protein misfolding, *Journal of Biological Chemistry 284*, 30148-30158.
5. Mittal, S., and Singh, L. R. (2014) Macromolecular crowding decelerates aggregation of a β-rich protein, bovine carbonic anhydrase: a case study, *The Journal of Biochemistry 156*, 273-282.

Appendices

Preparation of buffer of a particular pH

Buffer is termed as an aqueous system that tends to resist changes in pH when small amount of acid or base are added. It can be prepared by mixing aqueous solution of weak acid and its conjugate base.

The acid (*HA*) dissociation equilibrium in water is as follows,

$$HA(aq) + H_2O(aq) \leftrightarrows H_3O^+(aq) + A^-(aq)$$

The dissociation constant (K_a) is related to pH by the Henderson-Hasselbalch Equation given below,

$$pH = pK_a + \log\frac{[A^-(aq)]}{[HA(aq)]}$$

The buffer capacity range is $pK_a \pm 1$ and maximum capacity at pK_a.

In our experiment we have generally used sodium phosphate buffer (pH 7.4) or sometimes called **phosphate buffer saline (PBS)** which is isotonic with physiological fluid. Na_2HPO_4 and NaH_2PO_4 are mixed in a particular ratio to prepare the buffer solution.

Calculation:

$$pH = pK_a + \log\frac{[Na_2HPO_4]}{[NaH_2PO_4]}$$

or, $$\log\frac{[Na_2HPO_4]}{[NaH_2PO_4]} = pH - pK_a = 7.4 - 7.2 = 0.2$$

or, $$\frac{[Na_2HPO_4]}{[NaH_2PO_4]} = 10^{0.2}$$

If we take equimolar mixture (say 50 mM) of both the solution in a total volume 100 ml then we can write the equation in terms of volume,

$$\frac{V_{Na_2HPO_4}}{V_{NaH_2PO_4}} = 10^{0.2}$$

or, $$\frac{V_{Na_2HPO_4}}{100 - V_{Na_2HPO_4}} = 10^{0.2}$$

or, $$V_{Na_2HPO_4} = \frac{100 \times 10^{0.2}}{1 + 10^{0.2}} = 61.34\ ml$$

Therefore, 61.34 ml Na_2HPO_4 (50 mM) and 38.66 ml NaH_2PO_4 (50 mM) are mixed to make 100 ml 50 mM buffer of pH 7.4.

Debye relaxation model fitting in Origin 8.5 software

To fit the frequency (GHz/THz) dependent real and imaginary dielectric constants we have used **nonlinear curve fit** by origin 8.5 software.

Say, we have to fit into double Debye model,

$$\tilde{\varepsilon}(\nu) = \varepsilon_\infty + \frac{\varepsilon_1 - \varepsilon_2}{1 + i2\pi\nu\tau_1} + \frac{\varepsilon_2 - \varepsilon_\infty}{1 + i2\pi\nu\tau_2}$$

Following are the steps:

Step 1: Go to **Tools: Fitting Function Organizer** (or press **F9**)

Step 2: Define a new fitting function, say **DoubleDebye** in new category in the following window and put **Independent variable** as **x**, **dependent variable** as **y1, y2** and **parameters name** as **e, E1, E2, t1, t2** for ε_∞, ε_1, ε_2, τ_1 and τ_2 respectively.

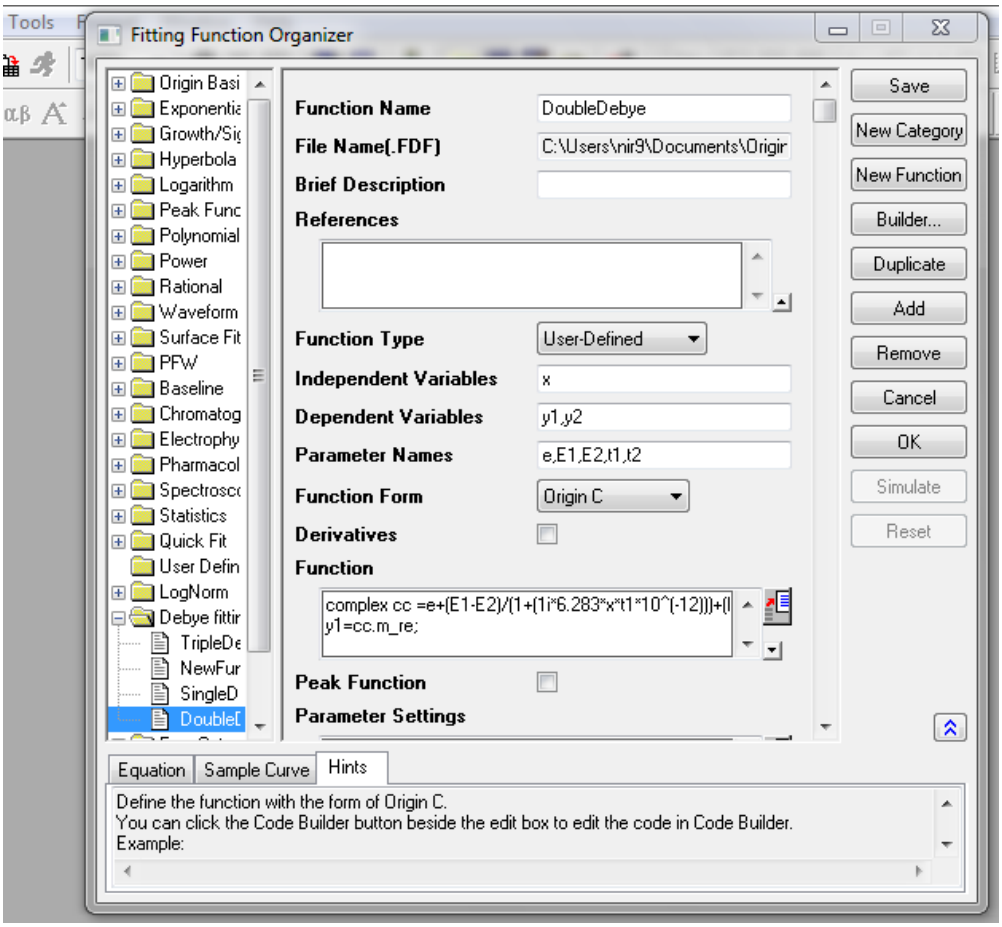

In **Function** put the equation as shown below and then compile:

```
complex cc =e+(E1-E2)/(1+(1i*6.283*x*t1*10^(-12)))+(E2-e)/(1+(1i*6.283*x*t2*10^(-12))) ;
y1=cc.m_re;
y2=-(cc.m_im);
```

Step 3: Save the fitting function named **DoubleDebye.**

Step 4: Now open a new Workbook and import the values of frequencies (X column) and real, imaginary dielectric constant values in two consecutive columns (Y column).

Step 5: Select the three columns and go to **Analysis/Fitting/Nonlinear Curve Fit/Open Dialog..** (or press **Ctrl Y**).

Step 6: Select the fitting function named **DoubleDebye** and put the guess values of the parameters accordingly.

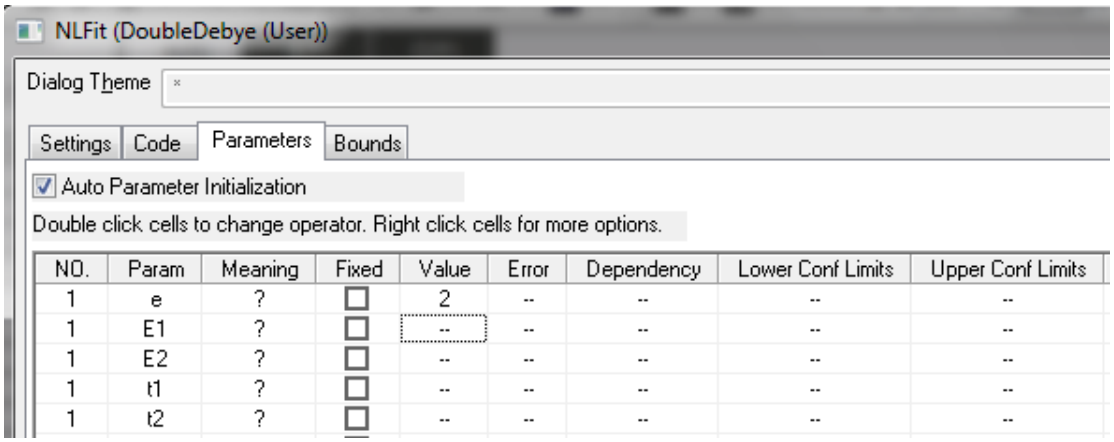

Step 7: Then fit until converged and check the good ness of fitting (adj. R-square ~0.99).

PUBLICATIONS RELATED TO THESIS

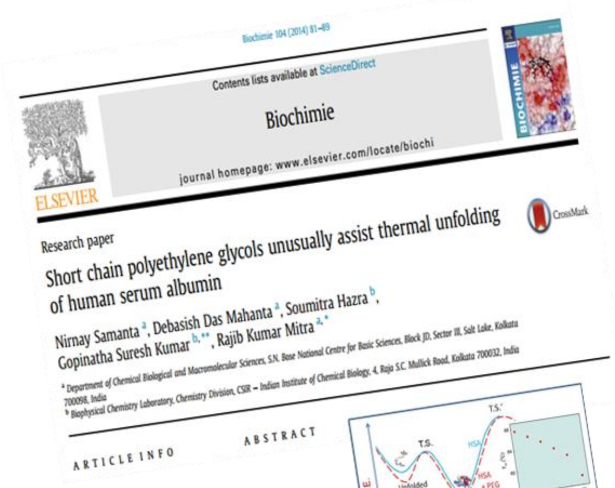
Biochimie 104 (2014) 81–89

Contents lists available at ScienceDirect

Biochimie

journal homepage: www.elsevier.com/locate/biochi

Research paper

Short chain polyethylene glycols unusually assist thermal unfolding of human serum albumin

Nirnay Samanta [a], Debasish Das Mahanta [a], Soumitra Hazra [b], Gopinatha Suresh Kumar [b,**], Rajib Kumar Mitra [a,*]

[a] Department of Chemical Biological and Macromolecular Sciences, S.N. Bose National Centre for Basic Sciences, Block JD, Sector III, Salt Lake, Kolkata 700098, India

[b] Biophysical Chemistry Laboratory, Chemistry Division, CSIR – Indian Institute of Chemical Biology, 4, Raja S.C. Mullick Road, Kolkata 700032, India

ARTICLE INFO

ABSTRACT


LANGMUIR

Effect of Short Chain Poly(ethylene glycol)s on the Hydration Structure and Dynamics around Human Serum Albumin

Nirnay Samanta, Trung Quan Luong, Debasish Das Mahanta, Rajib Kumar Mitra, and Martina Havenith

Supporting Information

ABSTRACT: We report the changes in the hydration ... globular protein, human serum albumin (HSA) ... short chain crowding agents, namely poly(ethylene glycol)s ... FTIR spectroscopy in the far-infrared (FIR) ...

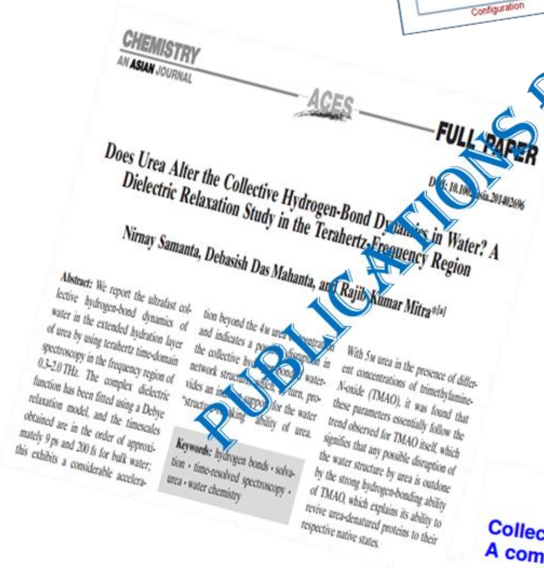
CHEMISTRY AN ASIAN JOURNAL

ACES

FULL PAPER

Does Urea Alter the Collective Hydrogen-Bond Dynamics in Water? A Dielectric Relaxation Study in the Terahertz-Frequency Region

Nirnay Samanta, Debasish Das Mahanta, and Rajib Kumar Mitra*[a]

Abstract: We report the ultrafast collective hydrogen-bond dynamics of water in the extended hydration layer of urea by using terahertz time-domain spectroscopy in the frequency region of 0.3–2.0 THz. The complex dielectric function has been fitted using a Debye relaxation model, and the timescales obtained are in the order of approximately 9 ps and 200 fs for bulk water; this exhibits a considerable accelera- tion beyond the 4M urea ... With 5M urea in the presence of different concentrations of trimethylamine-N-oxide (TMAO), it was found that these parameters essentially follow the trend observed for TMAO itself, which signifies that any possible disruption of the water structure by urea is outdone by the strong hydrogen-bonding ability of TMAO, which explains its ability to revive urea-denatured proteins to their respective native states.

Keywords: hydrogen bonds · solvation · time-resolved spectroscopy · urea · water chemistry


PCCP

PAPER

View Article Online

Collective hydration dynamics of guanidinium chloride solutions and its possible role in protein denaturation: a terahertz spectroscopic study†

Nirnay Samanta, Debasish Das Mahanta and Rajib Kumar Mitra*

Cite this: DOI: 10.1039/c4cp03273j

Received 23rd July 2014, Accepted 8th September 2014

DOI: 10.1039/c4cp03273j

www.rsc.org/pccp

The remarkable ability of guanidinium chloride (GdmCl) to denature proteins is a well studied yet controversial phenomenon; the exact molecular mechanism is still debatable, especially the role of hydration dynamics, which has been paid less attention. In the present contribution, we have addressed the issue of whether the collective hydrogen bond dynamics of water gets perturbed in the presence of GdmCl and its possible impact on the denaturation of a globular protein human serum albumin (HSA), using terahertz (THz) time domain spectroscopy (TTDS) in the frequency range of 0.3–2.0 THz. The collective hydrogen bond dynamics is determined by fitting the obtained complex dielectric response in a multiple Debye relaxation model. To compare the results, the studies were extended to two more salts: tetramethylguanidinium chloride (TMGdmCl) and sodium chloride (NaCl). It was concluded that the change in hydration dynamics plays a definite role in the protein denaturation process.

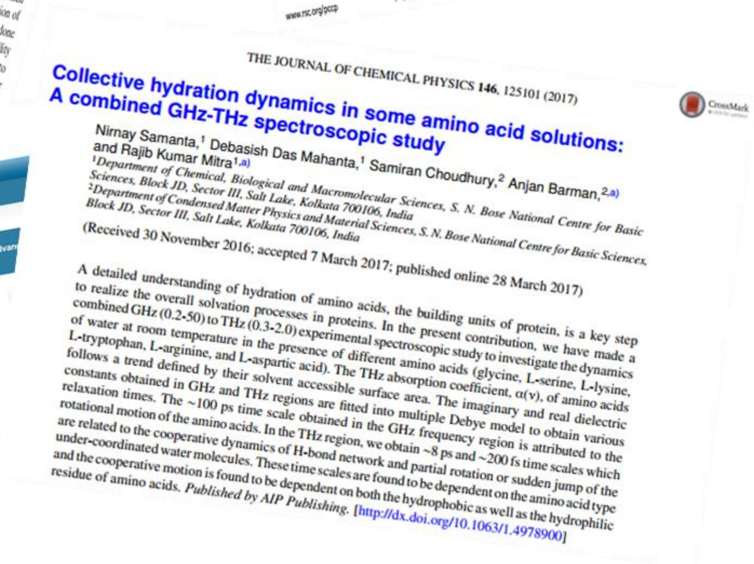
THE JOURNAL OF CHEMICAL PHYSICS 146, 125101 (2017)

Collective hydration dynamics in some amino acid solutions: A combined GHz-THz spectroscopic study

Nirnay Samanta,[1] Debasish Das Mahanta,[1] Samiran Choudhury,[2] Anjan Barman,[2,a)] and Rajib Kumar Mitra[1,a)]

[1]Department of Chemical, Biological and Macromolecular Sciences, S. N. Bose National Centre for Basic Sciences, Block JD, Sector III, Salt Lake, Kolkata 700106, India

[2]Department of Condensed Matter Physics and Material Sciences, S. N. Bose National Centre for Basic Sciences, Block JD, Sector III, Salt Lake, Kolkata 700106, India

(Received 30 November 2016; accepted 7 March 2017; published online 28 March 2017)

A detailed understanding of hydration of amino acids, the building units of protein, is a key step to realize the overall solvation processes in proteins. In the present contribution, we have made a combined GHz (0.2-50) to THz (0.3-2.0) experimental spectroscopic study to investigate the dynamics of water at room temperature in the presence of different amino acids (glycine, L-serine, L-lysine, L-tryptophan, L-arginine, and L-aspartic acid). The THz absorption coefficient, α(ν), of amino acids follows a trend defined by their solvent accessible surface area. The imaginary and real dielectric constants obtained in GHz and THz regions are fitted into multiple Debye model to obtain various relaxation times. The ~100 ps time scale obtained in the GHz frequency region is attributed to the rotational motion of the amino acids. In the THz region, we obtain ~8 ps and ~200 fs time scales which are related to the cooperative dynamics of H-bond network and partial rotation or sudden jump of the under-coordinated water molecules. These time scales are found to be dependent on the amino acid type and the cooperative motion is found to be dependent on both the hydrophobic as well as the hydrophilic residue of amino acids. *Published by AIP Publishing.* [http://dx.doi.org/10.1063/1.4978900]

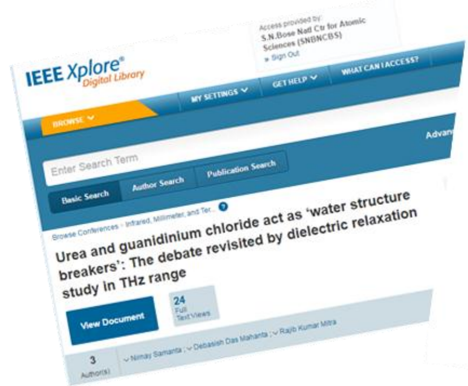
IEEE Xplore Digital Library

Urea and guanidinium chloride act as 'water structure breakers': The debate revisited by dielectric relaxation study in THz range

View Document

Nirnay Samanta ; Debasish Das Mahanta ; Rajib Kumar Mitra

Index